

Quantum wave packet revivals

R. W. Robinett*

*Department of Physics
The Pennsylvania State University
University Park, PA 16802 USA*

(Dated: November 5, 2018)

arXiv:quant-ph/0401031v1 7 Jan 2004

Abstract

The numerical prediction, theoretical analysis, and experimental verification of the phenomenon of wave packet revivals in quantum systems has flourished over the last decade and a half. Quantum revivals are characterized by initially localized quantum states which have a short-term, quasi-classical time evolution, which then can spread significantly over several orbits, only to reform later in the form of a quantum revival in which the spreading reverses itself, the wave packet relocalizes, and the semi-classical periodicity is once again evident. Relocalization of the initial wave packet into a number of smaller copies of the initial packet ('minipackets' or 'clones') is also possible, giving rise to fractional revivals. Systems exhibiting such behavior are a fundamental realization of time-dependent interference phenomena for bound states with quantized energies in quantum mechanics and are therefore of wide interest in the physics and chemistry communities.

We review the theoretical machinery of quantum wave packet construction leading to the existence of revivals and fractional revivals, in systems with one (or more) quantum number(s), as well as discussing how information on the classical period and revival time is encoded in the energy eigenvalue spectrum. We discuss a number of one-dimensional model systems which exhibit revival behavior, including the infinite well, the quantum bouncer, and others, as well as several two-dimensional integrable quantum billiard systems. Finally, we briefly review the experimental evidence for wave packet revivals in atomic, molecular, and other systems, and related revival phenomena in condensed matter and optical systems.

PACS numbers: 03.65.Ge, 03.65.Sq

*Electronic address: rick@phys.psu.edu

Contents

I. Introduction	6
II. General analysis	8
A. Autocorrelation function	8
B. Time-dependence of one-dimensional localized wave packets	9
C. Classical periodicity and approach to the collapsed state	13
D. Revivals and fractional revivals	14
1. Revival time	14
2. Fractional revivals	15
3. General structure of fractional revivals	16
E. Superrevivals	19
F. Revivals in systems with two or more quantum numbers	19
III. Model systems	22
A. Free particle wave packets	22
B. Wave packets and the constant force or uniform acceleration problem	23
C. Harmonic oscillator	26
D. The infinite well	30
1. General comments	30
2. Gaussian wave packets	32
3. Zero-momentum wave packets	33
4. Short-term, quasi-classical propagation	35
5. Revivals, fractional revivals, and mirror revivals	36
6. Expectation value analysis	37
7. Phase-space picture of fractional revivals using the Wigner function	39
8. Quantum carpets	42
E. Variations on the infinite well	43
F. The quantum bouncer	45
1. Energy eigenfunctions and eigenvalues	45
2. Classical period and revival time	46

G. 2D rotor and related systems	48
1. Two dimensional free quantum rotor	48
2. Quantum pendulum	49
IV. Two- and three-dimensional quantum systems	49
A. Two dimensional infinite well and variations	50
B. Isosceles ($45^\circ - 45^\circ - 90^\circ$) triangle billiard	51
C. Equilateral triangle billiard	52
1. Energy eigenvalues and eigenfunctions	52
2. Classical periodicity and revival times	53
D. Circular billiard and variations	55
1. Energy eigenvalues and eigenfunctions	55
2. Wave packets and time scales	59
3. Variations on the circular billiard	60
V. Experimental realizations of wavepacket revivals	61
A. Atomic systems	62
B. Molecular systems	64
C. Jaynes-Cummings model	65
D. Revivals in other systems	67
1. Atoms in optical lattices and Bose-Einstein condensates	67
2. Revivals and fractional revivals in optical systems	69
VI. Discussion and conclusions	70
A. Energy eigenvalues in power law potentials	71
B. General time scales	71
C. Fractional (p/q) revivals for even q	74
D. The ‘inverted’ oscillator	75
E. The full and annular circular wells: WKB energy eigenvalues, classical periods, and closed orbits	76

I. INTRODUCTION

The study of localized, time-dependent solutions to bound state problems in quantum mechanics has been of interest to both researchers and students of the subject alike since the earliest days of the development of the field. Schrödinger (1) and others (2) - (4) discussed the connections between the quantum and classical descriptions of nature by exhibiting explicit wave packet solutions to many familiar problems, including the cases of the free-particle, uniform acceleration (constant electric or gravitational field), harmonic oscillator (forerunner of coherent and squeezed states), and uniform magnetic field. Many such examples then appeared in early textbooks (5) - (7) only a decade later, discussing both wave packet spreading and periodic time-dependence in a way which is easily accessible to students even today.

Despite Schrödinger's hope (1) that "...wave groups can be constructed which move round highly quantised Kepler ellipses and are the representations by wave mechanics of the hydrogen electron..." (without spreading, as with the constant width harmonic oscillator packet he derived), early investigators soon found (3), (8) that such dispersion was a natural feature of wave packets for the Coulomb problem.

Attempts at constructing localized semi-classical solutions (of the coherent-state type) for the Coulomb problem, following up on Schrödinger's suggestions, continued with theoretical results (9) - (16) appearing in the literature much later. It was, however, the development of modern experimental techniques, involving the laser-induced excitation of atomic Rydberg wave packets, including the use of the 'pump-probe' (17) or 'phase-modulation' (18) techniques to produce, and then monitor the subsequent time-development of, such states which led to widespread interest in the physics of wave packets. (For reviews of the subject, see (19) - (23).) Updated proposals for the production of such states in the context of Rydberg atoms, where one could study the connections between localized quantum mechanical solutions and semi-classical notions of particle trajectories, led first to the creation of such spatially localized states (24), to experiments which observed their return to near the atomic core (25), and then the observation of the classical Kepler periodicity (26), (27) of Rydberg wave packets, over only a few cycles in the early experiments.

However, this interest also led to the prediction of qualitatively new features in the long-term time development in such bound state systems, such as quantum wave packet revivals. Parker and Stroud (28) were the first to find evidence for this behavior in numerical studies of Rydberg atoms, while Yeazell and Stroud (30), (31) and others (32), (33) soon confirmed their predictions experimentally.

The phenomenon of wave packet revivals, which has now been observed in many experimental situations, arises when a well-localized wave packet is produced and initially exhibits a short-term time evolution with almost classical periodicity (T_{cl}) and then spreads significantly after a number of orbits, entering a so-called collapsed phase where the probability is spread (not uniformly) around the classical trajectory. On a much longer time scale after the initial excitation, however, called the revival time (with $T_{rev} \gg T_{cl}$), the packet relocalizes, in the form of a quantum revival, in which the spreading reverses itself and the classical periodicity is once again apparent. Even more interestingly, many experiments have since observed additional temporal structures, with smaller periodicities (fractions of T_{cl}), found at times equal to rational fractions of the revival time (pT_{rev}/q). These have been elegantly interpreted (34) as the temporary formation of a number of 'mini-packets' or 'clones' of the original packet, often with $1/q$ of the total probability, exhibiting local periodicities T_{cl}/q , and have come to be known as fractional revivals. Observations of fractional revivals have been made in a number of atomic (31) - (33) and molecular (35) systems.

A simple picture (36) of the time-dependence of the quantum state leading to these behaviors, modeling the individual energy eigenstates and their exponential ($\exp(-iE_n t/\hbar)$) time-dependent factors as an ensemble of runners or race-cars on a circular track, is often cited. The quantum mechanical spreading arises from the differences in speed, while the classical periodicity of the system is observable over a number of revolutions (or laps.) For longer times, however, the runners/race-cars spread out and no correlations (or clumpings) are obvious, while after the fastest participants have lapped their slower competitors (once

or many times), obvious patterns can return, including smaller ‘packs’ of racers, clumped together, which model fractional revivals.

A different metaphor involves the (deterministic) shuffling of an initially highly ordered deck of playing cards. One shuffling method involves splitting the deck into two equal halves, and then alternately placing the bottom card from each half into a pile, reforming and reordering the deck. After only a few such shuffles, the original order is seemingly completely lost and the cards appear to have randomized. After only a few more turns, however, clear patterns of ordered subsets of suits and ranks appear, increasingly so until after only eight such shuffles the deck has returned to its original highly ordered state. Only the simplest of mathematical concepts is required to describes these analogs of fractional and full revivals.

The *Dynamics of wave packets of highly-excited states of atoms and molecules*, including a discussion of wave packet revivals and fractional revivals, and descriptions of the experimental observations of these phenomena, were discussed in the excellent 1991 review by Averbukh and Perelman (37), while a nicely accessible general discussion by Bluhm and Kostelecký (38) has also appeared. There have been developments in the field since then, and many of the basic quantum mechanical concepts behind revival behavior have also begun to appear in the pedagogical literature, so it seems appropriate to provide a review of some of the fundamental ideas behind the short- and long-term behavior of quantum wave packets, describing both the classical periodicity and revival behavior of wave packets in many model systems, and their experimental realizations.

The theoretical machinery required to understand many aspects of revival behavior is sufficiently accessible, and potentially of enough general interest, that our review of the subject will contain many tutorial aspects, such as

- (i) the use of familiar model systems (such as the infinite well and others) as illustrative of the fundamental concepts,
- (ii) an emphasis on examples in which exact revival behavior is found (to be used as benchmarks for more realistic systems),
- (iii) a focus on semi-classical methods, including the WKB approximation, which are appropriate for many wave packet systems constructed from large n energy eigenstates,
- (iv) general discussions of how information on both the classical periodicity and quantum revival times are encoded in the energy eigenvalue spectrum,
- (v) and references not only to the original research literature, but to many of the pedagogical papers appearing on the subject.

In these areas, and others, we hope to extend the reviews in Refs. (37) and (38) in useful ways.

We start in Sec. II with a general introduction to the theoretical tools required for understanding revival behavior, including the autocorrelation function. We then turn to discussions of many model systems (in Sec. III) which illustrate various aspects of the quantum mechanical time development of localized wave packets, including background material on unbound systems (free-particle and uniform acceleration cases) and for ones exhibiting only periodic behavior (the harmonic oscillator). The infinite well is then discussed in great detail, as are other familiar one-dimensional problems. Two-dimensional quantum systems, especially quantum billiard geometries, are studied in Sec. IV. We then briefly review experimental evidence for revival behavior in Sec. V in atomic (Coulomb) and molecular (vibrational, rotational) systems, as well as in situations where the quantum revivals are due to the quantized nature of the electromagnetic field in two-state atom-field systems, or in the excitation spectrum of Bose-Einstein condensates, and finally we discuss related revival phenomena in a variety of optical systems.

II. GENERAL ANALYSIS

A. Autocorrelation function

The study of the time-development of wave packet solutions of the Schrödinger equation has a long history and often makes use of the concept of the overlap ($\langle\psi_t|\psi_0\rangle$) of the time-dependent quantum state ($|\psi_t\rangle$) with the initial state ($|\psi_0\rangle$). For example, early work by Mandelstam and Tamm (39) on the time-development of isolated quantum systems led to the inequality

$$|\langle\psi_t|\psi_0\rangle|^2 \geq \cos^2\left(\frac{\Delta H t}{\hbar}\right), \quad \text{valid for} \quad 0 \leq t \leq \frac{\pi\hbar}{2\Delta H}, \quad (1)$$

where $\Delta H = \sqrt{\langle H^2 \rangle - \langle H \rangle^2}$ is the uncertainty in the free-particle energy of the wave packet. These ideas were used to study energy-time uncertainty relations, as well as the minimum time required to reach an orthogonal quantum state.

This overlap is most often referred to as the *autocorrelation function* and can be evaluated in either position- or momentum-space to give

$$A(t) \equiv \langle\psi_t|\psi_0\rangle = \int_{-\infty}^{+\infty} \psi^*(x, t) \psi(x, t) dx = \int_{-\infty}^{+\infty} \phi^*(p, t) \phi(p, t) dp \quad (2)$$

which emphasizes that in order for $|A(t)|$ to be large, the wave function at later times must have significant overlap with the initial state in both x - and p -space.

For one-dimensional bound state systems, where a wave packet is expanded in terms of energy eigenfunctions, $u_n(x)$, with quantized energy eigenvalues, E_n , in the form

$$\psi(x, t) = \sum_{n=0}^{\infty} a_n u_n(x) e^{-iE_n t/\hbar} \quad (3)$$

with

$$a_n = \int_{-\infty}^{+\infty} [u_n(x)]^* \psi(x, 0) dx \quad (4)$$

the most useful form for the autocorrelation function (40) is

$$A(t) = \sum_{n=0}^{\infty} |a_n|^2 e^{+iE_n t/\hbar} \quad (5)$$

and the evaluation of $A(t)$ in this form for initially highly localized wave packets will be one of the main topics of this review. Besides being of obvious theoretical value in the analysis of time-dependent systems, more physically, the autocorrelation function is important because it is very directly related to the observable ionization signal (17), (30) in the pump-probe type experiments where such behavior is studied experimentally.

Studies of the long-term time development of quantum states is also a topic with a long history, often being discussed from a more formal point of view. For example, Bocchieri and Loinger (41) produced statements of a ‘*quantum recurrence theorem*’ which attempted to generalize Poincaré’s theorem to show that systems with discrete energy eigenvalues would eventually return arbitrarily closely to the initial state, in the sense that the norm $\|\psi_t - \psi_0\|$ could be made smaller than any arbitrarily small number. (Such ideas have also been examined (42) from a pedagogical point of view.) Similar studies in the mathematical literature often deal with analyses of *almost periodic functions* (43), (44). Such long-term

time behavior has also been compared (45) to Fermi-Pasta-Ulam recurrences (46) in the dynamical behavior of non-linearly coupled oscillators. Investigations of recurrence (revival-like) phenomena in the context of non-stationary (time-dependent) Hamiltonians (47) have resulted in similar theorems.

In this context, Gutschick and Nieto (13) noted that “...if one waits long enough any state which has significant overlap with a finite number of states will eventually return to “almost” its original shape...it amounts to having a totally dispersed wave packet suddenly regenerate itself after very long times. Peres (48) also pointed out that very long time scale recurrences of this type would occur in systems with hydrogenic energy levels. However, both analyses focused on time scales which are much longer than those ultimately observed in wave packet experiments. For the laser-induced wave packets produced in modern experiments, the structure of the expansion in eigenstates in Eqn. (3) is such that a quite general systematic analysis of the time scales involved in the problem is possible and that is the topic of the next section.

B. Time-dependence of one-dimensional localized wave packets

In general, the time-dependence of an arbitrary time-dependent bound state wavefunction, $\psi(x, t)$, with the expansion in eigenstates, $u_n(x)$, of the form in Eqn. (3) can be quite complex. However, in many experimental realizations, a localized wave packet is excited with an energy spectrum which is tightly spread around a large central value of the quantum number, n_0 , so that $n_0 \gg \Delta n \gg 1$. In that case, it is appropriate to expand the individual energy eigenvalues, $E(n) \equiv E_n$, about this value, giving

$$E(n) \approx E(n_0) + E'(n_0)(n - n_0) + \frac{E''(n_0)}{2}(n - n_0)^2 + \frac{E'''(n_0)}{6}(n - n_0)^3 + \dots \quad (6)$$

where $E'(n_0) = (dE_n/dn)_{n=n_0}$ and so forth. This gives the time-dependence of each individual quantum eigenstate through the factors

$$\begin{aligned} e^{-iE_n t/\hbar} &= \exp \left(-i/\hbar \left[E(n_0)t + (n - n_0)E'(n_0)t + \frac{1}{2}(n - n_0)^2 E''(n_0)t \right. \right. \\ &\quad \left. \left. + \frac{1}{6}(n - n_0)^3 E'''(n_0)t + \dots \right] \right) \\ &\equiv \exp \left(-i\omega_0 t - 2\pi i(n - n_0)t/T_{cl} - 2\pi i(n - n_0)^2 t/T_{rev} \right. \\ &\quad \left. - 2\pi i(n - n_0)^3 t/T_{super} + \dots \right) \end{aligned} \quad (7)$$

where each term in the expansion (after the first) defines an important characteristic time scale, via

$$T_{cl} = \frac{2\pi\hbar}{|E'(n_0)|} \quad , \quad T_{rev} = \frac{2\pi\hbar}{|E''(n_0)|/2} \quad , \quad \text{and} \quad T_{super} = \frac{2\pi\hbar}{|E'''(n_0)|/6} \quad . \quad (8)$$

The first ($\omega_0 = E(n_0)/\hbar$) term is an unimportant, n -independent overall phase, common to all terms in the expansion, and which therefore induces no interference between them; it is similar to the time-dependent phase for a single stationary state solution and has no observable effect in $|\psi(x, t)|^2$.

The second term in the expansion is familiar from correspondence principle arguments (49) as being associated with the classical period of motion in the bound state, so that

$$T_{cl} \equiv \frac{2\pi\hbar}{|E'(n_0)|} \quad . \quad (9)$$

This connection is perhaps most easily seen using a semi-classical argument and the WKB quantization condition, familiar variations on classical action-angle methods (50) - (51).

For a particle of fixed energy E in a 1D bound state potential, $V(x)$, we have $E = mv(x)^2/2 + V(x)$ and the short time, dt , required to traverse a distance dx can be obtained from this and integrated over the range defined by the classical turning points; this then gives *half* the classical period as

$$dt = \frac{dx}{v(x)} = \sqrt{\frac{m}{2}} \frac{dx}{\sqrt{E - V(x)}} \quad \longrightarrow \quad \frac{\tau}{2} = \int_a^b dt = \sqrt{\frac{m}{2}} \int_a^b \frac{dx}{\sqrt{E - V(x)}}. \quad (10)$$

The WKB quantization condition in this same potential (with the same classical turning points, a, b) can be written in the form

$$\sqrt{2m} \int_a^b \sqrt{E_n - V(x)} dx = (n + C_L + C_R)\pi\hbar \quad (11)$$

in terms of the matching coefficients C_L, C_R . We recall that the appropriate values of these constants (52) are given by $C_{L,R} = 1/4$ at ‘linear’ or ‘smooth’ turning points, where functions are matched smoothly onto Airy function solutions (and $\psi(x)$ effectively penetrates roughly $1/8$ of a wavelength into the classically disallowed region (53)), while $C_{L,R} = 1/2$ at ‘infinite wall’ type boundaries where the wavefunction must vanish. This expression can then be differentiated implicitly with respect to the quantum number, n , to obtain

$$\sqrt{2m} \int_a^b \frac{|dE_n/dn| dx}{2\sqrt{E_n - V(x)}} = \pi\hbar. \quad (12)$$

This, in turn, can be related to the classical period in Eqn. (10) to give

$$T_{cl} \equiv \tau = \sqrt{2m} \int_a^b \frac{1}{\sqrt{E_n - V(x)}} dx = \frac{2\pi\hbar}{|dE_n/dn|}. \quad (13)$$

The most obvious example of such a connection is for the harmonic oscillator, where the WKB condition gives the exact eigenvalues, $E_n = (n + 1/2)\hbar\omega$, and the classical period from Eqn. (9) is

$$T_{cl} = \frac{2\pi\hbar}{|dE/dn|} = \frac{2\pi\hbar}{\hbar\omega} = \frac{2\pi}{\omega} \quad (14)$$

as expected. For the special case of the oscillator, all wave packets are exactly periodic and all higher order derivatives (E'', E''', \dots) vanish, so no other longer time scales are present. Nauenberg (40) has also provided an elegant argument connecting $E'(n_0)$, the classical periodicity, and the structure of the autocorrelation function, which we review in Appendix B.

For future reference, even in the presence of higher-order time scales, we define the *classical* component of the wave packet to be

$$\psi_{cl}(x, t) \equiv \sum_{n=0}^{\infty} a_n u_n(x) e^{-2\pi i(n-n_0)E'_n t/\hbar} \equiv \sum_k a_k u_k(x) e^{-2\pi i k t/T_{cl}} \quad (15)$$

where we define $k \equiv n - n_0$. This component can be used to describe the short-term ($t \approx T_{cl} \ll T_{rev}$) time-development and is especially helpful in discussing fractional revivals. We note that here, and elsewhere, we will henceforth ignore the overall $\exp(-iE(n_0)t/\hbar)$ phase factor.

The next term in the expansion in Eqn. (8) is given by

$$T_{rev} = \frac{2\pi\hbar}{|E''(n_0)|/2} \quad (16)$$

which will be associated with the quantum revival time scale. This time scale determines the relative importance of the $(n - n_0)^2$ term in the exponent for $t > 0$. It is responsible for the long-term ($t \gg T_{cl}$) spreading of the wave packet in the same way that the difference in the p -dependence of the px and $p^2t/2m$ terms in $\exp(i(px - p^2t/2m)/\hbar)$ in the plane wave expansion of free particle wave packets gives rise to dispersion; it can be shown quite directly (Ref. (40) and Appendix B) that the spreading time is proportional to T_{rev} for $t \ll T_{rev}$. More interestingly, for times of the order of T_{rev} , the additional $\exp(2\pi i(n - n_0)^2t/T_{rev})$ phase terms all return to unity, giving the $t \approx 0$ time-dependence in Eqn. (15) and a return to approximate semi-classical behavior.

The anharmonic oscillator provides an example of the calculation of the revival time of relevance to physically realizable systems such as the vibrational motion of molecules. For example, the addition of a cubic term, $\lambda\hbar\omega x^3$, to the usual oscillator Hamiltonian yields (in second-order perturbation theory (54)) the energy eigenvalues

$$E_n = \hbar\omega \left[(n + 1/2) - \frac{15\lambda^2}{4}(n + 1/2)^2 - \frac{7}{16}\lambda^2 \right] = \hbar\omega [\gamma + n(1 - \alpha) - \alpha n^2] \quad (17)$$

where $\gamma \equiv 1/2 - 11\lambda^2/8$ and $\alpha \equiv 15\lambda^2/4$. The effect of the anharmonicity (for either sign of λ) is to increase the classical period ($T_{cl} = 2\pi/(1 - \alpha)\omega$), but more importantly it also introduces a finite revival time given by

$$T_{rev} = \frac{2\pi}{\omega\alpha} \approx \frac{T_{cl}}{\alpha} \gg T_{cl} \quad \text{for } \alpha \ll 1. \quad (18)$$

As another example of the hierarchy of relative magnitudes of T_{rev} and T_{cl} which is possible, we consider a family of (symmetric) one-dimensional power-law potentials (55) – (58) defined by

$$V_{(k)}(x) \equiv V_0 \left| \frac{x}{L} \right|^k. \quad (19)$$

This family includes both the harmonic oscillator (when $k = 2$ and $V_0/L^2 = m\omega^2/2$) and the infinite well of width $2L$ (when $k \rightarrow +\infty$, for any V_0). The same WKB approximation considered above (see Appendix A for details) shows that the energy eigenvalues scale (for large n) as

$$E_n(k) \propto n^{2k/(k+2)} \quad (20)$$

which does indeed give the correct large n behavior for the oscillator ($E_n \propto n$) and the infinite well ($E_n \propto n^2$); it even gives the appropriate dependence on quantum number for the Coulomb problem ($E_n \propto n^{-2}$ for $k = -1$) so that these simple arguments are useful for the more realistic case of Rydberg atoms. (Many similar scaling laws can be derived for truly three-dimensional systems in different ways, as shown in Ref. (59).)

For this general class of potentials, we find that the ratio of the revival time to the classical period is given by

$$\frac{T_{rev}^{(k)}}{T_{cl}^{(k)}} = \left(\frac{4\pi\hbar}{|E''(n_0)|} \right) \left(\frac{|E'(n_0)|}{2\pi\hbar} \right) = 2 \left| \frac{k+2}{k-2} \right| n_0. \quad (21)$$

The revival time diverges for the special case of the oscillator ($k = 2$), as do all of the other higher-order time scales, while for the general ($k \neq 2$) case one can quite generally

have $T_{rev} \gg T_{cl}$ for $n_0 \gg 1$, which is typical for the localized wave packets studied experimentally. We note that for the experimentally important case of the Coulomb potential ($k = -1$), the hierarchy is given by $T_{rev}^{(Coul)} = (2n_0/3)T_{cl}^{(Coul)}$.

We note that several important model systems, including the infinite well, and the 2D ($E_m \propto m^2$) and 3D ($E_l \propto l(l+1)$) free rotors (38) have energy spectra with no higher than quadratic dependence on the quantum number, implying that higher order derivatives vanish and longer time scales are sent to infinity. The interaction energy of the particles in Bose-Einstein condensates can be modeled in the form $E_n = U_0 n(n-1)/2$ (60) providing another highly realizable physical example with a quadratic energy spectrum, and revival behavior.

Continuing in this fashion, we note that the next term in the expansion is typically an even longer time scale, called the *superrevival* time, defined by

$$T_{super} = \frac{2\pi\hbar}{|E'''(n_0)|/6} \quad (22)$$

with

$$\frac{T_{super}^{(k)}}{T_{rev}^{(k)}} = \frac{3(k+2)}{4}n_0 \quad (23)$$

for the power-law family of potentials; we discuss superrevivals in more detail in Sec. II.E.

Since this type of behavior is generic to localized wave packets, we will first exemplify the short-term semi-classical periodicity, then the approach to a collapsed (incoherent sum) state, as well as the structure of quantum revivals and fractional revivals using a simple model energy eigenvalue spectrum and standard Gaussian distribution of eigenstates. We will assume that the expansion coefficients are given by

$$a_n = \frac{1}{\sqrt{\Delta n} \sqrt{2\pi}} \exp \left[-\frac{(n-n_0)^2}{4\Delta n^2} \right] \quad (24)$$

which gives the required normalization

$$\sum_{n=0}^{\infty} |a_n|^2 \approx 1 \quad (25)$$

to exponential accuracy for $n_0 \gg \Delta n \gg 1$. For the examples in the rest of this section we use $n_0 = 400$ which is typically larger than that found in experimental realizations, but useful for making the visualized examples we present more transparent. We often use $\Delta n = 6$, but also will examine the effect of varying Δn as well; several notable experiments on Rydberg atoms (30), (33) have made use of wave packets constructed from 5 – 10 states, corresponding to $\Delta n \approx 2 - 5$ in our notation.

For the energy eigenvalues, we choose, for simplicity, a generalized anharmonic oscillator spectrum of the form

$$E_n = 2\pi(n - \alpha n^2/2 + \beta n^3/6) \quad (26)$$

and use two sets of parameters for comparison, namely

Case	A	B
α	1/800	1/800
β	0	$2 \cdot 10^{-6}$
T_{cl}	2	1.515
T_{rev}	1600	4444.4
T_{rev}/T_{cl}	800	2933.3

Table I.

For Case A, with only linear and quadratic terms, we expect exact revival behavior, and this case is arranged to be even more special by having T_{rev}/T_{cl} be an integer and so can be considered as an ideal case. The introduction of an additional small n^3 ($\beta \neq 0$) term in Case B will exemplify systems containing higher order terms, longer time scales, and hence only approximate revival behavior.

C. Classical periodicity and approach to the collapsed state

Even in the absence of a specific physical system, one can still examine, in great detail, the time-dependence of a generic wave packet using the autocorrelation function in the form

$$A(t) = \sum_{n=0}^{\infty} |a_n|^2 e^{iE_n t/\hbar}. \quad (27)$$

Nauenberg (40), for example, has shown how to elucidate the approximate periodicity apparent in $|A(t)|$ for bound state systems in a quite general way, and we discuss his approach in Appendix B, but we first present some numerical examples.

Using the values for Case A in Table I, we examine the behavior of $A(t)$ over the first 100 classical periods in Fig. 1, corresponding in this case to 1/8 of the entire revival time. In that plot (upper half), the initial classical periodicity is clear, as is the effect of the wave packet spreading, shown by the decreasing value of $A(t)$ at integral multiples of the classical period (also seen in the bottom half), as well as the increasing ‘width’ of the (decreasingly small) peaks in $A(t)$. In more specific model systems where we can examine the dynamics, we can elucidate the nature of the loss of coherence to the collapsed phase in more detail, as in Sec. III.D.4.

For times longer than approximately $50T_{cl}$ (in this case), the $|A(t)|$ oscillates (more or less rapidly) about a constant value, indicated by the horizontal dashed line. To understand this, we examine the general structure of $|A(t)|^2$ and note that

$$|A(t)|^2 = \left| \sum_n |a_n|^2 e^{iE_n t/\hbar} \right|^2 = \sum_n |a_n|^4 + 2 \sum_{n \neq m} |a_n|^2 |a_m|^2 \cos \left(\frac{(E_n - E_m)t}{\hbar} \right). \quad (28)$$

For time scales of the order of the classical period, the $\cos((E_n - E_m)t/\hbar)$ terms are still highly correlated and reproduce the approximate classical periodicity. For longer times, the oscillatory components become increasingly out of phase and can lead to high frequency ($f \gg 2\pi/T_{cl}$) excursions around the constant value given by the first term in Eqn. (28), namely

$$|A_{inc}|^2 \equiv \sum_{n=0}^{\infty} |a_n|^4 \quad (29)$$

which we will label the *incoherent* limit of $|A(t)|^2$. For the Gaussian expansion coefficients in Eqn. (24), this sum can also be done approximately (to the same accuracy as the normalization) giving

$$|A_{inc}|^2 \equiv \sum_{n=0}^{\infty} |a_n|^4 = \frac{1}{\Delta n 2\sqrt{\pi}} \approx 0.047 \quad \text{for } \Delta n = 6 \quad (30)$$

which is included in Fig. 1 as the dotted horizontal lines and indicated by the horizontal arrows. The larger the number of states contained in the expansion, the smaller the resulting

incoherent value during the collapsed state; because of the discrete nature of the bound state spectrum, the autocorrelation function does not asymptotically approach zero as it would in the free particle case, for example, but oscillates about this generic plateau value.

In the bottom half of Fig. 1, we also show the values of $A(t)$ at multiples of the classical period (squares) and at times a half period away ($t = (n + 1/2)T_{cl}$, stars) showing how the ‘in-phase’ (‘out-of-phase’) components first shrink (grow) until they are of the same order as the incoherent value of $|A_{inc}|^2$, and then clearly exhibit highly correlated behavior, which is the first hint of fractional revivals; some evidence of this is the appearance of highly oscillatory behavior at fractional multiples of T_{rev} (note the 1/9 - 1/11 labels in Fig. 1(a).)

We note, for future reference, that the form of the probability density, $|\psi(x, t)|^2$ during the collapsed or incoherent phase of the time-development can be similarly written in the form

$$|\psi(x, t)|^2 = \sum_n |a_n|^2 |u_n(x)|^2 + 2\Re \left[\sum_{n \neq m} a_n^* a_m u_n(x) u_m^*(x) e^{i(E_n - E_m)t/\hbar} \right]. \quad (31)$$

The probability density will then oscillate around a ‘static’ value determined by the incoherent sum of the probability densities for each eigenstate, $|u_n(x)|^2$. In the large n limit which is applicable here, WKB methods can be used to approximate the energy eigenstates, and one can write

$$P_n(x) = |u_n(x)|^2 \approx \frac{2}{\tau_n} \sqrt{\frac{m}{E_n - V(x)}} \quad (32)$$

where E_n, τ_n are the quantized WKB energies and classical periods in Eqns. (11) and (13). Similar statements can be made about the momentum-space probability densities.

D. Revivals and fractional revivals

1. Revival time

We now turn our attention to the longer term behavior of the autocorrelation function over an entire revival time and plot $|A(t)|^2$ over the interval $(0, T_{rev})$ in Fig. 2 for three cases. The top two plots, (a) and (b), correspond to the parameters of Case A in Table I, showing the effect of changing Δn ; for larger (smaller) values of Δn , the spread in momentum values is larger (smaller), so that the quantum mechanical spreading time, t_0 , is smaller (larger) and the rate at which the initial classical periodicity is lost is corresponding faster (slower). The initial size of the wave packet (and, as we will see, the subsequent size of the ‘mini’ wave packet components at fractional revivals) is smaller (larger) for bigger (smaller) values of Δn and this correlation is also obvious in that finer details are apparent for the larger Δn case.

In the bottom plot in Fig. 2(c), we show the results corresponding to case B in Table I, where one includes contributions from terms of order $(n - n_0)^3$. The overall pattern is similar, and many of the same individual distinct features are seen, but without the obvious symmetry or near exact revivals as in the case of purely quadratic n -dependence where no higher order time scales are present. The rich structure of features at rational fractions of T_{rev} which is apparent in both cases, and which are obviously highly correlated with fractional values of $|A(t = 0)|^2 = 1$, is seemingly a robust feature of all the examples, and we systematically explore their general structure next.

To examine the generic behavior of the wave packet near the revival time, T_{rev} , we use only the first two derivative terms in the expansion in Eqn. (8) and write

$$\psi(x, t \approx T_{rev}) = \sum_k a_k u_k(x) e^{-2\pi i k t / T_{cl}} e^{-2\pi i k^2} \quad \text{where } k = n - n_0 \quad (33)$$

and we focus on the effect of the $\mathcal{O}(t/T_{rev})$ or k^2 terms on the exponential time development. The additional phases arising from such terms all give unity and the wave packet is said to have revived since

$$\psi(x, t \approx T_{rev}) = \sum_k a_k u_k(x) e^{-2\pi i k t / T_{cl}} = \psi_{cl}(x, t) \quad (34)$$

has returned to something like its initial form, exhibiting the classical periodicity. In the special case when T_{rev}/T_{cl} is an integer (as in Case A in Table I, and the top two plots in Fig. 2) the revival occurs exactly in phase with the original time-development, and is exact (in that $|A(t)|$ returns to exactly unity).

The robust prediction that the wave packet exhibits approximately the classical periodicity (in phase or not) near $t = T_{rev}$ is also apparent in Fig. 3 (where we now plot $|A(t)|^2$ near several full or fractional revival times) even for admixtures of higher order terms, such as the Case B values in Table I where $|A(t \approx T_{rev})| < 1$, but the return to the initial periodicity is apparent.

2. Fractional revivals

We next examine $\psi(x, t)$ near half a revival time, and find that

$$\psi(x, t \approx T_{rev}/2) = \sum_k a_k u_k(x) e^{-2\pi i k t / T_{cl}} e^{-\pi i k^2} \quad (35)$$

with additional $\exp(-\pi i k^2) = \pm 1$ factors. We can compare this to the semi-classical time evolution by noting that

$$\psi_{cl}(x, t + T_{cl}/2) = \sum_k a_k u_k(x) e^{-2\pi i k (t + T_{cl}/2) / T_{cl}} = \sum_k a_k u_k(x) e^{-2\pi i k t / T_{cl}} e^{-\pi i k} \quad (36)$$

and the additional \pm phase factors in Eqn. (35) can be written in the same form since both the

$$\text{(Eqn. (35))} \quad e^{-\pi i k^2} = (-1)^{k^2} = (-1)^k = e^{-\pi i k} \quad \text{(Eqn. (36))} \quad (37)$$

terms give the same result for even and odd values of k . We thus see that

$$\psi(x, t \approx T_{rev}/2) = \psi_{cl}(x, t + T_{cl}/2) \quad (38)$$

and the wavepacket also reforms near the half revival time, with the original classical periodicity, but half a period of phase with the initial wave form (at least for integral T_{rev}/T_{cl}) and we see this behavior in Fig. 3 for both the A and B cases. The approximate revival at $T_{rev}/2$ seen for Case B is, in fact, somewhat better than at the full revival time T_{rev} since the higher order anharmonicities have had less time to effect the phase structure of the revivals.

We then turn our attention to the quarter-revival time where we can write

$$\psi(x, t \approx T_{rev}/4) = \sum_k a_k u_k(x) e^{-2\pi i k t / T_{cl}} e^{-\pi i k^2 / 2} \quad (39)$$

and the additional phase factor beyond the classical terms is given by

$$k = 2l \text{ even} \quad e^{-i\pi(2l)^2/2} = e^{-2\pi i} = 1 \quad (40a)$$

$$k = 2l + 1 \text{ odd} \quad e^{-i\pi(2l+1)^2/2} = e^{-2\pi i l^2} e^{-2\pi i l} e^{-i\pi/2} = -i \quad (40b)$$

or

$$e^{-i\pi k^2/2} = \begin{cases} +1 & \text{for } k \text{ even} \\ -i & \text{for } k \text{ odd} \end{cases} . \quad (41)$$

This factor can be written in the forms

$$e^{-i\pi k^2/2} = \frac{(1-i)}{2} + \frac{(1+i)}{2}(-1)^k = \frac{1}{\sqrt{2}} (e^{-i\pi/4} + e^{+i\pi/4}e^{-i\pi k}) \quad (42)$$

and, using the result in Eqn. (36), we can see that

$$\begin{aligned} \psi(x, t \approx T_{rev}/4) &= \sum_k a_k u_k(x) e^{-2\pi i k t / T_{cl}} e^{-\pi i k^2 / 2} \\ &= \sum_k a_k u_k(x) e^{-2\pi i k t / T_{cl}} \left[\frac{1}{\sqrt{2}} (e^{-i\pi/4} + e^{+i\pi/4} e^{-i\pi k}) \right] \\ &= \frac{1}{\sqrt{2}} [e^{-i\pi/4} \psi_{cl}(x, t) + e^{+i\pi/4} \psi_{cl}(x, t + T_{cl}/2)] . \end{aligned} \quad (43)$$

Thus, the wave packet near $T_{rev}/4$ (and $3T_{rev}/4$ as well) consists of two, high-correlated copies of the original packet, in- and out-of-phase, each containing half of the probability. This structure is similar to that proposed in early suggestions made for Schrödinger cat type states (61), and experimental work on Rydberg atom realizations of this state (62) has been discussed in just that context.

The signal for such behavior is the presence of peaks in $|A(t)|^2$ with half the magnitude, and half the classical periodicity, as each ‘mini-packet’ or ‘clone’ or ‘fractional revival’ state now approaches the same location in phase space as the initial wave form twice during each classical period; this behavior is indeed seen in Fig. 3, with the exact revival structure and phase relation to the initial state for Case A (with a maximum value of $|A(t)|^2 = (1\sqrt{2})^2 = 1/2$ as shown by the horizontal dashed line), and in a more approximate manner as for Case B.

3. General structure of fractional revivals

A very general pattern of well-defined revivals, characterized by temporally localized structures in $A(t)$, of local periodicity T_{cl}/q and with magnitude $|A(t)|^2 = 1/q$, at various rational multiples of the revival time given by $t = pT_{rev}/q$ (where p, q are mutually prime) is obvious from Fig. 2 and leads to the term *fractional revivals*. Averbukh and Perelman (34) were the first to analyze in detail the mathematical structure of the additional phase factors arising from the $\exp(-2\pi i k^2 t / T_{rev})$ terms at such times to discuss the “*Universality in the long-term evolution of quantum wave packets beyond the correspondence principle limit*” and we reproduce here, in part, their elegant arguments, for completeness. (We note that it has been pointed out (63), (64) that this problem, especially the calculation of the autocorrelation function at fractional revival times, is similar to that of the evaluation of Gauss sums (65) which has a long history in the mathematical literature (66).) The case of odd q is most straightforward and we consider the more general arguments for even q in Appendix C.

We are interested in the structure of the additional phase terms at times $t = pT_{rev}/q$ of the form

$$e^{-2\pi i k^2 t / T_{rev}} = e^{-2\pi i (p k^2 / q)} \equiv e^{-2\pi i \Theta_k} \quad (44)$$

and especially how to write these phases with k^2 in the exponential in terms of similar factors, but with linear dependence on k , as in Eqns. (37) and (42). We first note that the phase factor in Eqn. (44) will be periodic in k , namely

$$e^{-2\pi i\Theta_k} = e^{-2\pi i\Theta_{k+l}} \quad \text{or} \quad \frac{p}{q}k^2 = \Theta_k = \Theta_{k+l} = \frac{p}{q}(k+l)^2 \pmod{1}. \quad (45)$$

For this to occur, one requires that

$$\frac{2pk + pl^2}{q} = 0 \pmod{1} \quad (46)$$

which, for odd q , is satisfied if $l = q$. One can then expand any periodic function (periodic in k) in terms of the basis states

$$e^{-2\pi isk/l} \quad \text{with} \quad s = 0, 1, \dots, l-1 \quad (47)$$

and write

$$e^{-2\pi i\Theta_k} = e^{-2\pi ipk^2/q} = \sum_{s=0}^{l-1} b_s e^{-2\pi isk/l} \quad (48)$$

which can be described as a generalized trigonometric identity, finite Fourier series, or discrete Fourier transform. This is already a useful result as we can then write the wavefunction near a fractional (p/q) revival in the form

$$\begin{aligned} \psi(x, t \approx pT_{rev}/q) &= \sum_k a_k u_k(x) e^{-2\pi ikt/T_{cl}} e^{-\pi ipk^2/q} \\ &= \sum_{s=0}^{l-1} b_s \left[\sum_k a_k u_k(x) e^{-2\pi ikt/T_{cl}} e^{-2\pi isk/l} \right] \\ &= \sum_{s=0}^{l-1} b_s \psi_{cl}(x, t + sT_{cl}/l). \end{aligned} \quad (49)$$

This form implies that there will be as many as l ‘clones’ of the original wave packet, with amplitude b_s and probability $|b_s|^2$, differing in phase from the original packet by fractions (T_{cl}/l) of the classical period.

The expansion in Eqn. (48) can be inverted by multiplying both sides by $\exp(2\pi irk/l)$, summing over l possible states, and using the periodicity of the Θ_k to obtain

$$\sum_{k=0}^{l-1} e^{2\pi irk/l - 2\pi ipk^2/q} = \sum_{s=0}^{l-1} b_s \left[\sum_{k=0}^{l-1} e^{2\pi ik(r-s)/l} \right] = \sum_{s=0}^{l-1} b_s [l\delta_{r,s}] = lb_r \quad (50)$$

or

$$b_r = \frac{1}{l} \sum_{k=0}^{l-1} e^{2\pi i(rk/l - pk^2/q)}. \quad (51)$$

Using the arbitrariness of the summation index (due to the periodicity of the exponentials), we can formally relabel this relation using $k \rightarrow \bar{k} - 1$ and write

$$\begin{aligned}
b_r &= \frac{1}{l} \sum_{\bar{k}} e^{2\pi i(r(\bar{k}-1)/l - p(\bar{k}-1)^2/q)} \\
&= [e^{-2\pi i r/l} e^{-2\pi i p/q}] \frac{1}{l} \sum_{\bar{k}} e^{2\pi i(r\bar{k}/l + 2\bar{k}p/q - p\bar{k}^2/q)} \\
&= [e^{-2\pi i r/l} e^{-2\pi i p/q}] \left[\frac{1}{l} \sum_{\bar{k}} e^{2\pi i(\bar{k}/l(r+2pl/q) - p\bar{k}^2/q)} \right] \\
&= [e^{-2\pi i(r/l + p/q)}] b_{r'}
\end{aligned} \tag{52}$$

or

$$b_{r'} = e^{2\pi i(r/l + p/q)} b_r \quad \text{where} \quad r' \equiv r + \frac{2pl}{q} \tag{53}$$

which recursively relates the expansion coefficients. This implies that all of the (non-zero) $|b_r|$ have the same magnitude and, for odd values of q (and hence l), it gives

$$|b_r|^2 = \frac{1}{q} \quad \text{for all } r = 0, \dots, q-1 \tag{54}$$

and each of the $l = q$ ‘mini-packets’ contains $1/q$ of the total probability, overlapping with the original $t = 0$ packet in $A(t)$ with a periodicity T_{cl}/q .

As an example, consider the case of $T_{rev}/3$ where $p = 1$ and $q = l = 3$. In that case we use Eqn. (53), once with $r = 0$ and $r' = 2$ to obtain

$$b_2 = e^{2\pi i/3} b_0 \tag{55}$$

and again with $r = 2$ and $r' = 4 \longleftrightarrow r' = 1$ (recall the periodicity) to find

$$b_1 \longleftrightarrow b_4 = b_2. \tag{56}$$

The explicit value of b_0 is obtained by direct summation of Eqn. (51) giving

$$b_0 = \frac{1}{3} \sum_{k=0}^2 e^{-2\pi i k^2/3} = \frac{1}{3} [1 + e^{-2\pi i/3} + e^{-8\pi i/3}] = \frac{1}{3} [1 + 2e^{-2\pi i/3}] = -\frac{i}{\sqrt{3}}. \tag{57}$$

Thus, near $t \approx T_{rev}/3$, we find that

$$\begin{aligned}
\psi(x, t \approx T_{rev}/3) &= b_0 \psi_{cl}(x, t) + b_1 \psi_{cl}(x, t + T_{cl}/3) + b_2 \psi_{cl}(x, t + 2T_{cl}/3) \\
&= -\frac{i}{\sqrt{3}} [\psi_{cl}(x, t) + e^{2\pi i/3} \{\psi_{cl}(x, t + T_{cl}/3) + \psi_{cl}(x, t + 2T_{cl}/3)\}]
\end{aligned} \tag{58}$$

as first observed by Averbukh and Perelman in Ref. (34). The autocorrelation function near $T_{rev}/3$ is also shown in Fig. 3 for our two model systems, where the exact and approximate realizations of this behavior are apparent.

The arguments for even q are similar, but differ slightly depending on whether q is a multiple of 4, as discussed in Appendix C. The result however, is quite similar in that one finds $r = q/2$ copies of the classical wave packet, separated by multiples of T_{cl}/r , each with

maximum $|A(t)|^2 = 1/r$. The cases of $q = 2$ and $q = 4$ are considered again explicitly in Appendix C and are shown to reproduce the results in Eqns. (38) and (43) respectively.

Averbukh and Perelman used their results to correctly analyze the numerical calculations of Parker and Stroud (28), identifying the revival at $T_{rev}/2$ and fractional revivals of order $1/4, 1/6, 1/8$ which had earlier been described only as “...a complex pattern of quantum beats.” We reproduce the results of their analysis of the (simulated) data in Fig. 4. Fractional revival structures of order up to $1/7$ have been observed in other systems (33), as shown in Fig. 5.

The observability of higher-order revivals, which would have r distinct features in $|A(t)|^2$ separated by T_{cl}/r (for $r = q$ ($r = q/2$) for odd (even) q) depends on the level of the incoherent ‘background’ in Eqn. (30), so that in general such features would not be observable if

$$\frac{1}{q} = |A(t \approx pT_{rev}/q)|^2 < |A_{inc}|^2 = \frac{1}{\Delta n 2\sqrt{\pi}} \quad \text{or} \quad q \gtrsim \Delta n 2\sqrt{\pi} \quad (59)$$

so that larger Δn wave packets can ‘resolve’ higher-order fractional revivals, as noted in Fig. 2. The behavior at such times during the collapsed or incoherent phase is shown in Fig. 3 for our two model systems for a multiple of $T_{rev}/37$ where the dashed horizontal line indicates the value of $1/q$, while the $|A(t)|^2$ values are seen to oscillate instead about the incoherent value, shown by the dotted line.

We note that a number of authors have considered generalizations of these ideas (67), applications to specific model systems (68) - (75), and extensions to Hamiltonians that are time-dependent through a slow change in a parameter (76).

E. Superrevivals

For systems with purely quadratic energy dependence on a single quantum number (such as the infinite well, rigid rotor, and others), there are no independent time scales longer than the revival time, and the pattern of fractional and full revivals will repeat itself indefinitely with the T_{rev} time scale. For more realistic systems, with higher order terms in the expansion in Eqn. (8), the superrevival time, T_{super} becomes important, and Bluhm and Kostelecký (77), have exhaustively analyzed the long-term time-dependence of wave packets, with emphasis on Rydberg atom applications. They find qualitatively new patterns of revival behavior, with periodicities in the motion of the packet characterized by periods which are fractions of T_{rev} , giving a self-similar structure to the auto-correlation function plots for $t > T_{rev}$ and $t < T_{rev}$. The wave packet behavior on the T_{super} time scale is similar to that of the fractional revival structures seen on the T_{rev} scale, with integral multiples of $T_{super}/3$ appearing prominently, and smaller time scale periodicities of $3T_{rev}$ appearing, explicitly due to the presence of the third-derivative term in Eqn. (8). In performing their analyses, they necessarily had to generalize and extend the results of Averbukh and Perelman (34) to include the contributions of the $e^{-2\pi ip(n-n_0)^3/q}$ phase terms. Extensions to even more time scales (67), (78), with possible applications, have also been discussed.

F. Revivals in systems with two or more quantum numbers

The generalization of the discussion of classical periodicity and revivals (fractional or otherwise) to systems with more than one quantum number has been presented by several groups (40), (79), (80).

For the case of two quantum numbers, for example, one first assumes a time-dependent quantum state of the form

$$\psi(t) = \sum_{n_1, n_2} a_{(n_1, n_2)} u_{(n_1, n_2)} e^{-iE(n_1, n_2)t/\hbar} \quad (60)$$

where the coordinate labels have been suppressed, and could be either two position-space (e.g., (x, y) , (r, θ)) or two momentum-space ((p_x, p_y)) values. The energy eigenvalues are not assumed to factorize, but for localized wave packets, we do assume that they can be expanded about a central value (\bar{n}_1, \bar{n}_2) , with the resulting expression (to second order) given by

$$\begin{aligned}
E(n_1, n_2) = & E(\bar{n}_1, \bar{n}_2) + (n_1 - \bar{n}_1) \left(\frac{\partial E(n_1, n_2)}{\partial n_1} \right)_{(\bar{n}_1, \bar{n}_2)} + (n_2 - \bar{n}_2) \left(\frac{\partial E(n_1, n_2)}{\partial n_2} \right)_{(\bar{n}_1, \bar{n}_2)} \\
& + \frac{1}{2} (n_1 - \bar{n}_1)^2 \left(\frac{\partial^2 E(n_1, n_2)}{\partial n_1^2} \right)_{(\bar{n}_1, \bar{n}_2)} + \frac{1}{2} (n_2 - \bar{n}_2)^2 \left(\frac{\partial^2 E(n_1, n_2)}{\partial n_2^2} \right)_{(\bar{n}_1, \bar{n}_2)} \\
& + (n_1 - \bar{n}_1)(n_2 - \bar{n}_2) \left(\frac{\partial^2 E(n_1, n_2)}{\partial n_1 \partial n_2} \right)_{(\bar{n}_1, \bar{n}_2)} + \dots .
\end{aligned} \tag{61}$$

In the spirit of Eqn. (8), we can use this expansion to define important time scales. Two separate classical periods are given by

$$T_{cl}^{(n_1)} \equiv \frac{2\pi\hbar}{|\partial E/\partial n_1|} \quad \text{and} \quad T_{cl}^{(n_2)} \equiv \frac{2\pi\hbar}{|\partial E/\partial n_2|} \tag{62}$$

where we will henceforth suppress the subscripts indicating that the partial derivatives are evaluated at (\bar{n}_1, \bar{n}_2) . The corresponding longer-term, revival times are defined by

$$T_{rev}^{(n_1)} = \frac{2\pi\hbar}{(1/2)|\partial^2 E(n_1, n_2)/\partial n_1^2|} \quad , \quad T_{rev}^{(n_2)} = \frac{2\pi\hbar}{(1/2)|\partial^2 E(n_1, n_2)/\partial n_2^2|} \tag{63}$$

and the mixed term

$$T_{rev}^{(n_1, n_2)} = \frac{2\pi\hbar}{|\partial^2 E(n_1, n_2)/\partial n_1 \partial n_2|} . \tag{64}$$

There can be recognizable periodicities in the short-term semi-classical time-development, with the two classical periods beating against each other, with the most obvious case being when the two periods are commensurate with each other, namely when

$$\frac{T_{cl}^{(n_1)}}{T_{cl}^{(n_2)}} = \frac{a}{b} \tag{65}$$

where a, b are relatively prime integers. (Similar results hold for action-angle variables in classical systems (50), (51).) A simple example of such behavior is for a two-dimensional oscillator with differing frequencies, namely

$$V(x, y) = \frac{m}{2} (\omega_x^2 x^2 + \omega_y^2 y^2) \tag{66}$$

with quantized energies

$$E(n_x, n_y) = (n_x + 1/2)\hbar\omega_x + (n_y + 1/2)\hbar\omega_y \tag{67}$$

where the condition in Eqn. (65) reduces to

$$\frac{T_{cl}^{(n_1)}}{T_{cl}^{(n_2)}} = \frac{\omega_y}{\omega_x} = \frac{a}{b} \tag{68}$$

which is the familiar condition for the existence of Lissajous figures. Similar analyses will be shown below to lead to the appropriate conditions on closed or periodic orbits in simple two-dimensional quantum billiard systems such as the square (or rectangular) case in Sec. (IV.A), the equilateral triangle (Sec. IV.C), and circular (Sec. IV.D) footprints being the most familiar. Nauenberg (40) has also considered the patterns of classical periodicities in systems with several quantum numbers. We note that this connection of the quantized energy eigenvalue spectrum to the structure of classical recurring orbits is quite different from that found in another semiclassical approach, namely periodic orbit theory (81), (82).

The extension of these ideas to central potentials in three dimensions, where the energy eigenstates do not depend on the azimuthal quantum number ($E(n_r, l, m) = E(n_r, l)$ only), implies that one of the corresponding classical periods, $T_{cl}^{(m)} \rightarrow \infty$, is irrelevant, related to the fact that classical orbits are planar for all times. In a similar context, certain special 3D central potentials depend only on special combinations of quantum numbers with important semi-classical connections. For example, for the 3D isotropic harmonic oscillator, defined by

$$V(\mathbf{r}) = V(r) = \frac{m\omega^2}{2}(x^2 + y^2 + z^2) = \frac{m\omega^2}{2}r^2, \quad (69)$$

the quantized energies can be written in the form

$$E(N) = (N + 3/2)\hbar\omega \quad (70)$$

where N can be written in terms of Cartesian quantum numbers in the form $N = n_x + n_y + n_z$ or in cylindrical (n_r, m_ϕ, n_z) or spherical language (n_r, l) language. The fact that there is only one effective quantum number is related to the symmetry properties of the oscillator potential (and its factorizability in many coordinate systems) and implies that all classical periods are the same (or commensurate). This fact, in turn, is related to the result of Bertrand's theorem (83) which states that the only 3D power-law potentials for which all orbits are closed are given by $k = 2$ (the oscillator) and $k = -1$ (the Coulomb potential). For the latter problem, the quantized energies also exhibit special patterns of degeneracy (dependent on $S0(4)$ symmetries beyond the simple $SO(3)$ rotational invariance) so that the Coulomb energy spectrum (with Z the nuclear charge and μ the reduced mass of two-body system)

$$E(n_r, l) = -\frac{(Z\alpha)^2\mu c^2}{2(n_r + l)^2} = -\frac{(Z\alpha)^2\mu c^2}{2(n)^2} = E(n) \quad (71)$$

depends only the principal quantum number, n , and not on the radial and angular quantum numbers, n_r, l , separately. The factorizability of this problem in parabolic coordinates (84) leads to the same result for the quantized energies, and is useful for problems involving the addition of an external electric field (the Stark effect.)

The general time-development of wave packets which depend on two independent quantum numbers, on longer time scales, is then determined by the interplay of the three revival times, and the corresponding commensurability condition required to observe revivals is

$$T_{rev}^{(n_1)} = \left(\frac{c}{d}\right) T_{rev}^{(n_2)} = \left(\frac{e}{f}\right) T_{rev}^{(n_1, n_2)} \quad (72)$$

where c, d and e, f are again pairs of relatively prime integers. Fractional revivals are also possible if hierarchies such as

$$T_{frac} = \left(\frac{p_1}{q_1}\right) T_{rev}^{(n_1)} = \left(\frac{p_2}{q_2}\right) T_{rev}^{(n_2)} = \left(\frac{p_{12}}{q_{12}}\right) T_{rev}^{(n_1, n_2)} \quad (73)$$

exist and Bluhm, Kostelecký, and Tudose (79) have examined the structure of such fractional revivals, extending the results of Ref. (34) to the case of additional quantum numbers. We will provide examples of systems described by these time scales in the context of several 2D quantum billiard systems below.

III. MODEL SYSTEMS

The time-dependence of localized quantum wave packets, including possible quantum revival behavior, has been discussed for a large number of pedagogically familiar, and physically relevant, one-dimensional model systems. We briefly review several such cases, and then focus attention on the infinite well as a benchmark case where exact quantum revival behavior is found.

A. Free particle wave packets

The analysis of Gaussian free particle wave packets goes back at least to Darwin (3) and is a staple of introductory textbooks. While such systems do not exhibit quantum revivals (or even classical periodicity), it is useful to briefly review the basic formalism of Gaussian wave packet solutions to the free-particle Schrödinger equation in one dimension. It helps establish notation for later use, as well as providing an example for comparison with more realistic systems, especially illustrating important aspects of wave packet spreading in explicit form.

A general Gaussian free-particle wave packet, with arbitrary initial values of $\langle x \rangle_0 = x_0$ and $\langle p \rangle_0 = p_0$, can be written in momentum space as

$$\phi(p, t) = \phi_0(p) e^{-ip^2 t/2m\hbar} = \left[\sqrt{\frac{\alpha}{\sqrt{\pi}}} e^{-\alpha^2(p-p_0)^2/2} e^{-ipx_0/\hbar} \right] e^{-ip^2 t/2m\hbar}. \quad (74)$$

The various expectation values related to momentum are given by

$$\langle p \rangle_t = p_0, \quad \langle p^2 \rangle_t = p_0^2 + \frac{1}{2\alpha^2}, \quad \text{and} \quad \Delta p_t = \Delta p_0 = \frac{1}{\alpha\sqrt{2}} \quad (75)$$

so that the momentum-space probability density does not disperse in time, and the expectation value of kinetic energy, given by $\langle p^2 \rangle_t/2m$, is obviously constant, as it should for a free particle solution.

The corresponding solution in position-space is given by

$$\psi(x, t) = \frac{1}{\sqrt{\sqrt{\pi}\alpha\hbar(1+it/t_0)}} e^{ip_0(x-x_0)/\hbar} e^{-ip_0^2 t/2m\hbar} e^{-(x-x_0-p_0 t/m)^2/2(\alpha\hbar)^2(1+it/t_0)} \quad (76)$$

where

$$t_0 \equiv m\hbar\alpha^2 = \frac{m\hbar}{2(\Delta p_0)^2} = \frac{2m(\Delta x_0)^2}{\hbar} \quad (77)$$

is the spreading time. The corresponding position-space probability density is

$$P(x, t) = |\psi(x, t)|^2 = \frac{1}{\sqrt{\pi}\beta_t} e^{-(x-x(t))^2/\beta_t^2} \quad (78)$$

where

$$x(t) \equiv x_0 + p_0 t/m \quad \text{and} \quad \beta_t \equiv \alpha\hbar\sqrt{1+t^2/t_0^2} \quad (79)$$

and the time-dependent expectation values of position are

$$\langle x \rangle_t = x(t) = x_0 + p_0 t/m, \quad \langle x^2 \rangle_t = [x(t)]^2 + \frac{\beta_t^2}{2}, \quad \text{and} \quad \Delta x_t = \frac{\beta_t}{\sqrt{2}}, \quad (80)$$

which exhibits the classical constant rate of change for the expectation value (consistent with Ehrenfest's theorem) and the standard spreading.

For comparison to later examples, we note that the autocorrelation function for this class of solutions is easily obtained in either p - or x -space from Eqn. (2), and is given by

$$A(t) = \frac{1}{\sqrt{1 - it/2t_0}} \exp \left[\frac{i\alpha^2 p_0^2 t}{2t_0(1 - it/2t_0)} \right] \quad (81)$$

or

$$|A(t)|^2 = \frac{1}{\sqrt{1 + (t/2t_0)^2}} \exp \left[-2\alpha^2 p_0^2 \frac{(t/2t_0)^2}{(1 + (t/2t_0)^2)} \right]. \quad (82)$$

As expected, the only relevant time scale is the spreading time (actually $2t_0$) and we note that while for times satisfying $t \ll 2t_0$ there is an increasing exponential suppression of the overlap between ψ_t and ψ_0 , the exponential factor does 'saturate' for long times, giving

$$|A(t \gg 2t_0)|^2 \longrightarrow \frac{2t_0}{t} \exp \left[-\frac{p_0^2}{\Delta p_0^2} \right] \quad \text{since} \quad \alpha = \frac{1}{\sqrt{2}\Delta p_0}. \quad (83)$$

The asymptotic form of the exponential factor can perhaps be best understood by noting that the 'distance in position space' between the initial 'peak' at $\langle x \rangle_0 = x_0$, and that at later times when $\langle x \rangle_t = x_0 + p_0 t/m$, grows linearly with t , while for long times the position spread,

$$\Delta x_t = \Delta x_0 \sqrt{1 + (t/t_0)^2} \quad \longrightarrow \quad \Delta x_0 \frac{t}{t_0}, \quad (84)$$

increases in the same way. This leads to factors in the exponent of the form

$$\frac{(x(t) - x(0))^2}{(\Delta x_t)^2} \longrightarrow \frac{(p_0 t/m)^2}{(\Delta x_0 (t/t_0))^2} \approx \left(\frac{p_0 t_0}{m \Delta x_0} \right)^2 \approx (p_0 \alpha)^2 \quad \text{since} \quad \Delta x_0 = \frac{\alpha \hbar}{\sqrt{2}}. \quad (85)$$

We distinguish the exponential suppression factor in Eqn. (82) (which we can describe as 'dynamical' as it depends on the initial wave packet parameter, p_0) from the more intrinsic pre-factor term (containing only the spreading time) which is due to the natural dispersion of the wave packet (which we can therefore describe as 'dispersive'.)

We note here that the Gaussian packet in Eqns. (74) or (76) clearly satisfies the general bound on $A(t)$ in Eqn. (1) in Sec. II.A, saturating it to order $\mathcal{O}(t^2)$ for short times. In this case, one has

$$\langle H \rangle = \frac{1}{2m} \left(p_0^2 + \frac{1}{2\alpha^2} \right) \quad \text{and} \quad \langle H^2 \rangle = \left(\frac{1}{2m} \right)^2 \left(p_0^4 + \frac{3p_0^2}{\alpha^2} + \frac{3}{4\alpha^4} \right) \quad (86)$$

which give

$$(\Delta H)^2 = \left(\frac{1}{2m} \right)^2 \frac{2}{\alpha^2} \left(p_0^2 + \frac{1}{4\alpha^2} \right). \quad (87)$$

B. Wave packets and the constant force or uniform acceleration problem

The problem of a particle under the influence of a constant force is one of the most familiar in classical mechanics, but is less often treated in introductory quantum mechanics texts, especially in terms of time-dependent solutions, despite the fact that closed form solutions have been known since the time of Kennard (2). For that reason, we briefly review

the most straightforward momentum-space approach to this problem. This system also provides another example of the behavior of $A(t)$, this time in a more dynamical system.

In this case, where the potential is given by $V(x) = -Fx$, we can write the time-dependent Schrödinger equation in momentum-space as

$$\frac{p^2}{2m}\phi(p, t) - F \cdot \left[i\hbar \frac{\partial}{\partial p} \right] \phi(p, t) = i\hbar \frac{\partial \phi(p, t)}{\partial t} \quad (88)$$

or

$$i\hbar \left(F \frac{\partial \phi(p, t)}{\partial p} + \frac{\partial \phi(p, t)}{\partial t} \right) = \frac{p^2}{2m} \phi(p, t). \quad (89)$$

We note that the simple combination of derivatives guarantees that a function of the form $\Phi(p - Ft)$ will make the left-hand side vanish, so we assume a solution of the form $\phi(p, t) = \Phi(p - Ft)\tilde{\phi}(p)$, with $\Phi(p)$ arbitrary and $\tilde{\phi}(p)$ to be determined. Using this form, Eqn. (89) reduces to

$$\frac{\partial \tilde{\phi}(p)}{\partial p} = -\frac{ip^2}{2m\hbar F} \tilde{\phi}(p) \quad (90)$$

with the solution

$$\tilde{\phi}(p) = e^{-ip^3/6mF\hbar}. \quad (91)$$

We can then write the general solution as

$$\phi(p, t) = \Phi(p - Ft)e^{-ip^3/6mF\hbar} \quad (92)$$

or, using the arbitrariness of $\Phi(p)$, as

$$\phi(p, t) = \phi_0(p - Ft)e^{i((p - Ft)^3 - p^3)/6mF\hbar} \quad (93)$$

where now $\phi_0(p)$ is some initial momentum distribution, since $\phi(p, 0) = \phi_0(p)$. (We note that because the p^3 terms cancel in the exponential, we will be able to explicitly integrate Gaussian type initial momentum-space waveforms.) The momentum-space probability density now clearly satisfies

$$|\phi(p, t)|^2 = |\phi_0(p - Ft)|^2 \quad (94)$$

which demonstrates that the momentum distribution simply translates uniformly in time, with no change in shape.

For any general initial $\phi_0(p)$ we now have the time-dependent expectation values

$$\langle p \rangle_t = \langle p \rangle_0 + Ft \quad (95a)$$

$$\langle p^2 \rangle_t = \langle p^2 \rangle_0 + 2\langle p \rangle_0 Ft + (Ft)^2 \quad (95b)$$

$$\Delta p_t = \sqrt{\langle p^2 \rangle_t - \langle p \rangle_t^2} = \sqrt{\langle p^2 \rangle_0 - \langle p \rangle_0^2} = \Delta p_0 \quad (95c)$$

$$\langle \hat{x} \rangle_t = \langle \hat{x} \rangle_0 + \frac{\langle p \rangle_0 t}{m} + \frac{Ft^2}{2m} \quad (95d)$$

giving the expectation value

$$\langle H \rangle = \left\langle \frac{p^2}{2m} + V(x) \right\rangle = \frac{\langle p^2 \rangle_0}{2m} - F\langle \hat{x} \rangle_0 \quad (96)$$

which, in turn, also agrees with a similar calculation of $\langle \hat{E} \rangle_t$ using $\hat{E} = i\hbar(\partial/\partial t)$, all of which are consistent with a particle undergoing uniform acceleration.

Using the standard initial Gaussian momentum-space wavefunction, $\phi_0(p)$ in Eqn. (74), as the $\phi_0(p - Ft)$ in Eqn. (93), we can evaluate the position-space solution using the Fourier transform to obtain

$$\psi(x, t) = \left[e^{iFt(x_0 - Ft^2/6m)/\hbar} e^{i(p_0 + Ft)(x - x_0 - p_0 t/2m)/\hbar} \right] \left(\frac{1}{\sqrt{\sqrt{\pi} \alpha \hbar (1 + it/t_0)}} \right) \times e^{-(x - (x_0 + p_0 t/m + Ft^2/2m))^2 / 2(\alpha \hbar^2)^2 (1 + it/t_0)}. \quad (97)$$

The corresponding probability density is given by

$$P(x, t) = \frac{1}{\sqrt{\pi} \beta_t} e^{-(x - \tilde{x}(t))^2 / \beta_t^2} \quad (98)$$

where

$$\tilde{x}(t) \equiv x_0 + \frac{p_0 t}{m} + \frac{Ft^2}{2m} \quad (99)$$

and

$$\langle x \rangle_t = \tilde{x}(t), \quad \langle x^2 \rangle_t = [\tilde{x}(t)]^2 + \frac{\beta_t^2}{2}, \quad \text{and} \quad \Delta x_t = \frac{\beta_t}{\sqrt{2}} \quad (100)$$

so that this accelerating wave packet spreads in the same manner as the free-particle Gaussian example.

The calculation of the autocorrelation function can once again be done in either p - or x -space using Eqn. (2) to give

$$A(t) = \frac{1}{\sqrt{1 - it/2t_0}} \exp \left[\frac{(2ip_0^2 t/m\hbar - (\alpha Ft)^2 (1 + (t/2t_0)^2))}{4(1 - it/2t_0)} \right] e^{-iFt(x_0 - Ft^2/6m)/\hbar} \quad (101)$$

and the same factors of $1 - it/2t_0$ as in Eqn. (81) are obtained; this expression also reduces to that case in the free particle limit when $F \rightarrow 0$, as it must. The modulus-squared is given by

$$|A(t)|^2 = \frac{1}{\sqrt{1 + (t/2t_0)^2}} \exp \left[-2\alpha^2 (p_0^2 + (Ft_0)^2 (1 + (t/2t_0)^2)) \left(\frac{(t/2t_0)^2}{1 + (t/2t_0)^2} \right) \right] \quad (102)$$

and we note that this result can be obtained from Eqn. (82) by the simple substitution

$$p_0^2 \longrightarrow p_0^2 + (Ft_0)^2 (1 + (t/2t_0)^2). \quad (103)$$

For this case of uniform acceleration, the wave packet spreading is identical (same Δx_t) as in the free-particle case, which can be understood by noting that the distance between two classical particles starting at the same initial location, undergoing the same force, but with slightly different initial velocities (or momenta, $p_0^{(A)} - p_0^{(B)} = \Delta p_0$) would be

$$x_A(t) - x_B(t) = (x_0 + p_0^{(A)} t/m + Ft^2/2m) - (x_0 + p_0^{(B)} t/m + Ft^2/2m) = \frac{\Delta p_0 t}{m} \quad (104)$$

which increases linearly with time, in exactly the same way as for the free-particle solutions (when $F = 0$). The ‘distance’ between the peaks in ψ_0 and ψ_t , however, eventually grows as t^2 so that the exponential (‘dynamical’) suppression in $A(t)$ does not saturate, while the ‘dispersive’ pre-factor is exactly the same as for the free-particle case.

C. Harmonic oscillator

The harmonic oscillator provides the most straightforward example of a bound state system for which the periodic motion of wave packet solutions (especially Gaussian) is easily derivable. In this case, the initial value problem is perhaps most easily solved, especially for Gaussian wave packets, by propagator techniques (53). In this approach, one writes

$$\psi(x, t) = \int_{-\infty}^{+\infty} dx' \psi(x', 0) K(x, x'; t, 0) \quad (105)$$

where the propagator can be derived in a variety of ways (85) and can be written in the form

$$K(x, x'; t, 0) = \sqrt{\frac{m\omega}{2\pi i\hbar \sin(\omega t)}} \exp \left[\frac{im\omega}{2\hbar \sin(\omega t)} ((x^2 + (x')^2) \cos(\omega t) - 2xx') \right]. \quad (106)$$

Using the initial position-space wave function

$$\psi(x, 0) = \frac{1}{\sqrt{\beta}\sqrt{\pi}} e^{ip_0x/\hbar} e^{-(x-x_0)^2/2\beta^2}, \quad (107)$$

where $\beta \equiv \alpha\hbar$, one can evaluate the time-dependent wave function in closed form as

$$\psi(x, t) = \frac{1}{\sqrt{L(t)}\sqrt{\pi}} \exp \left[\frac{S(x, t)}{2\beta L(t)} \right] \quad (108)$$

where

$$L(t) \equiv \beta \cos(\omega t) + \frac{i\hbar}{m\omega\beta} \sin(\omega t) \quad (109)$$

and

$$\begin{aligned} S(x, t) \equiv & -x_0^2 \cos(\omega t) + 2xx_0 - x^2 \left[\cos(\omega t) + \frac{im\omega\beta^2 \sin(\omega t)}{\hbar} \right] \\ & - \frac{2x_0p_0 \sin(\omega t)}{m\omega} + \frac{2i\beta^2 p_0 x}{\hbar} - \frac{i\beta^2 p_0^2 \sin(\omega t)}{m\omega\hbar}. \end{aligned} \quad (110)$$

The corresponding position-space probability density can be written as

$$|\psi(x, t)|^2 = \frac{1}{\sqrt{\pi}|L(t)|} \exp \left[-\frac{(x - x_0 \cos(\omega t) - p_0 \sin(\omega t)/m\omega)^2}{|L(t)|^2} \right] \quad (111)$$

with

$$\langle x \rangle_t = x_0 \cos(\omega t) + \frac{p_0 \sin(\omega t)}{m\omega} \quad (112)$$

and

$$\Delta x_t = \frac{|L(t)|}{\sqrt{2}} = \frac{1}{\sqrt{2}} \sqrt{\beta^2 \cos^2(\omega t) + (\hbar/m\omega\beta)^2 \sin^2(\omega t)}. \quad (113)$$

Thus, the expectation value evolves in accordance with classical expectations (86), while the width in position-space oscillates (from wide to narrow, or vice versa.) The momentum-space variables behave in a similarly correlated manner with

$$\langle p \rangle_t = -m\omega x_0 \sin(\omega t) + p_0 \cos(\omega t) \quad (114)$$

$$\Delta p_t = \frac{1}{\sqrt{2}} \sqrt{(\hbar/\beta)^2 \cos^2(\omega t) + (m\omega\beta)^2 \sin^2(\omega t)}. \quad (115)$$

For the special case of the ‘minimum uncertainty’ wave packet, where

$$\beta^2 = \frac{\hbar}{m\omega} \equiv \beta_0^2, \quad (116)$$

the width of the packet is fixed as

$$\Delta x_t = \Delta x_0 = \frac{\beta_0}{\sqrt{2}} \quad (117)$$

which is the same as the ground state oscillator energy eigenvalue state, but simply oscillates at the classical frequency, which is similar to the famous example first cited by Schrödinger (1) or to later examples of coherent states (87).

The total energy of the general solution can be written in the form

$$\langle \hat{E} \rangle = \left(\frac{p_0^2}{2m} + \frac{1}{2} m\omega^2 x_0^2 \right) + \frac{\hbar\omega}{4} \left(\frac{\beta_0^2}{\beta^2} + \frac{\beta^2}{\beta_0^2} \right). \quad (118)$$

Since this is also a bound state problem, one can expand the solution in Eqn. (108) in eigenstates as

$$\psi(x, t) = \sum_{n=0}^{\infty} a_n u_n(x) e^{-iE_n t/\hbar} \quad \text{where } E_n = (n + 1/2)\hbar\omega. \quad (119)$$

We can then note that

$$\langle \hat{E} \rangle = \langle (n + 1/2) \rangle \hbar\omega = (\langle n \rangle + 1/2) \hbar\omega \quad (120)$$

which for $x_0, p_0 = 0$ and $\beta = \beta_0$ gives $\langle n \rangle = 0$ as expected, since in this limit we recover the ground state energy. The spread in n values is useful in discussions of wave packet behavior, and we note that

$$(\Delta E)^2 = \langle \hat{E}^2 \rangle - \langle \hat{E} \rangle^2 = \langle (n + 1/2)^2 \rangle - \langle (n + 1/2) \rangle^2 = (\Delta n)^2 (\hbar\omega)^2 \quad (121)$$

and we find that

$$(\Delta n)^2 = \frac{1}{2} \left[\frac{p_0^2}{(m\omega\beta)^2} + x_0^2 \left(\frac{m\omega\beta}{\hbar} \right)^2 \right] + \frac{1}{8} \left(\frac{\beta_0^4}{\beta^4} + \frac{\beta^4}{\beta_0^4} - 2 \right) \quad (122)$$

which will be useful. In the $x_0, p_0 = 0$ and $\beta = \beta_0$ limit, we find $\Delta n = 0$, as expected for an eigenstate.

All wave packet solutions (Gaussian or not) of the harmonic oscillator can be shown (using, for example (53), the expansion in Eqn. (119)), to satisfy

$$\psi(x, t + mT_d) = (-1)^m \psi(x, t) \quad (123)$$

with a similar result for $\phi(p, t)$ as well. This implies that the autocorrelation function will be periodic as well, with

$$A(t + kT_d) = (-1)^k A(t). \quad (124)$$

The evaluation of $|A(t)|^2$ for general values of β , x_0 , and p_0 is straightforward enough, but the resulting expressions are somewhat cumbersome, so we will focus on several special cases as illustrative.

Case I: Minimum uncertainty wave packets, $\beta = \beta_0$.

In this case the evaluation of $A(t)$ gives

$$A(t) = \sqrt{\cos(\omega t) + i \sin(\omega t)} \exp \left[- \left(\frac{x_0^2}{2\beta_0^2} + \frac{p_0^2}{2m\omega\hbar} \right) [(1 - \cos(\omega t)) - i \sin(\omega t)] \right] \quad (125)$$

where great simplifications have been made by noting that

$$\frac{1}{\cos(\omega t) - i \sin(\omega t)} = \cos(\omega t) + i \sin(\omega t). \quad (126)$$

(We note that a very similar expression arises in analyses of the macroscopic wavefunction for Bose-Einstein condensates (88) and the collapse and revival of the matter wave field has been observed experimentally (60).) Once again, the two important parameters appear together in quadrature, as in the uniform acceleration case, and we have

$$|A(t)|^2 = \exp \left[- \left(\frac{x_0^2}{\beta_0^2} + \frac{p_0^2}{m\omega\hbar} \right) \{1 - \cos(\omega t)\} \right] \quad (127)$$

which clearly exhibits the expected periodicity. All of the suppression can be attributed to the ‘dynamical’ factors (those in the exponential, containing x_0 and p_0) as there is no ‘dispersive’ pre-factor component for this constant width packet.

Case II: Arbitrary β , but $x_0, p_0 = 0$. For this case, the wave packet does not oscillate, but only ‘pulsates’ (89), and the time-dependent wave function simplifies to

$$\psi(x, t) = \frac{1}{\sqrt{(\beta \cos(\omega t) + (i\hbar/m\omega\beta) \sin(\omega t))}} \exp \left[\frac{-(x^2(\cos(\omega t) + (im\omega\beta^2/\hbar) \sin(\omega t)))}{2\beta^2(\cos(\omega t) + (i\hbar/m\omega\beta) \sin(\omega t))} \right]. \quad (128)$$

It is convenient to define the parameters

$$r \equiv \frac{\hbar}{m\omega\beta^2} = \frac{\beta_0^2}{\beta^2} \quad \text{so that} \quad \frac{1}{r} = \frac{\beta^2}{\beta_0^2} \quad (129)$$

in terms of which the resulting autocorrelation function in this case has the very simple form

$$A(t) = \sqrt{\frac{2}{2 \cos(\omega t) - i(r + 1/r) \sin(\omega t)}} \quad (130)$$

or

$$|A(t)|^2 = \frac{1}{\sqrt{\cos^2(\omega t) + (r + 1/r)^2 \sin^2(\omega t)/4}} \quad (131)$$

all of which can be attributed to a ‘dispersive’ (but in this case periodic) pre-factor.

We first note that in this case $A(t)$ is invariant under the transformation $r \rightarrow 1/r$, in other words, the time-dependence is the same for both initially wide ($\beta > \beta_0$) or narrow ($\beta < \beta_0$) packets. Plots of $|A(t)|^2$ over one classical period are shown in Fig. 6, where it is clear that the larger the deviation from the ‘minimum uncertainty’ wavepacket, the faster the wavepacket ‘pulsates’ away from its initial shape. It is also noteworthy that in this case $|A(T_c/2)| = 1$ so that the wave packet returns to its initial form (up to a constant complex phase) *twice* each classical period. This can be understood from the expansion of this wave

form in terms of energy eigenstates. In this case, where the parameters x_0, p_0 both vanish, one is expanding an even-parity function. In the eigenstate expansion,

$$\psi(x, t) = \sum_{n=0}^{+\infty} a_n u_n(x) e^{-iE_n t/\hbar} = e^{-i\omega t/2} \sum_{n=0}^{+\infty} a_n u_n(x) e^{-in\omega t}, \quad (132)$$

the $u_n(x)$ have parity $(-1)^n$, so that for an even-parity state, only the even (a_{2n}) terms are nonvanishing and the n -dependent exponential factors in Eqn. (132) therefore oscillate twice as rapidly as in the general case.

Finally, for the very special case where $\beta = \beta_0$ ($r = 1$) as well, we recover the ground state energy eigenstate of the oscillator, with its trivial stationary-state time-dependence ($\psi_0(x, t) = u_0(x) \exp(-iE_0 t/\hbar)$) and Eqn. (130) indeed reduces to

$$A(t) \xrightarrow{r \rightarrow 1} \sqrt{\frac{2}{2 \cos(\omega t) - 2i \sin(\omega t)}} = \sqrt{e^{i\omega t}} = e^{+i\omega t/2} \quad (133)$$

as expected.

Because of the specially symmetric nature of the potential, besides the relation in Eqn. (123), we also have

$$\psi(-x, t + T_{cl}/2) = (-i) \psi(x, t) \quad \text{and} \quad \phi(-p, t + T_{cl}/2) = (-i) \phi(p, t) \quad (134)$$

so that half a period later, the wave-packet is also reproduced, but at the opposite ‘corner’ of phase space, namely with $x \leftrightarrow -x$ and $p \leftrightarrow -p$; note that two applications of Eqn. (134) reproduce Eqn. (123). One can also show these connections using propagator techniques, provided one properly identifies the complex pre-factors, as described in detail in Ref. (53).

This type of ‘mirror’ behavior can be diagnosed using a variation on the standard auto-correlation function, namely

$$\tilde{A}(t) \equiv \int_{-\infty}^{+\infty} \psi^*(-x, t) \psi(x, 0) dx = \int_{-\infty}^{+\infty} \phi^*(-p, t) \phi(p, 0) dp \quad (135)$$

which measures the overlap of the initial state with the ‘across-phase-space’ version of itself at later times. Given the simple connections in Eqn. (134), we can immediately write, for Case I considered above,

$$|\tilde{A}(t)|^2 = \exp \left[- \left(\frac{x_0^2}{\beta_0^2} + \frac{p_0^2}{m\omega\hbar} \right) \{1 + \cos(\omega t)\} \right] \quad (136)$$

which is exponentially suppressed at integral multiples of T_{cl} , but unity at $t = (2k + 1)T_{cl}/2$. This type of *anti-correlation* function finds use in the study of wave packet revivals where quantum wave packets may reform near $t = T_{rev}/2$, as in Eqn. (38), but out of phase with the original packet.

Finally, we note that these results can be extended to the case of the ‘inverted’ oscillator (corresponding to a particle in unstable equilibrium, i.e., at a local maximum, instead of a local minimum of the potential) defined by

$$\tilde{V}(x) \equiv -\frac{1}{2} m \tilde{\omega}^2 x^2 \quad (137)$$

One can make the substitutions

$$\omega^2 \rightarrow -\tilde{\omega}^2, \quad \omega \rightarrow i\tilde{\omega}, \quad \sin(\omega t) \rightarrow i \sinh(\tilde{\omega} t), \quad \text{and} \quad \cos(\omega t) \rightarrow \cosh(\tilde{\omega} t) \quad (138)$$

and we briefly discuss this in Appendix D.

D. The infinite well

1. General comments

The one-dimensional infinite potential well is the most frequently encountered example of a 1D bound state system, finding its way into every introductory quantum mechanics text. Given its important pedagogical role, and familiar solutions, it is not surprising that many aspects of wave packet propagation in general, and quantum revivals in particular, in this system have been studied (38), (90) - (100). (Interestingly, the time development of quantum states in the infinite well was used as a debating point by Einstein and Born (101), (102) in more general discussions about the nature of quantum mechanics.)

In this review, we will examine both the short-term quasi-classical time-evolution of Gaussian wave packets, the spreading to a collapsed state, as well as the structure of the revivals, mirror or 'anti'-revivals, and fractional revivals using both the standard auto-correlation function, $A(t)$ and a related 'anti-correlated' $\overline{A}(t)$. We also focus on visualizing the same phenomena through the time-development of expectation values (and uncertainties), in both position- and momentum-space, as well as emphasizing the visualization of such effects in a variety of ways, including the Wigner quasi-probability (phase-space) distribution and the use of what have been dubbed *quantum carpets*. It is worth noting that bound-state wave packets in this system were examined in detail by Segre and Sullivan (90) in 1976 where the existence of exact wave packets revivals was discussed very explicitly, with the authors also noting in a footnote that "*We suspect that this almost periodic behavior of packet width is a general property of bound-state packets.*"

We begin by defining the familiar problem of a particle of mass m confined by the potential

$$V(x) = \begin{cases} 0 & \text{for } 0 < x < L \\ \infty & \text{otherwise} \end{cases} \quad (139)$$

which has energy eigenvalues and stationary state solutions given by

$$E_n = \frac{p_n^2}{2m} = \frac{\hbar^2 \pi^2 n^2}{2mL^2} = n^2 E_0 \quad \text{where} \quad p_n \equiv \frac{n\hbar\pi}{L} \quad \text{for } n = 1, 2, \dots \quad (140)$$

and

$$u_n(x) = \sqrt{\frac{2}{L}} \sin\left(\frac{n\pi x}{L}\right). \quad (141)$$

We note that the energy eigenfunctions have a generalized parity property (about the mid-point of the well), namely

$$u_n(L-x) = \sqrt{\frac{2}{L}} \sin\left(\frac{n\pi(L-x)}{L}\right) = -\sqrt{\frac{2}{L}} \cos(n\pi) \sin\left(\frac{n\pi x}{L}\right) = (-1)^{n+1} u_n(x) \quad (142)$$

so that for n odd (even), the eigenfunctions are even (odd) about the center ($L/2$) of the well. This connection suggests that we generalize the notion of the $\tilde{A}(t)$ 'anti-correlation' function in Eqn. (135) to the geometry of the standard infinite well by defining

$$\overline{A}(t) \equiv \int_0^L \psi^*(L-x, t) \psi(x, 0) dx. \quad (143)$$

The classical period for this system, obtained from Eqn. (9), is

$$T_{cl} = \frac{2\pi\hbar}{|E'_n|} = \frac{2mL^2}{\hbar\pi n} = \frac{2L}{[(\hbar\pi n/L)/m]} = \frac{2L}{v_n} \quad \text{where} \quad v_n \equiv \frac{p_n}{m} \quad (144)$$

and v_n is the analog of the classical speed, giving a result in agreement with classical expectations. The revival time is then given by

$$T_{rev} \equiv \frac{2\pi\hbar}{|E_n''|/2} = \frac{2\pi\hbar}{E_0} = \frac{4mL^2}{\hbar\pi} = (2n)T_{cl} \quad (145)$$

which is also consistent with Eqn. (21) for general 1D power law potentials. Thus, for $n \gg 1$, one can easily arrange to have $T_{rev} \gg T_{cl}$. The superrevival and higher order terms in the expansion in Eqn. (8) all vanish, making this an ideal system to study exact revival behavior.

The quantum revivals in this case are in a sense exact, since we have

$$\psi(x, t + T_{rev}) = \sum_{n=1}^{\infty} a_n u_n(x) e^{-iE_n t/\hbar} e^{-iE_n T_{rev}/\hbar} = \sum_{n=1}^{\infty} a_n u_n(x) e^{-iE_n t/\hbar} e^{-i2\pi n^2} = \psi(x, t) \quad (146)$$

for all times. The wave packet will also, however, reform itself at $t = T_{rev}/2$ (a so-called mirror revival or 'anti-revival') at a (possibly) different location in the well. To see this we note that

$$\begin{aligned} \psi(L-x, t + T_{rev}/2) &= \sum_{n=1}^{\infty} a_n u_n(L-x) e^{-iE_n t/\hbar} e^{-iE_n T_{rev}/2\hbar} \\ &= \sum_{n=1}^{\infty} a_n u_n(x) e^{-iE_n t/\hbar} \left[(-1)^{n+1} e^{-in^2\pi} \right] \\ &= -\psi(x, t) \end{aligned} \quad (147)$$

which implies that

$$|\psi(x, t + T_{rev}/2)|^2 = |\psi(L-x, t)|^2 \quad (148)$$

so that at half a revival time later, any initial wave packet will reform itself (same shape, width, etc.), but at a location mirrored (91) about the center of the well. The use of the anti-correlation function, $\bar{A}(t)$, defined in Eqn. (143), will then be useful not only for documenting the short-term, semi-classical periodicity of such packets, but especially in establishing this additional type of revival structure. This behavior is a special case of the more general $T_{rev}/2$ revival discussed in Eqn. (38).

The behavior of the wave packet in momentum space for such mirror packets is also easily derived using the Fourier transform connection, in this case

$$\phi(p, t) = \frac{1}{\sqrt{2\pi\hbar}} \int_0^L \psi(x, t) e^{ipx/\hbar} dx. \quad (149)$$

We simply note that

$$\begin{aligned} \phi(p, t + T_{rev}/2) &= \frac{1}{\sqrt{2\pi\hbar}} \int_0^L \psi(x, t + T_{rev}/2) e^{ipx/\hbar} dx \\ &= -\frac{1}{\sqrt{2\pi\hbar}} \int_0^L \psi(L-x, t) e^{ipx/\hbar} dx \\ &= -e^{ipL/\hbar} \left[\frac{1}{\sqrt{2\pi\hbar}} \int_0^L \psi(y, t) e^{-ipy/\hbar} dy \right] \\ &= -e^{ipL/\hbar} \phi(-p, t) \end{aligned} \quad (150)$$

so that

$$|\phi(p, t + T_{rev}/2)|^2 = |\phi(-p, t)|^2 \quad (151)$$

and half a revival time later the initial momentum profile is also reproduced, except flipped in sign ($p \rightarrow -p$), so that the particle is also moving in the 'other direction'.

It has been noted several times that the dynamical time dependence of wave packets in this system can be described by the free-space evolution of an infinite sequence of appropriately displaced initial wave functions (91), (103), which can be derived using a 'method of images' technique (104).

2. Gaussian wave packets

For definiteness, one typically considers Gaussian-like wave packets, corresponding approximately to initial momentum- or position-space wave functions as in the $t = 0$ limits of Eqns. (74) and (76). The expansion coefficients corresponding to such initial states can be well-approximated in an analytic form if we assume that the initial position-space wavefunction,

$$\psi_G(x, 0) = \frac{1}{\sqrt{b\sqrt{\pi}}} e^{-(x-x_0)^2/2b^2} e^{ip_0(x-x_0)/\hbar} \quad (152)$$

(where $b \equiv \alpha\hbar$) is sufficiently contained within the well so that we make an exponentially small error by neglecting any overlap with the region outside the walls, and may thus also ignore any problems associated with possible discontinuities at the wall. In practice, this condition only requires the wave packet to be a few times $\Delta x_0 = b/\sqrt{2}$ away from an infinite wall boundary.

With these assumptions, we can then extend the integration region from the finite $(0, L)$ interval to the entire 1D space, giving the (exponentially good) approximation for the expansion coefficients (97)

$$\begin{aligned} a_n &\approx \int_{-\infty}^{+\infty} [u_n(x)] [\psi_G(x, 0)] dx \\ &= \left(\frac{1}{2i}\right) \sqrt{\frac{4b\pi}{L\sqrt{\pi}}} [e^{in\pi x_0/L} e^{-b^2(p_0+n\pi\hbar/L)^2/2\hbar^2} - e^{-in\pi x_0/L} e^{-b^2(p_0-n\pi\hbar/L)^2/2\hbar^2}], \end{aligned} \quad (153)$$

because we can write

$$\sin\left(\frac{n\pi x}{L}\right) = \frac{1}{2i}(e^{in\pi x/L} - e^{-in\pi x/L}), \quad (154)$$

and we can perform Gaussian integrals such as

$$\int_{-\infty}^{+\infty} e^{-ax^2-bx} dx = \sqrt{\frac{\pi}{a}} e^{b^2/4a} \quad (155)$$

in closed form. This explicit expression goes back to at least Born (101) and in our context is very useful because it can speed up numerical calculation involving the expansion coefficients, such as the evaluation of $A(t)$. It also accurately encodes the sometimes delicate interplay between the oscillatory pieces of the Gaussian ($e^{-ip_0x/\hbar}$) and the bound state ($e^{\pm in\pi x/a}$) wavefunctions, which can be difficult to reproduce in a purely numerical evaluation, and it does so in a way that is valid for arbitrarily large values of p_0 , where the integrand would be highly oscillatory, as well as being valid even for small values of p_0 (or n_0 .) Finally, Eqn. (153) nicely illustrates how $\psi_G(x, 0)$ and the $u_n(x)$ must not only have an appropriate overlap in position space, but also must have an appropriate phase relationship between

their oscillatory terms. This phase connection leads to the $\exp(-b^2(p_0 \pm n\pi\hbar/a)^2/2\hbar^2)$ terms, which can be understood from a complementary overlap in momentum space.

With this approximation ($x_0, L - x_0 \gg b$), the normalization and energy expectation value conditions

$$\sum_{n=1}^{\infty} |a_n|^2 = 1 \quad (156a)$$

$$\sum_{n=1}^{\infty} |a_n|^2 E_n = \langle \hat{E} \rangle = \frac{1}{2m} \left(p_0^2 + \frac{\hbar^2}{2b^2} \right) \quad (156b)$$

can be satisfied to arbitrary accuracy. For the illustrative numerical results presented here, we use the nominal values

$$L = 1, \quad \hbar = 1, \quad \text{and} \quad 2m = 1 \quad (157)$$

and we will often denote $p_0 = n_0\pi\hbar/L$ to define the central value of n_0 used in the eigenstate expansion, which in the large n limit will also give

$$\frac{1}{\alpha\sqrt{2}} = \Delta p_0 = \frac{\Delta n\pi\hbar}{L} \quad \text{so that} \quad \Delta n = \frac{L}{(\alpha\hbar)\pi\sqrt{2}} = \frac{L}{\Delta x_0 2\pi}. \quad (158)$$

This is useful as it can provide an estimate of how many eigenstates must be included in a given expansion. In the limit that $n_0 \gg \Delta n \gg 1$, we can use this expression (relating $b \propto \Delta x_0 \propto L/\Delta n$) in Eqn. (153), which then reduces to the standardly used Gaussian expression coefficients in Eqn. (24).

For most cases we consider in this section, we will also use

$$\alpha = \frac{1}{10\sqrt{2}} \quad \text{so that} \quad \Delta x_0 = 0.05 \ll L, \quad \Delta p_0 = 10 \quad \text{and} \quad \Delta n = \frac{10}{\pi} \approx 3. \quad (159)$$

This choice of parameters also implies that the other relevant time in the problem, the spreading time, t_0 , defined by

$$t_0 = m\hbar\alpha^2 = \frac{m\hbar}{2\Delta p_0^2} = \frac{2m\Delta x_0^2}{\hbar}, \quad \text{gives} \quad \frac{T_{rev}}{t_0} = \frac{2}{\pi} \left(\frac{L}{\Delta x_0} \right)^2 \quad (160)$$

and $T_{rev}/t_0 \gg 1$ for any wave packet sufficiently localized to be contained in the well. While we will typically focus on wave packets characterized by $n_0 \gg 1$, which is what is typically obtained in experimental realizations exhibiting wave packet revivals, we start for simplicity with $p_0 = 0$ packets.

3. Zero-momentum wave packets

We can make immediate use of Eq. (153) by considering zero momentum ($p_0 = 0$) wave packets; this case corresponds to placing a particle ‘at rest’ inside the infinite well potential. For such cases, the only natural periodicity in the problem is the revival time in Eq. (145), because there is no corresponding classical periodic motion. In this special case, the expression for the a_n in Eq. (153) simplifies even further to

$$a_n = \sqrt{\frac{4b\pi}{L\sqrt{\pi}}} e^{-b^2 n^2 \pi^2 / L^2} \sin\left(\frac{n\pi x_0}{L}\right) \quad (161)$$

which shows that for several special values of x_0 in the well, a number of the expansion coefficients will vanish for obvious symmetry reasons.

For example, for $x_0/L = 1/2$, all of the even ($n = 2, 4, 6, \dots$) coefficients are zero and the only non-vanishing terms in the expansion are the odd ones ($n = 2k + 1$) which have energies of the form

$$E_n = \frac{\hbar^2 \pi^2}{2mL^2} (2k + 1)^2 = E_0(4k^2 + 4k + 1) = E_0 + 8E_0 \left[\frac{k(k + 1)}{2} \right]. \quad (162)$$

The first term in Eq. (162) contributes only to the same overall phase of the time-dependence of each term. The second term is of the form $8E_0$ times an integer and leads to revival times that are 8 times *shorter* than the standard $T_{rev} = 2\pi\hbar/E_0$ in Eq. (145). We illustrate this behavior in Fig. 7(a) where we also note that moving slightly away from $x_0/L = 1/2$ (as in Fig. 7(b)) removes these exact sub-revivals, while the required full revival is still present. (This was observed in Ref. (91) for any even parity eigenstate in the infinite well.)

Similarly, for the cases of $x_0/L = 1/3, 2/3$, the a_n with $n = 3k$ vanish, leading to special exact revivals at multiples of $T_{rev}/3$ for these two initial locations and this behavior is also shown in Fig. 7(c) where we find exact revivals at these shorter time intervals. For $x_0/L = 0.8$ (still far enough away from the walls to be considered reliably in this approximation), we also notice large partial (but not exact) revivals at $0.4T_{rev}$ and $0.6T_{rev}$ for similar reasons (because $\sin(4n\pi/5)$ vanishes for $n = 5k$.) (We note that it is also possible to construct odd-parity wave packets that have different patterns of special revivals at other locations in the well.) In the same plots, we also indicate the values of the a_n expansion coefficients and note the patterns of vanishing a_n values for the cases of special symmetry. For these $p_0 = 0$ states, the distribution of n -values is far from Gaussian.

We are more interested in semi-classical wave packets with $p_0 \neq 0$ and we next show, in Fig. 8, the effect of ‘turning on’ momentum values for an $x_0 = L/2$ wave packet. For $p_0 = 0$ (top line, (a)), we have the special pattern of exact revivals at multiples of $T_{rev}/8$ noted above, due to the vanishing of the even expansion coefficients (shown in the corresponding $|a_n|^2$ versus n plot in the right column). For a small, non-zero value ($p_0 = 3\pi \approx \Delta p_0$, Fig. 8(b)), only the exact revival at T_{rev} remains, because the even expansion coefficients are no longer forced to vanish. The autocorrelation function decreases somewhat more rapidly from its initial value than in the $p_0 = 0$ case, because the particle is now slowly moving away from its initial position, in addition to spreading out.

For still larger values of momentum, such as $p_0 = 40\pi$ (Fig. 8(c)), we see obvious evidence for the classical periodicity and the first appearance of fractional revivals (91) at rational fraction multiples of T_{rev} , as in Sec. II.D. The corresponding a_n now exhibit a more obvious Gaussian shape, with a spread, Δn , which closely approximates the result in Eqn. (158). For even larger momentum values (see the $p_0 = 400\pi$ case in Fig. 8(d), for example), the classical period becomes much shorter than any obvious fractional revival time scale, and the shape of the expansion coefficient distribution is unchanged (same Δn), but simply shifted to higher values of n , as expected.

In what follows, we will typically use this last case, $n_0 = 400$, in our visualizations. This implies that the appropriate relative time scales are

$$\frac{T_{rev}}{T_{cl}} = 2n_0 = 800 \quad \text{and} \quad \frac{t_0}{T_{cl}} = n_0\pi \left(\frac{\Delta x_0}{L} \right)^2 = \pi \quad (163)$$

so that much of the fractional revival structure is obvious, while a number of classical periods are present before significant spreading occurs.

4. Short-term, quasi-classical propagation

We expect the short-term propagation of wave packets in the semi-classical limit we study to share many properties with both the classical system, as well as with the quantum-mechanical free-particle in Sec. III.A. For example, well before the initial wave packet nears one of the infinite wall barriers, we expect the wave packet to propagate with time-dependence as in Eqn. (76), and with a decreasing auto-correlation function (Eqn. (82)) described by

$$|A_{free}(t)|^2 = \frac{1}{\sqrt{1 + (t/2t_0)^2}} \exp \left[-2\alpha^2 p_0^2 \frac{(t/2t_0)^2}{(1 + (t/2t_0)^2)} \right]. \quad (164)$$

The quasi-periodic wave packet in this confining potential must return to something like its original state at $t = T_{cl}$, so we expect also suspect that the behavior near that point will be approximately described by $A_{free}(T_{cl} - t)$. For later convenience, we will also find it useful to single out the dispersive pre-factor above as the ‘envelope’ and define

$$|A_{env}(t)|^2 = \frac{1}{\sqrt{1 + (t/2t_0)^2}}. \quad (165)$$

To see to what extent the free-particle autocorrelation function is relevant, we plot in Fig. 9 $|A(t)|^2$ over the first classical period, using Eqn. (76) for the Gaussian wave packet, and increasing numbers (N) of eigenstates used in the expansion (solid curves.) For comparison, we also plot $|A_{free}(t)|^2$ (dashed) and $|A_{free}(T_{cl} - t)|^2$ (dot-dashed) and find that they are indeed good representations of the numerically evaluated result for the Gaussian packet over much of the early and late parts of the classical period. The agreement improves as increasing numbers of states used in the expansion can more approximately reproduce the exponential suppression predicted by Eqn. (164). We also plot (as diamonds) values of $|A(t)|^2$ from the generic expression given by Nauenberg (40) for the short-term quasi-classical behavior, discussed in Appendix B, and note that especially for this case where there are no higher time scales, it is an excellent approximation.

Over longer times, we know that the wave packet will spread significantly and that $A(t), \bar{A}(t)$ will not be exactly periodic, but will decrease due to the dispersion, presumably described by Eqn (165). To confirm this, we plot both $|A(t)|^2$ and $|\bar{A}(t)|^2$ over the first 15 classical periods (corresponding to almost $15T_{CL}/t_0 = 15/\pi \approx 5$ spreading times) in Fig. 10, along with the ‘envelope’ function in Eqn. (165) and note that the initial decrease in the maximum values of the autocorrelation and anti-correlation functions is indeed well described by this prescription.

Continuing in this vein, we next examine, in Fig. 11, both $|A(t)|^2$ and $|\bar{A}(t)|^2$, now evaluated at integral multiples of T_{cl} over the first 150 classical periods. In this case we note that the dispersive prediction of Eqn. (165) is a good approximation for over 40 periods, while the anti-correlation function (evaluated at $t = nT_{cl}$) slowly grows from its exponentially suppressed value at $t = 0$ and eventually crosses the $|A(t)|$ curve. For comparison, we have plotted (horizontal dotted line) the value of $|A(t)|^2$ which might be expected if the wave packet were an incoherent sum of eigenstates, with no correlations, given by

$$|A(t)|^2 \implies |A_{inc}|^2 \equiv \sum_n |a_n|^4 = \frac{1}{\Delta n 2\sqrt{\pi}} \approx 0.089 \quad (\text{for } \Delta n = 10/\pi). \quad (166)$$

The relationship between $A(t)$ and $\bar{A}(t)$ at some of the first few fractional revival times is also obvious

5. Revivals, fractional revivals, and mirror revivals

The longer term structure of both $A(t)$ and $\overline{A}(t)$, showing evidence for revivals, fractional revivals, and mirror revivals, is illustrated in Fig. 12; only the interval $(0, T_{rev}/2)$ is shown as the plot is symmetric about $T_{rev}/2$ for this system. Many of the locations of possible low-lying fractional revivals are shown as vertical dashed lines, as well as the incoherent value, $|A_{inc}|$, from Eqn. (166). We can then examine the detailed behavior of $A(t)$, $\overline{A}(t)$ near various specific fractional revival times.

We begin, in Fig. 13, with $t = T_{rev}/2$, the $p/q = 1/2$ (or mirror or anti-revival) time, where we know that the wave packet will reform (Eqn. (148)) on the opposite side of the well, with momentum in the opposite direction (Eqn. (151).) The upper plots in Fig. 13 show the behavior of $|A(nT_{cl})|^2$ over the entire revival time (upper left) evaluated at integral values of T_{cl} , with the mirror revival indicated by the arrow, as well as the typical behavior of both $|A(t)|^2$ (solid) and $|\overline{A}(t)|^2$ (dashed) near T_{rev} (or $t = 0$ as well) in the upper right corner. The lower right shows the autocorrelation and anti-correlation functions for one classical period on either side of $T_{rev}/2$, showing how the anti-correlation function is unity at $T_{rev}/2$, with $A(t)$ being $T_{cl}/2$ out of phase with it, as described very generally in Eqn. (38). Finally, the position-space probability density is plotted (lower left) where the initial wave packet was located at $x_0/L = 2/3$ (solid), and was given positive momentum (illustrated by the arrow), while the value at $t = T_{rev}/2$ (dashed) is indeed centered at the mirror location $(L - x_0)$ and a short time later ($\Delta t = T_{cl}/20$, dotted curve) the packet is clearly moving to the left, consistent with Eqn. (151).

We next turn our attention, in Fig. 14, to an example of a fractional revival at $T_{rev}/3$. In this case, the plot of $|\psi(x, t)|^2$ in the lower left shows the pattern of three ‘mini’ versions (dashed) of the original wave packet (solid), moving in a highly correlated manner (note the time-development at a time $T_{cl}/20$ later, dotted curve, indicated by the arrows.) This is also reflected in the plots of $A(t)$ in the region around $t = T_{rev}/3$ where there is a periodicity of $T_{cl}/3$ due to the ‘mini’ packets (labeled a, b, c) being correlated with the initial wave form, and the same shorter periodicity is also apparent in the behavior of $\overline{A}(t)$, as predicted in Eqn. (58).

The case of the $T_{rev}/4$ revival, shown in Fig. 15, is interesting since in this case the maximal values of $|A(t)|$, $|\overline{A}(t)|$ near this fractional revival are identical ($1/2$) and they are both in phase (see the lower right of Fig. 15.) Once again, the two ‘mini’ packets are highly correlated in position-space (one packet reforming at x_0 , the other at $L - x_0$ as befits a mirror revival) and in momentum-space (with their momenta in opposite directions) just as in Eqn. (43).

Finally, if we look at many other times at random which are not near a fractional revival, as in Fig. 16, we see much smaller values of $|A(t)|$, $|\overline{A}(t)|$, typically consistent with the incoherent limit of Eqn. (166), and position-space probability densities (as in the lower left of Fig. 16) which exhibit far less obvious structure, being much more consistent with rapid oscillations about a uniform or ‘flat’ classical probability distribution, namely $P(x) = 1/L$ (denoted here by the two horizontal arrows.) This is typical of a collapsed phase where the wave packet is described more by an incoherent sum of energy eigenstates, with the probability density averaging about a semi-classical value, as in Eqn. (31), which in this case is the trivial constant value.

Since the phenomena of wave packet revivals (and fractional revivals) is first and foremost about the important phase relationships between the energy eigenstates, as well as between the individual ‘mini’-packets, it is instructive to examine both the real and imaginary parts of $A(t)$, both over the long term revival time scales, as well as near fractional revivals or during the collapsed phase.

We begin by examining in Fig. 17 both the real and imaginary parts of $A(t)$ as well as a parametric plot (in an Argand diagram) over half a revival time. The plots show $A(nT_{cl})$ sampled at multiples of the classical period (just as in Figs. 13 - 16), illustrating the intricate phase relationship present. The dashed circle corresponds to the value of $|A|^2 = 1/2$ and we

indicate the location of a 1/4 fractional revival showing how the autocorrelation function ‘lingers’ tangentially during the fractional revival period. Close-up versions of the fractional revivals at $T_{rev}/4$ and $T_{rev}/3$ are shown (in the same format) in Figs. 18 and 19 respectively, where the obvious phase correlations between the ‘mini’-packets are clearly present. For the case of the $T_{rev}/4$ fractional revival, the approximate wavefunction in Eqn. (43) implies that the autocorrelation function near that time can be generally written in the form

$$A(t \approx T_{rev}/4) = \frac{1}{\sqrt{2}} [e^{i\pi/4} A_{cl}(t) + e^{-i\pi/4} A_{cl}(t + T_{cl}/2)] \quad (167)$$

where we define

$$A_{cl}(t) \equiv \int_{-\infty}^{+\infty} \psi_{cl}^*(x, t) \psi_{cl}(x, 0) dx \quad (168)$$

and we see that this form is consistent with the visualization in Fig. 18.

For the $T_{rev}/3$ case in Fig. 19, the wavefunction in Eqn. (58) can be used to write

$$A(t \approx T_{rev}/3) = (iA_{cl}(t) + e^{-2\pi i/3} [A_{cl}(t + T_{cl}/3) + A_{cl}(t + 2T_{cl}/3)]) / \sqrt{3} \quad (169)$$

which describes the magnitude/phase relationships seen in Fig. 19.

Finally, the behavior of these quantities during a typical time, T^* , in the collapsed phase is shown in Fig. 20, where in this case the dotted circle corresponds to the incoherent value $|A_{inc}|^2 = \sum |a_n|^4$.

6. Expectation value analysis

While an analysis of the short-term quasi-classical and long-term revival structure of wave packets using autocorrelation function methods is often the most directly comparable to important experimental observables, the visualization of the time-dependence of quantum wave packets through their expectation values, both in position- and momentum-space, can also be a valuable tool (105) for understanding many of the effects arising in the quantum mechanical time evolution of wave functions. For example, the time-evolution of the uncertainty principle product, $\Delta r \cdot \Delta p_r$, has been used (30), (31) to distinguish between regimes of classical versus non-classical behavior in Rydberg atoms.

In this section, using the same parameter values as in earlier analyses, we examine the expectation values, $\langle x \rangle_t$ and $\langle p \rangle_t$, and uncertainties, Δx_t and Δp_t , for Gaussian wave packets in the infinite well (94), both for short times (several classical periods) and over the entire revival time.

Once again, comparisons to both the classical limits and the results of the free-particle wave packet in Sec. III.A can be useful. For example, the time-dependence of a classical particle in the infinite well potential, starting with velocity $+v_0$, at the center of the well, is shown in Fig. 21, with cusps in $x(t)$ at the ‘bounces’ at the infinite walls, and a discontinuous change in momentum (from $\pm mv_0$ to $\mp mv_0$) at the same points. We might expect somewhat similar behavior, softened by quantum effects, at least at early times for the quantum problem. For comparison, we recall that the free-particle Gaussian wave packet in Eqns. (74) and (76) is characterized by

$$\langle x \rangle_t = p_0 t / m + x_0 \quad , \quad \Delta x_t = \Delta x_0 \sqrt{1 + (t/t_0)^2} \quad (170a)$$

$$\langle p \rangle_t = p_0 \quad , \quad \Delta p_t = \Delta p_0 \quad (170b)$$

The short-term, quasi-classical time-development can be seen in Fig. 22 for the position-space variables and in Fig. 23 for the momentum-space quantities, over the first 10 classical periods (approximately 3 spreading times.) The classical looking behavior of $\langle x \rangle_t$ is apparent,

but with the maximal values near odd integral multiples of $T_{cl}/2$ (corresponding to the ‘hits’ on the walls) becoming smaller and smaller, as the wave packet spreads, becomes wider and finds it increasingly harder to get near the wall. The results for Δx_t are also consistent with expectations, namely there are small ‘dips’ in Δx_t at $t = (2n + 1)T_{cl}/2$ arising from the ‘compression’ of the packet (106) as it strikes the wall, superimposed on a uniform increase (the dotted line) consistent with the free-particle spreading in Eqn. (170a).

In our exemplary cases, the initial wave packet is characterized by positive momentum $p_0 = 400\pi \approx 1260$ and we see distinct evidence of ‘flips’ between $\pm p_0$, at times consistent with the classical ‘bounces’ in the $\langle p \rangle_t$ plot at the top of Fig. 23. The initial momentum spread from Eqn. (159) is $\Delta p_0 = 10$ and we expect this to stay roughly constant between successive collisions with the wall. During the collision times, however, the spread arising from the momentum-space probability density is dominated not by the intrinsic spread of a single peak, but rather by the ‘distance’ between the two peaks at $p = \pm p_0$. In the limit where $P(p)$ can be approximated by two highly peaked features at $\pm p_0$, namely

$$P(p) = \frac{1}{2} [\delta(p - p_0) + \delta(p + p_0)] \quad (171)$$

the corresponding spread in momentum is actually closer to $\Delta p_{cl} = p_0$, and this type of behavior is also evident from Fig. 23.

For the autocorrelation function analysis, we found that the approach to the collapsed state could be discussed in terms of the decrease of $|A(t)|$ from its highly correlated value of unity near classical periods to something closer to the incoherent value of $|A_{inc}|$ given by Eqn. (166). In more physical terms, we expect the increasingly wide quantum wave packet to approach a collapsed state which is uniformly spread over the entire well, consistent with the classical probability density $P_{cl}(x) = 1/L$. For that distribution, we have position spread is given by

$$\langle x \rangle_{cl} = \frac{L}{2} \quad , \quad \langle x^2 \rangle_{cl} = \frac{L^2}{3} \quad \text{so that} \quad \Delta x_{cl} = \frac{L}{\sqrt{12}} \approx 0.288L. \quad (172)$$

To visualize this approach to the collapsed state, we plot in Fig. 24, the time-dependent position spread, Δx_t corresponding to three different values of Δx_0 and note that they all ‘saturate’ at $\Delta x_{flat} = L/\sqrt{12}$, at different times, due to the difference in spreading times ($t_0 = 2m(\Delta x_0)^2/\hbar$). In each case, the bound state values initially follow the free-particle prediction of Eqn. (170a) for short times. The time scale for this collapse can be estimated by equating

$$\frac{L}{\sqrt{12}} \equiv \Delta x_{cl} = \Delta x_{(t=T_{coll})} = \Delta x_0 \sqrt{1 + (T_{coll}/t_0)^2} \quad (173)$$

giving

$$T_{coll} = t_0 \left(\frac{L}{\sqrt{12}\Delta x_0} \right) = \frac{1}{\sqrt{3}} \left(\frac{mL\Delta x_0}{\hbar} \right) = \sqrt{\frac{\pi T_{rev} t_0}{24}} \quad (174)$$

which defines another time scale, intermediate between t_0 and T_{rev} .

The same type of approach to the values appropriate for a collapsed state can also be seen (in Fig. 25) for $\langle x \rangle_t$ (approaching $\langle x \rangle_{cl} = L/2$), for $\langle p \rangle_{cl} = 0$ (equal admixtures of left and right moving states), and for $\Delta p_{cl} = +p_0$ (same reason) over the same time scales, and with the same dependence on the spreading time (via its dependence on the initial width.)

Finally, the behavior of selected average values over the entire revival time, illustrating both the revival and mirror revival times, as well as ‘close up’ views at intermediate times, are shown in Figs. 26, 27, and 28. The plots are shown for times given by $t = (n + 1/8)T_{cl}$ (solid) and $(n + 5/8)T_{cl}$ (dashed) to help distinguish standard versus mirror revivals. The magnitude of excursions from the classical value of $\langle x \rangle_{cl} = L/2$ for the collapsed state are shown on an

expanded scale in Fig. 26, which includes a fractional revival at $t = T_{rev}/6 = 133T_{CL}$ and $t = T_{rev}/5 = 160T_{cl}$.

For the time-dependent spread in position, Δx_t , in Fig. 27, we see that Δx_t returns to the initial value, Δx_0 , at T_{rev} (full revival) and $T_{rev}/2$ ($p/q = 1/2$ or mirror revival) as expected, but also at $T_{rev}/4$ and $3T_{rev}/4$. These last two instances are special cases and are due to the choice of $x_0 = L/2$ for the initial wave packet (compared to $x_0 = 2L/3$ as shown in Fig. 15) where the two 'mini' packets are superimposed at the same location (the midpoint of the well), but moving with opposite momenta. This is consistent with the $\langle p \rangle_t$ and Δp_t values at the same times in Fig. 28.

We note that the observed agreement of a number of expectation values and spreads with results obtained from the classical probability distributions (as in Eqn. (172)) during times much longer than the spreading time, while consistent with the approach to a purely 'flat' distribution, can also be thought of, during periods of fractional revivals, as being due to the correlated behavior of a number of 'mini-packets' or 'clone' wave packets, which can give similar results (100).

7. Phase-space picture of fractional revivals using the Wigner function

Another useful way to visualize the correlated position- and momentum-space structure of wave packets in a phase-space type picture is by using the Wigner quasi- or pseudo probability density (107) defined by

$$W(x, p; t) \equiv \frac{1}{\pi\hbar} \int_{-\infty}^{+\infty} \psi^*(x+y, t) \psi(x-y, t) e^{2ipy/\hbar} dy \quad (175)$$

$$= \frac{1}{\pi\hbar} \int_{-\infty}^{+\infty} \phi^*(p+q, t) \phi(p-q, t) e^{-2iqx/\hbar} dq. \quad (176)$$

(The Wigner distribution for Gaussian wave packet solutions in the infinite square well has been discussed in Ref. (108) to which we refer the reader for many calculational and visualization details.) The general properties of the Wigner distribution have been discussed in a number of accessible reviews (109) - (117), where, among other features, it is noted that integration of $W(x, p; t)$ over one variable or the other is seen to give the correct marginal quantum mechanical probability distributions for x and p separately, since

$$\int_{-\infty}^{+\infty} W(x, p; t) dp = |\psi(x, t)|^2 = P_{QM}(x, t) \quad (177)$$

$$\int_{-\infty}^{+\infty} W(x, p; t) dx = |\phi(p, t)|^2 = P_{QM}(p, t). \quad (178)$$

The Wigner function is also easily shown to be real, but need not, however, be positive definite, hence the name quasi- or pseudo-probability density.

The Wigner distribution for a standard time-dependent Gaussian free-particle solution of the form in Eqns. (74) or (76) is easily obtained, using standard Gaussian integrals, and is given by

$$W^{(G)}(x, p; t) = \frac{1}{\pi\hbar} e^{-\alpha^2(p-p_0)^2} e^{-(x-x_0-pt/m)^2/\beta^2} \quad (179)$$

where $\beta \equiv \hbar\alpha$; in this case, the ultra-smooth Gaussian form does give a positive $W(x, p; t)$, as has been discussed in the literature (118).

Another result which will prove useful in what follows is the expression for the Wigner function for the case of a linear combination of two 1D Gaussians, characterized by different values of x_0 and p_0 . For example, if we assume that at some instant of time we have

$$\begin{aligned}\psi^{(A,B)}(x) &= \gamma\psi_{(G)}(x; x_A, p_A) + \delta\psi_{(G)}(x; x_B, p_B) \\ &= \gamma \left[\frac{1}{\sqrt{\beta}\sqrt{\pi}} e^{-(x-x_A)^2/2\beta^2} e^{ip_A(x-x_A)/\hbar} \right] + \delta \left[\frac{1}{\sqrt{\beta}\sqrt{\pi}} e^{-(x-x_B)^2/2\beta^2} e^{ip_B(x-x_B)/\hbar} \right],\end{aligned}\quad (180)$$

the corresponding Wigner function is given by

$$\begin{aligned}P_W^{(A,B)} &= \frac{1}{\pi\hbar} \left[|\gamma|^2 e^{-\alpha^2(p-p_A)^2} e^{-(x-x_A)^2/\beta^2} + |\delta|^2 e^{-\alpha^2(p-p_B)^2} e^{-(x-x_B)^2/\beta^2} \right. \\ &\quad \left. + 2e^{-\alpha^2(p-\bar{p})^2} e^{-(x-\bar{x})^2/\beta^2} \text{Re} \left\{ \gamma\delta^* e^{i(x_A p_B - x_B p_A)/\hbar} e^{-i(x_A - x_B)(p-\bar{p})/\hbar} e^{i(p_A - p_B)x/\hbar} \right\} \right]\end{aligned}\quad (181)$$

where

$$\bar{x} \equiv \frac{x_A + x_B}{2} \quad \text{and} \quad \bar{p} \equiv \frac{p_A + p_B}{2}.\quad (182)$$

In this case, the Wigner function is characterized by two smooth ‘lumps’ in phase space, corresponding to the values of (x_A, p_A) and (x_B, p_B) of the individual Gaussians, but also by an oscillatory term, centered at a point in phase space defined by the average of these values; the oscillations are either in x (if $p_A \neq p_B$), p (if $x_A \neq x_B$) or both. (See Ref. (119) for a similar result for the case when $p_A = p_B = 0$; see also Ref. (63) for a related expression involving coherent states.)

For a general, time-dependent wave packet constructed from energy eigenstates of the form in Eqn. (3), the Wigner distribution is given by

$$\begin{aligned}W^{(\psi)}(x, p; t) &\equiv \frac{1}{\pi\hbar} \int_{-\infty}^{+\infty} \psi^*(x+y, t) \psi(x-y, t) e^{2ipy/\hbar} dy \\ &= \sum_{m=1}^{\infty} \sum_{n=1}^{\infty} [a_m]^* a_n e^{i(E_m - E_n)t/\hbar} \left[\frac{1}{\pi\hbar} \int_{-\infty}^{+\infty} u_m(x+y) u_n(x-y) e^{2ipy/\hbar} dy \right] \\ &\equiv \sum_{m=1}^{\infty} \sum_{n=1}^{\infty} [a_m]^* a_n e^{i(E_m - E_n)t/\hbar} P_W^{(m,n)}(x, p)\end{aligned}\quad (183)$$

where, in general, we must calculate both diagonal ($m = n$) and off-diagonal ($m \neq n$) terms of the form

$$W^{(m,n)}(x, p) = \frac{1}{\pi\hbar} \int_{-\infty}^{+\infty} u_m(x+y) u_n(x-y) e^{2ipy/\hbar} dy\quad (184)$$

where we have assumed that the individual position-space bound state eigenfunctions, $u_n(x)$, can be made purely real. The off-diagonal Wigner terms are, however, not real, but do satisfy

$$[W^{(m,n)}(x, p)]^* = W^{(n,m)}(x, p).\quad (185)$$

For the infinite square well, the diagonal ($m = n$) terms are given by

$$W^{(n,n)}(x, p) = \frac{1}{\pi\hbar} \int u_n(x+y) u_n(x-y) e^{2ipy/\hbar} dy\quad (186)$$

and the limits of integration are determined by the restriction that the $u_n(x \pm y)$ in Eqn. (141) are non-vanishing only in the range $(0, L)$ and they must therefore simultaneously satisfy the requirements

$$0 \leq x + y \leq L \quad \text{and} \quad 0 \leq x - y \leq L.\quad (187)$$

This leads to upper and lower bounds for the integral over y in Eqn. (186) which depend on x via

$$-x \leq y \leq +x \quad \text{for } 0 \leq x \leq L/2 \quad (188)$$

$$-(L-x) \leq y \leq +(L-x) \quad \text{for } L/2 \leq x \leq L. \quad (189)$$

Thus, over the left-half of the allowed x interval, $(0, L/2)$, we have

$$\begin{aligned} W^{(n)}(x, p) &= \frac{1}{\pi\hbar} \int_{-x}^{+x} \left[\sqrt{\frac{2}{L}} \sin\left(\frac{n\pi(x+y)}{L}\right) \right] \left[\sqrt{\frac{2}{L}} \sin\left(\frac{n\pi(x-y)}{L}\right) \right] e^{2ipy/\hbar} dy \\ &= \left(\frac{2}{\pi\hbar L} \right) \left\{ \frac{\sin[2(p/\hbar - n\pi/L)x]}{4(p/\hbar - n\pi/L)} + \frac{\sin[2(p/\hbar + n\pi/L)x]}{4(p/\hbar + n\pi/L)} \right. \\ &\quad \left. - \cos\left(\frac{2n\pi x}{L}\right) \frac{\sin(2px/\hbar)}{(2p/\hbar)} \right\}, \end{aligned} \quad (190)$$

while over the right-half of the interval, $(L/2, L)$, one simply makes the replacement $x \rightarrow L-x$. This form has been derived before (115) - (117), although in at least one reference it is written in terms of Bessel functions ($j_0(z)$) which somewhat obscures its simple derivation.

For a general wave packet solution for the infinite square well, we also require the off-diagonal terms in Eqn. (184). Using the position-space eigenstates in Eqn. (141), over the interval $(0, L/2)$ we find that

$$\begin{aligned} W^{(m,n)}(x, p) &= \frac{1}{\pi\hbar} \int_{-x}^{+x} \left[\sqrt{\frac{2}{L}} \sin\left(\frac{m\pi(x+y)}{L}\right) \right] \left[\sqrt{\frac{2}{L}} \sin\left(\frac{n\pi(x-y)}{L}\right) \right] e^{2ipy/\hbar} dy \\ &= \frac{1}{\pi\hbar} \left[e^{+i(m-n)\pi x/L} \frac{\sin[(2p/\hbar + (m+n)\pi/L)x]}{2pL/\hbar + (m+n)\pi} \right. \\ &\quad + e^{-i(m-n)\pi x/L} \frac{\sin[(2p/\hbar - (m+n)\pi/L)x]}{2pL/\hbar - (m+n)\pi} \\ &\quad - e^{+i(m+n)\pi x/L} \frac{\sin[(2p/\hbar + (m-n)\pi/L)x]}{2pL/\hbar + (m-n)\pi} \\ &\quad \left. - e^{-i(m+n)\pi x/L} \frac{\sin[(2p/\hbar - (m-n)\pi/L)x]}{2pL/\hbar - (m-n)\pi} \right] \end{aligned} \quad (191)$$

and it is easy to check that this result reduces to the expression in Eqn. (190) when $m = n$. In order to extend this to the interval $(L/2, L)$, it is important to note that the substitution $x \rightarrow L-x$ should be made *only* in those terms arising from the integration over dy , namely, the $\sin[(2p/\hbar \pm (m \pm n)/L)x]$ terms.

Using these expressions, the expansion in Eqn. (183), and the Gaussian expansion coefficients in Eqn. (153) for the a_n , we can evaluate the time-dependent Wigner function for the infinite well. As examples, we show in Figs. 29 and 30, $W(x, p; t)$ versus (x, p) at two fractional revival times, namely $T_{rev}/3$ and $T_{rev}/4$, for direct comparison to the position-space probability densities in Figs. 14 and 15 for the same values. (The same initial values of x_0 are used in each case, but we use $n_0 = 40$ here for ease of visualization.) The results are consistent with the expression in Eqn. (181) with smooth isolated Gaussian ‘lumps’ and oscillatory cross-terms; for example, in Fig. 29, the cross-term between the two Gaussians which have the same momentum ($-40\pi\hbar/L \approx -126$ in this case, so $p_A = p_B$), but different central locations ($x_A \neq x_B$) is seen to be oscillatory only in the p variable. These views make clearer the Schrödinger-cat like behavior of the split wave packet at fractional revival times.

8. Quantum carpets

A semi-classical visualization of the initial spreading of bound state wave packets in the infinite well was provided by Born (101), (102) who examined the diverging classical trajectories of particles with differing initial velocities (momenta) in (x, t) plots where such classical paths can be identified with individual ‘world-lines’. An example of such a plot is shown in Fig. 31, which illustrates how the spreading can lead to an almost uniform probability density, giving rise to calculations such as in Eqn. (172).

The corresponding quantum mechanical picture of such behavior can be obtained by examination of the quantum mechanical position-space probability density as a function of time, given by plots of $P(x, t) = |\psi(x, t)|^2$ versus (x, t) . As examples, we show in Fig. 32, the probability density over the first classical period, comparing it to the more interesting structures present over the same time interval starting at the $T_{rev}/3$ fractional revival, as seen in Fig. 33.

To visualize these over even longer time scales, we note that because of the periodicity of the system given by the revival time, it suffices to plot $P(x, t) = |\psi(x, t)|^2$ over the two-dimensional (x, t) space given by $(0, L)$ and $(0, T_{rev}/2)$, such as in Fig. 34, which were first produced by Kinzel (120); such plots have come to be known as *quantum carpets*. The rich structure of ridges and canals apparent in such plots, which are clearly correlated with the spatio-temporal structure of revivals and fractional revivals, have been discussed in a number of approaches (92), (120) - (128), including making use of a traveling wave decomposition of the wavefunction or using Wigner quasi-probability densities.

One useful approach (123), (124) to the visualization of this pattern formation, based on an expansion of the wavepacket in traveling waves, begins by writing the stationary state solutions in the form

$$\begin{aligned}\psi_n(x, t) &= \left[\sqrt{\frac{2}{L}} \sin\left(\frac{n\pi x}{L}\right) \right] e^{-iE_n t/\hbar} \\ &= \left[\frac{1}{i\sqrt{2L}} (e^{in\pi x/L} - e^{-in\pi x/L}) \right] e^{-2\pi i n^2 t/T_{rev}}\end{aligned}\quad (192)$$

so that

$$\psi(x, t) = \sum_{n=1}^{\infty} a_n \psi_n(x, t) \quad (193)$$

for any more general time-dependence state, including localized wave packets. The probability density can then be written as

$$P(x, t) = \psi^*(x, t)\psi(x, t) = P_{cl}(x, t) + P_{qc}(x, t) \quad (194)$$

where one defines *classical* (P_{cl}) and *quantum carpet* (P_{qc}) contributions by

$$P_{cl}(x, t) = \left(\frac{1}{2L}\right) \sum_{n,m=1}^{\infty} a_m^* a_n \left\{ e^{i(n-m)\pi[x/L+2(n+m)t/T_{rev}]} + e^{-i(n-m)\pi[x/L-2(n+m)t/T_{rev}]} \right\} \quad (195)$$

$$P_{qc}(x, t) = \left(\frac{-1}{2L}\right) \sum_{n,m=1}^{\infty} a_m^* a_n \left\{ e^{i(n+m)\pi[x/L+2(n-m)t/T_{rev}]} + e^{-i(n+m)\pi[x/L-2(n-m)t/T_{rev}]} \right\} \quad (196)$$

The contributions to the *classical* component (P_{cl}) are dominated by (x, t) locations at integral multiples of $[x/L \pm 2(n+m)t/T_{rev}]$. For localized wave packets, the n, m values will be peaked near n_0 and using the fact that $T_{rev} = 2n_0 T_{cl}$, the factors in the exponents can be approximated $[x/L \pm 2t/T_{cl}]$ which are therefore similar to those seen in Fig. 31 for

classical trajectories. Since $T_{cl} \ll T_{rev}$, or equivalently, since $n, m \gg 1$, these world-lines, when plotted over the ranges $(0, L)$ and $(0, T_{rev})$, have very ‘flat’ slopes and, also taking into account their diverging paths, soon cover the (x, t) plane almost uniformly, as illustrated in Fig. 35, providing a ‘background’.

The *quantum carpet* (P_{qc}) terms, on the other hand, have dominant contributions from terms in the exponentials of the form $[x/L \pm 2(n - m)t/T_{rev}]$. The $(n - m)$ terms will only contribute significantly for n, m values for which $|n - m| \leq \mathcal{O}(\Delta n)$. This implies that the world-line slopes for these factors will cover a significant fraction of the entire (x, t) ‘plane’, in a few ‘bounces’, with two typical cases shown in Figs. 35 (b) and (c); the interference of such terms with the *classical* background can then give rise to the observed patterns of ridges and canals.

For initial wave packets which are more highly localized (smaller Δx_0 , larger Δn), more obvious features can be resolved (129), similarly to the dependence seen in Fig. 2. The relative ‘sharpness’ of the features can also be seen to arise from the differing pre-factors in the exponentials. For example, the $(n - m)$ pre-factors in the P_{cl} terms will be dominated by small values of $|n - m|$, so that relatively large changes in the corresponding $[x \pm 2(n + m)t/T_{rev}]$ terms will still contribute significantly, enhancing the uniformity of the classical contributions; on the other hand, for the P_{qc} terms, the $(n + m)$ pre-factors are large ($\mathcal{O}(2n_0)$), so that small changes in the accompanying $[x \pm 2|n - m|t/T_{rev}]$ factors will rapidly lead to cancellations, helping to define the ‘contrast’ seen in the quantum carpet images.

It has also been observed that the 2D (in (x, t)) probability density patterns observed here are similar to what have been described as ‘scars’ (130) in spatially two-dimensional $((x, y))$ quantum mechanical systems. We also note that similar techniques have been used to examine other systems which also exhibit exact revivals (125).

E. Variations on the infinite well

Given the pedagogical familiarity and simplicity of the infinite well potential, a number of variations on this system have been studied and we briefly mention three of them.

We have noted that the important time scales for wave packet propagation are determined by the energy eigenvalues through Eqns. (9), (16), and (22), so it is clear that systems with identical (isospectral) or closely related energy spectra will have similar patterns of classical periodicity, wave packet collapse, and revival. For example, pairs of systems defined by superpartner potentials which are related by one-dimensional supersymmetry (131) - (133) have energy spectra which are identical except for the ground state energy and would be expected to exhibit almost the same pattern of revival behavior, at least for $n_0 \gg 1$. The construction of superpartner potentials (134) starts with the assumption of a 1D Hamiltonian with a zero-energy ground state, namely one such that

$$\hat{H}_{(-)}\psi_0(x) = \left(-\frac{\hbar^2}{2m} \frac{d^2}{dx^2} + V_{(-)}(x) \right) \psi_0(x) = 0. \quad (197)$$

Since $\psi_0(x)$ is assumed known, one can define a superpotential for the problem by the identification

$$W(x) \equiv -\frac{\hbar}{\sqrt{2m}} \left(\frac{\psi'_0(x)}{\psi_0(x)} \right). \quad (198)$$

The pair of systems defined by the Hamiltonians

$$\hat{H}_{(\pm)} \equiv -\frac{d^2}{dx^2} + V_{(\pm)}(x) \equiv -\frac{d^2}{dx^2} + \left\{ [W(x)]^2 \pm \frac{\hbar}{\sqrt{2m}} W'(x) \right\} \quad (199)$$

can then be shown to have the same energy level spectrum, with $E_n^{(+)} = E_{n+1}^{(-)}$, except that the zero-energy ground state of $\hat{H}_{(-)}$ ($E_0^{(-)} = 0$) has no counterpart in $\hat{H}_{(+)}$. The wavefunctions in the two systems are related by generalized raising and lowering operators.

The standard infinite well potential of Eqn. (139) can be put into the form of $\hat{H}_{(-)}$ by subtracting the appropriate zero-point energy to write

$$V_{(-)}(x) = V(x) - \frac{\hbar^2 \pi^2}{2mL^2} \quad \text{with} \quad \psi_0^{(-)}(x) = \sqrt{\frac{2}{L}} \sin\left(\frac{\pi x}{L}\right) \quad (200)$$

with quantized energies given by

$$E_n^{(-)} = \frac{\hbar^2 \pi^2}{2mL^2} n(n+2). \quad (201)$$

The superpotential is then given by

$$W(x) = -\frac{\hbar}{\sqrt{2m}} \frac{\pi}{L} \cos\left(\frac{\pi x}{L}\right) \quad (202)$$

and the superpartner potential of the infinite well potential is given by

$$V_{(+)}(x) = \frac{\hbar^2 \pi^2}{2mL^2} \left[2 \csc^2\left(\frac{\pi x}{L}\right) - 1 \right] \quad (203)$$

so that large n wave packets in this potential will have the same pattern of semi-classical periodicity, and exact revivals, as for the infinite well. We note that this potential is a special case of a larger class of Pöschl-Teller potentials and the authors of Ref. (135) have constructed coherent states (see also Refs. (11) - (13)) for such systems, making use of their $SU(1,1)$ symmetries, while the revival structure in Pöschl-Teller and Rosen-Morse (125) and other related potentials (136) have also been considered. Revivals and fractional revivals in other $SU(1,1)$ symmetric systems have also been discussed (137).

We note in passing that the same approach can be used with the harmonic oscillator potential, defining

$$V_{(-)}(x) = \frac{m\omega^2}{2} x^2 - \frac{\hbar\omega}{2} \quad (204)$$

but trivially returns the supersymmetric partner potential

$$V_{(+)}(x) = \frac{m\omega^2}{2} x^2 + \frac{\hbar\omega}{2} \quad (205)$$

and the raising/lowering operator formalism is the standard one seen in textbooks. The use of a phenomenological supersymmetry involving atomic energy levels, has been discussed (138) as it relates to the revivals and fractional revivals of Rydberg atoms and radial squeezed states.

The finite well has been studied by several groups (139), (140) with an eye towards providing a more realistic model system, focusing on the appearance of superrevival time scales since the energy eigenvalue spectrum is no longer exactly quadratic. Aronstein and Stroud (141) have provided a useful description of the bound state energy eigenvalue spectrum which is helpful for the determination of both the global energy spectrum as well as local approximations, useful for wave packet construction. Finally, the addition of a δ -function to the infinite well problem is a staple of the pedagogical literature (142), and its effects on the revival structure of wave packet development has been discussed in Ref. (143).

F. The quantum bouncer

1. Energy eigenfunctions and eigenvalues

One of the more familiar systems of classical mechanics, the ‘bouncer’, has been considered in the context of quantum mechanical wave packet propagation and revivals. This system, defined by the potential

$$V(z) = \begin{cases} +\infty & \text{for } z \leq 0 \\ Fz & \text{for } z > 0 \end{cases}, \quad (206)$$

corresponds to a particle under the influence of a constant force F (such as gravity), but with an infinite wall at $z = 0$ from which the particle bounces. While this system has long been a popular non-trivial example in the pedagogical literature and in collections of problems in quantum mechanics, advances in experimental techniques (144), using reflection from laser-induced evanescent waves, have allowed the observation of such ‘bouncing’ atoms (145), (146) and even the quantum mechanical interference between different atomic trajectories (147).

The classical periodicity for this system is simply twice the time a particle takes to fall from its maximum height, z_0 , and is given by

$$T_{cl} = 2\sqrt{\frac{2mz_0}{F}} \quad (207)$$

and several groups (148) - (151) have considered different aspects of the time-development of (Gaussian) quantum mechanical wave packets, initially centered at z_0 , including their subsequent revival behavior. (The effect on the bouncer of the application of a periodic external driving force, especially on the structure of revivals, has also been discussed (152), (153).)

The Schrödinger equation for this system can be written as

$$-\frac{\hbar^2}{2m} \frac{d^2\psi(z)}{dz^2} + Fz\psi(z) = E\psi(z) \quad (208)$$

and the change of variables

$$z = \rho y + \sigma, \quad \text{where} \quad \rho = \left(\frac{\hbar^2}{2mF}\right)^{1/3} \quad \text{and} \quad \sigma = \frac{E}{F}, \quad (209)$$

reduces it to the familiar Airy equation

$$\frac{d^2\psi(y)}{dy^2} = y\psi(y). \quad (210)$$

The condition that the wavefunction be well-behaved as $z/y \rightarrow +\infty$ excludes the divergent $Bi(y)$ solution, while the boundary condition at the infinite wall, $\psi(z = 0) = 0$, implies that

$$Ai\left(-\frac{\sigma}{\rho}\right) = 0 = Ai(-y_n) \quad (211)$$

and the quantized energy eigenvalues are determined by the zeros (y_n) of the well-behaved $Ai(y)$ solution. (This problem is discussed in a variety of textbooks, but the first analysis using the Schrödinger equation seems to have been done by Breit (154).)

The energy spectrum then has the form

$$E_n = y_n \left(\frac{\hbar^2 F^2}{2m} \right)^{1/3}. \quad (212)$$

The Airy function zeros (y_n) can be derived from standard handbook results, but the energies in the large n limit relevant for wave packet construction can also be easily obtained from a WKB approximation. The WKB quantization condition is

$$\int_0^{z_0} \sqrt{2m(E_n - Fz)} dz = \left(n + \frac{1}{2} + \frac{1}{4} \right) \hbar\pi \quad (213)$$

where we use the appropriate matching coefficients, $C_L = 1/2$ for the infinite wall, and $C_R = 1/4$ for the linear barrier. The resulting energies are given by

$$E_n = \left(\frac{3\pi}{2}(n + 3/4) \right)^{2/3} \left(\frac{\hbar^2 F^2}{2m} \right)^{1/3} \quad \text{where } n = 0, 1, 2, \dots, \quad (214)$$

which agrees with the Airy function analysis (149) to this order in n . (We note that experimental evidence for the quantized nature of the bound state spectrum of neutrons in the Earth's gravitational field (155) has recently appeared, motivating additional studies of wave packet dynamics (156) of such systems.) This expression can also be used to associate the central value of n_0 in the eigenstate expansion with the initial position, z_0 , via

$$Fz_0 = E_{initial} = \left(\frac{3\pi}{2}(n_0 + 3/4) \right)^{2/3} \left(\frac{\hbar^2 F^2}{2m} \right)^{1/3} \quad (215)$$

which will prove useful.

2. Classical period and revival time

The classical periodicity of the system, as encoded in the energy eigenvalue spectrum, is given by

$$T_{cl} = \frac{2\pi\hbar}{|E'(n_0)|} = \frac{3\pi\hbar(n_0 + 3/4)}{E(n_0)} = 2\sqrt{\frac{2mz_0}{F}} \quad (216)$$

(where we have used the z_0/n_0 identification in Eqn. (215)) and is consistent with the classical result. As an example of the semi-classical, short-term time-development of a Gaussian wave packet in this potential, we show in Fig. 36 the position- and momentum-space probability densities for such a packet with

$$z_0 = 25 \quad \text{and} \quad \Delta z_0 = 1 \quad (217)$$

using the parameters

$$\hbar = 1 \quad , \quad 2m = 1 \quad , \quad F = 1 \quad (218)$$

so that $T_{cl} = 10$. On the left of Fig. 36, the position-space probability is initially seen to spread in a manner which is numerically consistent with Eqn. (100), while the calculated position value $\langle z \rangle_t$ (solid curve) agrees well with the classical expectation for the trajectory (dashed) except, of course, for the cusp at the 'bounce'. The packet exhibits the standard 'interference' pattern during the collision with the wall (106), (157), (158) at the 'bounce',

and then reforms into something like the initial packet (compare to the dotted initial packet superimposed on the $t = 10$ case), only wider.

For the momentum-space distributions (shown on the right of Fig. (36)), we also see features of both the classical motion and the uniformly accelerated wave packet, as in Eqn. (95a). The expectation value of momentum $\langle p \rangle_t$, calculated from $|\phi(p, t)|^2$ and plotted as the solid curve, is once again consistent with the classical trajectory (dashed curve), except near the discontinuous, impulsive change in momentum values at the ‘bounce’. The shape of the momentum-distribution follows the form expected from Eqn. (94), namely uniform translation with no change in shape, from $t = 1 \rightarrow t = 3$ and then again from $t = 8 \rightarrow t = 10$, that is, during the time when it is not in collision with the wall, but with a definite final change in shape, compared to the initial $|\phi_0(p)|^2$ superimposed on the $t = 10$ result, resulting from the collision with the wall. The dotted vertical lines indicate the values of $p = 0$, and also the classically expected minimum and maximum values of momentum given by $\pm p_M = \pm\sqrt{2mE} = \pm\sqrt{2mFz_0}$. The change in shape can be understood, in great part, from purely classical arguments (149), (151).

Using Eqn. (16), the revival time is then given by

$$T_{rev} = \frac{4\pi\hbar}{|E''(n_0)|} = \frac{16mz_0^2}{\pi\hbar} \quad (219)$$

which can be compared to the similar result for the infinite well in Eqn. (145) which obviously has the same dimensions, but a differing dependence on the initial energy. Gea-Banacloche (149) examined the explicit time-dependence of Gaussian wave packets for the ‘quantum bouncer’ and noted that packets returned to their classical periodicity, but half a period out of phase, at a time half that of Eqn. (219), which he described as the revival time and this would correspond to a $p/q = 1/2$ revival in the language of Averbukh and Perelman (34); discussions of the structure of fractional revivals (148) in this system have also appeared. The probability density at $t = 0$ and near the first two (complete) revivals are shown in Fig. 37, showing the revival structure becoming increasingly approximate as the effect of higher order $((n - n_0)^3/T_{super})$ terms becomes important.

As noted in Sec. II.C, during the collapsed phase, the probability density will be consistent with an incoherent sum of the individual probability densities, as in Eqn. (31). We observe this behavior at the bottom of Fig. 37 where we plot $|\psi(x, T^*)|^2$ at a time T^* which is not close to any obvious fractional revival time. The anti-correlation between the ‘wiggleness’ of the wavefunction and its magnitude, familiar from semi-classical discussions of stationary states or from the WKB approximation, is apparent. For additional comparison, we plot a purely classical probability density, given by

$$P_{cl}(z) = \frac{2}{\tau} \frac{1}{\sqrt{E - V(z)}}, \quad (220)$$

based on simple “*How much time, dt , does the particle spend in a given position bin, dx ?*” arguments or, equivalently, given by the pre-factor of a WKB wavefunction. In this case, the classical distribution is given by

$$P_{cl}(z; z_0) = \frac{1}{2\sqrt{z_0(z_0 - z)}} \quad (221)$$

and is shown in Fig. 37(b) as the dotted curve. The visualization of the time-dependent expectation values in both the short-term semiclassical and the long-term revival phases have been discussed in Ref. (151), where, for example, the classical position-space average values, using Eqn. (221), are given by

$$\langle z \rangle = \frac{2z_0}{3}, \quad \langle z^2 \rangle = \frac{8z_0^2}{15} \quad \text{and} \quad \Delta z = \frac{2z_0}{\sqrt{45}} \approx 0.3z_0 \quad (222)$$

and quantum wave packets collapse to near these values during much of the time between revivals.

G. 2D rotor and related systems

1. Two dimensional free quantum rotor

The problem of a particle confined to a circle of radius L , but otherwise free to rotate, defines the free quantum rotor, and is described by the Schrödinger equation

$$-\frac{\hbar^2}{2I} \frac{d^2\psi_m(\theta)}{d\theta^2} = E_m\psi_m(\theta) \quad (223)$$

where $I \equiv \mu L^2$ is the moment of inertia. (We will occasionally denote the particle mass by μ to avoid confusion with standard notation for angular quantum numbers when appropriate.) The quantized energies and normalized wavefunctions are then given by

$$E_m = \frac{\hbar^2 m^2}{2I} \quad \text{and} \quad \psi_m(\theta) = \frac{1}{\sqrt{2\pi}} e^{im\theta} \quad (224)$$

for $m = 0, \pm 1, \pm 2, \dots$. The solutions with $+m, -m$ for $|m| \neq 0$ are doubly degenerate, corresponding to the equivalence of clockwise and counter clockwise motion. The angular wavefunctions can also be written in the form

$$\psi_m(\theta) = \begin{cases} 1/\sqrt{2\pi} & \text{for } m = 0 \\ \cos(m\theta)/\sqrt{\pi} & \text{for } m > 0 \\ \sin(m\theta)/\sqrt{\pi} & \text{for } m < 0 \end{cases} \quad (225)$$

which displays the pattern of degeneracies in a different way.

The classical system would have an energy, classical frequency, and period associated by

$$E = \frac{1}{2} I \omega^2 \quad \text{and} \quad T_{cl} = \frac{2\pi}{\omega} = 2\pi \sqrt{\frac{I}{2E}}. \quad (226)$$

The corresponding quantum mechanical period requires

$$|E'_m| = \frac{\hbar^2 m}{I} = \hbar \sqrt{\frac{2E_m}{I}} \quad (227)$$

so that

$$T_{cl} = \frac{2\pi\hbar}{|E'_m|} = 2\pi / \sqrt{2E_m/I} \quad (228)$$

as expected.

For this system, with purely quadratic dependence on the single quantum number, the revival time is given by

$$T_{rev} = \frac{4\pi I}{\hbar} = \frac{4\pi\mu L^2}{\hbar}. \quad (229)$$

This system can, of course, be thought of as a free particle with periodic boundary conditions, to be compared to 1D infinite well (with reflecting boundary conditions) which has a very similar energy spectrum. Localized (angular) wave packets can then be constructed with many of the same properties as those in the 1D infinite well, including zero (angular) momentum states with shorter revival times, and fractional revivals at p/q multiples of T_{rev} . The related problem of quantum diffusion (159) on a circular one-dimensional lattice has been found to have similar revival-like behavior, while a propagator approach (98), (99) for the 1D problem has also shown explicit evidence for fractional revivals. The time evolution of the quantum rotor has also been examined in an interesting way in Ref. (64).

2. Quantum pendulum

A related problem, with a far richer structure of classical time-dependence and quantum energy eigenvalue spectra, is the quantum pendulum, defined by the potential

$$V(\theta) = -V_0 \cos(\theta) \quad (230)$$

where $V_0 = mgl$ for a pendulum under the influence of gravity, or $V_0 = qEL$ for a point charge q acted on by a constant electric field, E . This problem was first studied by Condon (160) in the early days of quantum theory, and is a staple of the pedagogical literature, appearing as an example of perturbation theory in many textbooks and collections of problems. The corresponding Schrödinger equation can be written in the form

$$-\frac{\hbar^2}{2I} \frac{d^2\psi(\theta)}{d\theta^2} - V_0 \cos(\theta)\psi(\theta) = E_m\psi(\theta). \quad (231)$$

This problem is of interest since it reduces to the free-rotor case in the high energy limit ($E_n \gg +V_0$), while it has the harmonic oscillator case in the limit of small oscillations, with predictable anharmonic corrections derivable from the $\cos(\theta)$ term. The classical problem is also more interesting as the periodicity can be evaluated in both limits, as well as in general case (using elliptic integrals), with the limiting case of $E \approx +V_0$ defining the separatrix where the classical period diverges, namely the ‘stuck on top’ point.

The quantum mechanical problem can be written as one of the familiar equations of mathematical physics, namely Mathieu’s equation. Recently, this problem has been studied both in the context of understanding the connections between the classical periodicity and the quantum energy eigenstates, but also in terms of the revival behavior. The authors of Ref. (161) use fourth-order perturbation theory and numerical evaluation of the energy eigenvalues to discuss the classical periodicity in the low-energy, high-energy, and separatrix limits, where the classical divergence in T_{cl} is ‘softened’ by quantum effects, while also discussing the energy dependence of the quantum revival and super-revival times. For example, the lowest-order anharmonic correction to the energies in the low-energy limit is given by

$$E_n^{(1)} = \frac{\hbar^2}{32I}(2n^2 + 2n + 1) \quad (232)$$

which gives a (non-infinite) revival time

$$T_{rev} = \frac{2\pi\hbar}{|E_n''|/2} = \frac{32\pi I}{\hbar} \quad (233)$$

which is independent of V_0 and 8 times larger than the revival time for the high-energy, pure-rotor limit in Eqn. (229).

Revivals in 3D rotational systems (with energy eigenvalues proportional to $l(l+1)$) have also been studied (38), (163), (164).

IV. TWO- AND THREE-DIMENSIONAL QUANTUM SYSTEMS

A number of integrable two-dimensional infinite well or quantum billiard geometries lend themselves to the study of quantum revival behavior in systems with several quantum numbers, and we focus here on three polygonal billiard footprints, namely the square ($N = 4$), equilateral triangle ($N = 3$), and circular ($N \rightarrow \infty$) infinite wells. Discussions of time-dependent wave packet solutions of the first and third cases go back to at least de Broglie (4) and also provide useful examples of the connections of the short-term time-development of wavepackets to classical periodic orbits.

We note that evidence of wave packet revivals has been presented from numerical simulations of quantum systems with classically chaotic behavior (165), with specific examples being illustrated for the stadium billiard.

A. Two dimensional infinite well and variations

For the two-dimensional infinite square well (with dimensions $L_x \times L_y = L \times L$), the problem simplifies to two copies of a single 1-D infinite well because of the separability of the potential. For example, the energy eigenvalues, $E(n_x, n_y)$, and position-space eigenstates, $w_{(n_x, n_y)}(x, y)$, are given by

$$E(n_x, n_y) = \frac{\hbar^2 \pi^2 (n_x^2 + n_y^2)}{2mL^2} \quad \text{and} \quad w_{(n_x, n_y)}(x, y) = u_{(n_x)}(x)u_{(n_y)}(y) \quad (234)$$

where $n_x, n_y = 1, 2, 3, \dots$ are the appropriate quantum numbers and the $u_n(x)$ are given by Eqn. (141). The two non-vanishing revival times are given by Eqn. (63) and are simply related to each other via

$$T_{rev}^{(n_x)} = \frac{4mL^2}{\hbar\pi} = T_{rev}^{(n_y)} \quad (235)$$

with no cross-term ($T_{rev}^{(n_x, n_y)}$) present. Therefore, the quantum revival structure is very simply related to that of the 1-D infinite well, including the possibilities of special ‘symmetric’ revivals for zero-momentum ($\mathbf{p}_0 = (0, 0)$) wave packets at particular locations, such as for initial values of $(x_0, y_0) = (L/2, L/2)$ or $(L/3, 2L/3)$, as well as the same rich structure of fractional revivals. For rectangular infinite wells with commensurate ($L_x \times L_y$, $L_x/L_y = p/q$) or incommensurate ($L_x/L_y \neq p/q$) sides, the structure of the revival times may be more complex and interesting examples have been given in Refs. (79) and (80).

The pattern of closed or periodic orbits is also interesting as the path lengths for closed orbits in the 2-D square billiard can be readily deduced from simple geometric arguments and are given by

$$L(p, q) = 2L\sqrt{p^2 + q^2} \quad (236)$$

where $2p, 2q$ count the number of ‘hits’ on the horizontal and vertical walls respectively, before returning to the starting point in phase space. The corresponding classical periods for such closed trajectories are given by

$$T_{cl}^{(po)} = \frac{L(p, q)}{v_0} \quad (237)$$

where v_0 is the classical speed. Such orbits can be produced by point particles in the 2-D billiard, starting from any initial location, (x_0, y_0) , inside the box, provided they are ‘pointed’ appropriately, namely in the $\tan(\theta) = q/p$ direction. The values of

$$\theta = \tan^{-1}(q/p) \quad \text{and} \quad T_{cl}^{(po)}/\tau = \sqrt{p^2 + q^2} \quad (238)$$

(where $\tau \equiv 2L/v_0$ is the period for the simplest, ‘back-and-forth’ closed trajectory) for many of the low-lying cases are tabulated in Ref. (97).

The condition for periodic orbits in Eqn. (65) can be implemented very easily in this case, and we will examine this example in detail. For such closed orbits to occur we require that

$$p \left(\frac{2mL^2}{\hbar\pi n_x} \right) = pT_{cl}^{(n_x)} = qT_{cl}^{(n_y)} = q \left(\frac{2mL^2}{\hbar\pi n_y} \right) \quad (239)$$

or $n_y = n_x(q/p)$. Substituting this back into Eqn. (234), as well as equating the quantized total energy, $E(n_x, n_y)$, with the classical kinetic energy, gives

$$\begin{aligned} \frac{1}{2}mv_0^2 \longleftrightarrow E(n_x, n_y) &= \frac{\hbar^2 \pi^2}{2mL^2} (n_x^2 + n_y^2) \\ &= \frac{\hbar^2 \pi^2}{2mL^2} \left(n_x^2 + n_x^2 \left(\frac{q}{p} \right)^2 \right) \\ &= \frac{\hbar^2 \pi^2}{2mL^2} \left[\frac{n_x^2 (p^2 + q^2)}{p^2} \right] \end{aligned} \quad (240)$$

or

$$n_x = \left(\frac{mLv_0}{\hbar\pi} \right) \frac{p}{\sqrt{p^2 + q^2}} \quad \text{and} \quad n_y = \left(\frac{mLv_0}{\hbar\pi} \right) \frac{q}{\sqrt{p^2 + q^2}} \quad (241)$$

so that

$$T_{cl}^{(p_0)} = pT_{cl}^{(n_x)} = p \left(\frac{2mL^2}{\hbar\pi n_x} \right) = \frac{2L\sqrt{p^2 + q^2}}{v_0} \quad (242)$$

which is consistent with the purely classical, and geometrical, result from Eqn. (237).

We illustrate the short-term time-dependence of such wave packets, through plots of $|A(t)|^2 = |A_x(t)A_y(t)|^2$ versus t , in Fig. 38. The results shown there are for wave packets characterized by initial positions $(x_0, y_0) = (L/2, L/2)$ and initial momenta given by $(p_{0x}, p_{0y}) = (p_0 \cos(\theta), p_0 \sin(\theta))$ where we use $p_0 = 400\pi$ and vary $\theta = \tan^{-1}(p_{0y}/p_{0x})$; we also use $\Delta x_0 = \Delta y_0 = 0.05$ and the same physical parameters as in Eqn. (157). With these values, the classical period (for the simplest back-and-forth motion), $\tau = 2L/v_0$, the spreading time, t_0 (from Eqn. (77)), and the revival time, T_{rev} (from Eqn. (235)), are given numerically by

$$\tau = \frac{(2\mu)L}{p_0} = \frac{1}{400\pi} \approx 0.8 \times 10^{-3}, \quad (243)$$

$$t_0 = \left(\frac{2\mu}{\hbar} \right) \Delta x_0^2 = (0.05)^2 = 2.5 \times 10^{-3} \quad (244)$$

$$T_{rev} = \frac{4\mu L^2}{\hbar\pi} = \frac{2}{\pi} \approx 0.64. \quad (245)$$

The wave packet is seen to exhibit a reasonable number of classical periods before significant spreading occurs, with the revival time scale being much larger than both; the locations of classical closed or periodic orbits are denoted by stars, with the closed orbit patterns indicated for some of the simpler 2D trajectories.

B. Isosceles ($45^\circ - 45^\circ - 90^\circ$) triangle billiard

The energy eigenvalues and wavefunctions for a special 2-D triangular billiard ‘footprint’ can be easily derived (166) - (168) from those of the two-dimensional square infinite well solutions in Eqn. (234). The standard results for the 2-D square well

$$E(n_x, n_y) = \frac{\hbar^2\pi^2}{2mL^2} (n_x^2 + n_y^2) \quad \text{and} \quad w_{(n_x, n_y)}(x, y) = u_{(n_x)}(x)u_{(n_y)}(y) \quad (246)$$

hold for any integral $n_x, n_y \geq 1$ and for $n_x = n_y$ there is a single state, while for $n_x \neq n_y$, there is a two-fold degeneracy. Linear combinations of these solutions can be written in form

$$w_{(n,m)}^{(-)}(x, y) = \frac{1}{\sqrt{2}} [u_{(n)}(x)u_{(m)}(y) - u_{(m)}(x)u_{(n)}(y)] \quad (m \neq n) \quad (247)$$

$$w_{(n,m)}^{(+)}(x, y) = \frac{1}{\sqrt{2}} [u_{(n)}(x)u_{(m)}(y) + u_{(m)}(x)u_{(n)}(y)] \quad (m \neq n) \quad (248)$$

$$w_{(n,n)}^{(o)}(x, y) = u_{(n)}(x)u_{(n)}(y) \quad (249)$$

which have the same energy degeneracy, but exhibit different patterns of nodal lines. These alternative forms are useful since they allow one to discuss the energy eigenvalues and

eigenfunctions of the $45^\circ - 45^\circ - 90^\circ$ triangle billiard formed by ‘folding’ the square along a diagonal, since the $w_{(n,m)}^{(-)}(x, y)$ now satisfy the appropriate boundary condition along the new hypotenuse as one can easily see from Eqn. (247) that $w_{(n,m)}^{(-)}(x, y = x) = 0$, by construction. The allowed eigenvalues for this case are still given by

$$E(n_x, n_y) = \frac{\hbar^2 \pi^2}{2mL^2} (n_x^2 + n_y^2) \quad \longrightarrow \quad E(n, \tilde{n}) = \frac{\hbar^2 \pi^2}{2mL^2} (n^2 + \tilde{n}^2) \quad (250)$$

but now with only a single $(n_x, n_y) \rightarrow (n, \tilde{n})$ state allowed, with corresponding wavefunctions given by Eqn. (247), but multiplied by $\sqrt{2}$ to account for the different normalization needed in the smaller area billiard.

The single common revival time in the $45^\circ - 45^\circ - 90^\circ$ triangle billiard is then still given by Eqn. (235) and localized wave packets can also be constructed, now using the appropriately normalized analogs of the wavefunctions in Eqn. (247), once again, provided they are kept away from any of the infinite wall boundaries.

The structure of the classical closed or periodic orbits in this case is the same as for the square billiard, since all of the standard (p, q) orbits in the 2-D square well are simply reflected off the new diagonal wall (along the hypotenuse), giving rise to the same allowed orbits as in Eqn. (238). The only new feature in the semi-classical propagation of such wave packet solutions in this ‘folded’ geometry is the existence of a special isolated closed orbit (97), (168) at 135° (one which bisects the 90° right angle, bouncing normally off the hypotenuse, and returning to the corner) which has path lengths which are multiples of $(\sqrt{1^2 + 1^2})L/2 = \sqrt{2}L/2$, namely half that of the standard $(p, q) = (1, 1)$ features. When we construct wave packets using parameters appropriate to this geometry, we see twice as many features in the $A(t)$ plot for the $(1, 1)$ case because of this special classical closed orbit, but otherwise reproduce the results shown in Fig. 38. Extensions to 3D cubic or rectangular parallelepiped billiard systems are also possible.

C. Equilateral triangle billiard

1. Energy eigenvalues and eigenfunctions

It is perhaps an under-appreciated fact that the energy eigenvalues and position-space wave functions for a particle in an equilateral ($60^\circ - 60^\circ - 60^\circ$) triangular infinite well (or billiard) of side L are available in closed form. They have been discussed by many authors, in a variety of different contexts, using complementary methods of derivation (169) - (172) and more recently in the context of wave packet revivals (173). For definiteness in what follows, we will assume such a triangular billiard with vertices located at $(0, 0)$, $(L/2, \sqrt{3}L/2)$, and $(-L/2, \sqrt{3}L/2)$ and we will denote the particle mass by μ to avoid confusion with standardly used notation for various quantum numbers. With this notation, the resulting energy spectrum is given by

$$E(m, n) = \frac{\hbar^2}{2\mu L^2} \left(\frac{4\pi}{3} \right)^2 (m^2 + n^2 - mn) \quad (251)$$

for integral values of m, n , with the restriction that $m \geq 2n$. (In what follows, we will use the notation of Ref. (171) except for a minor relabeling, for the energies and wavefunctions.)

For the case of $m > 2n$, there are two degenerate states with different symmetry properties which can be written in the forms

$$w_{(m,n)}^{(-)}(x, y) = \sqrt{\frac{16}{L^2 3 \sqrt{3}}} \left[\sin\left(\frac{2\pi(2m-n)x}{3L}\right) \sin\left(\frac{2\pi ny}{\sqrt{3}L}\right) - \sin\left(\frac{2\pi(2n-m)x}{3L}\right) \sin\left(\frac{2\pi my}{\sqrt{3}L}\right) - \sin\left(\frac{2\pi(m+n)x}{3L}\right) \sin\left(\frac{2\pi(m-n)y}{\sqrt{3}L}\right) \right] \quad (252)$$

and

$$w_{(m,n)}^{(+)}(x, y) = \sqrt{\frac{16}{L^2 3 \sqrt{3}}} \left[\cos\left(\frac{2\pi(2m-n)x}{3L}\right) \sin\left(\frac{2\pi ny}{\sqrt{3}L}\right) - \cos\left(\frac{2\pi(2n-m)x}{3L}\right) \sin\left(\frac{2\pi my}{\sqrt{3}L}\right) + \cos\left(\frac{2\pi(m+n)x}{3L}\right) \sin\left(\frac{2\pi(m-n)y}{\sqrt{3}L}\right) \right]. \quad (253)$$

One can confirm by direct differentiation that they satisfy the 2-D Schrödinger equation, with the energy eigenvalues in Eqn. (251), as well as the appropriate boundary conditions. Extending earlier results, we have here also included the correct normalizations, since we are, of course, interesting in expanding Gaussian wave packets in such eigenstates.

For the special case of $m = 2n$, there is a single non-degenerate state for each value of n , given by

$$w_{(2n,n)}^{(o)}(x, y) = \sqrt{\frac{8}{L^2 3 \sqrt{3}}} \left[2 \cos\left(\frac{2\pi nx}{L}\right) \sin\left(\frac{2\pi ny}{\sqrt{3}L}\right) - \sin\left(\frac{4\pi ny}{\sqrt{3}L}\right) \right]. \quad (254)$$

Clearly these states satisfy

$$w_{(m,n)}^{(\pm)}(-x, y) = \pm w_{(m,n)}^{(\pm)}(x, y), \quad w_{(m,n)}^{(o)}(-x, y) = +w_{(m,n)}^{(o)}(x, y) \quad (255)$$

and the $w_{(m=2n,n)}^{(\pm)}(x, y)$ states also satisfy

$$w_{(m=2n,n)}^{(+)}(x, y) = \sqrt{2} w_{(2n,n)}^{(o)}(x, y) \quad (256)$$

$$w_{(m=2n,n)}^{(-)}(x, y) = 0.$$

The pattern of energy level degeneracies, and wavefunction symmetries is thus very similar to that for the 2-D square billiard, especially when the solutions for that problem are written in the form in Eqns. (247), (248), and (249). (See Ref. (174) for a discussion of such pairwise degeneracies in 2D polygonal billiards.)

2. Classical periodicity and revival times

Turning now to the time-dependence of wave packets in this geometry, the long-term, revival time scales in this two quantum number system are given by Eqns. (63) and (64) as

$$T_{rev}^{(m)} = \frac{2\pi\hbar}{|\partial^2 E / \partial m^2|/2}, \quad T_{rev}^{(n)} = \frac{2\pi\hbar}{|\partial^2 E / \partial n^2|/2}, \quad \text{and} \quad T_{rev}^{(m,n)} = \frac{2\pi\hbar}{|\partial^2 E / \partial m \partial n|} \quad (257)$$

which all give the single common revival time

$$T_{rev}^{(m)} = T_{rev}^{(n)} = T_{rev}^{(m,n)} \equiv T_{rev} = \frac{9\mu L^2}{4\hbar\pi} \quad (258)$$

and exact revivals (just as for the 2-D square well) and fractional revivals are present in this system, with a single revival time guaranteed for any and all possible initial wave packets. Thus, both the $N = 3$ and $N = 4$ polygonal billiards (the equilateral triangle and square) exhibit similar and simple energy eigenvalues and exact quantum revivals. Just as with the 1D and 2D infinite wells, we note that special, shorter-time scale revivals are also possible in the equilateral triangle case for zero-momentum ($(p_{0x}, p_{0y}) = (0, 0)$) wave packets initially centered at ‘symmetric’ locations within the triangular billiard, such as at the geometric center, and half-way down a bisector (173).

The short-term, classical periodicity of quantum wave packets in this geometry can also be determined from calculations of

$$T_{cl}^{(m)} = \frac{2\pi\hbar}{|\partial E/\partial m|} = \left[\frac{9\mu L^2}{4\hbar\pi} \right] \frac{1}{(2m - n)} \quad (259)$$

$$T_{cl}^{(n)} = \frac{2\pi\hbar}{|\partial E/\partial n|} = \left[\frac{9\mu L^2}{4\hbar\pi} \right] \frac{1}{(2n - m)}. \quad (260)$$

The condition leading to closed orbits can then be written as

$$\frac{(2m - n)}{(2n - m)} = \frac{T_{cl}^{(n)}}{T_{cl}^{(m)}} = \frac{p}{q} \quad \text{or} \quad n = m \left(\frac{2p + q}{2q + p} \right). \quad (261)$$

If we substitute this condition into the energy spectrum in Eqn. (251), as well as equating the quantum energies with the classical kinetic energy, $\mu v_0^2/2$ (where v_0 is the classical speed), we are led to the association

$$\frac{1}{2}\mu v_0^2 \longleftrightarrow E(m, n) = \left(\frac{16\pi^2}{9} \right) \left(\frac{\hbar^2}{2\mu L^2} \right) \left[m^2 + m^2 \left(\frac{2p + q}{2q + p} \right)^2 - m^2 \left(\frac{2p + q}{2q + p} \right) \right] \quad (262)$$

or

$$\left(\frac{2\mu v_0 L}{4\pi\hbar} \right)^2 = m^2 \left[\frac{3(p^2 + pq + q^2)}{(2q + p)^2} \right]. \quad (263)$$

This implies that

$$m = \left(\frac{2\mu v_0 L}{4\pi\hbar} \right) \frac{(2q + p)}{\sqrt{3}\sqrt{p^2 + pq + q^2}} \quad \text{and} \quad n = \left(\frac{2\mu v_0 L}{4\pi\hbar} \right) \frac{(2p + q)}{\sqrt{3}\sqrt{p^2 + pq + q^2}}. \quad (264)$$

The period for classical, closed/periodic orbits is then given by

$$T_{cl}^{(p_0)} = p T_{cl}^{(m)} = \frac{L\sqrt{3}\sqrt{p^2 + pq + q^2}}{v_0} = \frac{L(p, q)}{v_0} \quad (265)$$

where

$$L(p, q) = d(p, q) = L\sqrt{3}\sqrt{p^2 + pq + q^2} \quad (266)$$

are the corresponding path lengths for periodic orbits. The possible classical closed or periodic orbits can be derived from a geometric construction (involving tiling of the 2-D plane, just as for the square case) giving this same result. (See Refs. (174) and (175))

for discussions of the derivation of energy eigenvalues and eigenfunctions for convex plane polygonal billiards using tiling methods.)

We note that the special cases of $2m = n$ and $2n = m$ correspond to $q = 0$ and $p = 0$ respectively, both of which give $L(p, q) = \sqrt{3}L$. In these cases, one of the classical periods from Eqn. (260) formally goes to infinity and this can be understood classically from the corresponding path length, which corresponds to periodic, ‘back and forth’ motion from one corner, along a bisector, to the opposite side, but with no repetition in the complementary direction. (See also Ref. (171) for a derivation of the quantized energies from which this effect can be also inferred.)

Because of the (relatively) simple form of the allowed wavefunctions in Eqns. (252) and (253), involving trigonometric functions, just as for the 1-D infinite well, one can evaluate the expansion coefficients for any 2-D Gaussian wave packet by extending the region of integration from the (finite) triangular region to the entire 2-D space, so long as the initial wave packet is well away from any of the walls. The required Gaussian-type integrals are of the forms

$$\int_{-\infty}^{+\infty} e^{ip_0(x-x_0)/\hbar} e^{-(x-x_0)^2/2b^2} \cos\left(\frac{Cx}{a}\right) dx = \frac{b\sqrt{2\pi}}{2} \left[e^{iCx_0/a} e^{-b^2(C/a+p_0/\hbar)^2/2} \right. \\ \left. + e^{-iCx_0/a} e^{-b^2(-C/a+p_0/\hbar)^2/2} \right] \quad (267)$$

and

$$\int_{-\infty}^{+\infty} e^{ip_0(x-x_0)/\hbar} e^{-(x-x_0)^2/2b^2} \sin\left(\frac{Cx}{a}\right) dx = \frac{b\sqrt{2\pi}}{2i} \left[e^{iCx_0/a} e^{-b^2(C/a+p_0/\hbar)^2/2} \right. \\ \left. - e^{-iCx_0/a} e^{-b^2(-C/a+p_0/\hbar)^2/2} \right] \quad (268)$$

with similar expressions for y -integrations. The resulting closed form expressions for the expansion coefficients can be used in calculations of the auto-correlation function to illustrate the long-term revival structure of wave packets, as well as the short-term, semi-classical propagation giving rise to closed orbits of the form in in Eqn. (265); for example, the analog of Fig. 38 for the equilateral triangle billiard have been presented in Ref. (173).

A ‘folding’ of the equilateral ($60^\circ - 60^\circ - 60^\circ$) triangle along a bisector yields another special triangular geometry, namely a $30^\circ - 60^\circ - 90^\circ$ right triangle. The energy eigenvalues and eigenfunctions for this case can also be trivially obtained from those of Eqn. (252) as they satisfy the new boundary condition along the ‘fold’. Such a system will have the same energy eigenvalues as in Eqn. (251) (but with only one (m, n) combination, with $m > 2n$, possible) and the same common revival time, T_{rev} , as in Eqn. (258). Wave packet solutions can also be constructed (remembering to include an additional factor of $\sqrt{2}$ to account for the normalization difference) from the $w_{(m,n)}^{(-)}(x, y)$ in Eqn. (252).

Finally, we note that Liboff (176) has displayed a subset of the wavefunctions and energy eigenstates for the hexagonal ($N = 6$ regular polygon) which can be seen to also give exact revival behavior.

D. Circular billiard and variations

1. Energy eigenvalues and eigenfunctions

We finally turn our attention to the $N \rightarrow \infty$ limit of the N -sided regular polygonal billiard, namely the circular infinite well, which has been explored (177) in terms of quantum

revivals. The potential for this problem can be defined by

$$V_C(r) = \begin{cases} 0 & \text{for } r < R \\ \infty & \text{for } r \geq R \end{cases} \quad (269)$$

and we once again use the notation μ for the particle mass. The (unnormalized) solutions of the corresponding 2-D Schrödinger equation are given by

$$u_{(m)}(r, \theta) = J_{|m|}(kr)e^{im\theta} \quad (270)$$

where the quantized angular momentum values are given by $L_z = m\hbar$ for $m = 0, \pm 1, \pm 2, \dots$ and the $J_{|m|}(kr)$ are the (regular) Bessel functions of order $|m|$. The angular eigenstates can also be written in the form in Eqn. (225).

The wavenumber, k , is related to the energy via $k = \sqrt{2\mu E/\hbar^2}$ and the energy eigenvalues are quantized by application of the boundary conditions at the infinite wall at $r = R$, namely $J_{|m|}(z = kR) = 0$. The quantized energies are then given by

$$E_{(m,n_r)} = \frac{\hbar^2 [z_{(m,n_r)}]^2}{2\mu R^2} \quad (271)$$

where $z_{(m,n_r)}$ denotes the zeros of the Bessel function of order $|m|$, and n_r counts the number of radial nodes. A general time-dependent state in this system can be written in the form

$$\psi(r, \theta, t) = \sum_{n_r=0}^{\infty} \sum_{m=-\infty}^{+\infty} a_{(m,n_r)} [N_{(m,n_r)} J_{|m|}(k_{(m,n_r)} r)] \left(\frac{e^{im\theta}}{\sqrt{2\pi}} \right) e^{-iE_{(m,n_r)} t/\hbar} \quad (272)$$

where the radial normalization factors are determined by insisting that

$$\int_0^R [N_{(m,n_r)} J_{|m|}(k_{(m,n_r)} r)]^2 r dr = 1. \quad (273)$$

The energy spectrum is doubly degenerate for $|m| \neq 0$ corresponding to the equivalence of clockwise and counter-clockwise ($m > 0$ and $m < 0$) motion. We therefore see a pattern of degeneracies very similar to that of both the square and equilateral triangle wells, with two equal energy states for each ($|m| > 0, n_r$) value, and a single one for each ($m = 0, n_r$). Because the quantum number dependence of the energy eigenvalues is the determining factor in the structure of wave packet revivals, we need to examine the m, n_r dependence of the $E_{(m,n_r)} \propto [z_{(m,n_r)}]^2$.

As a first approximation, one can look at the large z behavior of the Bessel function solutions for fixed values of $|m|$, namely

$$J_{|m|}(z) \longrightarrow \sqrt{\frac{2}{\pi z}} \cos \left(z - \frac{|m|}{2} - \frac{\pi}{4} \right) + \dots \quad (274)$$

With this approximation, the zeros are given by

$$z_{(m,n_r)} - \frac{|m|}{2} - \frac{\pi}{4} \approx (2n_r + 1) \frac{\pi}{2} \quad \text{or} \quad z_{(m,n_r)} \approx \left(n_r + \frac{|m|}{2} + \frac{3}{4} \right) \pi. \quad (275)$$

If this result were exact, the quantized energies would depend on two quantum numbers, in at most a quadratic manner, and there would be exact wave packet revivals, just as for

the 2-D square or equilateral triangle billiards. However, there are important corrections to this first-order formula which means that the Bessel function zeros are not given by exact integral values: however, a useful approximation in the large quantum number limit relevant for wave packet expansions can be obtained in a straightforward and accessible way by use of the WKB approximation.

The two-dimensional Schrödinger equation for the radial wavefunction can be written in the form

$$-\frac{\hbar^2}{2\mu} \left(\frac{d^2 R(r)}{dr^2} + \frac{1}{r} \frac{dR(r)}{dr} \right) + \frac{\hbar^2 m^2}{2\mu r^2} R(r) = ER(r) \quad (276)$$

and to recast this into a one-dimensional equation suitable for the WKB approximation we write $u(r) \equiv R(r)/\sqrt{r}$ to obtain

$$-\frac{\hbar^2}{2\mu} \frac{d^2 u(r)}{dr^2} + \frac{\hbar^2(m^2 - 1/4)}{2\mu r^2} u(r) = Eu(r). \quad (277)$$

In order to obtain WKB wavefunctions with the correct behavior (same phase for large r as the exact solutions), one makes use of the Langer transformation (52), (52), (178) - (181) which effectively replaces $m^2 - 1/4$ with m^2 . This substitution is valid for all but s -states, which must be treated differently (182), (185).

In this approach, we note that in the radial direction the particle moves freely up to the infinite wall at $r = R$, but is subject to an effective centrifugal potential given by $V_{eff}(r) = L_z^2/2\mu r^2 = (m\hbar)^2/2\mu r^2$. The classical particle cannot penetrate this centrifugal barrier and has an associated inner radius or distance of closest approach, R_{min} , given by

$$V_{eff}(R_{min}) = \frac{m^2 \hbar^2}{2\mu R_{min}^2} = E \quad \text{or} \quad R_{min} = \frac{|m|\hbar}{\sqrt{2\mu E}}. \quad (278)$$

We can also write this in the useful form

$$R_{min} = \frac{|m|R}{z} \quad \text{where} \quad E \equiv \frac{\hbar^2 z^2}{2\mu R^2} \quad (279)$$

more directly in terms of the desired dimensionless variable z , which is equivalent to the energy eigenvalue.

The WKB quantization condition on the radial variable, r , is then given by

$$\int_{R_{min}}^R k_r(r) dr = (n_r + C_L + C_R)\pi \quad \text{where} \quad k_r(r) \equiv \sqrt{\frac{2\mu E}{\hbar^2}} \sqrt{1 - \frac{R_{min}^2}{r^2}}. \quad (280)$$

The matching coefficients are given by $C_L = 1/4$ and $C_R = 1/2$ which are appropriate for 'linear' boundaries (at the inner centrifugal barrier) and 'hard' or 'infinite wall' boundaries (such as at $r = R$), respectively. The WKB energy quantization condition for the quantized energies, in terms of n_r explicitly and $|m|$ implicitly, via both the E and R_{min} terms, can then be written in the form

$$\sqrt{\frac{2\mu E}{\hbar^2}} \int_{R_{min}}^R \sqrt{1 - \frac{R_{min}^2}{r^2}} dr = (n_r + 3/4)\pi. \quad (281)$$

(This result was obtained earlier in Ref. (183). We also note that an improved approximation for $m \neq 0$ eigenvalues has also been obtained through the use of periodic orbit theory (184).) The integral on the left can be evaluated in the form

$$\begin{aligned} \int_{R_{min}}^R \frac{\sqrt{r^2 - R_{min}^2}}{r} dr &= \sqrt{R^2 - R_{min}^2} - R_{min} \sec^{-1} \left(\frac{R}{R_{min}} \right) \\ &= R \left[\sqrt{1 - x^2} - x \sec^{-1}(1/x) \right] \end{aligned} \quad (282)$$

where we define $x \equiv R_{min}/R = |m|/z$. This result can be expanded for small values of x (i.e., $R_{min}/R \ll 1$ or $|m|/z \ll 1$) to obtain

$$\sqrt{1-x^2} - x \sec^{-1}(1/x) = 1 - \frac{\pi x}{2} + \frac{x^2}{2} + \frac{x^4}{24} + \frac{x^6}{80} + \frac{5x^8}{896} + \dots \quad (283)$$

The WKB quantization condition in Eqn. (281) can then be written, in terms of z , in the form

$$z \left(1 - \frac{\pi |m|}{2z} + \frac{m^2}{2z^2} + \frac{m^4}{24z^4} + \dots \right) = (n_r + 3/4)\pi \quad (284)$$

If we keep only the first two terms on the left-hand side, we find that

$$z \approx (n_r + |m|/2 + 3/4)\pi \equiv z_0(m, n_r) \quad (285)$$

which is the lowest-order result obtained directly from the limiting form of the wavefunction.

To improve on this result, we simply keep successively higher order terms, solving iteratively at each level of approximation using a lower-order result for z , and we find the much improved approximation

$$\begin{aligned} z_{(m, n_r)} = z_0(m, n_r) &- \frac{m^2}{2z_0(m, n_r)} - \frac{7}{24} \frac{m^4}{[z_0(m, n_r)]^3} - \frac{83}{240} \frac{m^6}{[z_0(m, n_r)]^5} \\ &- \frac{6949}{13440} \frac{m^8}{[z_0(m, n_r)]^7} + \dots \end{aligned} \quad (286)$$

which we have confirmed numerically is an increasingly good approximation, especially for $n_r \gg 1$. For the study of wave packet revivals, we only require the energy eigenvalue dependence on m, n_r to second order, but higher order terms such as those above might be useful for super-revivals and even longer-term time-dependence studies.

For the special case of $m = 0$, this WKB technique only returns the zero-th order result, $z = z(0, n_r)$, and the authors of Ref. (177), motivated by the form of the expansion in Eqn. (286), numerically fit the first 50 lowest-lying $m = 0$ zeros to a similar form and find the result

$$z_{(0, n_r)} = z_0(0, n_r) + \frac{1}{8z_0(0, n_r)} + \dots \quad (287)$$

which gives a much improved approximation. Friedrich and Trost (185) have obtained an improved WKB approximation for the 2D circular well for the $m = 0$ case which, when expanded in terms of $z_{(0, n_r)}$, gives the first two terms in Eqn. (287), so we will use that next-to-leading result in what follows.

Using Eqns. (286) and (287), we can evaluate the energy eigenvalues to quadratic order in n_r, m in order to probe the revival structure of wave packets. For the special case of $m = 0$, we find that

$$E_{(0, n_r)} = \frac{\hbar^2 [z_{(0, n_r)}]^2}{2\mu R^2} = \frac{\hbar^2 \pi^2}{2\mu R^2} \left[\left(n_r + \frac{3}{4} \right)^2 + \frac{1}{4\pi^2} \right] \quad (288)$$

while for the more general case with $m \neq 0$, we find

$$E_{(m, n_r)} = \frac{\hbar^2 [z_{(m, n_r)}]^2}{2\mu R^2} = \frac{\hbar^2 \pi^2}{2\mu R^2} \left[\left(n_r + \frac{|m|}{2} + \frac{3}{4} \right)^2 - \frac{m^2}{\pi^2} \right]. \quad (289)$$

The fact that these energies depend on non-integral values of the effective quantum numbers is reminiscent of the case of Rydberg wave packets in alkali-metal atoms due to quantum defects (186), (187) and methods similar to those used there might prove useful. In what follows, however, we simply examine the time-dependence of typical $m = 0$ and $m \neq 0$ wave packets directly.

2. Wave packets and time scales

We begin by focusing on the special case of zero-momentum wave packets, centered at the origin, namely with vanishing values of (p_{0x}, p_{0y}) and (x_0, y_0) . For such states, where only the $m = 0$ eigenstates contribute, we can write the energy eigenvalues from Eqn. (288) in the form

$$\begin{aligned} E(n_r) &= \frac{\hbar^2 \pi^2}{2\mu R^2} \left[\left(n_r + \frac{3}{4} \right)^2 + \frac{1}{4\pi^2} + \mathcal{O} \left(\frac{1}{(n_r + 3/4)^2} \right) \right] \\ &\approx \frac{\hbar^2 \pi^2}{32\mu R^2} \left[8n_r(2n_r + 3) + \left(9 + \frac{4}{\pi^2} \right) \right] \\ &= \frac{\hbar^2 \pi^2}{4\mu R^2} \left[l(n_r) + \left(\frac{9}{8} + \frac{1}{2\pi^2} \right) \right] \end{aligned} \quad (290)$$

where $l(n_r) \equiv n_r(2n_r + 3)$ is an integer (neither even nor odd in general). The last term in the square brackets is independent of n_r and will make the same, constant, overall phase contribution to the autocorrelation function, so we focus on the $l(n_r)$ term. Since this integer has no special evenness/oddness properties, its contribution to the phase of each $|a_{(n,n_r)}|^2$ term in Eqn. (272) will be identically unity at a revival time given by

$$\left(\frac{\hbar^2 \pi^2}{4\mu R^2} \right) \frac{T_{rev}^{(m=0)}}{\hbar} = 2\pi \quad \text{or} \quad T_{rev}^{(m=0)} = 4 \left[\frac{2\mu R^2}{\hbar\pi} \right] \equiv 4T_0 \quad (291)$$

Thus, at integral multiples of $4T_0$, we expect nearly perfect revivals because of the almost regularly spaced structure of the $m = 0$ Bessel function zeros. At these recurrences, we can also predict the overall phase corresponding to the last term in Eqn. (290), namely

$$e^{-i\hbar^2 \pi^2 / 4\mu R^2 (4T_0)(9/8 + 1/2\pi^2)} = e^{-2\pi i(9/8 + 1/2\pi^2)} = e^{-2\pi i} e^{-2\pi i(1/8 + 1/2\pi^2)} \equiv e^{-i\pi F} \quad (292)$$

where $F = 1/4 + 1/\pi^2 \approx 0.351$.

To investigate these predictions numerically, we have used an initial Gaussian wave packet consisting of a product of two forms as in Eqn. (107) with the specific values

$$2m, \hbar, R = 1 \quad \text{and} \quad b = \frac{1}{10\sqrt{2}} \quad \text{so that} \quad \Delta x_0 = \Delta y_0 = 0.05. \quad (293)$$

The expansion coefficients $a_{(m,n_r)}$ in Eqn. (272) are calculated by numerical evaluation of the required ‘overlap’ integrals of the initial state with the eigenstates.

Using the expansion coefficients for this state, we plot the modulus squared of the autocorrelation function, $|A(t)|^2$, in the bottom plots of both Figs. 39 and 40, with time ‘measured’ in units of T_0 . The almost exact revival structure at integral multiples of $4T_0$ is evident. As a further check, we can evaluate the phase of $A(t)$ at each revival and find that to an excellent approximation it is given by $-nF\pi$, as in Eqn. (292).

We next move away from the special case of the zero-momentum, central wave packet by considering individually the case of $x_0 \neq 0$ and $p_{0y} \neq 0$ (but not both). In each case, the average angular momentum of the state is still vanishing, but $m \neq 0$ values of the expansion coefficients are now required. We must now use the more general case for the energies, which to second order in $m \neq 0, n_r$, are given by Eqn. (289) as

$$\begin{aligned} E_{(m,n_r)} &= \frac{\hbar^2 \pi^2}{2\mu R^2} \left[\left(n_r + \frac{|m|}{2} + \frac{3}{4} \right)^2 - \frac{m^2}{\pi^2} \right] \\ &= \frac{\hbar^2 \pi^2}{32\mu R^2} \left[(16n_r^2 + 24n_r + 16|m|n_r) + 4|m|(|m| + 3) - \frac{16m^2}{\pi^2} \right] \\ &= \frac{\hbar^2 \pi^2}{32\mu R^2} \left[8\tilde{l}(n_r) + 8\bar{l}(|m|) - \frac{16m^2}{\pi^2} + 9 \right] \end{aligned} \quad (294)$$

where

$$\tilde{l}(n_r) \equiv n_r(2n_r + 3 + 2|m|) \quad \text{and} \quad \bar{l}(|m|) \equiv |m|(|m| + 3)/2 \quad (295)$$

are both integers, again, with no special even or oddness properties. We can then write these energies in the form

$$E_{(m,n_r)} = \frac{2\pi\hbar}{4T_0} \left[\tilde{l}(n_r) + \bar{l}(|m|) - \frac{2m^2}{\pi^2} + \frac{9}{8} \right]. \quad (296)$$

At integral multiples of the $m = 0$ revival time, $t_N = N(4T_0)$, the first two terms give $e^{-N(2\pi i)} = 1$ phases to each (m, n_r) term in the autocorrelation function, while the last term gives an overall, (m, n_r) -independent phase, just as in the $m = 0$ case. The other term, however, gives a contribution

$$e^{-(2\pi i)(m^2 N)/(2/\pi^2)} \quad (297)$$

which depends on m explicitly and which therefore eliminates the revivals, increasingly so, as the wave packet is dominated by $m \neq 0$ terms. However, because of a seeming numerical accident, at integral multiples of $5T_{rev}^{(m=0)} = 20T_0$, we recover approximate revivals due to the fact that $5 \times (2/\pi^2) = 1.013$. We thus find approximate revivals for the more general $m \neq 0$ case given by $T_{rev}^{(m \neq 0)} = (\pi^2/2)T_{rev}^{(m=0)} \approx 5T_{rev}^{(m=0)}$.

This effect is illustrated in more detail in Figs. 39 and 40 where we plot $|A(t)|^2$ versus t as we move from the central, zero-momentum wave packet by first moving away from the origin ($x_0 \neq 0$, in Fig. 39) or having non-zero momentum values ($p_{0y} \neq 0$, in Fig. 40.) In each case, as we increase the parameter (x_0 or p_{0y}), we necessarily include more and more $|m| \neq 0$ eigenstates. For even a small mix of such states, the $T_{rev}^{(m=0)}$ revival periods at most integral multiples of $4T_0$ disappear, while evidence for the more general $T_{rev}^{(m \neq 0)} = 20T_0$ revivals remains evident.

We note that this 'lifting' of a seemingly 'accidental' degeneracy in the pattern of revival times is somewhat similar to the special case of a zero-momentum Gaussian wave packet in a 2D square or equilateral triangular billiard, initially placed at the center.

This pattern of revival times depending on two distinct quantum numbers is also somewhat reminiscent of that encountered in a rectangular billiard with differing sides of length L_x, L_y where if the sides are incommensurate one would expect a less elaborate revival structure. Since the revival times typically scale as $T_{rev} \propto L^2$, the appearance of a π^2 scale factor which can give rise to very close to an integer ratio $10/\pi^2 \approx 1$ (to within 1.3%) is appropriate; in this case, the relevant length scales for the radial quantum number and azimuthal quantum numbers are most likely multiples of R and $2\pi R$ respectively, so that relative factors of π^2 in the revival times can appear naturally.

The presence of the $\Delta m \neq 0$ revivals becomes increasingly less obvious as the average angular momentum is increased away from zero (with both x_0 and p_{0y} now non-vanishing), since the required energy eigenvalues are in a region of large $|m|/z$ where the lowest-order approximation (from Eqn. (285)) of evenly spaced z values becomes worse. We also note that even with $\langle \hat{L} \rangle = 0$, as we increase p_{0y} , the spread in m values required also increases, so that the overall number of states required to reproduce the initial Gaussian, and which have to 'beat' against each other appropriately, increases as well, making revivals more difficult to produce.

3. Variations on the circular billiard

The discussion of the circular billiard can be easily extended to the case of the half-circular footprint, with the addition of an infinite wall along any diameter. The resulting energy eigenvalue spectrum is obtained in a similar way as in the cases of the square and

equilateral triangle billiards when ‘cut’ along a diagonal. The angular wavefunctions for the half-circle problem can be obtained from the form in Eqn. (225) by choosing only the $\sin(m\theta)$ ($m > 1$) forms which vanish on the new boundary. Thus, the energy eigenvalue spectrum consists of one copy of the $m \neq 0$ energies of the full well, very similar to the cases encountered in Sec. IV.B and at the end of Sec. IV.C. However, because purely $m = 0$ wave packets are no longer possible, the existence of recognizable quantum revivals is less obvious

While we have focused on the long-term revival structure of quantum wave packets in the circular well, the short-term, semi-classical propagation leading to closed orbits in this geometry can also be studied using the same methods as in Secs. IV.A and IV.C and we present such an analysis in Appendix E. The 2D annular billiard, where an additional infinite wall at $r = R_{in} < R$ is added, can be studied with the same WKB methods used here, and we discuss that case in Appendix E as well.

The problem of the spherical billiard, with an otherwise free particle confined to a circular region of radius R , is an obvious extension, with the (unnormalized) solutions in spherical coordinates given by

$$\psi(r, \theta, \phi) = j_l(k_{(l,n_r)}r) Y_{(l,m)}(\theta, \phi) \quad (298)$$

and the quantized energies determined by the zeros of the regular *spherical* Bessel functions via

$$E_{(l,n_r)} = \frac{\hbar^2}{2\mu R^2} [z_{(l,n_r)}]^2 \quad \text{where} \quad j_l(z_{(l,n_r)}) = 0. \quad (299)$$

For such a central potential, the energy eigenvalues do not depend on the m quantum number, so the corresponding classical period ($T_{cl}^{(m)}$) and revival times ($T_{rev}^{(m)}, T_{rev}^{(n_r,m)}, T_{rev}^{(l,m)}$) decouple from the problem. For the special case of spherically symmetric ($l = 0$) solutions, one has

$$j_0(z) \propto \frac{\sin(z)}{z} \quad (300)$$

and the $l = 0$ eigenvalues are exactly quadratic in the n_r quantum number; this implies that initially central ($\mathbf{r}_0 = (0, 0, 0)$) Gaussian wave packets with vanishing initial momentum ($\mathbf{p}_0 = (0, 0, 0)$) will exhibit exact revival behavior, with no higher order time scales present, while all other packets, which necessarily include $l \neq 0$ components, will have less obvious revival behavior.

Finally, the addition of a single infinite wall along any radius (not diameter) of the 2D circular billiard (adding a ‘baffle’) can be analyzed in detail (188), with the result that half-integral values of the 2D angular momentum ($m = 1/2, 3/2, \dots$) are allowed. Then, noting that the 2D ($J_m(z)$) and 3D ($j_m(z)$) Bessel functions are related by

$$j_m(z) = \sqrt{\frac{\pi}{2z}} J_{m+1/2}(z), \quad (301)$$

we see that wave packets constructed from only $m = 1/2$ eigenstates in this geometry will also exhibit purely quadratic dependence on the radial quantum number and also have exact revival behavior.

V. EXPERIMENTAL REALIZATIONS OF WAVEPACKET REVIVALS

The existence of revival and fractional revival behavior in quantum bound states, first found numerically in simulations of Rydberg atoms (28), has led to a number of experimental tests in atomic, molecular, and other systems. We briefly review some of the experimental evidence for quantum wave packet revivals, while noting that excellent reviews of wave packet physics (19) - (23), (37) have appeared elsewhere. In addition, we discuss other experimental realizations of quantum revivals found in the occupation probability of a two-state atom system in a quantized electromagnetic field, described by the Jaynes-Cummings model, and in the behavior of the macroscopic wave function of Bose-Einstein condensates. We also discuss revival-like behaviors which arise in various optical phenomena.

A. Atomic systems

As mentioned above, early formal studies (9) - (16) of the construction of Coulomb wave packets were expanded upon by a number of authors (189) - (201), including suggestions for experimental production of localized wave packets. Since excellent reviews (19) - (23), (37) exist on this subject, we limit ourselves to a few comments.

The production of localized Rydberg wave packets makes use of the fact that the large n energy levels in such atoms are very closely spaced; for example, the energy difference between successive Rydberg levels for $n_0 = 50$ ($\Delta n = \pm 1$) is approximately $\Delta E_n = 2 \times 10^{-3} eV$. Short-duration ($\Delta t \sim \tau_{pump}$) laser pulses necessarily have a range of energies ($\Delta E = \hbar/\Delta t$) and can therefore simultaneously excite a number of states (experiments have been done where wavepackets containing of order 3 - 10 states have been produced, corresponding to roughly $\Delta n = 1.5 - 5$ in our notation.) One-electron-like atoms such as potassium and rubidium have ionization potentials of order 4 eV, requiring laser wavelengths of roughly this order to excite states to $E_n = -E_0/n_0^2 \lesssim 0$ for $n_0 \gg 1$. As examples, several classic experiments (30) ((32), (33)) used potassium (rubidium) atoms which have ionization potentials given by 4.341 eV (4.177 eV) and produced excited Rydberg states with $n_0 = 65$ ($n_0 = 62$, $n_0 = 46.5$) using single photon excitation corresponding to laser wavelengths of 2858 Å (297 nm); an earlier experiment (26) also used rubidium, but utilized two-photon excitation with $\lambda = 594 nm$, and contained only 2 - 3 component states.

The time-development of the wave packet can be subsequently probed with a second laser pulse, as a function of the time delay from the first pulse. A classical description (30) of the process involves noting that the rate of energy absorption from the laser pulse by the wave packet is given by $R(t) = \mathbf{J}(t) \cdot \mathbf{E}(t)$ where $\mathbf{J}(t) = e\mathbf{v}(t)$ is the classical electron current and $\mathbf{E}(t)$ is the time-dependent electric field. This rate is large (small) near the inner (outer) Keplerian turning point, where the electron speed is big (small), so that when the electron is near the nucleus, energy from the 'probe' laser can be efficiently absorbed, resulting in an increased probability of ionization (which is the observable signal), a method first proposed by Alber, Ritsch, and Zoller (17). Other experiments (33) have used different techniques (18) to monitor the dynamic behavior of the packets.

For systems described by the Coulomb-like spectrum in Eqn. (71), such as large- n Rydberg states where Z is effectively unity, the classical period will be given by

$$T_{cl}^{(Coul)}(n_0) = \frac{2\pi\hbar}{|E'(n_0)|} = (1.52 \times 10^{-16} s)(n_0)^3 \approx 20 ps (n_0/50)^3. \quad (302)$$

and the corresponding revival time is then given by

$$T_{rev}^{(Coul)} = (2n_0/3)T_{cl}^{(Coul)} \approx 670 ps (n_0/50)^4. \quad (303)$$

For example, the original numerical predictions of Parker and Stroud (28) used an effective $n_0 = 85$ which gives

$$T_{cl} = 93.5 ps \quad \text{and} \quad T_{rev} = 5.3 ns \quad (304)$$

so that the $p/q = 1/2$ revival shown in Fig. 4 is indeed observed to occur at roughly $T_{rev}/2 = 2.7 ns$ as seen in their simulations (where Averbukh and Perelman (34) added the appropriate labeling to the original data, as in Fig. 4.)

In one of the early experimental observations of fractional revivals by Yeazell and Stroud (31), the initial wave packet was excited with $n_0 = 72$ (and including roughly 5 states, or $\Delta n \sim 2.5$) which gives

$$T_{cl} = 57 ps \quad \text{and} \quad T_{rev} = 2.7 ns. \quad (305)$$

In the data from Ref. (31), reproduced here in Fig. 41, that initial periodicity is clearly visible, and a fractional revival, with local periodicity roughly half that of T_{cl} , corresponding

to a $p/q = 1/4$ fractional revival at $T_{rev}/4 \approx 680 ps$ is also apparent (note the two closely spaced vertical dashed lines); similar results were obtained by Meacher *et al.* (32).

Experimental data on rubidium from Ref. (33), shown in Fig. 5, corresponding to $n_0 = 46.5$ and $\Delta n \approx 3$ (6.5 states), gives $T_{cl} = 15 ps$, and a $p/q = 1/2$ revival is evident, with the initial local classical periodicity, at $T_{rev}/2 = 237 ps$ (which is labeled there as T_{rev} .) The inset shows similar data from the same experiment, but obtained with $n_0 = 53.3$ and almost 10 states excited in the wavepacket expansion, where fractional revivals up to order $T_{rev}/7$ are now visible, due in part to the larger value of Δn used, and connections such as those in Eqn. (59). Observations of fractional revivals in two-electron atoms such as calcium (202) have also been reported.

In contrast to most studies where localized electron wave packets are excited by short optical pulses, it has also been shown possible to generate Rydberg wave packets using THz frequency half cycle pulses (203). While the short-term Kepler orbit motion and longer-term revival behavior of packets produced in this way are comparable, the THz wavepacket is initially delocalized and only becomes localized after half a revival time.

States where the effects of the inner atomic core are important are often described by quantum defects, where the effective principal quantum number is given by $n^* = n - \delta(n, l)$, with an angular-momentum quantum number dependent correction characterizing the effect of the inner core electrons. The effects of quantum defects on the structure of wave packet revivals has been examined in Refs. (186) and (187), while its effect on the detailed recurrence spectrum has been documented (33) experimentally.

The time-evolution of localized electron packets in an external electric field (Stark wave packets) (204) has been studied experimentally (205) - (208). The effect of the field on the energy spectrum is most easily determined by solving the Schrödinger equation using parabolic coordinates (84) where the principal quantum number, n , can be written in terms of two parabolic quantum numbers, n_1, n_2 , and the azimuthal (magnetic) quantum number, m in the form

$$n = n_1 + n_2 + |m| + 1. \quad (306)$$

The linear (in applied field) correction to the energy spectrum due to an external electric field of the form $V(z) = -eFz$ can be written (84) as

$$E^{(1)}(k, n) = \frac{3}{2}nk[eFa_0] \quad (307)$$

where $k \equiv n_1 - n_2$ and $a_0 = \hbar^2/me^2$ is the Bohr radius. For fixed n , the spacing between adjacent energy levels is given by $\Delta E^{(1)} = 3n[eFa_0]$, due to the form in Eqn. (306) which implies $\Delta k = 2$ jumps, which is therefore similar to the even spaced levels of an oscillator spectrum. The classical periodicity associated with the k quantum number will then be given by Eqn. (62), suitably modified to read,

$$T_{cl}^{(k)} = \frac{2\pi\hbar}{2|\partial E/\partial k|} = \frac{2\pi\hbar}{3n[eFa_0]} = \frac{2.6 ps}{n[F/(100 V/cm)]} \quad (308)$$

and experimental observations of up to 10 periods have been reported (205) - (208). Since one is here concerned with only the classical periodicity, the application of variations of periodic orbit theory have also proved useful (207) - (209). The dynamics of Stark wave packets above the field-ionization threshold (210) have also been measured experimentally, observing that part of the electron wave function returns to the core, before escaping over the saddle point, with classical periodicities consistent with Eqn. (308).

Novel Stark wave packets consisting of an $H^+ - H^-$ ion pair have been produced (211) in which the energy states are scaled from the simple hydrogen results by

$$\mu \sim m_e \quad \longrightarrow \quad \mu \sim \frac{M_p}{2} \quad (309)$$

since it is now the nuclear motion which is relevant; the classical periodicity in Eqn. (308) is increased by roughly 3 orders of magnitude and data for this system (211) show good, but not perfect, agreement with that prediction.

The longer-term, revival structure of Stark wave packets, in the case where the time-dependent states contain components of both varying n and k have been analyzed in Ref. (212). The purely Coulomb revival time in Eqn. (303) is unchanged, but there is a non-vanishing cross-revival time given by

$$T_{rev}^{(n,k)} = \frac{2\pi\hbar}{3[eFa_0]} = nT_{cl}^{(k)} \quad (310)$$

and the revival (and fractional revival) structure of Stark wave packets differs in interesting ways from the free Rydberg case.

B. Molecular systems

The vibrational states of diatomic systems, described by anharmonic potentials with unequally spaced energy levels, constitute another physical system in which wave-packet excitations have been prepared. The subject has been reviewed in Ref. (37), where it is rightly pointed out that the excitation of localized packets in such molecular systems can be easier because of the one-dimensional nature of the vibrational degree of freedom, versus the 3D nature of hydrogen-like atoms. Vibrational wave packet motion has been seen in a number of systems, including I_2 (213), (214), NaI (215), and ICl (216), often with a large number of classical periods apparent.

For example, the recurrence of the semi-classical periodicity of a vibrational wave packet at a longer revival time in the sodium dimer Na_2 was exhibited in Ref. (217), with a hierarchy of classical periodicity versus revival times given by $T_{cl} \sim 300 fs$ and $T_{rev} \sim 47 ps$. More recent experiments on Br_2 (35) have presented evidence for fractional revivals (of order $p/q = 1/2$ and $1/4$) in such vibrational wave packets, as have experiments on I_2 (219).

An especially illustrative method of visualizing the appearance of revivals (and fractional revivals) in such systems involves the calculation of a time-windowed Fourier transform power spectrum, or spectrogram, $S(\omega, \tau)$; this is basically a two-dimensional map of frequency content of the packet versus time delay. The experimentally obtained time delay scan signal, $s(t)$, is convoluted with a window function, $g(t)$ to obtain

$$S(\omega, \tau) = \int_0^\infty s(t) g(t - \tau) e^{i\omega t} dt \quad (311)$$

where the window function is often chosen to be an Gaussian of the form $g(t) = \exp(-t^2/t_0^2)$; it is typical to plot $\ln(|S(\omega, \tau)|^2)$ versus (ω, τ) . An example of such a plot (taken from Ref. (35)) is shown in Fig. 42. The dark regions near $\tau = 0$ and $\tau \approx 88 ps$ and $f = 95 cm^{-1}$ correspond to the initial wave packet and the $p/q = 1/2$ revival, while the features along $2f = 190 cm^{-1}$ (i.e, at half the classical periodicity) and structures at $3f$ show evidence of fractional revivals.

Revivals and fractional revivals in NaK systems for different isotope-selected samples (220) have shown evidence for fractional revivals of up to order $p/q = 1/6$, as well as being able to distinguish differing classical periods and revival times for different isotopes; isotope-selective studies of K_2 (221) have also appeared. A novel application of such vibrational wave packet revival behavior has been demonstrated in the laser separation of isotopes. Standard methods of isotope separation (222) involve gaseous diffusion and centrifugation which, in turn, rely on the differences in isotopic masses. More modern laser separation methods (223) make use of the isotopic shifts in various atomic or molecular lines. The excitation of vibrational wave packets in diatomic molecules with differing isotopes can yield quantum

revival behavior which depends on the detailed structure of the vibrational eigenfrequencies (and anharmonicities) which then determine the long-term free evolution and revival times. The difference in revival time can yield spatial separation of the two species and this effect has been demonstrated experimentally (224), (225) and patented (226).

Observations of revival behavior (up to order $p/q = 1/8$) in triatomic molecules have been reported (227), while other proposals (228) to use differences in revival times in more complex molecules, ones with several vibrational degrees of freedom, have also appeared.

Evidence for coherence in the time-development of rotational wave packets goes back to at least 1975 (229) with observations of short-duration birefringence in CS_2 vapor with periodicity of order 40 ps. The theoretical background and many experimental realizations of such molecular structures arising from coherent production of rotational wave packets has been nicely reviewed by Felker and Zewail (230). Evidence for revival behavior in the rotational behavior of molecular wave packets has also been presented (214), (231) - (232) and reviewed (233), while more recent experiments (234), (235) have made use of the revivals in such molecular rotational wavepackets to manipulate the form (phase and spectral content) of ultrashort laser pulses. The revival time is determined by the difference in energy eigenvalues of the rotational states making up the coherent packet. Using a standard notation for the rotational eigenvalues, $E_J = BJ(J + 1)$, the relevant differences are given by

$$\Delta E_J = E_{J+N} - E_J = B[2JN + N(N + 1)] = 2B[JN + N(N + 1)/2] \quad (312)$$

where two states differ by N rotational quanta. For molecules with no special symmetries, the JN and $N(N + 1)/2$ values are integers (neither even nor odd) and the time to return to original state will be determined by

$$\frac{\Delta E_J T_{rev}}{\hbar} = 2\pi \quad \text{or} \quad T_{rev} = \frac{\pi \hbar}{B} \quad (313)$$

with shorter revival times possible for molecules of specific symmetries where only certain rotational states are allowed (229). Predictions of cross-revivals (236) due to vibration-rotation coupling and discussions of the wavepacket dynamics of rotational quantum states of C_{60} (237) have also appeared.

C. Jaynes-Cummings model

One of the most frequently discussed fully quantum mechanical models of the interaction of a two-level atom with a single mode of the quantized electromagnetic field was proposed by Jaynes and Cummings (238). The Hamiltonian for this system is given by

$$\hat{H} = \frac{\hbar\omega_0}{2}\hat{\sigma}_3 + \hbar\omega\hat{a}\hat{a}^\dagger + \hbar\lambda(\hat{\sigma}_+\hat{a} + \hat{a}^\dagger\hat{\sigma}_-) \quad (314)$$

where \hat{a}^\dagger, \hat{a} are the raising and lowering operators for the boson field mode of frequency ω , and the $\hat{\sigma}_+, \hat{\sigma}_-, \hat{\sigma}_3$ are the Pauli matrices representing the two-state system, with $\hbar\omega_0$ being the energy difference between the two levels. Discussions of this system have routinely appeared in reviews of the subject (239) - (242) and the model is known to have analogs in many other areas of physics.

Applied to a two-level atom in a resonant cavity with n photons, the system will undergo Rabi oscillations with frequency given by

$$\Omega_n = (n\lambda^2 + \Delta^2/4)^{1/2} \quad \text{with} \quad \Delta = \omega_0 - \omega \quad (315)$$

which simplifies in the de-tuning limit when $\omega \rightarrow 0$. For that case, the probability that the system is in the excited state is given by

$$P_{e,n}(t) = \frac{1}{2} (1 + \cos(2\sqrt{n}\lambda t)) \quad (316)$$

while for a system with a distribution of photons, the solution is averaged over the initial probability distribution, p_n , to give

$$P_e(t) = \sum_{n=0}^{\infty} p_n P_{e,n}(t) = \frac{1}{2} + \frac{1}{2} \sum_{n=0}^{\infty} p_n \cos(\sqrt{n}\lambda t). \quad (317)$$

For an initial coherent state distribution, one has p_n given by the Poisson distribution, yielding

$$P_e(t) = \frac{1}{2} + \frac{e^{-|\alpha|^2}}{2} \sum_{n=0}^{\infty} \frac{|\alpha|^{2n}}{n!} \cos(2\sqrt{n}\lambda t) \quad (318)$$

and the average value of n is given by $\bar{n} = |\alpha|^2$, while the spread is $\Delta n = |\alpha|$. This expression for $P_e(t)$ has many obvious similarities to the autocorrelation function, $A(t)$, for wave packets, namely highly localized expansion coefficients (when $\bar{n} = |\alpha|^2 \gg |\alpha| = \Delta n \gg 1$) and oscillatory terms which are not purely harmonic, so it is not surprising that some aspects of the short- and long-term behavior of Eqn. (318) have features in common with $A(t)$.

The dynamics of this system exhibit Rabi oscillations with a frequency centered at $\Omega_{\bar{n}}$, but with a dephasing given by a Gaussian envelope, $\exp(-(\lambda t)^2/2)$, first derived in Refs. (243) and (244), and later improved upon (245) for $\Delta \neq 0$. For longer times, using familiar physical reasoning (or more formal expansions about $n - \bar{n}$), one can see that at the time that neighboring terms in Eqn. (318) acquire a common 2π phase difference, one expects the Jaynes-Cummings summation to return to close to its $t = 0$ behavior, exhibiting revivals, this time due to the quantized nature of the electromagnetic field. The condition for this to occur is

$$2\Omega_{\bar{n}+1}T_{rev} - 2\Omega_{\bar{n}}T_{rev} \equiv \phi_{\bar{n}+1} - \phi_{\bar{n}} = 2\pi \quad (319)$$

yielding a revival time given by

$$T_{rev} = \frac{2\pi\sqrt{\lambda^2\bar{n} + \Delta^2/4}}{\lambda^2} \longrightarrow \frac{2\pi\sqrt{\bar{n}}}{\lambda} \quad \text{as } \Delta = 0. \quad (320)$$

This time scale, given by how long it takes the phases from consecutive frequencies to catch up to each other, is more akin to the classical periodicity in Eqn. (9) in the formalism we have used so far, but is routinely referred to as the revival time.

The result in Eqn. (320) was derived in numerical simulations by Eberly, Narozhny, and Sanchez-Mondragon (245), (246), but one should also note the much earlier work by J. Frahm (247) who also demonstrated very similar results in this system. Eberly *et al.* also found evidence of subsequent revivals at integral multiples of T_{rev} , as well as accurate representations of the decreasing magnitudes at $t = kT_{rev}$, and discussed as well the even longer-term approach to more irregular behavior, due to overlapping revivals (248). For example, they were able to demonstrate that the peak heights were bounded by the long-term limits (when $\Delta = 0$)

$$B(t) = \frac{1}{2} \pm \frac{1}{2} \frac{1}{(1 + \lambda^2 t^2 / 4\bar{n})^{1/4}}. \quad (321)$$

As an example of their solutions, we show in Fig. 43 plots of $P_e(t)$ for $\bar{n} = 36$ and $\lambda = 0.01$. We note the short-term Rabi oscillations, with Gaussian dephasing factor in

Fig. 43(a), as well as the presence of increasingly width revivals at integral multiples of T_{rev} in Fig. 43(b). (Plotted as a function of $\tau = \lambda t/\pi$, the revivals predicted by Eqn. (320) are expected at $\tau = k(2\sqrt{\bar{n}}) = 12k$ for this example.) The reappearance of the ‘classical’ periodicity near the first two revivals ((c) and (d)) is also apparent. We note that there are similarities in the spreading time formalism appearing in the envelope functions found by them with the formulae by Nauenberg (40): Fleischhauer and Schleich (249) have, in fact, applied a Poisson summation approach to the evaluation of Eqn. (318) which makes this connection more apparent. The time-development of this system in phase space, in terms of the quasiprobability distribution of Cahill and Glauber (251) (or Q-function), has been presented by Eiselt and Risken (252).

The direct observation of these effects (with at least two obvious revivals) was first demonstrated by Rempe, Walther, and Klein (253) using Rydberg atom states interacting with single field modes in a superconducting cavity constituting a one-atom maser (254). More detailed observations (255) have been able to extract discrete Fourier components of the Rabi oscillation time-dependence proportional to the square root of integers, as in Eqn. (318), providing very direct evidence of the quantization of the electromagnetic field. (It should be noted that Wright and Meystre (256) have examined in detail the collapses and revivals in micromaser systems and found subtle differences with those in the Jaynes-Cummings model.)

Theoretical work extending these results further to fractional revivals (257), (258) and to sub-Poisson photon distributions (258) has also appeared, as well as suggestions for using the revivals in the population inversion to measure novel phenomena (259); variations on these results in an optical (as opposed to a microwave) cavity have also been discussed (260). Studies have shown (261) - (263) that at half the revival time it is possible to obtain a entangled, Schrödinger-cat-like, atom-field state, similar in some ways to the structure in Eqn. (43) and Fig. 30, but with no short-term periodicity (no Rabi oscillations), while extensions to N -level atoms (264) have been observed to give different behaviors.

Other similar models which are soluble in closed form have been presented (265), (266), while realizations of similar phenomena in the context of laser-driven excitation of electronic transitions in diatomic molecules (268) have also been discussed.

Using harmonically bound ions, it has proved possible to create non-classical motional states of trapped atoms, including thermal, Fock, coherent and squeezed states of motion (269), including observations of the classical periodicity. The coupling between the internal and motional states is in a regime which can be described by the Jaynes-Cummings model, so that the evolution of the atomic state can provide information on the number distribution of the motional state.

D. Revivals in other systems

1. Atoms in optical lattices and Bose-Einstein condensates

Optical lattices, formed by the interference of multiple laser beams, can act as local periodic potentials for atoms. Anharmonicities present in the potential well can cause dispersive spreading of wave packets formed in such systems, while dissipation can also arise from spontaneous emission, leading to loss of coherence. Localized coherent-state-like wave packets can be formed by suddenly shifting the optical lattice and two groups (270), (271) have examined the interplay between wave packet spreading, dissipation, and tunneling between adjacent wells and their impact on wave packet revival times.

Motivated by the production of Bose-Einstein condensates, several groups analyzed the time-dependence of the macroscopic wave function (272) - (275) and found periodic collapses and revival behavior. The energy of the external potential experienced by the atoms could

be modeled as being due to the interaction energy between the atoms, giving an effective Hamiltonian of the form

$$\hat{H} = \frac{U_0 \hat{n}(\hat{n} - 1)}{2} \quad (322)$$

where \hat{n} is the number operator for atoms in the confining potential, and U_0 is determined by the inter-particle interactions through the s -wave scattering length, a , and the ground state wavefunction, $w(x)$, to be $U_0 = (4\pi\hbar^2 a/m) \int |w(\mathbf{x})|^4 d\mathbf{x}$.

In this case, the initial coherent state excitations can be of the form

$$|\alpha\rangle_t = \left\{ e^{-|\alpha|^2/2} \sum_{n=0}^{\infty} \frac{\alpha^n}{\sqrt{n!}} e^{-iU_0 n(n-1)t/2\hbar} \right\} |n\rangle \quad (323)$$

where $|\alpha|^2 = N$ and $|\alpha| = \Delta N$; the time-dependence has at most a quadratic dependence on n . Using by now familiar techniques, we see that since $n(n-1)/2$ is an integer (neither even nor odd), there is a common revival time given by $T_{rev} = 2\pi\hbar/U_0$ at which $|\alpha\rangle_{t+T_{rev}} = |\alpha\rangle_t$. This effect was confirmed experimentally for a Bose-Einstein condensate (60) confined to a three-dimensional optical lattice, where the collapse and (approximate) revivals of the number of atoms in the coherent state was monitored.

We note that the macroscopic matter field, $\psi = \langle \alpha_t | \hat{a} | \alpha \rangle_t$, can be written in the form (88)

$$\psi(t) = \alpha \exp \left\{ -|\alpha|^2 \left[\left(1 - \cos \left(\frac{2\pi t}{T_{rev}} \right) + i \sin \left(\frac{2\pi t}{T_{rev}} \right) \right) \right] \right\} \quad (324)$$

which is very similar in form to the autocorrelation function, $A(t)$, in Eqn. (125) for the minimum-uncertainty, coherent-state like solution of the harmonic oscillator. The collapse time for this system can also be derived (88), (272) - (275) from the short-term time-dependence of Eqn. (324) giving $T_{coll} \propto T_{rev}/|\alpha| = T_{rev}/\Delta N$.

The dynamical behavior of $|\alpha\rangle_t$ can also be examined in the context of fractional revival behavior by evaluating the time-dependence (especially the interplay between the n and n^2 terms in the exponentials) of each term at p/q multiples of T_{rev} . For example, at $T_{rev}/2$, each term in the coherent state expansion contains a term of the form

$$\begin{aligned} e^{i\pi n/2} e^{-i\pi n^2/2} &= e^{i\pi n/2} \left[\frac{1}{\sqrt{2}} (e^{-i\pi/4} + e^{+i\pi/4} e^{-in\pi}) \right] \\ &= \frac{1}{\sqrt{2}} (e^{-i\pi/4} e^{i\pi n/2} + e^{+i\pi/4} e^{-i\pi n/2}), \end{aligned} \quad (325)$$

using the expansion in Eqn. (42). When used in the evaluation of $|\alpha\rangle_t$ one finds

$$|\alpha\rangle_{t=T_{rev}/2} = \frac{1}{\sqrt{2}} (e^{-i\pi/4} |e^{+i\pi/2} \alpha\rangle + e^{+i\pi/4} |e^{-i\pi/2} \alpha\rangle) \quad (326)$$

which is another Schrödinger-cat like superposition, with two distinct states rotated by 90° from the initial $|\alpha\rangle$ state. The structure of these coherent states are visualized in a standard way by defining the overlap of $|\alpha\rangle_t$ with an arbitrary coherent state, $|\beta\rangle$, via

$$\langle \beta | \alpha \rangle_t = e^{-|\alpha|^2/2} e^{-|\beta|^2/2} \sum_{n=0}^{\infty} \frac{\alpha^n (\beta^*)^n}{n!} e^{-i\pi n(n-1)t/T_{rev}} \quad (327)$$

and then plotting

$$P[Re(\beta), Im(\beta); t] = P(\beta; t) \equiv |\langle \beta | \alpha \rangle_t|^2 \quad (328)$$

and several examples are shown in Fig. 44; for example, the case of Fig. 44(c) corresponds to the state in Eqn. (326). Related ways of visualizing such coherence phenomena include the use of Wigner quasi-probability distributions (as in Ref. (34) for fractional wave packet revivals or Figs 29 and 30) and the so-called Q function (63), (277) in quantum optics.

2. Revivals and fractional revivals in optical systems

The quantized structure of important physical properties (energy eigenvalues for quantum wave packets, or the quantized EM field for Jaynes-Cummings systems) are not limited to purely quantum phenomena. The existence of full revivals, mirror revivals (with a reformation of the original coherence, but out of phase), and fractional revivals, due to the discrete nature of classical wave systems, has been observed experimentally in several optical phenomena. In most cases, the observation of revivals in the spatial distributions of light is referred to as *self-imaging* (for an excellent review of this general topic, see Ref. (278)) and we will focus on two examples, the Talbot effect and self-imaging in waveguides, as they are the most analogous to wave packet revivals in their mathematical structure and analyses.

In 1836 H. F. Talbot (279) (a co-inventor of photography, with Daguerre) illuminated a diffraction grating with a small (coherent) white light source and examined the resulting transmitted light with a magnifying glass. He noted recurring patterns of colored bands, repeating themselves as the lens was moved further away from the grating. Rayleigh (280) correctly interpreted these as resulting from the interference of the diffracted beams, in what would now be called the near-field regime. Subsequent work showed that the self-images of the original periodic structure, illuminated in plane wave approximation, with monochromatic light, would appear at multiples of a distance $L_T = 2a^2/\lambda$ where a is the grating distance and λ is the wavelength. The detailed mathematical analysis showed that the same pattern would also recur at $z = L_T/2$, but shifted in space by half the spatial periodicity (the analog of a mirror revival.) Higher order fractional revivals, at rational multiples of L_T ($z = pL_T/q$) consist of q copies of the original grating, separated by a/q . In the context of self-imaging, the revivals (and mirror revivals) are often called Fourier images, while the fractional versions are referred to as Fresnel images (281). The clear physical and mathematical analogies to the structure of wave packet revivals, and their intricate dependence on number theoretic identities, has been extensively discussed (282) - (285) and the Talbot effect (286), along with corresponding effects in wave packet revivals (64) (129), have been put forward as a novel way to factorize numbers.

The Talbot effect is not limited to purely electromagnetic waves, but has also been discussed for matter waves in atom optics (287) and observed experimentally with relatively light atoms (288) - (290) as well as with large molecules such as C_{60} (291). Fractional revivals, i.e., higher order Talbot fringes, of up to 7-th order have been observed (290), which is coincidentally quite similar to the fractional revival resolution obtained with the best wave packet studies (33).

The formation of images by *phase coincidences* in optical waveguides is another example of such self-imaging processes. The prediction that real optical images could form in planar optical waveguides was made by Bryngdahl (292), was then demonstrated in a series of elegant experiments by Ulrich and collaborators (293) and resulted in several patents (294). For this system, the recurrence length is given by $L = 4n_f W_a^2/\lambda$ where W_a is the effective aperture size in this slab geometry (including penetration depth effects) and n_f is the index of refraction of the dielectric slab. Multiple/fractional image formation (293), (295) has also been observed, and the phenomenon has also been demonstrated with x -ray waveguides (296). The planar waveguide geometry corresponds to the one-dimensional infinite well, with W corresponding to the well size, and the length along the waveguide corresponding to time. The ray tracing visualization of the intensity patterns in this geometry leading to fractional revivals (see especially Ref. (298) for a nice example) are therefore quite similar to the semi-classical pictures discussed by Born (101), (102) for trajectories in the infinite square well, leading to quantum carpets.

The application of this effect for use in novel optical beam splitters has been advocated (298). The generalization of this self-imaging method to two-dimensional waveguides of rectangular cross-sections (297) has also been demonstrated and fiber optic geometries of equilateral triangle and hexagonal cross-sections (as in Sec. IV.C), have also been discussed.

Finally, we note that while observations of wavepacket revival behavior has been mainly limited to atomic and molecular systems, the possible use of localized low-energy wave packet

excitations (299) localized at the edge of a 2D electron system (edge magnetoplasmons) to probe the dynamical properties of the integer and quantum Hall effects has also been proposed.

The study of classical and quantum mechanical systems subject to external periodic forces, focusing on issues related to chaotic behavior, has a rich literature. A number of such studies have focused on the appearance of revival-type behaviors (152), (153), (300) - (303) in such systems.

VI. DISCUSSION AND CONCLUSIONS

The connections between the energy eigenvalue spectrum of a quantum bound state system and the classical periodicities of the system have been a standard subject in quantum theory since the first discussions of the correspondence principle by Bohr.

Some semiclassical techniques, such as periodic orbit theory, can connect the quantum energy spectrum with classical closed or periodic orbits, but often do so in a way which does not exhibit the time-dependence of quantum wave packets. Truly dynamic observations of localized quantum wave packets, exhibiting the classical periodicities expected in such semi-classical limits, have become possible with observations in atomic, molecular, and other systems, with analog behaviors seen in atom-field, BEC, optical, and other systems as well. The medium-term collapse of localized quantum states also present in such systems is familiar from simple examples of spreading wave packets which were constructed during the early days of the development of quantum theory. It can be analyzed quite generally for such bound state systems and has been observed in a number of systems as well.

The truly novel observation that such wave packets can relocalize and once again exhibit the classical periodicity, first observed in numerical simulations, has now been widely confirmed by experiments in a large number of different physical systems including atomic (Coulomb and Stark effect) systems using both electronic and nuclear states, and vibrational and rotational states in molecules. Besides being a fundamental realization of the discrete nature of quantum bound states, the simple time-dependence of such eigenstates, and interference effects, the phenomenon of quantum packet revivals has been increasingly used in the development of modern quantum control experiments, to assist in the shaping of specific quantum states, and is likely to remain an important aspect of the production of specific target states in the future. Given the relative simplicity of the quantum mechanical background which is needed to understand many aspects of these effects, and the connections to a wide variety of other revival phenomena (in optics and elsewhere), it is likely that this important manifestation of the time-development of quantum mechanical bound states could easily find a place in the undergraduate and graduate curricula, and this review can be seen as one step towards that end.

Acknowledgments

We thank M. Doncheski for fruitful and enjoyable collaborations on many projects. We are very grateful to I. Averbukh, M. Belloni, R. Bluhm, H. Fielding, A. Kostelecký, I. Marzoli, W. Schleich, C. Stroud, W. van der Zande, and D. Villeneuve for helpful comments and communications. Some of the original work of the author cited here was supported, in part, by the National Science Foundation under Grant DUE-9950702.

APPENDIX A: Energy eigenvalues in power law potentials

The energy eigenvalue spectrum in the family of power-law potentials (55) – (58) given by

$$V_{(k)}(x) \equiv V_0 \left| \frac{x}{L} \right|^k \quad (\text{A1})$$

can be obtained for large n (which is the situation encountered in wave packet revivals) by the use of the WKB approximation. In this case one writes

$$\int_{-x_0}^{+x_0} \sqrt{2m(E_n^{(k)} - V_{(k)}(x))} dx = (n + C_L + C_R) \hbar\pi \quad (\text{A2})$$

where

$$\pm x_0 = \pm \left(\frac{E_n}{V_0} \right)^{1/k} L \quad (\text{A3})$$

are the classical turning points. The matching coefficients have been discussed in detail in Ref. (52) and are given by $C_L, C_R = 1/4$ for smooth potentials, but with $C_L, C_R \rightarrow 1/2$ for the case of infinite walls (i.e., in the limit when $k \rightarrow \infty$). The integrals can be done using standard handbook results to give

$$\begin{aligned} E_n^{(k)} &= \left[(n + C_L + C_R) \frac{\hbar\pi}{2L\sqrt{2m}} V_0^{1/k} \frac{\Gamma(1/k + 3/2)}{\Gamma(1/k + 1)\Gamma(3/2)} \right]^{2k/(k+2)} \\ &= \mathcal{E}^{(k)} (n + C_L + C_R)^{2k/(k+2)} \end{aligned} \quad (\text{A4})$$

which does reproduce both the oscillator ($k = 2$) and infinite well $k \rightarrow \infty$ limits, for large n , and even gives the appropriate scaling for the Coulomb ($k = -1$) case. The same approach can also be used for ‘half’ well potentials, where an infinite barrier at $x = 0$ is introduced, as for the case of the ‘quantum bouncer’ in Sec. III.F, for appropriate values of C_L, C_R .

APPENDIX B: General time scales

The general expansion in Eqn. (8) defines three time scales, namely the classical periodicity, the revival, and superrevival times, all of which we have discussed in detail. In this Appendix, we describe two other relevant time scales, as well as another quite general approach to visualizing the short-term classical periodicity and subsequent spreading.

Nauenberg (40) noted that, for the Gaussian coefficients in Eqn. (24), the autocorrelation function could be written (in the notation used here) as

$$A(t) = \langle \psi_t | \psi_0 \rangle = \sum_{n=0}^{\infty} \left[\frac{e^{-(n-n_0)^2/2\Delta n^2}}{\Delta n \sqrt{2\pi}} \right] e^{i[E(n_0)t + E'(n_0)(n-n_0)t + E''(n_0)(n-n_0)^2/2]/\hbar} \quad (\text{B1})$$

to second order in $(n - n_0)$. Using the Poisson formula,

$$\sum_{q=0}^{\infty} f(q) = \sum_{m=-\infty}^{+\infty} \left[\int_0^{+\infty} f(q) e^{2\pi i q m} dq \right] + \frac{f_0}{2}, \quad (\text{B2})$$

he found he could write $A(t)$ in the suggestive form

$$A(t) = \frac{e^{iE(n_0)t/\hbar}}{2\pi\Delta n\sqrt{\alpha(t)}} \sum_{m=-\infty}^{+\infty} e^{-(m-t/T_c)^2/2\alpha(t)} \quad (\text{B3})$$

where

$$\alpha(t) \equiv \frac{1}{4\pi^2} \left(\frac{1}{(\Delta n)^2} + \frac{4\pi i t}{T_{rev}} \right) \quad (\text{B4})$$

and T_{cl} and T_{rev} are defined, in the notation used here, by Eqns. (9) and (16). This form exhibits, in a quite general way, the periodicity of the autocorrelation function, with the summation of exponentials centered at integral multiples of T_{cl} . It also exhibits the spreading (due to dispersion) apparent in the time-dependent width given by

$$\Delta(t) = \frac{1}{2\pi\Delta n} \left(1 + \left(\frac{4\pi\Delta n^2 t}{T_{rev}} \right)^2 \right)^{1/2} = \frac{1}{2\pi\Delta n} \left(1 + \left(\frac{t}{T_s} \right)^2 \right)^{1/2} \quad (\text{B5})$$

where

$$T_s \equiv \frac{T_{rev}}{4\pi(\Delta n)^2}. \quad (\text{B6})$$

This type of spreading is similar to that due to the pre-factor terms in Eqns. (82) and (102), which were written in terms of the familiar spreading times, t_0 , in the free-particle (infinite well) or uniform acceleration (quantum bouncer) cases. In order to exhibit this connection more generally, we use the power-law potential in Eqn. (A1) and the results in Appendix A. For example, we can write the quantized energies (in the large n limit) for the general $V_{(k)}(x)$ potential in the form

$$\frac{p_n^2}{2m} = E_n^{(k)} = \mathcal{E}^{(k)} n^{2k/(k+2)} \quad (\text{B7})$$

which we also equate to the maximum value of momentum, p_n . In these systems, we have

$$T_{rev}^{(k)} = \frac{4\pi\hbar}{\mathcal{E}^{(k)}} n^{4/(k+2)} \left| \frac{(k+2)^2}{2k(k-2)} \right|. \quad (\text{B8})$$

For an initial Gaussian wave packet of width Δp_n , the spreading time can be written in the form

$$t_0^{(k)} = \frac{m\hbar}{2\Delta p_n^2} \quad (\text{B9})$$

and we can use the identification in Eqn. (B7) to equate

$$\Delta p_n = \sqrt{2m\mathcal{E}^{(k)}} n^{-2/(k+2)} \left(\frac{k}{k+2} \right) \Delta n \quad (\text{B10})$$

which gives

$$t_0^{(k)} = \left(\frac{\hbar}{4\mathcal{E}^{(k)}} \right) \frac{n^{4/(k+2)}}{(\Delta n)^2} \left(\frac{k+2}{k} \right)^2. \quad (\text{B11})$$

Thus, for this family of potentials, we have the relation

$$\frac{T_{rev}^{(k)}}{t_0^{(k)}} = 8\pi \left| \frac{k}{k-2} \right| (\Delta n)^2 \quad (\text{B12})$$

and this ratio is equal to $8\pi(\Delta n)^2$ for both $k=1$ (quantum bouncer, uniform acceleration) and $k \rightarrow \infty$ (infinite well, free particle). We then note that the spreading time, T_s , given by the Nauenberg formula for these cases, is calculated to be

$$T_s^{(k)} = \frac{T_{rev}^{(k)}}{4\pi(\Delta n)^2} = 2t_0 \quad (\text{B13})$$

which agrees with the results in Eqn. (82) and (102).

Nauenberg also pointed out that the wavepacket spreads sufficiently that *quantum self-interference* occurs on a time scale of (in our notation) $T_{rev}/\Delta n$, marking the approach the collapsed state. The notation of a *collapse time* has also been studied in the context of the infinite (94) well and the quantum bouncer (149), with quite different approaches. For the infinite well, the time required for the various expectation values to approach their semi-classical limits was given approximately by Eqn. (174) which can be written in the form

$$T_{coll} = \frac{T_{rev}}{4\sqrt{12}\Delta n} \quad (\text{B14})$$

while for the quantum bouncer, a direct examination of the phase differences between various terms in the eigenstate expansion led to the result

$$T_{coll} \sim \frac{T_{rev}}{(8/\pi)\Delta n} \quad (\text{B15})$$

(where we use our notation for T_{rev} , since the one described in Eqn. (42) of Ref. (149) is more rightly associated with the $p/q = 1/2$ revival in the language of Averbukh and Perelman.) A third, quite general measure of the time taken to collapse to the incoherent state would be to use the spreading (*dispersive*) pre-factors in Eqn. (B3), or the similar ones in Eqns. (82) and (102), and define the collapse time as how long it takes for the envelope of $|A(t)|^2$ to decrease to $|A_{inc}|^2$, namely when

$$\frac{2t_0}{T_{coll}} \approx \frac{1}{\sqrt{1 + (T_{coll}/2t_0)^2}} = |A(T_{coll})|^2 \equiv |A_{inc}|^2 = \frac{1}{\Delta n 2\sqrt{\pi}} \quad (\text{B16})$$

which gives

$$T_{coll} = (4\sqrt{\pi}\Delta n) t_0 = \frac{T_{rev}}{(2\sqrt{\pi})\Delta n} \left(\frac{k-2}{k} \right) \quad (\text{B17})$$

which gives the same general form as the explicit analyses resulting in Eqns. (B14) and (B15). We note that the earliest time at which a possible fractional revival which might be resolvable (over the incoherent background) is given by the condition

$$\left| A \left(\frac{T_{rev}}{q} \right) \right|^2 = \frac{1}{q} = \frac{1}{\Delta n 2\sqrt{\pi}} \quad \text{at the time} \quad T_{early} = \frac{T_{rev}}{q} = \frac{T_{rev}}{\Delta n 2\sqrt{\pi}} \quad (\text{B18})$$

so that this time scale is also singled out as one ‘comes down’ in time from T_{rev} , as well as from ‘going up’ in time from $t = 0$. We note that Fleischhauer and Schleich (249) made similar use of the Poisson summation formula to obtain improved approximate expressions for the Jaynes-Cummings sum in Eqn. (318).

Finally, the presence of the T_{rev} term provides the dispersion necessary for the decay to the collapsed state. For the harmonic oscillator system, when $T_{rev} \rightarrow \infty$, we would expect to reproduce something like the result of Eqn. (125). Using Eqn. (B3), with $T_{rev} \rightarrow \infty$, we find that

$$A(t) = e^{iE(n_0)t/\hbar} \sum_{m=-\infty}^{+\infty} e^{-(m-t/T_{cl})^2(2\pi\Delta n)^2/2}. \quad (\text{B19})$$

Near $t \approx 0$, this reduces to

$$A(t) = e^{iE(n_0)t/\hbar} e^{-(\Delta n)^2\omega^2 t^2/2} \quad (\text{B20})$$

since $2\pi/T_{cl} = \omega$. The exact result in Eqn. (125) was derived for $\beta = \beta_0$, but arbitrary x_0, p_0 , and using Eqns. (118) (to evaluate $\langle E \rangle$) and (122) (to evaluate Δn), we find that the oscillator result for $\omega t \ll 1$ can be written in the form

$$A(t) = e^{+i\langle E \rangle t/\hbar} e^{-(\Delta n)^2(\omega t)^2/2} \quad (\text{B21})$$

which agrees with Eqn. (B20) in that limit. More generally, the two formulae agree very well for $|t - kT_{cl}| \ll T_{cl}$, i.e., near any multiple of the classical period.

APPENDIX C: Fractional (p/q) revivals for even q

The derivations of Averbukh and Perelman (34) for the temporal structure of fractional wave packet revivals at $t = pT_{rev}/q$ for odd values of q was discussed in Sec. II.D and we extend the analysis here. For case of even q values (implying p is odd, since p, q are assumed to be relatively prime), the periodicity in l required to satisfy Eqn. (45) is given by

$$l = q \quad \text{for } q = 2 \pmod{4} \quad (\text{C1})$$

$$l = q/2 \quad \text{for } q = 4 \pmod{4} \quad (\text{C2})$$

and we can treat each case separately.

For the first case, we note that the recursion relation in Eqn. (53) will connect b_r values with even and odd r separately. Since $q = 2 \pmod{4}$, $q/2$ will be an odd integer and we can rewrite the expression for b_0 , using the relabeling $\bar{n} = n + q/2$, to write

$$\begin{aligned} b_0 &= \frac{1}{l} \sum_n e^{-2\pi i p n^2 / q} \\ &= \frac{1}{l} \sum_{\bar{n}} e^{-2\pi i p (\bar{n} + q/2)^2 / q} \\ &= \frac{1}{l} \sum_{\bar{n}} e^{-2\pi i p \bar{n}^2 / q} e^{-2\pi i p \bar{n}} e^{-\pi i p q / 2} \\ &= -\frac{1}{l} \sum_{\bar{n}} e^{-2\pi i p \bar{n}^2 / q} \\ &= -b_0 \end{aligned} \quad (\text{C3})$$

since

$$e^{-2\pi i p \bar{n}} = 1 \quad \text{and} \quad e^{-\pi i p q / 2} = [e^{-\pi i q / 2}]^p = (-1)^p \quad (\text{C4})$$

because $q/2$ is an odd integer and p is necessarily odd if q is even. Since b_0 vanishes, all of the even b_r do as well, and only the $q/2$ b_r values with odd r are non-vanishing, leading to $q/2$ ‘clones’ or ‘mini-packets’ near the fractional revival time in these cases.

An explicit example is for the half-revival time, $T_{rev}/2$ where $p = 1$, $q = 2$, and $l = q/2 = 1$ where one can explicitly find that

$$b_0 = \frac{1}{2} \sum_{k=0}^1 e^{-2\pi i k^2 / 2} = \frac{1}{2}(1 - 1) = 0 \quad (\text{C5})$$

and

$$b_1 = \frac{1}{2} \sum_{k=0}^1 e^{2\pi i (k/2 - k^2/2)} = \frac{1}{2}(1 + 1) = 1 \quad (\text{C6})$$

and we obtain the result of Eqn. (38). The next case in this series is for multiples of $T_{rev}/6$, which turn out to be similar to the $p/q = 1/3, 2/3$ cases.

Finally, for the case of $q = 4 \pmod{4}$, the periodicity in Eqn. (45) is given by $l = q/2$ and the analysis proceeds in a similar fashion. For example, for the case of $T_{rev}/4$, we have

$p = 1$, $q = 4$, $l = q/2 = 2$, and the various expansion coefficients in Eqn. (48) are

$$\begin{aligned}
b_0 &= \frac{1}{2} \sum_0^1 e^{-2\pi i k^2/4} = \frac{1}{2}(1 - i) = \frac{1}{\sqrt{2}} e^{-i\pi/4} \\
b_1 &= \frac{1}{2} \sum_0^1 e^{2\pi i(k/4 - k^2/4)} = \frac{1}{2}(1 - 1) = 0 \\
b_2 &= \frac{1}{2} \sum_0^1 e^{2\pi i(2k/4 - k^2/4)} = \frac{1}{2}(1 + i) = \frac{1}{\sqrt{2}} e^{+i\pi/4}
\end{aligned} \tag{C7}$$

which explains the result of Eqn. (43) in a more ‘turnkey’ fashion.

We note that Bluhm and Kostelecký (77) have obtained similar results for the algebra of the complex phases arising from the *superrevival* terms of the form $\exp(-2\pi i p k^3/q)$. They have also extended this formalism of fractional revival analysis to the case of systems with two or more quantum numbers (79).

APPENDIX D: The ‘inverted’ oscillator

For the case of the so-called ‘inverted’ oscillator, the general wave packet solution in Eqn. (111), for example, can be directly carried over using the identifications in Eqn. (138) to obtain the ‘runaway’ wavepacket, with probability density given by

$$|\psi(x, t)|^2 = \frac{1}{\sqrt{\pi}|B(t)|} \exp \left[-\frac{(x - x_0 \cosh(\tilde{\omega}t) - p_0 \sinh(\tilde{\omega}t)/m\tilde{\omega})^2}{|B(t)|^2} \right] \tag{D1}$$

with

$$\langle x \rangle_t = x_0 \cosh(\tilde{\omega}t) + \frac{p_0 \sinh(\tilde{\omega}t)}{m\tilde{\omega}} \quad \text{and} \quad \Delta x_t = \frac{|B(t)|}{\sqrt{2}} \tag{D2}$$

where

$$|B(t)| = \sqrt{\beta^2 \cosh^2(\tilde{\omega}t) + (\hbar/m\tilde{\omega}\beta)^2 \sinh^2(\tilde{\omega}t)}. \tag{D3}$$

Just as for the harmonic oscillator, the expression for $A(t)$ for the general case is cumbersome, so we only examine it for one specific case as an example, namely the case where $\beta = \beta_0 = \sqrt{\hbar/m\tilde{\omega}}$. This situation no longer corresponds to a constant width wave packet, since

$$\Delta x_t \longrightarrow \frac{\beta_0}{\sqrt{2}} \sqrt{\cosh^2(\tilde{\omega}t) + \sinh^2(\tilde{\omega}t)} \tag{D4}$$

increases exponentially, as the individual momentum components comprising the wave packet quickly diverge in p -space. For the case of $x_0 = 0$, we have the general expression

$$A(t) = \frac{1}{\sqrt{\cosh(\tilde{\omega}t)}} \exp \left[\left(\frac{p_0^2}{2m\tilde{\omega}\hbar} \right) \left\{ \frac{\cosh(\tilde{\omega}t) - 1 + i \sinh(\tilde{\omega}t)(2 \cosh(\tilde{\omega}t) - 1)}{\cosh(\tilde{\omega}t)(\cosh(\tilde{\omega}t) - i \sinh(\tilde{\omega}t))} \right\} \right] \tag{D5}$$

In the limit when $t \gg 1/\tilde{\omega}$, the hyperbolic functions both approach $\exp(\tilde{\omega}t)/2$ and we have the limiting case

$$A(t) \longrightarrow \frac{1}{\sqrt{\exp(\tilde{\omega}t)/2}} \exp \left[-\frac{p_0^2}{2m\tilde{\omega}\hbar} (1 - i) \right]. \tag{D6}$$

The exponential (‘dynamical’) suppression once again is seen to ‘saturate’, as in the free-particle case, and for the same reason, namely that both $x(t) - x_0$ and Δx_t have the same large t behavior. The resulting modulus is given by

$$|A(t)|^2 \longrightarrow 2e^{-\tilde{\omega}t} \exp \left[-\frac{p_0^2}{m\tilde{\omega}\hbar} \right] \quad (\text{D7})$$

which still becomes exponentially small, but now due to the (‘dispersive’) prefactor. If one also has $x_0 \neq 0$, the expression above includes an additional factor of $\exp(-x_0^2/\beta_0^2)$ (similar to that in Eqn. (81), with no cross-term involving x_0 times p_0).

APPENDIX E: The full and annular circular wells: WKB energy eigenvalues, classical periods, and closed orbits

While we focus on the information about wave packet revival times encoded in the energy eigenvalue spectrum of quantum systems, it is also interesting to see how the pattern of closed (or periodic) orbits supported in a number of simple 2D quantum billiards arise from the connections between the classical periods in systems with more than two quantum numbers. This is especially true since most of the experimentally observed data from 2D circular billiard systems (304), (305) have involved measurements which are relevant for short-term, quasi-classical ballistic propagation. Such closed orbits are also the ones of relevance to periodic orbit theory (306) - (308) analyses of such billiard systems.

We have illustrated these connections using the explicit expressions for $E(n, m)$ for both the square and equilateral triangle billiard and we now turn to the cases of the circular and annular infinite wells. (The arguments presented here are adapted and extended from Ref. (177), but see also Ref. (309) for discussions of the circular billiard in the context of what has come to be known as periodic orbit theory.) For the circular well, we first note that the allowed closed orbits are characterized by two integers (p, q) , where q counts the number of ‘net revolutions’ the trajectories make before closing on themselves, while p counts the number of ‘hits’ on the circular walls. For consistency, one must have $p \geq 2q$ and when p, q have common factors, say $\bar{p} = np$ and $\bar{q} = nq$, one simply has an n -fold recurrence of a basic (or primitive) closed path. A number of low-lying trajectories of this type are shown in Ref. (309). The total path length for one classical period in any of these closed orbits is given by

$$L(p, q) = 2pR \sin \left(\frac{\pi q}{p} \right) \quad (\text{E1})$$

so that the classical period is simply

$$T(p, q) = \frac{L(p, q)}{v_0} \quad (\text{E2})$$

where v_0 is again the classical speed of the point particle inside the billiard. The minimum distance to the origin for any of these trajectories (distance of closest approach) is given by

$$R_{min} = R \cos \left(\frac{\pi q}{p} \right). \quad (\text{E3})$$

For the quantum case, the two appropriate quantum numbers give rise to classical periods given by

$$T_{cl}^{(n_r)} \equiv \frac{2\pi\hbar}{|\partial E/\partial n_r|} \quad \text{and} \quad T_{cl}^{(m)} \equiv \frac{2\pi\hbar}{|\partial E/\partial m|} \quad (\text{E4})$$

and the two periods can beat against each other to produce the classical periodicity ($T_{cl}^{(po)}$) for closed or periodic orbits if they satisfy

$$pT_{cl}^{(n_r)} = T_{cl}^{(po)} = qT_{cl}^{(m)} \quad (\text{E5})$$

again, with $p \geq 2q$ for this geometry.

We can then use this formalism to understand how these conditions can give rise to the classical expressions for the path lengths and minimum radii in Eqns. (E1) and (E3). Instead of using the approximate expression in Eqn. (289) for the (m, n_r) -dependent energies, we make use of the WKB condition in Eqn. (281), namely

$$\sqrt{\frac{2\mu E}{\hbar^2}} \int_{R_{min}}^R \sqrt{1 - \frac{R_{min}^2}{r^2}} dr = (n_r + 3/4)\pi \quad (\text{E6})$$

where the appropriate $C_L + C_R = 1/2 + 1/4 = 3/4$ factor corresponds to infinite wall boundary conditions at $r = R$ and ‘linear’ boundary conditions at the inner ‘turning point’,

$$R_{min} = \frac{|m|\hbar}{\sqrt{2\mu E}} \quad \text{or} \quad R_{min} = \frac{|m|R}{z} \quad (\text{E7})$$

which defines the useful parameter z .

We then simply take partial derivatives of both sides with respect to n_r and m respectively. We thus obtain the conditions

$$\sqrt{\frac{\mu}{2\hbar^2}} \left[\int_{R_{min}}^R \frac{dr}{\sqrt{E - m^2\hbar^2/2\mu r^2}} \right] \left| \frac{\partial E}{\partial n_r} \right| = \pi \quad (\text{E8})$$

$$\sqrt{\frac{\mu}{2\hbar^2}} \left[\int_{R_{min}}^R \frac{dr}{\sqrt{E - m^2\hbar^2/2\mu r^2}} \left(\left| \frac{\partial E}{\partial n_r} \right| - \frac{|m|\hbar^2}{\mu r^2} \right) \right] = 0. \quad (\text{E9})$$

The condition to be satisfied for periodic orbits can then be written as

$$\frac{q}{p} = \frac{T_{cl}^{(n_r)}}{T_{cl}^{(m)}} = \frac{|\partial E/\partial m|}{|\partial E/\partial n_r|} = \left(\frac{|m|\hbar}{\pi\sqrt{2\mu E}} \right) \left[\int_{R_{min}}^R \frac{dr}{r\sqrt{r^2 - R_{min}^2}} \right] \quad (\text{E10})$$

Evaluating the integral and using $R_{min} \equiv |m|\hbar/\sqrt{2\mu E}$, we find that

$$\frac{q}{p} = \frac{1}{\pi} \sec^{-1} \left(\frac{R}{R_{min}} \right) \quad \text{or} \quad R_{min}(p, q) \equiv R_{min} = R \cos \left(\frac{\pi q}{p} \right) \quad (\text{E11})$$

as the condition on periodic orbits, as expected. To find the classical period for such closed orbits, we note that

$$\begin{aligned} T_{cl}^{(po)} = pT_{cl}^{(n_r)} &= p \left(\frac{2\pi\hbar}{|\partial E/\partial n_r|} \right) = \left(2p\sqrt{R^2 - R_{min}^2} \right) \sqrt{\frac{\mu}{2E}} \\ &= \frac{[2pR \sin(\pi q/p)]}{v_0} = \frac{L(p, q)}{v_0} \end{aligned} \quad (\text{E12})$$

where we identify $v_0 = \sqrt{2E/\mu}$ with the classical speed which reproduces the purely geometric result of Eqn. (E1).

This type of analysis can be easily generalized to the case of an annular billiard, a circular system with infinite walls at both the outer radius R as well as at an inner radius $R_0 \equiv fR$ (where $0 < f < 1$), defined by the potential

$$V_A(r) = \begin{cases} 0 & \text{for } R_0 < r < R \\ \infty & \text{for } r \leq R_0 \text{ and } r \geq R \end{cases}. \quad (\text{E13})$$

This system has also been studied in the context of periodic orbit theory (310). The appropriate quantum wave functions are given by

$$\psi(r, \theta) = (\alpha J_{|m|}(kr) + \beta Y_{|m|}(kr)) \left(e^{im\theta} / \sqrt{2\pi} \right) \quad (\text{E14})$$

where one now includes the ‘irregular’ (divergent at the origin) $Y_{|m|}(kr)$ since the inner wall now guarantees that $r > 0$. Application of the boundary conditions at $r = R$ and $r = R_0 = fR$ yields the corresponding energy eigenvalue condition

$$J_{|m|}(kR)Y_{|m|}(kR_{inner}) - J_{|m|}(kR_{inner})Y_{|m|}(kR) = 0 \quad (\text{E15})$$

which can be solved numerically just as easily as in the purely circular case.

In terms of the connection between the classical closed orbits and the quantum periods, we note that the same periodic orbits described by Eqns. (E1) and (E3) are still allowed, so long as

$$\frac{R_{min}}{R} = \cos\left(\frac{\pi q}{p}\right) \geq f \equiv \frac{R_0}{R} \quad (\text{E16})$$

as shown in Fig. 45. Another set of orbits is allowed, also characterized by the same set of integers (p, q) , which bounce off the inner wall, an example of which is also shown in Fig. 45. For this geometry, the corresponding path lengths are always at least as large as those in Eqn. (E1), and are given by

$$\tilde{L}(p, q) = 2pR\sqrt{1 + f^2 - 2f \cos(\pi q/p)}. \quad (\text{E17})$$

The two classes of periodic orbits and path lengths coalesce in the limit that $f \rightarrow f_{max} = \cos(\pi q/p)$ and then both disappear from the allowed set of paths. We know that the effective distance of closest approach is an important parameter in this geometry, and for the case of the annular ring, we can define $R_{min} = zR$ as before, but we now have

$$z = f \frac{\sin(\pi q/p)}{\sqrt{1 + f^2 - 2f \cos(\pi q/p)}} \quad (\text{E18})$$

as illustrated in Fig. 46. We note that $z \leq f$ (as expected) for these trajectories which bounce off the inner wall, with the limiting case (‘just touching’) arising when $f = f_{max} = \cos(\pi q/p)$.

The WKB analysis for this geometry proceeds as in Sec. IV.D.1, with the lower integration limit changed from R_{min} to R_0 , and the WKB ‘matching coefficient’ changed to reflect the fact that the inner boundary is now also of the ‘infinite wall type’. These changes give

$$\sqrt{\frac{2\mu E}{\hbar^2}} \int_{R_0}^R \sqrt{1 - \frac{R_{min}^2}{r^2}} dr = (n_r + 1)\pi \quad (\text{E19})$$

with $R_{min} = zR$ with $f < z$ as noted above. The implicit differentiation proceeds as before and the condition for closed orbits becomes

$$\frac{q}{p} = \frac{|\partial E / \partial m|}{|\partial E / \partial n_r|} = \sqrt{\frac{2\mu}{E}} \left(\frac{|m|\hbar}{2\mu\pi} \right) \left[\int_{R_0}^R \frac{dr}{r\sqrt{r^2 - R_{min}^2}} \right]. \quad (\text{E20})$$

The integral can be done exactly and using $R_{min} = zR$ and $R_0 = fR$, we obtain

$$\frac{\pi q}{p} = \sec^{-1} \left(\frac{1}{z} \right) - \sec^{-1} \left(\frac{f}{z} \right) \quad (\text{E21})$$

as the condition for closed orbits, or

$$\sec^{-1} \left(\frac{1}{z} \right) = \frac{\pi q}{p} + \sec^{-1} \left(\frac{f}{z} \right) \quad (\text{E22})$$

This can be inverted to give

$$z = \cos \left(\frac{\pi q}{p} \right) \left(\frac{z}{f} \right) - \sin \left(\frac{\pi q}{p} \right) \sqrt{1 - \frac{z^2}{f^2}} \quad (\text{E23})$$

which can be solved for z to yield

$$z = f \frac{\sin(\pi q/p)}{\sqrt{1 + f^2 - 2f \cos(\pi q/p)}} \quad (\text{E24})$$

which is the appropriate condition for these ‘inner touching’ closed orbits. The corresponding classical periods, $T_{cl}^{(po)}$, which then give the corresponding path lengths, are given by

$$\begin{aligned} T_{cl}^{(po)} &= pT_{cl}^{(p)} = p \left(\frac{2\pi\hbar}{|\partial E/\partial n_r|} \right) \\ &= p \left[\sqrt{\frac{2\mu}{E}} \right] \left[\int_{R_0}^R \frac{r dr}{\sqrt{r^2 - R_{min}^2}} \right] \\ &= p \left[\frac{2R}{v_0} \right] \left(\sqrt{1 - z^2} - \sqrt{f^2 - x^2} \right) \\ &= \frac{2pR\sqrt{1 + f^2 - 2f \cos(\pi q/p)}}{v_0} \end{aligned} \quad (\text{E25})$$

where we have used the relation in Eqn. (E24) and the classical connection $E = \mu v_0^2/2$ and recover the expected result.

The spherical billiard can also be discussed in the same context, using these methods. The centrifugal barrier term, in a WKB expansion, is obtained from Eqn. (281) by the substitution $l(l+1) \rightarrow l(l+1) + 1/4 = (l+1/2)^2$, the so-called Langer modification (178) - (181).

References

- [1] E. Schrödinger, *Der stetige Übergang von der Mikro- zur Makromechanik* Naturwissenschaften **14** (1926) 664-666; translated and reprinted as *The continuous transition from micro- to macro mechanics*, *Collected papers on wave mechanics* (Chelsea Publishing, New York, 1982) pp. 41-44.

- [2] E. H. Kennard, *The quantum mechanics of an electron or other particle*, J. Franklin Institute **207** (1929) 47-78; see also *Zur Quantenmechanik einfacher Bewegungstypen* (translated as *The quantum mechanics of simple types of motion*), Z. Phys. **44** (1927) 326-352.
- [3] C. G. Darwin, *Free motion in the wave mechanics*, Proc. Roy. Soc (London) **A117** (1928) 258-293.
- [4] L. de Broglie, *Einführung in die Wellenmechanik* (Akad. Verlag., Leipzig, 1929).
- [5] E. C. Kemble, *The fundamental principles of quantum mechanics with elementary applications* (McGraw-Hill, New York, 1937) pp. 35-41.
- [6] S. Dushman, *The elements of quantum mechanics* (Wiley, New York, 1938) pp. 405-407.
- [7] V. Rojansky, *Introductory quantum mechanics* (Prentice-Hall, New York, 1938), pp. 66-70.
- [8] Letter from Lorentz to Schrödinger, 1926, reprinted in *Letters on wave mechanics*, edited by K. Przibram (Philosophical Library, New York, 1967) pp. 67-75.
- [9] L. S. Brown, *Classical limit of the hydrogen atom*, Am. J. Phys. **41** (1973) 525-530.
- [10] J. Mostowski, *On the classical limit of the Kepler problem*, Lett. Math. Phys. **2** (1977) 1-5.
- [11] M. M. Nieto and L. M. Simmons, Jr., *Coherent states for general potentials*, Phys. Rev. Lett. **41** (1978) 207-210.
- [12] M. M. Nieto *Coherent states for general potentials IV. Three-dimensional systems*, Phys. Rev. **D22** (1980) 391-402.
- [13] V. P. Gutschick and M. M. Nieto *Coherent states for general potentials V. Time evolution* Phys. Rev. **D22** (1980) 403-418.
- [14] D. R. Snider, *Elliptical orbits in quantum mechanics*, Am. J. Phys. **51** (1983) 801-803.
- [15] C. C. Gerry, *Coherent states and the Kepler-Coulomb problem*, Phys. Rev. **A33** (1986) 6-11.
- [16] D. Bhaumik, B. Dutta-Roy, and G. Ghosh, *Classical limit of the hydrogen atom*, J. Phys. A: Math. Gen **19** (1986) 1355-1364.
- [17] G. Alber, H. Ritsch, and P. Zoller, *Generation and detection of Rydberg wave packets by short laser pulses*, Phys. Rev. **A34** (1986) 1058-1064.
- [18] L. D. Noordam, D. I. Duncan, and T. F. Gallagher, *Ramsey fringes in atomic Rydberg wave packets*, Phys. Rev. **A45** (1992) 4734-4737.
- [19] G. Alber and P. Zoller, *Laser excitation of electronic wave packets in Rydberg atoms*, Phys. Rep. **199** (1991) 231-280.
- [20] B. M. Garraway and K.-A. Suominen, *Wave-packet dynamics: new physics and chemistry in*

- femto-time*, Rep. Prog. Phys. **58** (1995) 365-419.
- [21] *The Physics and Chemistry of Wave Packets*, eds. J. A. Yeazell and T. Uzer (Wiley, New York, 2000).
- [22] J. R. R. Verlet and H. H. Fielding, *Manipulating electron wave packets*, Int. Reviews in Physical Chemistry **20** (2001) 283-312.
- [23] R. A. L. Smith, J. R. R. Verlet, and H. H. Fielding, *Rydberg wave packets in molecules*, Phys. Chem. Chem. Phys. **5** (2003) 3567-3579.
- [24] J. A. Yeazell and C. R. Stroud, Jr., *Observation of spatially localized atomic electron wave-packets*, Phys. Rev. Lett. **60** (1988) 1494-1497.
- [25] L. D. Noordam, A. ten Wolde, H. G. Muller, A. Lagendijk, and H. B. van Linden van den Heuvell, *Return of an electronic wavefunction to the core*, J. Phys. B: At. Mol. Opt. Phys. **21** (1988) L533-L538.
- [26] A. ten Wolde, L. D. Noordam, A. Lagendijk, and H. B. van Linden van den Heuvell, *Observation of radially localized atomic electron wave packets*, Phys. Rev. Lett. **61** (1988) 2099-2101.
- [27] J. A. Yeazell, M. Mallalieu, J. Parker, and C. R. Stroud, Jr., *Classical periodic motion of atomic-electron wave packets*, Phys. Rev. **A40** (1989) 5040-5043.
- [28] J. Parker and C. R. Stroud, Jr., *Coherence and decay of Rydberg wave packets*, Phys. Rev. Lett. **56** (1986) 716-719. See also Ref. (29).
- [29] J. Parker and C. R. Stroud, Jr., *Rydberg wave packets and the classical limit*, Phys. Scr. **T12** (1986) 70-75.
- [30] J. A. Yeazell, M. Mallalieu, and C. R. Stroud, Jr., *Observation of the collapse and revival of a Rydberg electronic wave packet*, Phys. Rev. Lett. **64** (1990) 2007-2010.
- [31] J. A. Yeazell and C. R. Stroud, Jr., *Observation of fractional revivals in the evolution of a Rydberg atomic wave packet*, Phys. Rev. **A43** (1991) 5153-5156.
- [32] D. R. Meacher, P. E. Meyler, I. G. Hughes, and P. Ewart, *Observation of the collapse and revival of a Rydberg wavepacket in atomic rubidium*, J. Phys. B. **24** (1991) L63-L69.
- [33] J. Wals, H. H. Fielding, J. F. Christian, L. C. Snoek, W. J. van der Zande, and H. B. van Linden van den Heuvell, *Observation of Rydberg wave packet dynamics in a Coulombic and magnetic field*, Phys. Rev. Lett. **72** (1994) 3783-3786.
- [34] I. Sh. Averbukh and N. F. Perelman, *Fractional revivals: Universality in the long-term evolution of quantum wave packets beyond the correspondence principle dynamics*, Phys.

- Lett. **A139** (1989) 449-453; *Fractional revivals of wave packets*, Acta Phys. Pol. **78** (1990) 33-40. This paper includes much of the material in the citation above, correcting some minor typographical errors; *Fractional regenerations of wave-packets in the course of long-term evolution of highly excited quantum-systems*, Zh. Eksp. Teor. Fiziki. **96** (1989) 818-827 (Sov. Phys. JETP **69** (1989) 464-469.)
- [35] M. J. J. Vrakking, D. M. Villeneuve, and A. Stolow, *Observation of fractional revivals of a molecular wave packet*, Phys. Rev. **A54** (1996) R37-R40.
- [36] M. Nauenberg, C. Stroud, and J. Yeazell, *The classical limit of an atom*, Sci. Am. **270** (June) (1994) 44-49.
- [37] I. Sh. Averbukh and N. F. Perelman, *The dynamics of wave packets of highly-excited atoms and molecules*, Usp. Fiz. Nauk **161** (1991) 41-81 (Sov. Phys. Usp. **34** (1991) 572-591.)
- [38] R. Bluhm, V. A. Kostelecký, and J. Porter, *The evolution and revival structure of localized quantum wave packets*, Am. J. Phys. **64** (1996) 944-953 [arXiv:quant-ph/9510029].
- [39] L. Mandelstam and I. Tamm, *The uncertainty relation between energy and time in nonrelativistic quantum mechanics*, J. Phys. (USSR) **9** (1945) 249-254.
- [40] M. Nauenberg, *Autocorrelation function and quantum recurrence of wave packets*, J. Phys. B. At. Mol. Opt. Phys. **23** (1990) L385-L390.
- [41] P. Bocchieri and A. Loinger, *Quantum recurrence theorem*, Phys. Rev. **107** (1957) 337-338.
- [42] R. von Baltz, *Distance between quantum states and the motion of wave packets*, Eur. J. Phys. **11** (1990) 215-220.
- [43] H. Bohr, *Almost periodic functions* (Chelsea, New York, 1947).
- [44] I. C. Percival, *Almost periodicity and the quantal H theorem*, J. Math. Phys. **2** (1961) 235-239; **3** (1962) 386 where Percival cites earlier work by S. Ono and Ref. (41).
- [45] V. A. Ermoshin, M. Erdmann, and V. Engel, *Fermi-Pasta-Ulam recurrences, normal modes, and wave-packet revivals*, Chem. Phys. Lett. **356** (2002) 29-35.
- [46] E. Fermi, J. Pasta, and S. Ulam, Document LA-1940 Los Alamos Preprint (May 1995). Reprinted as *Studies of non-linear problems in Collected papers of Enrico Fermi*, Vol. II, Senior Editor, E. Segrè (University of Chicago, Chicago, 1965), pp. 978-988.
- [47] T. Hogg and B. A. Huberman, *Recurrence phenomena in quantum dynamics*, Phys. Rev. Lett. **48** (1982) 711-714.
- [48] A. Peres, *Multiple time scales for recurrences of Rydberg states*, Phys. Rev. **A47** (1993)

- 5196-5197.
- [49] N. Bohr, *Über die Anwendung der Quantentheorie auf den Atombau. I. Die Grundpostulate der Quantentheorie*, Z. Phys. **13** (1923) 117-165.
- [50] H. Goldstein, *Classical Mechanics*, 2nd edition (Addison-Wesley, Reading, 1980) pp. 457-471.
- [51] A. L. Fetter and J. D. Walecka, *Theoretical mechanics of particles and continua* (McGraw-Hill, New York, 1980) pp. 191-196.
- [52] A. B. Migdal and V. Krainov, *Approximation Methods in Quantum Mechanics* (Benjamin, New York, 1969) pp. 111-144.
- [53] D. W. Saxon, *Elementary Quantum Mechanics* (McGraw-Hill, New York, 1968).
- [54] See, e.g., C. Cohen-Tannoudji, D. Diu, and F. Laloë, *Quantum Mechanics Volume II* (Wiley, New York, 1977) pp. 1110-1116.
- [55] U. P. Sukhatme, *WKB energy levels for a class of one-dimensional potentials*, Am. J. Phys. **41** (1973) 1015-1016.
- [56] M. M. Nieto and L. M. Simmons, Jr., *Limiting spectra from confining potentials*, Am. J. Phys. **47** (1979) 634-635.
- [57] R. L. Liboff, *On the potential x^{2N} and the correspondence principle*, Int. J. Theor. Phys. **18** (1979) 185-191.
- [58] R. W. Robinett, *Wave packet revivals and quasirevivals in one-dimensional power law potentials*, J. Math. Phys. **41** (2000) 1801-1813.
- [59] C. Quigg and J. L. Rosner, *Quantum mechanics with applications to quarkonium*, Phys. Rep. **56** (1979) 167-235.
- [60] M. Greiner, O. Mandel, T. W. Hänsch, and I. Bloch, *Collapse and revival of the matter wave field of a Bose-Einstein condensate*, Nature **419** (2002) 51-54.
- [61] B. Yurke and D. Stoler, *Generating quantum mechanical superpositions of macroscopically distinguishable states via amplitude dispersion*, Phys. Rev. Lett. **57** (1986) 13-16; *Quantum behavior of a four-wave mixer operated in a nonlinear regime*, Phys. Rev. **A35** (1987) 4846-4849; *The dynamic generation of Schrödinger cats and their detection*, Physica **B151** (1988) 298-301; G. J. Milburn, *Quantum and classical Liouville dynamics of the anharmonic oscillator*, Phys. Rev. **A33** (1986) 674-685.
- [62] M. W. Noel and C. R. Stroud, Jr., *Young's double-slit interferometry within an atom*, Phys. Rev. Lett. **75** (1995) 1252-1255; *Excitation of an atomic electron to a coherent superposition*

- of macroscopically distinct states*, Phys. Rev. Lett. **77** (1996) 1913-1916.
- [63] W. P. Schleich, *Quantum optics in phase space*, (Wiley-VCH, Berlin, 2001).
- [64] H. Mack, M. Bienert, F. Haug, M. Freyberger, and W. P. Schleich, *Wave packets can factorize numbers*, Phys. Stat. Sol. (B) **233** (2002) 408-415; H. Mack, M. Bienert, F. Haug, F. S. Straub, M. Freyberger, and W. P. Schleich, *Wave packet dynamics and factorization of numbers*, in *Experimental quantum computation and information*, edited by F. de Martini and C. Monroe, Proc. of the International School of Physics “Enrico Fermi” (IOS Press, Amsterdam, 2002) pp. 369-384.
- [65] B. C. Berndt, R. J. Evans, and K. S. Williams, *Gauss and Jacobi sums*, (Wiley, New York, 1998).
- [66] C. F. Gauss, *Disquisitiones Arithmeticae*, (Fleischer, Leipzig, 1801); *Summatio quarundam serierum singularium*, Comment. Soc. Reg. Sci. Gottingensis **1** (1811).
- [67] C. Leichtle, I. Sh. Averbukh, and W. P. Schleich, *Generic structure of multilevel quantum beats*, Phys. Rev. Lett. **77** (1996) 3999-4002; *Multilevel quantum beats: An analytical approach*, Phys. Rev. **A54** (1996) 5299-5312.
- [68] S. I. Vetchinkin, A. S. Vetchinkin, V. V. Eryomin, and I. M. Umanskii, *Gaussian wavepacket dynamics in an anharmonic system*, Chem. Phys. Lett. **215** (1993) 11-16.
- [69] V. V. Eryomin, S. I. Vetchinkin, and I. M. Umanskii, *Manifestations of wave packet fractional revivals in a Morse-like anharmonic system*, J. Chem. Phys. **101** (1994) 10730-10735.
- [70] S. I. Vetchinkin and V. V. Eryomin, *The structure of wavepacket fractional revivals in a Morse-like anharmonic system*, Chem. Phys. Lett. **222** (1994) 394-398.
- [71] K. Dupret and D. Delande, *Nonlinear wave-packet dynamics for a generic one-dimensional time-independent system and its application to the hydrogen atom in a weak magnetic field*, Phys. Rev. **A53** (1996) 1257-1272.
- [72] P. A. Braun and V. I. Savichev, *The influence of higher-order anharmonic corrections to the energy spectrum on the evolution of quantum wavepackets*, J. Phys. B: At. Mol. Opt. Phys. **29** (1996) L329-L335.
- [73] U. Leonhardt, *State reconstruction of anharmonic molecular vibrations: Morse-oscillator model*, Phys. Rev. **A55** (1997) 3164-3172.
- [74] Q.-L. Jie, S.-J. Wang, and L.-F. Wei, *Partial revivals of wave packets: An action-angle phase-space description*, Phys. Rev. **A57** (1998) 3262-3267.

- [75] Q.-L. Jie and S.-J. Wang, *Equal partial revivals of wavepackets in long time scales*, J. Phys. A: Math. Gen. **33** (2000) 2513-2525.
- [76] G. G. de Polavieja, *Noncyclic geometric phase shift for quantal revivals*, Phys. Rev. Lett. **81** (1998) 1-5.
- [77] R. Bluhm and V. A. Kostelecký, *Long-term evolution and revival structure of Rydberg wave packets for hydrogen and alkali-metal atoms*, Phys. Rev. **A51** (1995) 4767-4786 [arXiv:quant-ph/9506009]; *Long-term evolution and revival structure of Rydberg wave packets*, Phys. Lett. **A200** (1995) 308-313 [arXiv:quant-ph/9508024]
- [78] O. Knospé and R. Schmidt, *Revivals of wave packets: General theory and application to Rydberg clusters*, Phys. Rev. **A54** (1996) 1154-1160.
- [79] R. Bluhm, V. A. Kostelecký, and B. Tudosé, *Wave-packet revivals for quantum systems with nondegenerate energies*, Phys. Lett. **A222** (1996) 220-226 [arXiv:quant-ph/9609020].
- [80] G. S. Agarwal and J. Banerji, *Fractional revivals in systems with two time scales*, Phys. Rev. **A57** (1998) 3880-3884.
- [81] M. Gutzwiller, *Chaos in classical and quantum mechanics*, (Springer-Verlag, New York, 1990); *The interplay between classical and quantum mechanics* (American Association of Physics Teachers, College Park, MD, 2001);
- [82] M. Brack and R. K. Bhaduri, *Semiclassical Physics* (Addison-Wesley, Reading MA, 1997)
- [83] A. K. Grant and J. L. Rosner, *Classical orbits in power-law potentials*, Am. J. Phys. **62** (1994) 310-315.
- [84] H. A. Bethe and E. E. Salpeter, *Quantum mechanics of one- and two-electron atoms* (Springer-Verlag, Berlin, 1957) pp. 27-29, 228-232; L. D. Landau and E. M. Lifschitz, *Quantum mechanics: non-relativistic theory*, 2nd edition (Pergamon Press, Oxford 1965) pp. 125-128, 269-274.
- [85] B. R. Holstein, *The harmonic oscillator propagator*, Am. J. Phys. **66** (1998) 583-589.
- [86] D. F. Styer, *The motion of wave packets through their expectation values and uncertainties*, Am. J. Phys. **58** (1990) 742-744.
- [87] R. J. Glauber, *Photon correlations*, Phys. Rev. Lett. **10** (1963) 84-86; *The quantum theory of optical coherence*, Phys. Rev. **130** (1963) 2529-2539; *Coherent and incoherent states of the radiation field*, Phys. Rev. **131** (1963) 2766-2788; E. C. G. Sudarshan, *Equivalence of semiclassical and quantum mechanical descriptions of statistical light beams*, Phys. Rev. Lett.

- 10** (1963) 277-279.
- [88] E. M. Wright, D. F. Walls, and J. C. Garrison, *Collapses and revivals of Bose-Einstein condensates formed in small atomic samples*, Phys. Rev. Lett. **77** (1996) 2158-2161.
- [89] K. Razi Naqvi and S. Waldenstrøm, *Revival, mirror revival, and collapse may occur even in a harmonic oscillator wave packet*, Phys. Scr. **62** (2000) 12-16. See also S. Waldenstrøm and K. Razi Naqvi, *A neglected aspect of the pulsating Gaussian wave packet*, Eur. J. Phys. **20** (1999) L41-L43.
- [90] C. U. Segre and J. D. Sullivan, *Bound-state wave packets*, Am. J. Phys. **44** (1976) 729-732. This paper contains one of the first references to what have become known as wave packet revivals.
- [91] D. L. Aronstein and C. R. Stroud Jr., *Fractional wave-function revivals in the infinite square well*, Phys. Rev. **A55** (1997) 4526-4537.
- [92] P. Stifter, W. E. Lamb Jr., and W. P. Schleich, *The particle in a box revisited*, in: Frontiers of Quantum Optics and Laser Physics, Proceedings of the International Conference on Quantum Optics and Laser Physics eds S. Y. Zhu, M. S. Zubairy, and M. O. Scully, (Springer, Singapore, 1997) pp. 236-246. See also Ref. (93).
- [93] W. E. Lamb, Jr., *Suppose Newton had invented wave mechanics*, Am. J. Phys. **62** (1994) 201-206.
- [94] R. W. Robinett, *Visualizing the collapse and revival of wave packets in the infinite square well using expectation values*, Am. J. Phys. **68** (2000) 410-420 [arXiv:quant-ph/0307041].
- [95] D. F. Styer, *Quantum revivals versus classical periodicity in the infinite square well*, Am. J. Phys. **69** (2001) 56-62.
- [96] K. Razi Naqvi, S. Waldenstrøm, and T. Haji Hassan, *Fractional revival of wave packets in an infinite square well: a Fourier perspective*, Eur. J. Phys. **22** (2001) 395-402.
- [97] M. A. Doncheski, S. Heppelmann, R. W. Robinett, and D. C. Tussey, *Wave packet construction in two-dimensional quantum billiards: Blueprints for the square, equilateral triangle, and circular cases*, Am. J. Phys. **71** (2003) 541-557 [arXiv:quant-ph/0307070].
- [98] F. Gori, D. Ambrosini, R. Borghi, V. Mussi, and M. Santarsiero, *The propagator for a particle in a well*, Eur. J. Phys. **22** (2001) 53-66.
- [99] S. A. Fulling and K. S. Güntürk, *Exploring the propagator of a particle in a box*, Am. J. Phys. **71** (2003) 55-63.

- [100] S. Waldenström, K. R. Naqvi, and K. J. Mork, *The force exerted by the walls of an infinite square well on a wave packet: Ehrenfest theorem, revivals and fractional revivals*, Phys. Scr. **68** (2003) 45-53.
- [101] M. Born, *Continuity, determinism, and reality*, Kgl. Danske Videns. Sels. Mat.-fys. Medd., **30** (2) (1955) 1-26. Born was addressing concerns made by Einstein in *Elementare Überlegungen zur Interpretation der Grundlagen der Quanten-Mechanik*, in *Scientific papers presented to Max Born* (Oliver and Boyd, Edinburgh, 1953) pp. 33-40.
- [102] M. Born and W. Ludwig, *Zur Quantenmechanik der kräftefreien Teilchens*, Z. Phys. **150** (1958) 106-117.
- [103] P. Stifter, C. Leichtle, W. P. Schleich, and J. Marklov, *Das Teilchen im Kasten: Strukturen in der Wahrscheinlichkeitsdichte* (translated as *The particle in a box: Structures in the probability density*), Z. Naturforsch **52 a** (1997) 377-385.
- [104] M. Kleber, *Exact solutions for time-dependent phenomena in quantum mechanics*, Phys. Rep. **236** (1994) 331-393.
- [105] P. A. Braun and V. I. Savichev, *Time dependence of physical observables in wave-packet states*, Phys. Rev. **A49** (1994) 1704-1708.
- [106] M. A. Doncheski and R. W. Robinett, *Anatomy of a quantum 'bounce'*, Eur. J. Phys. **20** (1999) 29-37 [arXiv:quant-ph/0307010].
- [107] E. Wigner, *On the quantum correction for thermodynamic equilibrium*, Phys. Rev. **40** (1932) 749-759.
- [108] M. Belloni, M. Doncheski, and R. W. Robinett, *Wigner quasi-probability distribution for the infinite square well: energy eigenstates and time-dependent wave packets*, to be submitted for publication.
- [109] V. I. Tatarskiĭ, *The Wigner representation of quantum mechanics*, Usp. Fiz. Nauk **139** (1983) 587-619 (Sov. Phys. Usp. **26** (1983) 311-327.)
- [110] N. L. Balaczs and B. K. Jennings, *Wigner's function and other distribution functions in mock phase space*, Phys. Rep. **105** (1984) 347-391.
- [111] P. Carruthers and F. Zachariasen, *Quantum collision theory with phase-space distributions*, Rev. Mod. Phys. **55** (1983) 245-285.
- [112] M. Hillery, R. F. O'Connell, M. O. Scully, and E. P. Wigner, *Distribution functions in physics: Fundamentals*, Phys. Rep. **106** (1984) 121-167.

- [113] Y. S. Kim and E. P. Wigner, *Canonical transformations in quantum mechanics*, Am. J. Phys. **58** (1990) 439-448.
- [114] Y. W. Kim and M. E. Noz, *Phase space picture of quantum mechanics: Group theoretical approach*, Lecture Notes in Physics Series, Vol. 40 (World Scientific, Singapore, 1990).
- [115] M. Casas, H. Krivine, and J. Martorell, *On the Wigner transforms of some simple systems and their semiclassical interpretations*, Eur. J. Phys. **12** (1991) 105-111.
- [116] H.-W. Lee, *Theory and application of the quantum phase-space distribution functions*, Phys. Rep. **259** (1995) 147-211.
- [117] A. M. Ozorio de Almeida, *The Weyl representation in classical and quantum mechanics*, Phys. Rep. **295** (1998) 265-342.
- [118] R. L. Hudson, *When is the Wigner quasi-probability density non-negative?*, Rep. Math. Phys. **6** (1974) 249-252; F. Sofo and P. Claverie, *When is the Wigner function of multi-dimensional systems nonnegative?*, J. Math. Phys. **24** (1983) 97-100.
- [119] L. E. Ballentine, *Quantum mechanics: A modern development*, (World Scientific, Singapore, 1998).
- [120] W. Kinzel, *Bilder elementarer Quantenmechanik*, Phys. Bl. **51** (1995) 1190-1191.
- [121] M. V. Berry, *Quantum fractals in boxes*, J. Phys. A: Math. Gen. **29** (1996) 6617-6629.
- [122] F. Großmann, J. -M. Rost, and W. P. Schleich, *Spacetime structures in simple quantum systems*, J. Phys. **A30** (1997) L277-L283.
- [123] I. Marzoli, F. Saif, I. Bialynicki-Birula, O. M. Friesch, A. E. Kaplan, W. P. Schleich, *Quantum carpets made simple*, Acta Phys. Slov. **48** (1998) 323-333 [arXiv:quant-ph/9806033].
- [124] A. E. Kaplan, P. Stifter, K. A. H. van Leeuwen, W. E. Lamb, Jr., and W. P. Schleich, *Intermode traces – Fundamental interference phenomena in quantum and wave physics*, Phys. Scr. **T76** (1998) 93-97.
- [125] W. Loinaz and T. J. Newman, *Quantum revivals and carpets in some exactly solvable systems*, J. Phys. A: Math. Gen. **32** (1999) 8889-8895 [arXiv:quant-ph/9902039].
- [126] M. J. W. Hall, M. S. Reineker, W. P. Schleich, *Unravelling quantum carpets: a travelling wave approach*, J. Phys. **A32** (1999) 8275-8291, [arXiv:quant-ph/9906107].
- [127] A. E. Kaplan, I. Marzoli, W. E. Lamb, Jr., and W. P. Schleich, *Multimode interference: Highly regular pattern formation in quantum wave-packet evolution*, Phys. Rev. **A61** (2000) 032101 - 1-6.

- [128] O. M. Friesch, I. Marzoli, and W. P. Schleich, *Quantum carpets woven by Wigner functions*, New. J. Phys. **2** (2000) 4.1-4.11 <http://www.jnp.org/>
- [129] W. G. Harter, *Quantum-fractal revival structure in C_N quadratic spectra: Base- N quantum computer registers*, Phys. Rev. **A64** (2001) 012312 - 1-17; *Wave node dynamics and revival symmetry in quantum rotors*, J. Mol. Spec. **210** (2001) 166-182.
- [130] E. J. Heller, *Bound-state eigenfunctions of classical chaotic Hamiltonian systems: Scars of periodic orbits*, Phys. Rev. Lett. **53** (1984) 1515-1518; L. Kaplan and E. J. Heller, *Linear and non-linear theory of eigenfunction scars*, Ann. Phys. **264** (1998) 171-206; *Measuring scars of periodic orbits*, Phys. Rev. **E59** (1999) 6609-6628.
- [131] F. Cooper, A. Khare, and U. Sukhatme, *Supersymmetry and quantum mechanics*, Phys. Rep. **251** (1995) 267-385.
- [132] R. Dutt, A. Khare, and U. Sukhatme, *Supersymmetry, shape invariance, and exactly solvable potentials*, Am. J. Phys. **56** (1988) 163-168.
- [133] F. Cooper and B. Freedman, *Aspects of supersymmetric quantum mechanics*, Ann. Phys. **146** (1983) 262-288.
- [134] E. Witten, *Dynamical breaking of supersymmetry*, Nucl. Phys. **B188** (1981) 513-554.
- [135] J.-P. Antoine, J.-P. Gazeau, P. Monceau, J. R. Klauder, and K. A. Penson, *Temporally stable coherent states for infinite well and Pöschl-Teller potentials*, J. Math. Phys. **42** (2001) 2349-2387.
- [136] F. Gori and L. de la Torre, *Diophantine equation for the \tan^2 well*, Eur. J. Phys. **24** (2003) 1-5.
- [137] J. Banerji and G. W. Agarwal, *Revival and fractional revival in the quantum dynamics of $SU(1,1)$ coherent states*, Phys. Rev. **A59** (1999) 4777-4783.
- [138] R. Bluhm and V. A. Kostelecký, *Atomic supersymmetry, Rydberg wave packets, and radial squeezed states*, Phys. Rev. **A** (1994) 4628-4640 [arXiv:quant-ph/9508020].
- [139] A. Venugopalan and G. S. Agarwal, *Superrevivals in the quantum dynamics of a particle confined in a finite square-well potential*, Phys. Rev. **A59** (1999) 1413-1421 [arXiv:quant-ph/9811012].
- [140] D. L. Aronstein and C. R. Stroud Jr., *Analytical investigation of revival phenomena in the finite square-well potential*, Phys. Rev. **A62** (2000) 022102 - 1-9.
- [141] D. L. Aronstein and C. R. Stroud Jr., *General series solution for finite square-well energy*

- levels for use in wave-packet studies, *Am. J. Phys.* **68** (2000) 943-949.
- [142] S. T. Epstein, *Application of the Rayleigh-Schrödinger perturbation theory to the delta-function potential*, *Am. J. Phys.* **28** (1960) 495-496; W. E. Gettys, *Quantum theory of a square well plus delta function potential*, *Am. J. Phys.* **41** (1973) 670-677; D. Atkinson and H. W. Crater, *An exact treatment of the Dirac δ -function in the Schrödinger equation*, *Am. J. Phys.* **43** (1974) 301-304; I. R. Lapidus, *One-dimensional hydrogen atom in an infinite square well*, *Am. J. Phys.* **50** (1982) 563-564; I. R. Lapidus, *Particle in a square well with a δ -function potential*, *Am. J. Phys.* **55** (1987) 172-174; P. Senn, *Time evolutions of quantum mechanical states in a symmetric double-well potential*, *Am. J. Phys.* **60** (1992) 228-231; J. Goldstein, C. Lebedzik, and R. W. Robinett, *Supersymmetric quantum mechanics: Examples with Dirac δ functions*, *Am. J. Phys.* **62** (1994) 612-618.
- [143] G. A. Vugalter, A. K. Das, and V. A. Sorokin, *Revivals in an infinite square well in the presence of a δ well*, *Phys. Rev.* **A66** (2002) 012104 - 1-7.
- [144] J. P. Dowling and J. Gea-Banacloche, *Evanescent light-wave atom mirrors, resonators, waveguides, and traps*, in *Adv. At. Mol. Opt.* **37**, edited by B. Bederson and H. Walther (Academic Press, San Diego, 1996) pp. 1-94.
- [145] C. G. Aminoff, A. M. Steane, P. Bouyer, P. Desbiolles, J. Dalibard, and C. Cohen-Tannoudji, *Cesium atoms bouncing in a stable gravitational cavity*, *Phys. Rev. Lett.* **71** (1993) 3083-3086.
- [146] T. M. Roach, H. Abele, M. G. Boshier, H. L. Grossman, K. P. Zetie, and E. A. Hinds, *Realization of a magnetic mirror for cold atoms*, *Phys. Rev. Lett.* **75** (1995) 629-632.
- [147] P. Szriftgiser, D. Guéry-Odelin, M. Arndt, and J. Dalibard, *Atomic wave diffraction and interference using temporal slits*, *Phys. Rev. Lett.* **77** (1996) 4-7.
- [148] W. -Y. Chen and G. J. Milburn, *Fractional quantum revivals in the atomic gravitational cavity*, *Phys. Rev.* **A51** (1995) 2328-2333.
- [149] J. Gea-Banacloche, *A quantum bouncing ball*, *Am. J. Phys.* **67** (1999) 776-782.
- [150] O. Vallée, Comment on Ref. (149), *Am. J. Phys.* **68** (2000) 672-673; D. M. Goodmanson, *A recursion relation for matrix elements of the quantum bouncer*, *Am. J. Phys.* **68** (2000) 866-868.
- [151] M. A. Doncheski and R. W. Robinett, *Expectation value analysis of wave packet solutions for the quantum bouncer: Short-term classical and long-term revival behaviors*, *Am. J. Phys.* **69** (2001) 1084-1090 [arXiv:quant-ph/0307046].

- [152] F. Saif, G. Alber, V. Savichev, and W. P. Schleich, *Quantum revivals in a periodically driven gravitational cavity*, J. Opt. B: Quant. Semiclass. Opt. **2** (2000) 668-671 [arXiv:quant-ph/0006041].
- [153] F. Saif, *Quantum recurrences: Probe to study quantum chaos*, Phys. Rev. **E62** (2000) 6308-6311.
- [154] G. Breit, *The propagation of Schroedinger waves in a uniform field of force*, Phys. Rev. **32** (1928) 273-276.
- [155] V. V. Nesvizhevsky *et al.*, *Quantum states of neutrons in the Earth's gravitational Field*, Nature **415** (2002) 297-299; *Measurement of quantum states of neutrons in the Earth's gravitational field*, Phys. Rev. **D67** (2003) 102002 - 1-9.
- [156] B. O. Kerbikov, A. E. Kudryavtsev, and V. A. Lensky, *Neutron-antineutron oscillations in a trap revisited*, [arXiv:hep-ph/0306039].
- [157] M. Andrews, *Wave packets bouncing off walls*, Am. J. Phys. **66** (1998) 252-254.
- [158] L. de la Torre and F. Gori, *The bouncing bob: quasi-classical states*, Eur. J. Phys. **24** (2003) 253-259.
- [159] A. C. de la Torre, H. O. M'artin, and D. Goyeneche, *Quantum diffusion on a cyclic one dimensional lattice*, Phys. Rev. **E68** (2003) 031103 - 1-9 [arXiv:quant-ph/0304065].
- [160] E. U. Condon, *The physical pendulum in quantum mechanics*, Phys. Rev. **31** (1928) 891-894.
- [161] M. A. Doncheski and R. W. Robinett, *Wave packet revivals and the energy eigenvalue spectrum of the quantum pendulum*, Ann. Phys. **308** (2003) 578-598 [arXiv:quant-ph/0307079]. See also Ref. (162).
- [162] J. C. Ross and H. W. Capel, *Fractional revivals of coherence in quantum mechanical oscillators*, Physica **A287** (2000) 217-258.
- [163] P. Rozmej and R. Arvieu, *Clones and other interference effects in the evolution of angular-momentum coherent states*, Phys. Rev. **A58** (1998) 4314-4329.
- [164] M. Auzinsh, *The evolution and revival structure of angular momentum wave packets (Tutorial)*, Can. J. Phys. **77** (1999) 491-503 [arXiv:physics/9905019].
- [165] S. Tomsovic and J. H. Lefebvre, *Can wave packet revivals occur in chaotic quantum systems?*, Phys. Rev. Lett. **79** (1997) 3629-3632.
- [166] M. V. Berry and M. Wilkinson, *Diabolical points in the spectra of triangles*, Proc. of the Royal Society, London, **A392** (1984) 15-43.

- [167] W. -K. Li, *A particle in an isosceles right triangle*, J. Chem. Educ. **61** (1984) 1034.
- [168] R. W. Robinett, *Isolated versus non-isolated periodic orbits in variants of the two-dimensional square and circular billiards*, J. Math. Phys. **40** (1999) 101-122.
- [169] J. Mathews and R. L. Walker, *Mathematical Methods of Physics*, 2nd edition (W. A. Benjamin, Menlo Park, 1970) pp. 237-239.
- [170] C. Jung, *An exactly soluble three-body problem in one-dimension*, Can. J. Phys. **58** (1980) 719-728.
- [171] P. J. Richens and M. V. Berry, *Pseudointegrable systems in classical and quantum mechanics*, Physica **2D** (1981) 495-512.
- [172] W. -K. Li and S. M. Blinder, *Particle in an equilateral triangle: Exact solution of a nonseparable problem*, J. Chem. Educ. **64** (1987) 130-132.
- [173] M. A. Doncheski and R. W. Robinett, *Quantum mechanical analysis of the equilateral triangle billiard: periodic orbit theory and wave packet revivals*, Ann. Phys. (New York) **299** (2002) 208-227. [arXiv:quant-ph/0307063].
- [174] R. L. Liboff, *The polygon quantum-billiard problem*, J. Math. Phys. **35** (1994) 596-607.
- [175] V. Amar, M. Pauri, and A. Scotti, *Schrödinger equation for convex plane polygons: A tiling method for the derivation of eigenvalues and eigenfunctions*, J. Math. Phys. **32** (1991) 2442-2449; *Schrödinger equation for convex plane polygons. II. A no-go theorem for plane waves representation of solutions*, J. Math. Phys. **34** (1993) 3343-3350.
- [176] R. L. Liboff, *The hexagon quantum billiard*, J. Stat. Phys. **105** (2001) 389-402.
- [177] R. W. Robinett and S. Heppelmann, *Quantum wave-packet revivals in circular billiards*, Phys. Rev. **A65** (2002) 062103 - 1-10 [arXiv:quant-ph/0307020].
- [178] R. E. Langer, *On the connection formulas and the solutions of the wave equation*, Phys. Rev. **51** (1937) 669-676.
- [179] L. D. Landau and E. M. Lifschitz, *Quantum mechanics: non-relativistic theory*, (Pergamon Press, London, 1958) pp. 166-171
- [180] M. V. Berry and K. E. Mount, *Semiclassical approximations in wave mechanics*, Rep. Prog. Phys. **35** (1972) 315-397.
- [181] N. Fröman and P. O. Fröman, *Phase-integral method*, (Springer, New York, 1996)
- [182] M. V. Berry and A. M. Ozorio de Almeida, *Semiclassical approximation of the radial equation with two-dimensional potentials*, J. Phys. A: Math **6** (1973) 1451-1460.

- [183] M. Robnik, *Quantising a generic family of billiards with analytic boundaries*, J. Phys. A: Math. Gen. **17** (1984) 1049-1074; T. Prosen and M. Robnik, *Failure of semiclassical methods to predict individual energy levels*, J. Phys. A: Math. Gen. **26** (1993) L37-L44.
- [184] J. Main, K. Weiberg, and G. Wunner, *\hbar expansion for the periodic orbit quantization by harmonic inversion*, Phys. Rev. **E58** (1998) 4436-4439.
- [185] H. Friedrich and J. Trost, *Accurate WKB wave functions for weakly attractive inverse square potentials*, Phys. Rev. **A59** (1999) 1683-1686.
- [186] R. Bluhm and V. A. Kostelecký, *Quantum defects and the long-term behavior of radial Rydberg wave packets*, Phys. Rev. **A50** (1994) R4445-R4448 [arXiv:hep-ph/9410325].
- [187] J. Wals, H. H. Fielding, and H. B. van Linden van den Heuvell, *The role of the quantum defect and of high-order dispersion in Rydberg wave packets*, Phys. Scr. **T58** (1995) 62-68.
- [188] R. W. Robinett, *Quantum mechanics of the two-dimensional circular billiard plus baffle system and half-integral angular momentum*, Eur. J. Phys. **24** (2003) 231-243 [arXiv:quant-ph/0307035].
- [189] J. A. Yeazell and C. R. Stroud, Jr., *Rydberg-atom wave packets localized in angular variables*, Phys. Rev. **A35** (1987) 2806-2809.
- [190] W. A. Henle, H. Ritsch, and P. Zoller, *Rydberg wave packets in many-electron atoms excited by short laser pulses*, Phys. Rev. **A36** (1987) 683-692.
- [191] J. Grochmalicki and M. Lewenstein, *Excitation of Rydberg wavepackets by short laser pulses*, J. Phys. B: At. Mol. Opt. Phys. **21** (1988) 3285-3302.
- [192] M. Nauenberg, *Quantum wave packets on Kepler elliptic orbits*, Phys. Rev. **A40** (1989) 1133-1136.
- [193] J. Parker and C. R. Stroud, Jr., *Population trapping in short-pulse laser ionization*, Phys. Rev. **A41** (1990) 1602-1608.
- [194] Z. D. Gaeta and C. R. Stroud, Jr., *Classical and quantum-mechanical dynamics of a quasi-classical state of the hydrogen atom*, Phys. Rev. **A42** (1990) 6308-6313; Z. D. Gaeta, M. W. Noel, and C. R. Stroud, Jr., *Excitation of the classical-limit state of an atom*, Phys. Rev. Lett. **73** (1994) 636-639.
- [195] I. M. Suarez Barnes, M. Nauenberg, M. Nockleby, and S. Tomsovic, *Semiclassical theory of quantum propagation: The Coulomb potential*, Phys. Rev. Lett. **71** (1993) 1961-1964.
- [196] M. Mallalieu and C. R. Stroud, Jr., *Semiclassical dynamics of circular orbit Rydberg wave*

- packets*, Phys. Rev. **A49** (1994) 2329-2339.
- [197] M. Mallalieu and C. R. Stroud, Jr., *Semiclassical theory of Rydberg-wave-packet interferometry*, Phys. Rev. **A51** (1995) 1827-1835.
- [198] R. Bluhm and V. A. Kostelecký, *Radial squeezed states and Rydberg wave packets*, Phys. Rev. **A48** (1993) R4047-R4050 [arXiv:quant-ph/9508019]; *Elliptical squeezed states and Rydberg wave packets*, Phys. Rev. **A52** (1995) 2234-2244 [arXiv:quant-ph/9509010]; *Keplerian squeezed states and Rydberg wave packets*, Phys. Rev. **A53** (1996) 937-945 [arXiv:quant-ph/9510023].
- [199] R. Bluhm, V. A. Kostelecký, and B. Tudosé, *Revivals of Rydberg wave packets*, Phys. At. Nucl. **61** (1998) 1948-1953 [arXiv:quant-ph/9711073].
- [200] H. Carlsen and O. Goscinski, *Dynamics of particles for circular Rydberg states*, Phys. Rev. **A59** (1999) 1063-1069.
- [201] D. Delande and J. C. Gay, *A new method for producing circular Rydberg states*, Europhys. Lett. **5** (1988) 303-308; J. Hare, M. Gross, and P. Goy, *Circular atoms prepared by a new method of crossed electric and magnetic fields*, Phys. Rev. Lett. **61** (1988) 1938-1941; J.-C. Gay, D. Delande, and A. Bommier, *Atomic quantum states with maximum localization on classical elliptical orbits*, Phys. Rev. **A39** (1989) 6587-6590; F. Penent, D. Delande, and J. C. Gay, *Rydberg states of rubidium in crossed electric and magnetic fields*, Phys. Rev. **37** (1988) 4707-4719.
- [202] M. Strehle, U. Weichmann, and G. Gerber, *Femtosecond time-resolved Rydberg wave-packet dynamics in the two-electron system calcium*, Phys. Rev. **A58** (1998) 450-455.
- [203] A. Wetzels, A. Gürtler, H. G. Muller, and L. D. Noordam, *The dynamics of a THz Rydberg wavepacket*, Eur. Phys. J. **D14** (2001) 157-165.
- [204] *Laser excitation of Stark-induced resonances*, Phys. Rev. **A40** (1989) 1321-1329.
- [205] A. ten Wolde, L. D. Noordam, A. Lagendijk, H. B. van Linden van den Heuvell, *Atomic electron wave packets in an electrical field*, Phys. Rev. **A40** (1989) 485-488.
- [206] L. D. Noordam, A. ten Wolde, A. Lagendijk, H. B. van Linden van den Heuvell, *Time dependence of an atomic electron wave function in an electrical field*, Phys. Rev. **A40** (1989) 6999-7006.
- [207] H. H. Fielding, J. Wals, W. J. van der Zande, and H. B. van Linden van den Heuvell, *Rydberg-electron wave-packet dynamics in parallel electric and magnetic fields and evidence*

- for stabilization, Phys. Rev. **A51** (1995) 611-619.
- [208] M. L. Naudeau, C. I. Sukenik, and P. H. Bucksbaum, *Core scattering of Stark wave packets*, Phys. Rev. **A56** (1997) 636-639.
- [209] J. Wals, H. H. Fielding, H. V. van Linden van den Heuvell, *Rydberg electron dynamics in external fields*, Mod. Phys. Lett. **B9** (1995) 1845-1871.
- [210] B. Broers, J. F. Christian, J. H. Hoogenraad, W. J. van der Zande, H. B. van Linden van den Heuvell, and L. D. Noordam, *Time-resolved dynamics of electronic wave packets above the classical field-ionization threshold*, Phys. Rev. Lett. **71** (1993) 344-347; J. F. Christian, B. Broers, J. H. Hoogenraad, W. J. van der Zande, and L. D. Noordam, *Rubidium electronic wave packets probed by a phase-sensitive pump-probe technique*, Opt. Comm. **103** (1993) 79-84; B. Broers, J. F. Christian, and H. B. van Linden van den Heuvell, *Experimental investigation of rubidium atoms above the field-ionization limit using a time-resolved wave packet approach*, Phys. Rev. **A49** (1994) 2498-2507; G. M. Lankhuijzen and L. D. Noordam, *Frequency- and time-resolved study of the dynamics of rubidium Rydberg wave packets in an electric field*, Phys. Rev. **A52** (1995) 2016-2028.
- [211] E. Reinhold and W. Ubachs, *Observation of coherent wave packets in a heavy Rydberg system*, Phys. Rev. Lett. **88** (2002) 013001 - 1-4.
- [212] R. Bluhm, V. A. Kostelecký, and B. Tudosé, *Revival structure of Stark wave packets*, Phys. Rev. **A55** (1997) 819-822 [arXiv:quant-ph/9608040].
- [213] R. M. Bowman, M. Dantus, and A. H. Zewail, *Femtosecond transition-state spectroscopy of iodine: From strongly bound to repulsive surface dynamics*, Chem. Phys. Lett. **161** (1989) 297-302.
- [214] M. Dantus, R. M. Bowman, and A. H. Zewail, *Femtosecond laser observations of molecular vibration and rotation*, Nature **343** (1990) 737-739.
- [215] M. J. Rosker, T. S. Rose, and A. H. Zewail, *Femtosecond real-time dynamics of photofragment-trapping resonances on dissociative potential energy surfaces*, Chem. Phys. Lett. **146** (1988) 175-179; T. S. Rose, M. J. Rosker, and A. H. Zewail, *Femtosecond real-time probing of reactions. IV. The reactions of alkali halides*, J. Chem. Phys. **91** (1989) 7415-7436.
- [216] M. H. M. Janssen, R. M. Bowman, and A. H. Zewail, *Femtosecond temporal spectroscopy of ICl: inversion to the $A^3\Pi_1$ state potential*, Chem. Phys. Lett. **172** (1990) 99-108.
- [217] T. Baumert, V. Engel, C. Röttgermann, W. T. Strunz, and G. Gerber, *Femtosecond pump-*

- probe study of the spreading and recurrence of a vibrational wave packet in Na₂*, Chem. Phys. Lett. **191** (1992) 639-44. See also Ref. (218).
- [218] S. Rutz, S. Greschik, E. Schreiber, and L. Wöste, *Femtosecond wave packet propagation in spin-orbit coupled electronic states of the Na₂ molecule*, Chem. Phys. Lett. **257** (1996) 365-373.
- [219] I. Fischer, M. J. J. Vrakking, D. M. Villeneuve, and A. Stolow, *Femtosecond time-resolved zero kinetic energy photoelectron and photoionization spectroscopy studies of I₂ wavepacket dynamics*, Chem. Phys. **207** (1996) 331-354.
- [220] J. Heufelder, H. Ruppe, S. Rutz, E. Schreiber, and L. Wöste, *Fractional revivals of vibrational wave packets in the NaK A¹Σ⁺ state*, Chem. Phys. Lett. **269** (1997) 1-8.
- [221] S. Rutz, R. de Vivie-Riedle, and E. Schreiber, *Femtosecond wave-packet propagation in spin-orbit-coupled electronic states of ^{39,39}K₂ and ^{39,41}K₂*, Phys. Rev. **A54** (1996) 306-313; S. Rutz and E. Schreiber, *Isotope-selective femtosecond wave packet dynamics: The rare ^{41,41}K₂ molecule*, Eur. Phys. J. **D4** (1998) 151-158.
- [222] See, e.g., *Separation of isotopes*, edited by H. London (George Newnes Limited, London, 1961).
- [223] P. T. Greenland, *Laser isotope separation*, Contemp. Phys. **31** (1990) 405-424; W. H. King, *Isotope shifts in atomic spectra* (Plenum, New York, 1984).
- [224] I. Sh. Averbukh, M. J. J. Vrakking, D. M. Villeneuve, and A. Stolow, *Wave packet isotope separation*, Phys. Rev. Lett. **77** (1996) 3518-3521.
- [225] M. Leibscher and I. Sh. Averbukh, *Optimal control of wave-packet isotope separation*, Phys. Rev. **A63** (2001) 043407 - 1-9
- [226] *Laser isotope separation by excitation of wavepackets*, I. Sh. Averbukh, United States Patent 5827405 (October 27, 1998).
- [227] S. Yu. Grebenshchikov, C. Beck, H. Flöthmann, D. H. Mordaunt, and R. Schinke, *Revivals in triatomic molecules: influence of mode mixing*, Chem. Phys. Lett. **271** (1997) 197-203.
- [228] S. Meyer and V. Engel, *Vibrational revivals and the control of photochemical reactions*, J. Phys. Chem. **101** (1997) 7749-7753.
- [229] J. P. Heritage, T. K. Gustafson, and C. H. Lin, *Observation of coherent transient birefringence in CS₂ vapor*, Phys. Rev. Lett. **34** (1975) 1299-1302.
- [230] P. M. Felker and A. H. Zewail, *Molecular structures from ultrafast coherence spectroscopy*, in

- Femtosecond Chemistry* Volume 1 (VCH, Weinheim, 1995) edited by J. Manz and L. Wöste, pp. 193-260.
- [231] T. Seideman, *Revival structure of aligned rotational wave packets*, Phys. Rev. Lett. **83** (1999) 4971-4974.
- [232] F. Rosca-Pruna and M. J. J. Vrakking, *Experimental observation of revival structures in picosecond laser-induced alignment of I_2* , Phys. Rev. Lett. **87** (2001) 152902 - 1-4.
- [233] F. Rosca-Pruna and M. J. J. Vrakking, *Revival structures in picosecond laser-induced alignment of I_2 molecules. I. Experimental results*, J. Chem. Phys. **116** (2002) 6567-6578; *Revival structures in picosecond laser-induced alignment of I_2 molecules. II. Numerical modeling*, J. Chem. Phys. **116** (2002) 6579-6588.
- [234] R. A. Bartels, T. C. Weinacht, N. Wagner, M. Baertschy, C. H. Greene, M. M. Murnane, and H. C. Kapteyn, *Phase modulation of ultrashort light pulses using molecular rotational wave packets*, Phys. Rev. Lett. **88** (2002) 013903 - 1-4.
- [235] M. Comstock, V. V. Lozovoy, and M. Dantus, *Rotational wavepacket revivals for phase modulation of ultrafast pulses*, Chem. Phys. Lett. **372** (2003) 739-744.
- [236] S. C. Althorpe and T. Seideman, *Predictions of rotation-vibration effects in time-resolved photoelectron angular distributions*, J. Chem. Phys. **113** (2000) 7901-7910; T. Hansson, *Cross-revival of molecular wave packets*, Phys. Rev. **A61** (2000) 033404 - 1-7.
- [237] I. Jex and G. Alber, *Rotational wavepacket dynamics of the C_{60} molecule*, J. Phys. B: At. Mol. Opt. Phys. **33** (2000) 1663-1674.
- [238] E. T. Jaynes and F. W. Cummings, *Comparison of quantum and semiclassical radiation theories with applications to the beam maser*, Proc. IEEE **51** (1963) 89-109.
- [239] S. Stenholm, *Quantum theory of electromagnetic fields interacting with atoms and molecules*, Phys. Rep. **6** (1973) 1-122.
- [240] P. L. Knight and P.W. Milloni, *The Rabi frequency in optical spectra*, Phys. Rep. **66** (1980) 21-107.
- [241] H.-I. Yoo and J. H. Eberly, *Dynamical theory of an atom with two or three levels interacting with quantized cavity fields*, Phys. Rep. **118** (1985) 239-337.
- [242] S. M. Barnett, P. Filipowicz, J. Javanainen, P. L. Knight, and P. Meystre, *The Jaynes-Cummings model and beyond* in *Frontiers in Quantum Optics*, edited by E. R. Pike and S. Sarkar (Adam Hilger, Bristol, 1986).

- [243] F. W. Cummings, *Stimulated emission of radiation in a single mode*, Phys. Rev. **140** (1965) A1051-A1056.
- [244] P. Meystre, A. Quattropani, and H. P. Baltes, *Quantum mechanical approach to Rabi flipping*, Phys. Lett. **49A** (1974) 85-86.
- [245] J. H. Eberly, N. B. Narozhny, and J. J. Sanchez-Mondragon, *Periodic spontaneous collapse and revival in a simple quantum model*, Phys. Rev. Lett. **44** (1980) 1323-1326.
- [246] N. B. Narozhny, J. J. Sanchez-Mondragon, and J. H. Eberly, *Coherence versus incoherence: Collapse and revival in a simple quantum model*, Phys. Rev. **A23** (1981) 236-247.
- [247] J. Frahm, *Quantenmechanische Streuung der elektrischen Feldstärke einer gestörten Resonator-Eigenschwingung*, Ann. Phys (Leipzig) **18** (1966) 205-208.
- [248] H.-I. Yoo, J. J. Sanchez-Mondragon, and J. H. Eberly, *Non-linear dynamics of the fermion-boson model: Interference between revivals and the transition to irregularity*, J. Phys. A: Math. Gen. **14** (1981) 1383-1397.
- [249] M. Fleischhauer and W. P. Schleich, *Revivals made simple: Poisson summation formula as a key to the revivals in the Jaynes-Cummings model*, Phys. Rev. **A47** (1993) 4258-4269. See also Ref. (250).
- [250] P. Filipowicz, *Quantum revivals in the Jaynes-Cummings model*, J. Phys. A: Math. Gen. **19** (1986) 3785-3795.
- [251] K. E. Cahill and R. J. Glauber, *Density operators and quasiprobability distributions*, Phys. Rev. **177** (1969) 1882-1902.
- [252] J. Eiselt and H. Risken, *Calculation of quasiprobabilities for the damped Jaynes-Cummings model*, Opt. Comm. **72** (1989) 351-355; *Quasiprobability distributions for the Jaynes-Cummings model with cavity damping*, Phys. Rev. **A43** (1991) 346-360.
- [253] G. Rempe, H. Walter, and N. Klein, *Observation of quantum collapse and revival in a one-atom maser*, Phys. Rev. Lett. **58** (1987) 353-356. See also F. Diedrich, J. Krause, G. Rempe, M. O. Scully, and H. Walther, *Laser experiments with single atoms as a test of basic physics*, IEEE J. Quant. Electron. **24** (1988) 1314-1319.
- [254] D. Meschede, H. Walther, and G. Müller, *One-atom maser*, Phys. Rev. Lett. **54** (1985) 511-554
- [255] M. Brune, F. Schmidt-Kaler, A. Maali, J. Dreyer, E. Hagley, J. M. Raimond, and S. Haroche, *Quantum Rabi oscillations: A direct test of field quantization in a cavity*, Phys. Rev. Lett.

- 76** (1996) 1800-1805.
- [256] E. M. Wright and P. Meystre, *Collapse and revival in the micromaser*, Opt. Lett. **14** (1989) 177-179.
- [257] I. Sh. Averbukh, *Fractional revivals in the Jaynes-Cummings model*, Phys. Rev. **A46** (1992) R2205-R2208.
- [258] P. F. Góra and C. Jędrzejek, *Superstructures, fractional revivals, and optical Schrödinger-cat states in the Jaynes-Cummings model*, Phys. Rev. **A48** (1993) 3291-3300; *Revivals and superstructures in the Jaynes-Cummings model with a small number of photons*, Phys. Rev. **A49** (1994) 3046-3056.
- [259] J. I. Cirac, R. Blatt, A. S. Parkins, and P. Zoller, *Quantum collapse and revival in the motion of a single trapped ion*, Phys. Rev. **A49** (1994) 1202-1207.
- [260] T. Quang, P. L. Knight, and V. Bužek, *Quantum collapses and revivals in an optical cavity*, Phys. Rev. **A44** (1991) 6092-6096.
- [261] J. Gea-Banacloche, *Collapse and revival of the state vector in the Jaynes-Cummings model: An example of state preparation by a quantum apparatus*, Phys. Rev. Lett. **65** (1990) 3385-3388; *Atom- and field-state evolution in the Jaynes-Cummings model for large initial fields*, Phys. Rev. **A44** (1991) 5913-5931.
- [262] S. J. D. Phoenix and P. L. Knight, Comment on Ref. (261), Phys. Rev. Lett. **66** (1991) 2833; *Establishment of an entangled atom-field state in the Jaynes-Cummings model*, Phys. Rev. **A44** (1991) 6023-6029.
- [263] V. Bužek, H. Moya-Cessa, P. L. Knight, and S. J. D. Phoenix, *Schrödinger-cat states in the resonant Jaynes-Cummings model: Collapse and revival of oscillations of the photon-number distribution*, Phys. Rev. **A45** (1992) 8190-8203.
- [264] P. L. Knight and B. W. Shore, *Schrödinger-cat states of the electromagnetic field and multi-level atoms*, Phys. Rev. **A48** (1993) 642-655.
- [265] B. Buck and S. V. Sukumar, *Exactly soluble model of atom-phonon coupling showing periodic decay and revival*, Phys. Lett. **81A** (1981) 132-135.
- [266] K.-P. Marzlin and J. Audretsch, *Collapse and revival of ultracold atoms in a microwave cavity and of photons in parametric down-conversion*, Phys. Rev. **A57** (1998) 1333-1337. See also Ref. (267).
- [267] G. Drobný and I. Jex, *Collapses and revivals in the energy exchange in the process of k -photon*

- down-conversion with quantized pump*, Phys. Rev. **A45** (1992) 1816-1821.
- [268] P. Domokos, T. Kiss, J. Janszky, A. Zucchetti, Z. Kis, and W. Vogel, *Collapse and revival in the vibronic dynamics of laser-driven diatomic molecules*, Chem. Phys. Lett. **322** (2000) 255-262.
- [269] D. M. Meekhof, C. Monroe, B. E. King, W. M. Itano, and D. J. Wineland, *Generation of nonclassical motional states of a trapped atom*, Phys. Rev. Lett. **76** (1996) 1796-1799.
- [270] G. Raithel, W. D. Phillips, and S. L. Rolston, *Collapse and revivals of wave packets in optical lattices*, Phys. Rev. Lett. **81** (1998) 3615-3618; *Decay of atomic wave-packet motion in optical lattices*, Fortschr. Phys. **46** (1998) 791-799.
- [271] F. B. J. Buchkremer, R. Dumke, H. Levsen, G. Birkl, and W. Ertmer, *Wave packet echoes in the motion of trapped atoms*, Phys. Rev. Lett. **85** (2000) 3121-3124.
- [272] A. S. Parkins and D. F. Walls, *The physics of trapped dilute-gas Bose-Einstein condensates*, Phys. Rep. **303** (1998) 1-80.
- [273] J. A. Dunningham, M. J. Collett, and D. F. Walls, *Quantum state of a trapped Bose-Einstein condensate*, Phys. Lett. **A245** (1998) 49-54.
- [274] E. M. Wright, T. Wong, M. J. Collett, S. M. Tan, and D. F. Walls, *Collapses and revivals in the interference between two Bose-Einstein condensates formed in small atomic samples*, Phys. Rev. **A56** (1997) 591-602.
- [275] A. Imamoglu, M. Lewenstein, and L. You, *Inhibition of coherence in trapped Bose-Einstein condensates*, Phys. Rev. Lett. **78** (1997) 2511-2514. The possibility of collapse and revival times in the context of Josephson junctions has also been discussed, as in Ref. (276).
- [276] F. Sols, *Randomization of the phase after suppression of the Josephson coupling*, Physica **B194-196** (1994) 1389-1390.
- [277] M. O. Scully and M. Suhail Zubairy, *Quantum Optics* (Cambridge University Press, Cambridge, 1997) pp. 79-95.
- [278] K. Patorski, *The self-imaging phenomenon and its applications*, in *Progress in Optics*, Vol. 27 edited by E. Wolf (North Holland, Amsterdam, 1989) pp. 1-108.
- [279] W. H. Fox Talbot, *Facts related to optical science. No. IV*, Phil. Mag. **9** (1836) 401-405
- [280] L. Rayleigh, *On copying diffraction-gratings and on some phenomena connected therewith*, Phil. Mag. **11** (1881) 196-205
- [281] J. T. Winthrop and C. R. Worthington, *Theory of Fresnel images I. Plane periodic objects*

- in monochromatic light*, J. Opt. Soc. Am. **55** (1965) 373-381.
- [282] M. V. Berry and S. Klein, *Integer, fractional, and fractal Talbot effects*, J. Mod. Opt. **43** (1996) 2139-2164.
- [283] K. Banaszek, K. Wódkiewicz, and W. P. Schleich, *Fractional Talbot effect in phase space: A compact summation formula*, Optics Express **2** (1998) 169-172; *Fractional dynamics in phase space*, Laser Physics **10** (2000) 123-126.
- [284] M. V. Berry and E. Bodenschatz, *Caustics, multiply reconstructed by Talbot interference*, J. Mod. Opt. **46** (1999) 349-365.
- [285] M. Berry, I. Marzoli, and W. P. Schleich, *Quantum carpets, carpets of light*, Phys. World **14** (6) (2001) 39-44
- [286] J. F. Clauser and J. P. Dowling, *Factoring integers with Young's N-slit interferometer*, Phys. Rev. **A53** (1996) 4587-4590.
- [287] B. Rohwedder, *Atom optical elements based on near-field grating sequences*, Fortschr. Phys. **47** (1999) 883-911.
- [288] J. F. Clauser and S. Li, *Talbot - von Lau atom interferometry with cold slow potassium*, Phys. Rev. **A49** (1994) R2213-R2216.
- [289] M. S. Chapman, C. R. Ekstrom, T. D. Hammond, J. Schmiedmayer, B. E. Tannian, S. Wehinger, and D. E. Pritchard, *Near-field imaging of atom diffraction gratings: the atomic Talbot effect*, Phys. Rev. **A51** (1995) R14-R17.
- [290] S. Nowak, Ch. Kurtsiefer, T. Pfau, and C. David, *High-order Talbot fringes for atomic matter waves*, Opt. Lett. **22** (1997) 1430-1432.
- [291] B. Brezger, L. Hackermüller, S. Uttenthaler, J. Petschinka, M. Arndt, and A. Zeilinger, *Matter-wave interferometer for large molecules*, Phys. Rev. Lett. **88** (2002) 100404 - 1-4
- [292] O. Bryngdahl, *Image formation using self-imaging techniques*, J. Opt. Soc. Am. **63** (1973) 416-418.
- [293] R. Ulrich, *Image formation by phase coincidences in optical waveguides*, Opt. Comm. **13** (1975) 259-264; R. Ulrich and G. Ankele, *Self-imaging in homogeneous planar optical waveguides*, App. Phys. Lett. **27** (1975) 337-339; R. Ulrich and T. Kamiya, *Resolution of self-images in planar optical waveguides*, J. Opt. Soc. Am. **68** (1978) 583-592.
- [294] *Self-imaging with an optical tunnel for image formation*, O. Bryngdahl, United States Patent 3832029 (August 27, 1974); *Self imaging system using a waveguide*, R. Ulrich, United States

- Patent 4087159 (May 2, 1978).
- [295] Yu. B. Ovchinnikov, *Revivals of light in a planar metal waveguide*, Opt. Comm. **182** (2000) 35-43; Yu. B. Ovchinnikov and T. Pfau, *Revivals and oscillations of the momentum of light in a planar multimode waveguide*, Phys. Rev. Lett. **87** (2001) 123901 - 1-4.
 - [296] B. Fischer and R. Ulrich, *Self-imaging in a planar x-ray waveguide*, Appl. Phys. Lett. **36** (1980) 356-358.
 - [297] A. Simon and R. Ulrich, *Fiber-optical interferometer*, Appl. Phys. Lett. **31** (1977) 77-79.
 - [298] J. M. Heaton, R. M. Jenkins, D. R. Wright, J. T. Parker, J. C. H. Birbeck, and K. P. Hilton, *Novel 1-to-N integrated optical beam splitters using symmetric mode mixing in GaAs/AlGaAs multimode waveguides*, Appl. Phys. Lett. **61** (1992) 1754-1756.
 - [299] U. Zülicke, R. Bluhm, V. A. Kostelecký, and A. H. MacDonald, *Edge-magnetoplasmon wave-packet revivals in the quantum-Hall effect*, Phys. Rev. **B55** (1997) 9800-9186.
 - [300] J.-Y. Shin and H.-W. Lee, *Quantum tunneling, dynamical symmetry, and quantum revival*, Phys. Rev. **E53** (1996) 3096-3100.
 - [301] J. K. Breslin, C. A. Holmes, and G. J. Milburn, *Quantum signatures of chaos in the dynamics of a trapped ion*, Phys. Rev. **A56** (1997) 3022-3027.
 - [302] F. Saif and M. Fortunato, *Quantum revivals in periodically driven systems close to nonlinear resonances*, Phys. Rev. **A65** (2001) 013401 - 1-5.
 - [303] A. Buchleitner, D. Delande, and J. Zakrzewski, *Non-dispersive wave packets in periodically driven quantum systems*, Phys. Rep. **368** (2002) 409-547.
 - [304] C. M. Marcus, A. J. Rimberg, R. M. Westervelt, P. F. Hopkins, and A. C. Gossard, *Conductance fluctuations and chaotic scattering in ballistic microstructures*, Phys. Rev. Lett. **69** (1992) 506-509.
 - [305] N. Friedman, A. Kaplan, D. Carasso, and N. Davidson, *Observation of chaotic and regular dynamics in atom-optics billiards*, Phys. Rev. Lett. **86** (2001) 1518-1521.
 - [306] H.-J. Stöckmann and J. Stein, *Quantum chaos in billiards studied by microwave absorption*, Phys. Rev. Lett. **64** (1990) 2215-2218.
 - [307] E. Doron, U. Smilansky, and A. Frenkel, *Experimental demonstration of chaotic scattering of microwaves*, Phys. Rev. Lett. **65** (1990) 3072-3075.
 - [308] S. Sridhar and E. J. Heller, *Physical and numerical experiments on the wave mechanics of classically chaotic systems*, Phys. Rev. **A46** (1992) R1728-R1731.

- [309] R. Balian and C. Bloch, *Distribution of eigenfrequencies for the wave equation in a finite domain: III. Eigenfrequency density oscillations*, Ann. Phys. **69** (1972) 76-160.
- [310] S. M. Reimann, M. Brack, A. G. Magner, and M. V. N. Murthy, *Applications of classical periodic orbit theory to circular billiards with small scattering centers*, Surf. Rev. Lett. **3** (1996) 19-23; R. W. Robinett, *Energy eigenvalues and periodic orbits for the circular disk or annular infinite well*, Surf. Rev. Lett. **5** (1998) 519-526; *Periodic orbit theory analysis of the circular disk or annular billiard: Nonclassical effects and the distribution of energy eigenvalues*, Am. J. Phys. **67** (1999) 67-77.

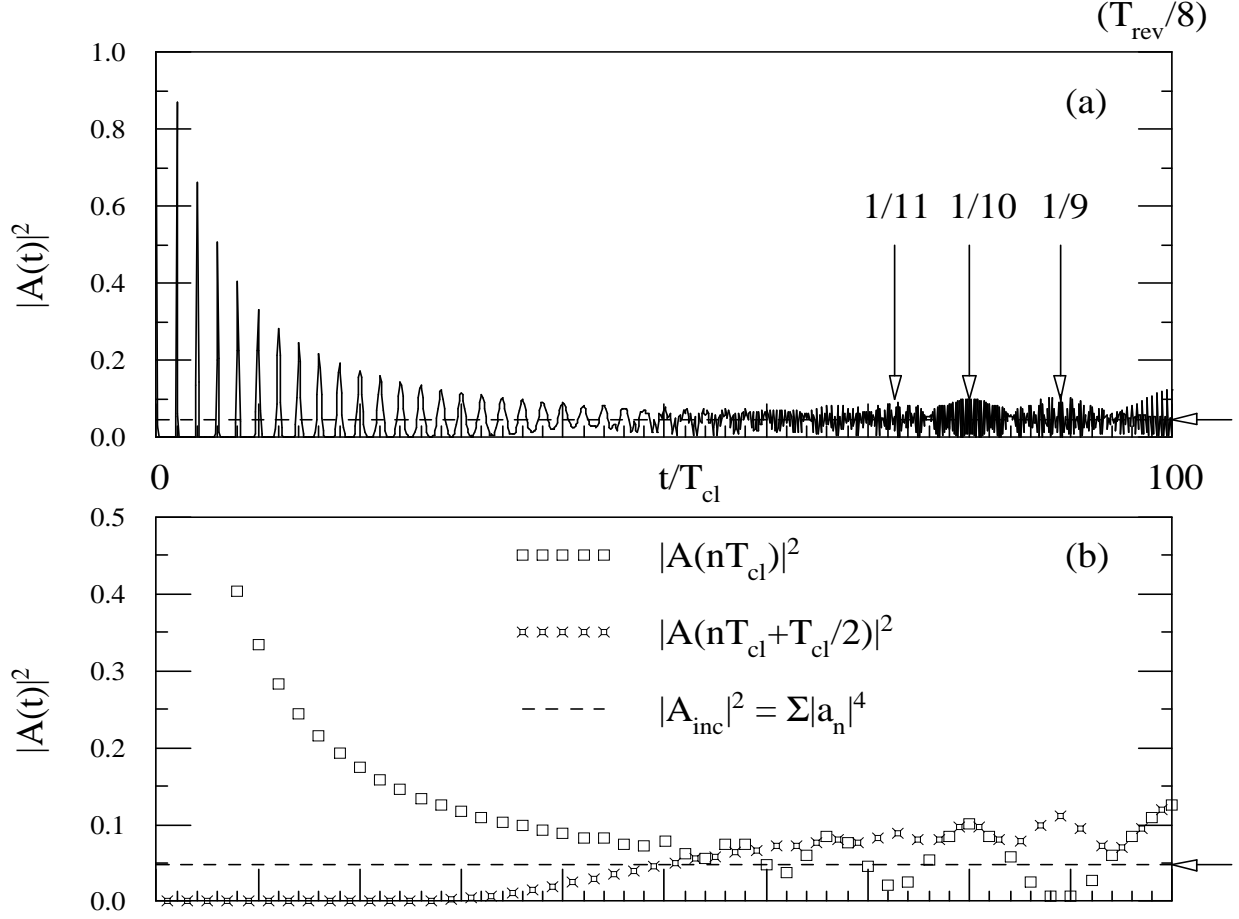


FIG. 1 Plot of the autocorrelation function, $|A(t)|^2$, over the first 100 classical periods, for the model system described by Eqns. (24) and (26) and Case A in Table I. The value of $|A(t)|^2$ at multiples of the classical period (squares) and at half a period out of phase (stars) is shown in the bottom (b), compared to the ‘incoherent’ value of $|A_{inc}|^2 = \sum_n |a_n|^4 = 1/(\Delta n 2\sqrt{\pi}) \approx 0.047$ in Eqn. (30), shown as the dotted horizontal lines (and indicated by arrows.) Locations of fractional revivals are indicated by vertical arrows.

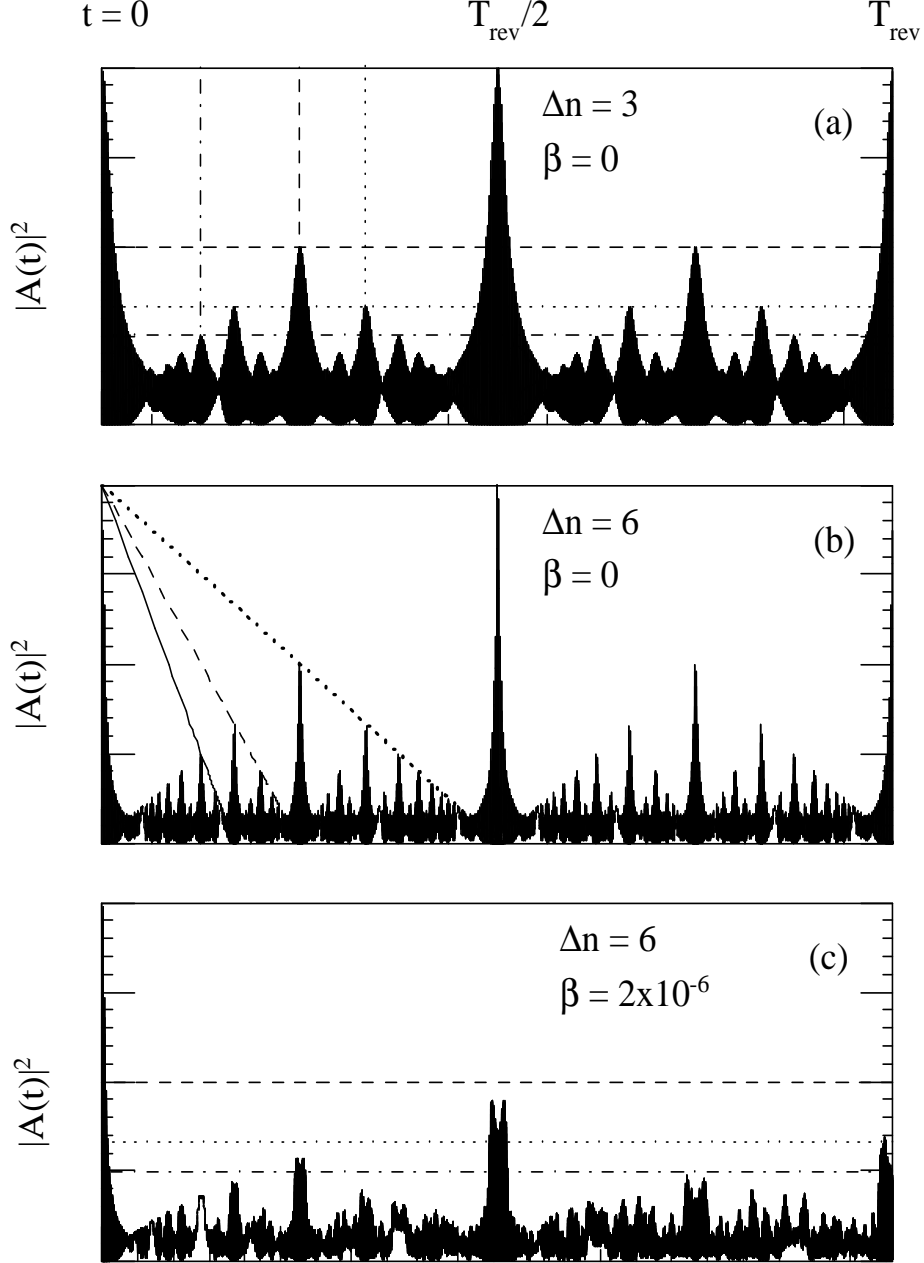


FIG. 2 Plot of the autocorrelation function, $|A(t)|^2$, over the interval $(0, T_{rev})$ for the energy spectrum in Eqn. (26) and the Gaussian distribution of energy eigenstates in Eqn. (24) with $n_0 = 400$ and $\alpha = 1/800$ and three different sets of parameters: (a) $\Delta n = 3$, and $\beta = 0$, (b) $\Delta n = 6$, and $\beta = 0$, and (c) $\Delta n = 6$, and $\beta = 2 \times 10^{-6}$. The horizontal lines indicate several fractional values of $|A|^2 = 1$, namely $1/2$ (dashed), $1/3$ (dotted), and $1/4$ (dot-dash), at rational fractions of t/T_{rev} given by $1/4$, $1/3$, and $1/8$ respectively.

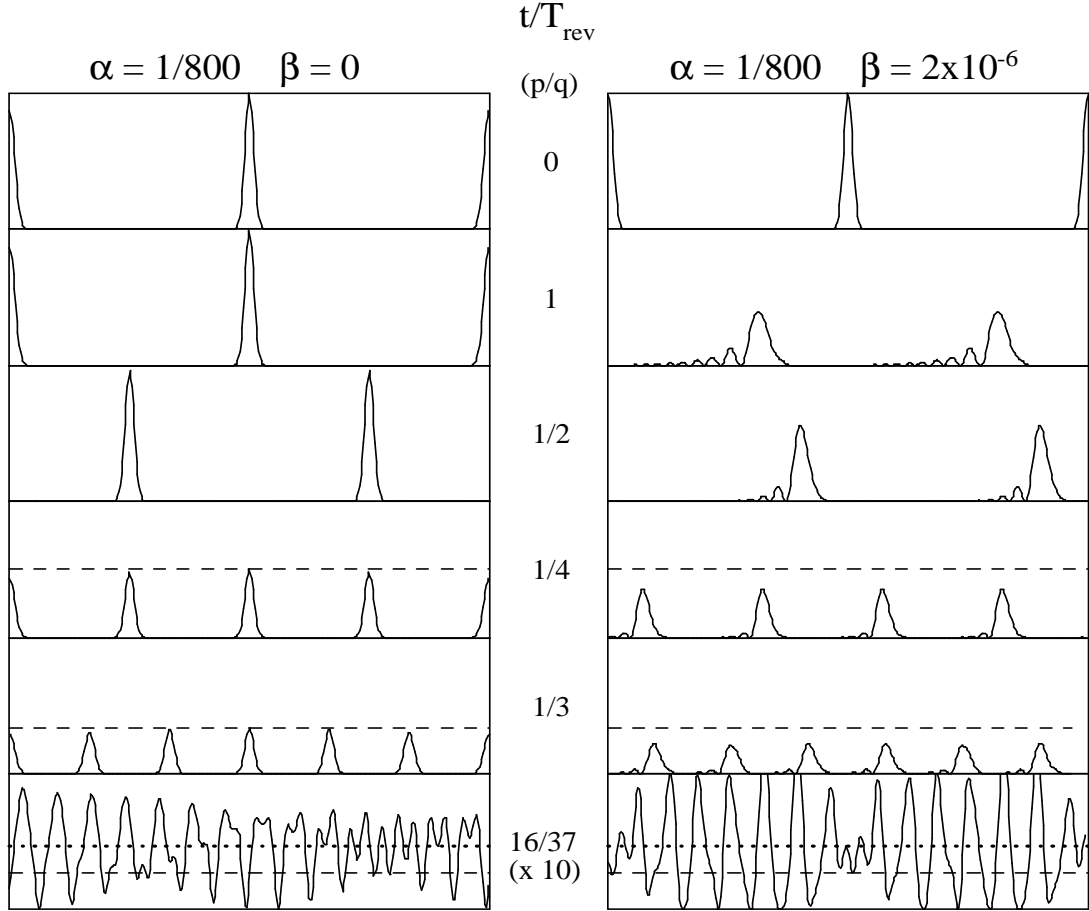


FIG. 3 Plot of the autocorrelation function, $|A(t)|^2$, near various full or fractional revivals, i.e. over the intervals $(pT_{rev}/q - T_{cl}, pT_{rev}/q + T_{cl})$ for various values of p/q and for the parameters in Eqns. (24) and (26) and Table I. The values at the bottom are multiplied by 10 to illustrate the oscillations about the constant incoherent value $|A_{inc}|^2$ (shown as the dotted horizontal line) for times not near resolvable fractional revivals. For comparison, the constant value of $|A|^2 = p/q = 1/37$ is indicated by the horizontal dashed line to compare a large q fractional revival versus a collapsed or incoherent state.

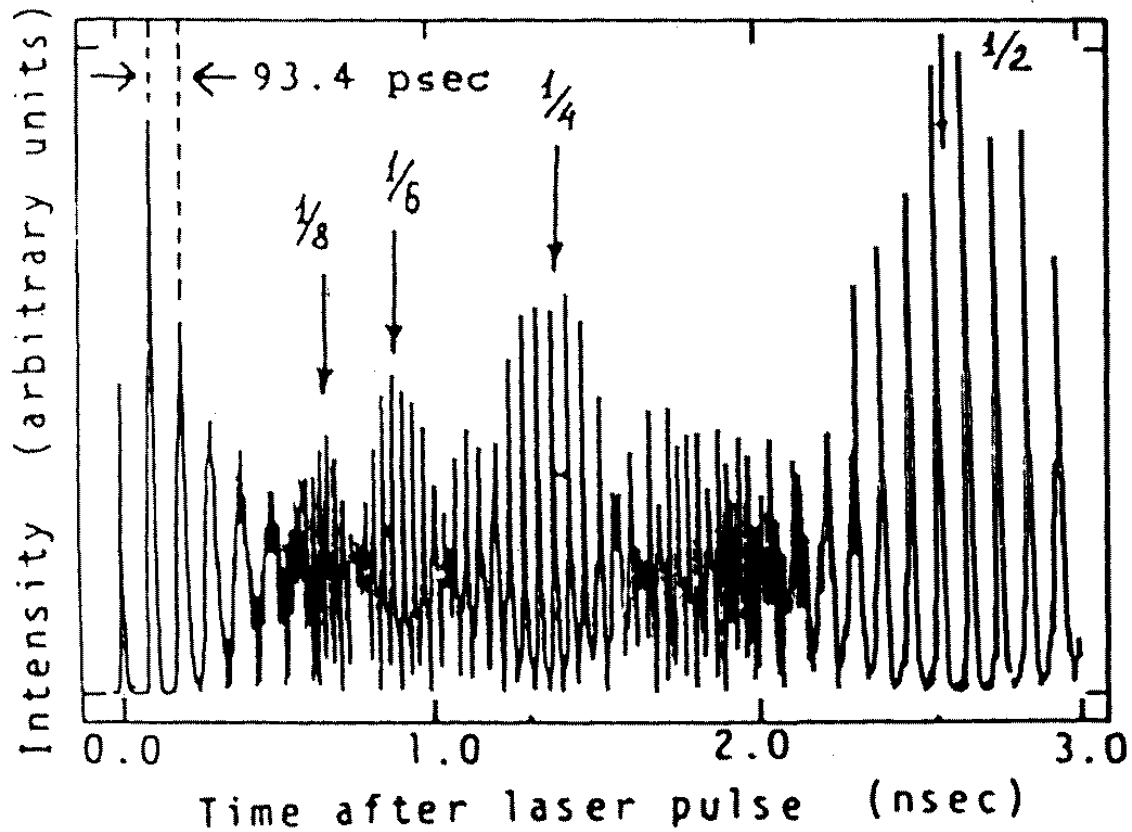


FIG. 4 Numerical calculations by Parker and Stroud (originally from Ref. (28)) for the intensity of the ionization probability for atoms excited by short laser pulses, showing numerical evidence for revival behavior, as explained in Ref. (34). The additional notations, identifying the locations of the fractional revivals, were added by Averbukh and Perelman. (Reprinted from Ref. (34).)

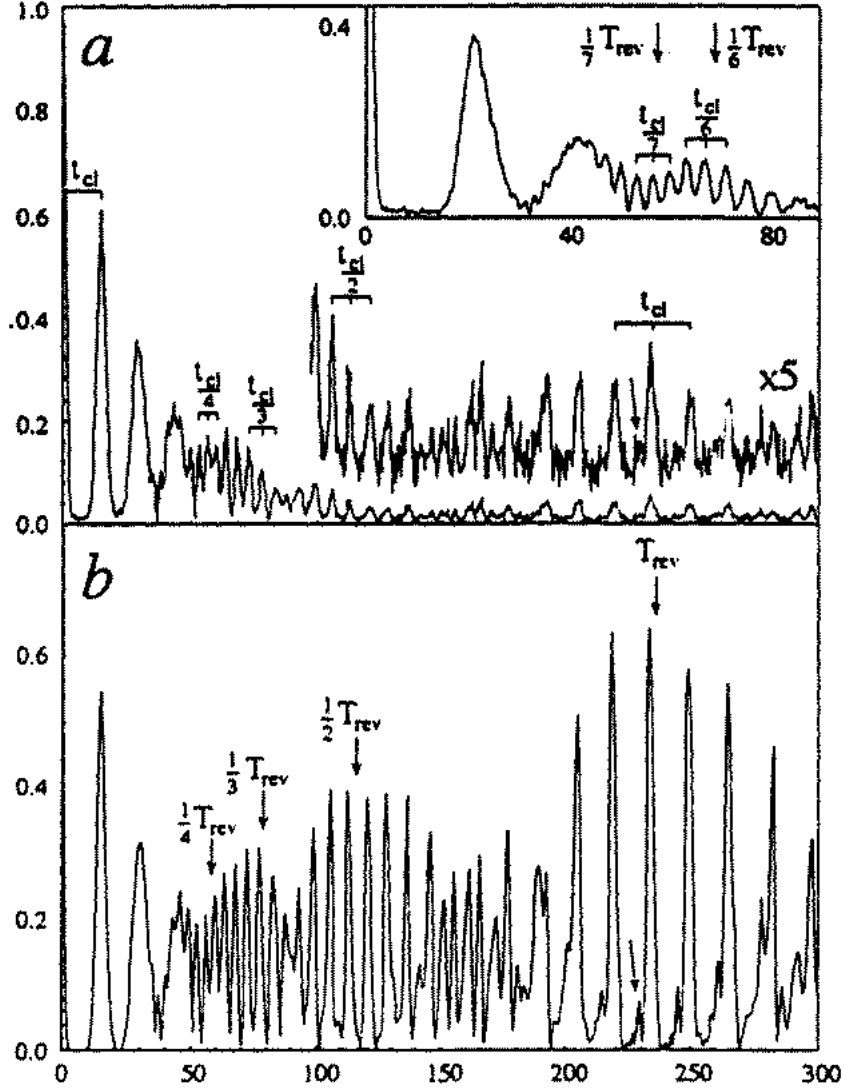


FIG. 5 Recurrence spectra for the excitation of a Rydberg electron wave packet from Ref. (33) showing fractional revivals of up to order $T_{rev}/7$. The top plot shows measurements taken using rubidium atoms, with $n_0 = 46.5$ and roughly 6.5 states excited, while the inset shows data for $n_0 = 53.5$ and 9.9 states, showing the improved resolution as one increases Δn . The bottom plot shows the calculated time-dependent transition probabilities for the same system. We note that some of the identifications with various fractional revivals differ from the notation used by Averbukh and Perelman (34). (Reprinted from Ref. (33).)

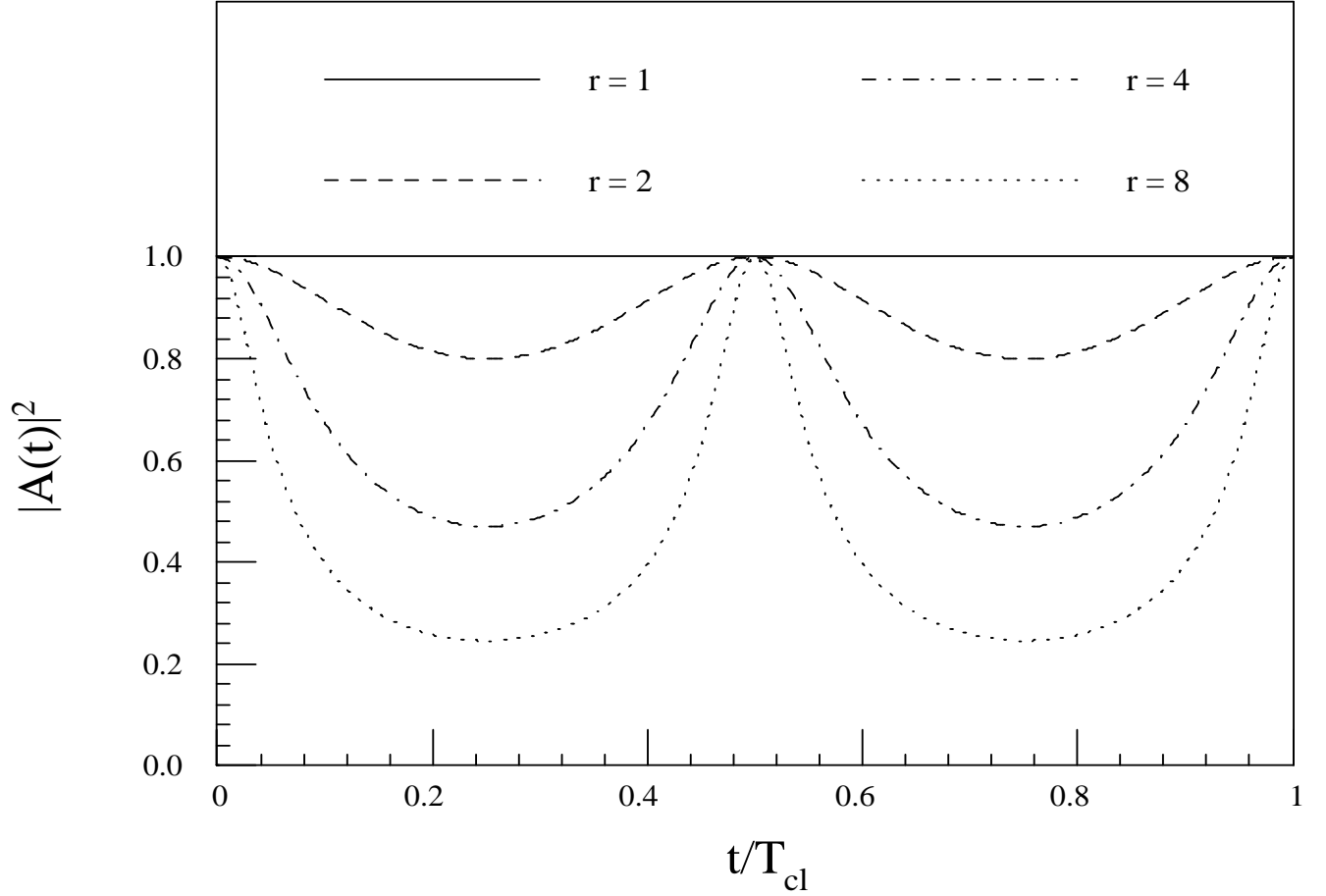


FIG. 6 Plot of the autocorrelation function, $|A(t)|^2$, over one classical period, for the ‘pulsating’ Gaussian wave packets solutions in the harmonic oscillator, with $x_0, p_0 = 0$, described by Eqn. (130), for various values of $r = \beta^2/\beta_0^2$. Note that the plots are invariant under $r \rightarrow 1/r$. For $r = 1$ the solution reduces to the ground state energy eigenstate, with trivial time dependence, and $|A(t)| = 1$.

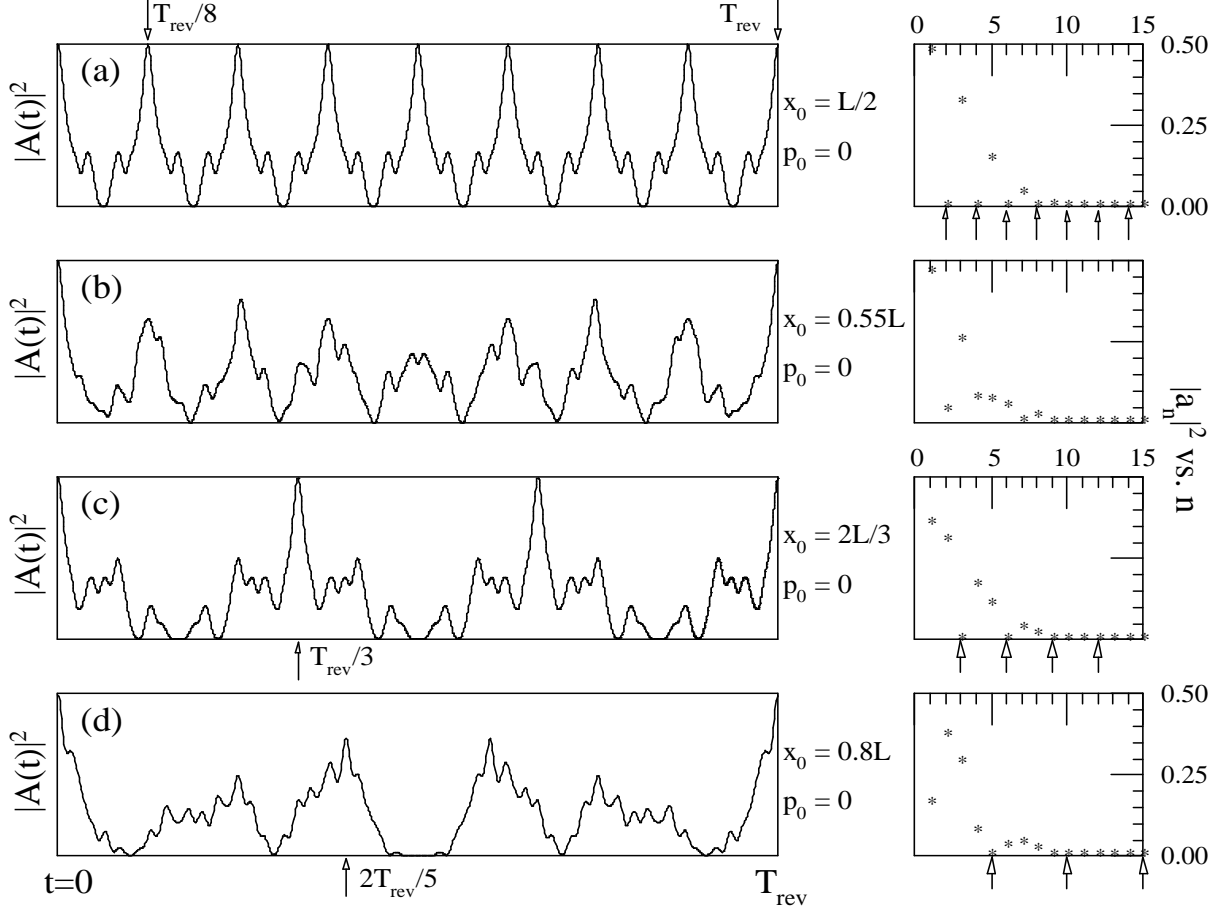


FIG. 7 Plots of the autocorrelation function, $|A(t)|^2$ over one revival time, for zero-momentum Gaussian wave packets in the infinite well, for various values of the initial position, x_0 . Note the special shorter time-scale revivals for cases with additional symmetries, such as for (a) $x_0 = L/2$ ($T_{rev}/8$) and (b) $x_0 = 2L/3$ ($T_{rev}/3$). The corresponding expansion coefficients from Eqn. (153) are shown alongside.

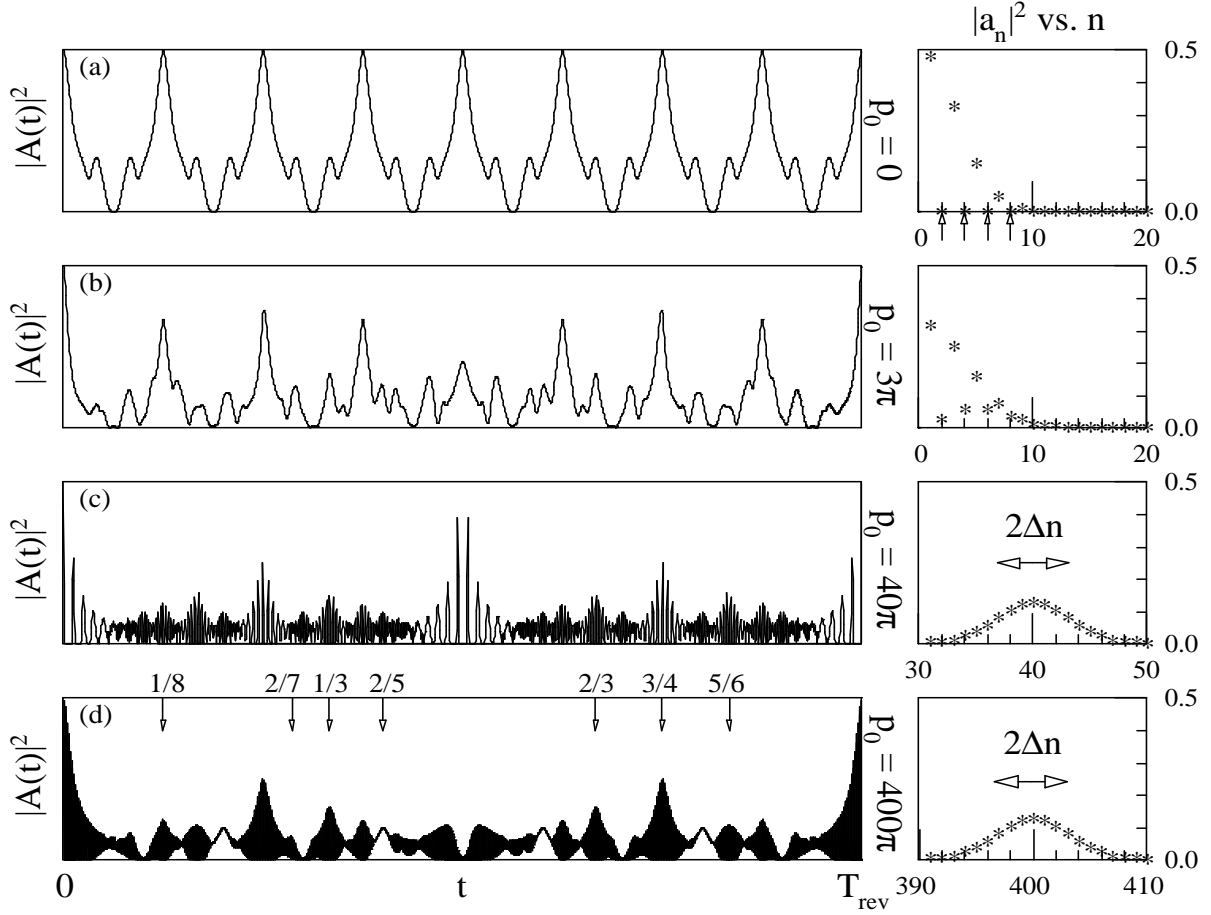


FIG. 8 Same as Fig. 7, but for $x_0 = L/2$ wave packets with increasing momentum values. Note the appearance of the classical periodicity for $p_0 \gg \Delta p_0$ for the bottom two cases, where the $|a_n|$ versus n distribution approaches the expected Gaussian form in Eqn. (24) for $n_0 \gg 1$.

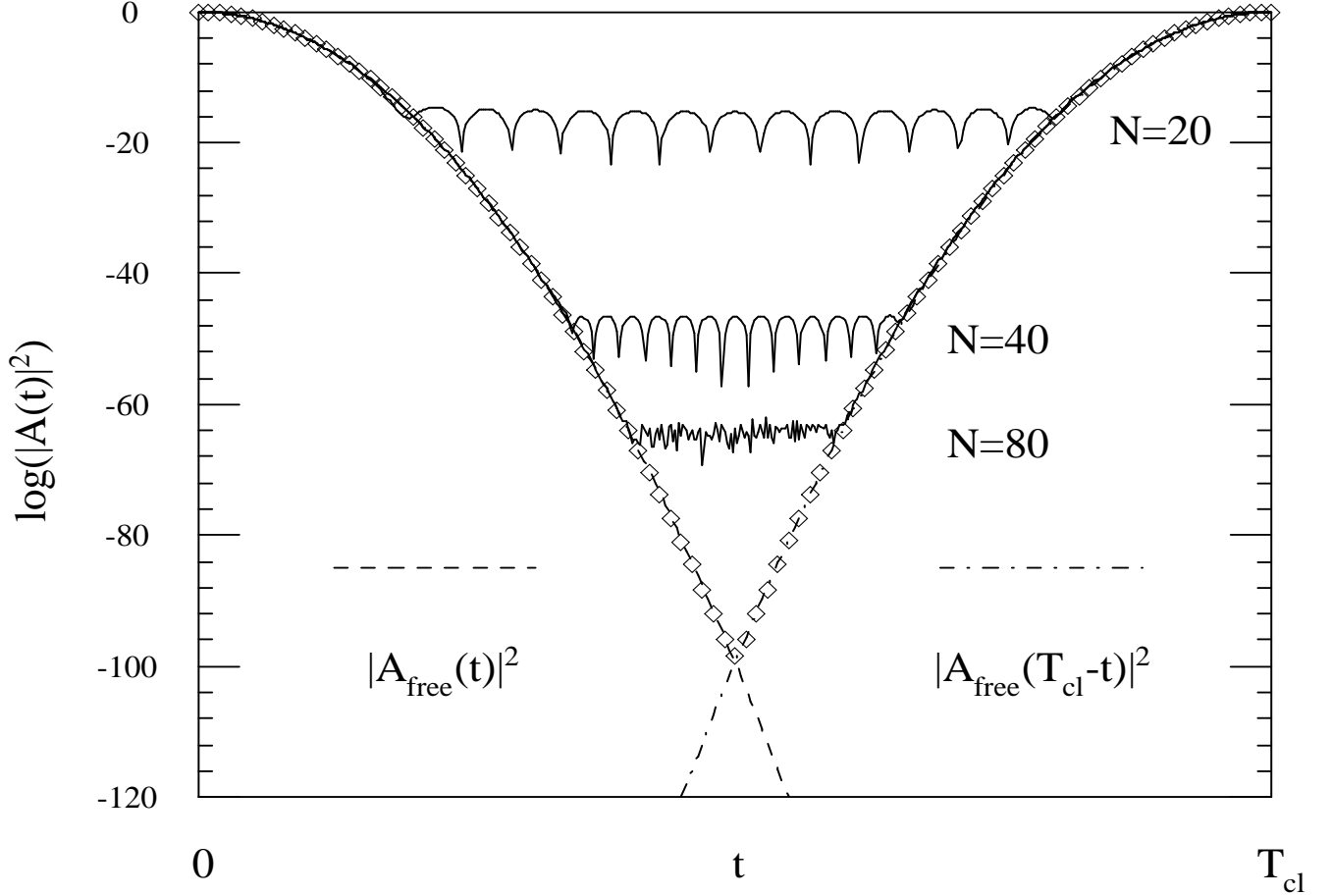


FIG. 9 Plot of the auto-correlation function ($\log(|A(t)|^2)$) for the Gaussian wave packet in the 1D infinite well for the first classical period, for increasing values of the number of eigenstates ($N = 20, 40, 80$) (with a_n given by Eqn. (153)) used in the expansion (solid curves). The free-particle autocorrelation function in Eqn. (164) as a function of t (dashed) and $T_{cl} - t$ (dot-dash) are shown for comparison. The values plotted as diamonds are from the generic result given by Nauenberg in Eqn. (B3).

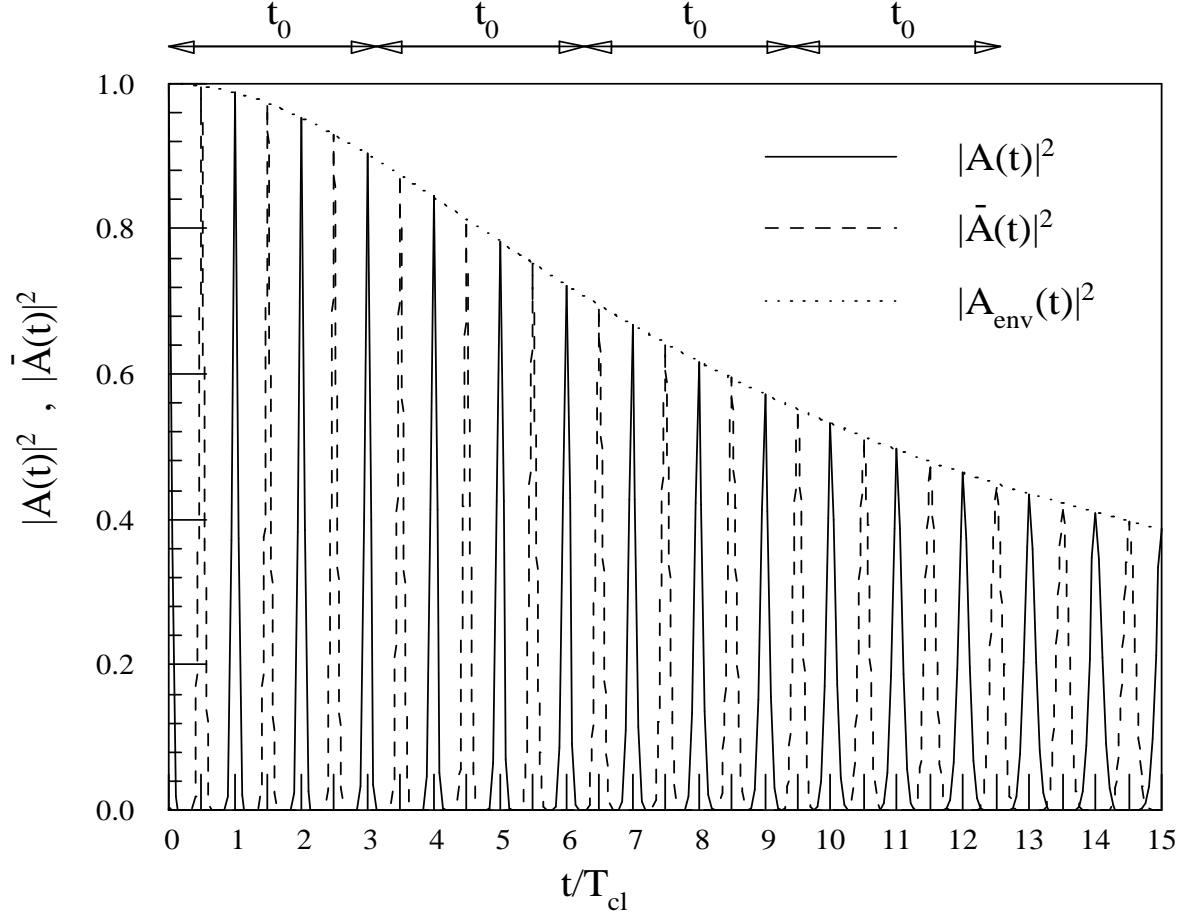


FIG. 10 Plot of $|A(t)|^2$ (solid) and $|\bar{A}(t)|^2$ (dashed) over the first 15 classical periods, along with the dispersive part of the free-particle autocorrelation function, $|A_{env}(t)|^2$ (dotted), in Eqn. (165). The value of the spreading times, t_0 are shown for comparison.

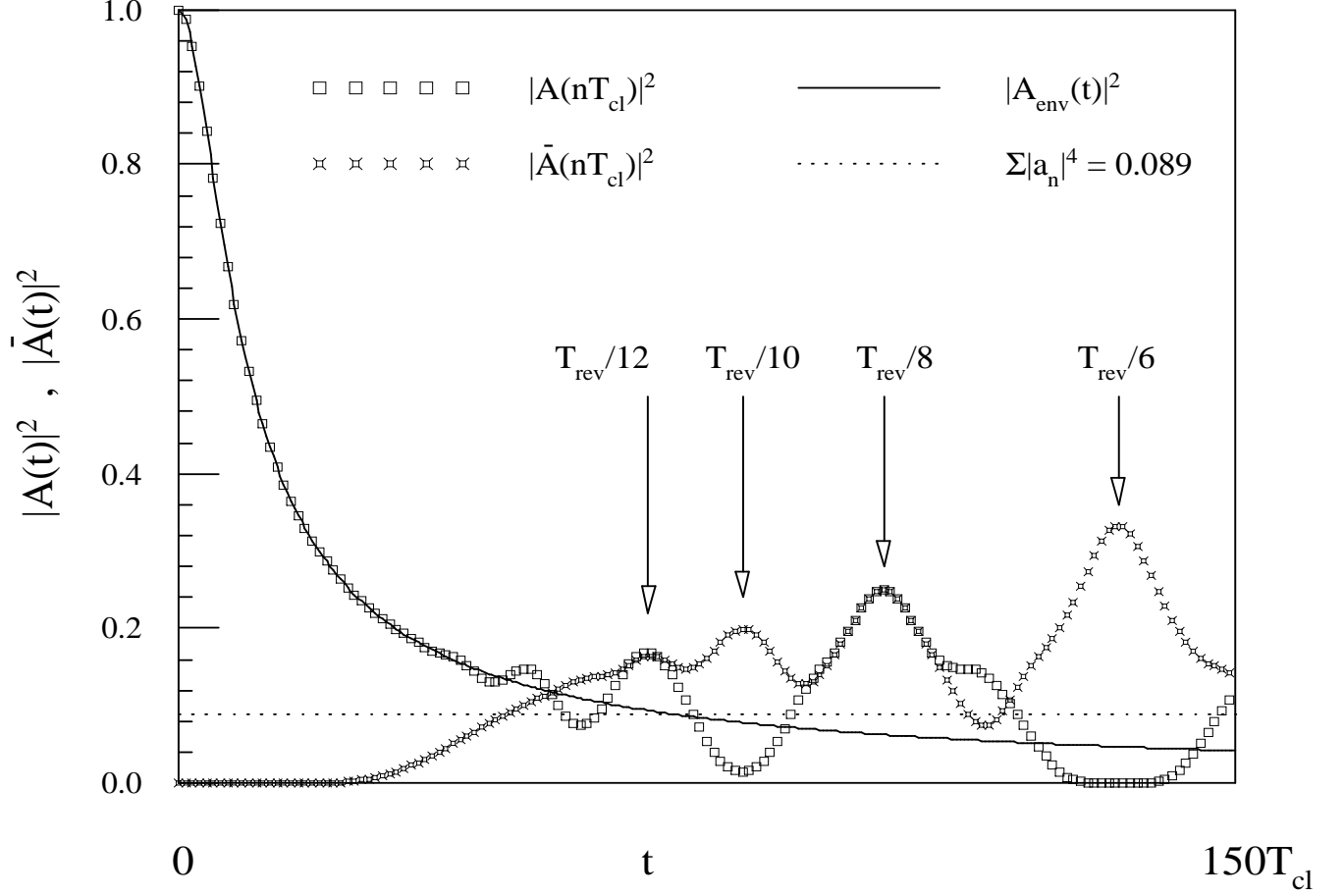


FIG. 11 Plot of $|A(nT_{cl})|^2$ (square) and $|\bar{A}(nT_{cl})|^2$ (stars) over the first 150 classical periods, along with the dispersive part of the free-particle autocorrelation function, $|A_{env}(t)|^2$ (solid), in Eqn. (165). The horizontal dotted line corresponds to the incoherent sum of uncorrelated energy eigenstates, given by Eqn. (166).

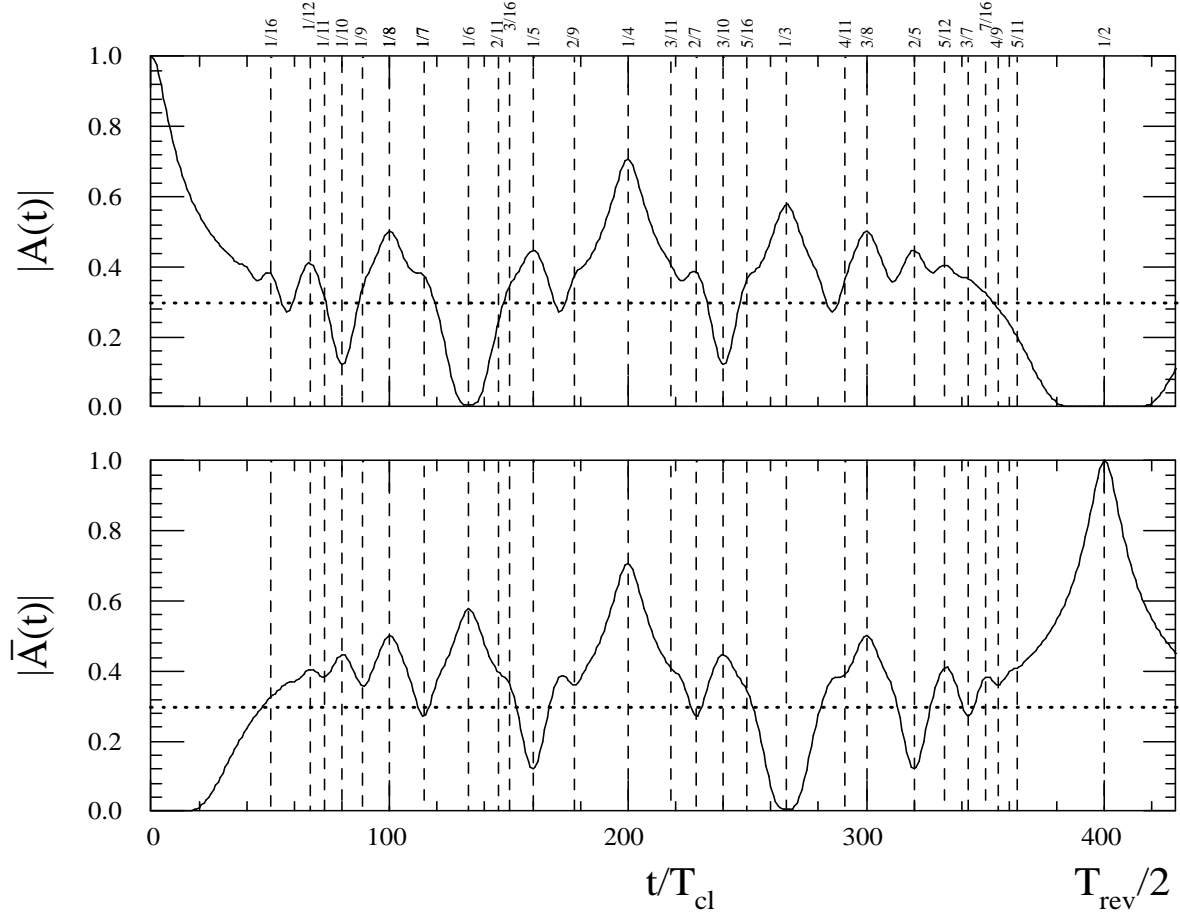


FIG. 12 Plot of $|A(nT_{cl})|$ (top) and $|\bar{A}(nT_{cl})|$ (bottom) over half a revival time (just over $T_{rev}/2$.) A large number of possible fractional revivals are denoted by vertical dashed lines, while the value of $|A_{inc}|$ for an incoherent sum of eigenstates, as in Eqn. (166), is also shown for comparison. A number of the higher order fractional revivals are obvious. For example, the revivals at $T_{rev}/2$ and $T_{rev}/6$ are obvious in the ‘out-of-phase’ $\bar{A}(t)$ anti-correlation function, while that at $T_{rev}/3$ is apparent in $A(t)$; the fractional revival at $T_{rev}/4$ is equally distinct in both plots, consistent with the form in Eqn. (43).

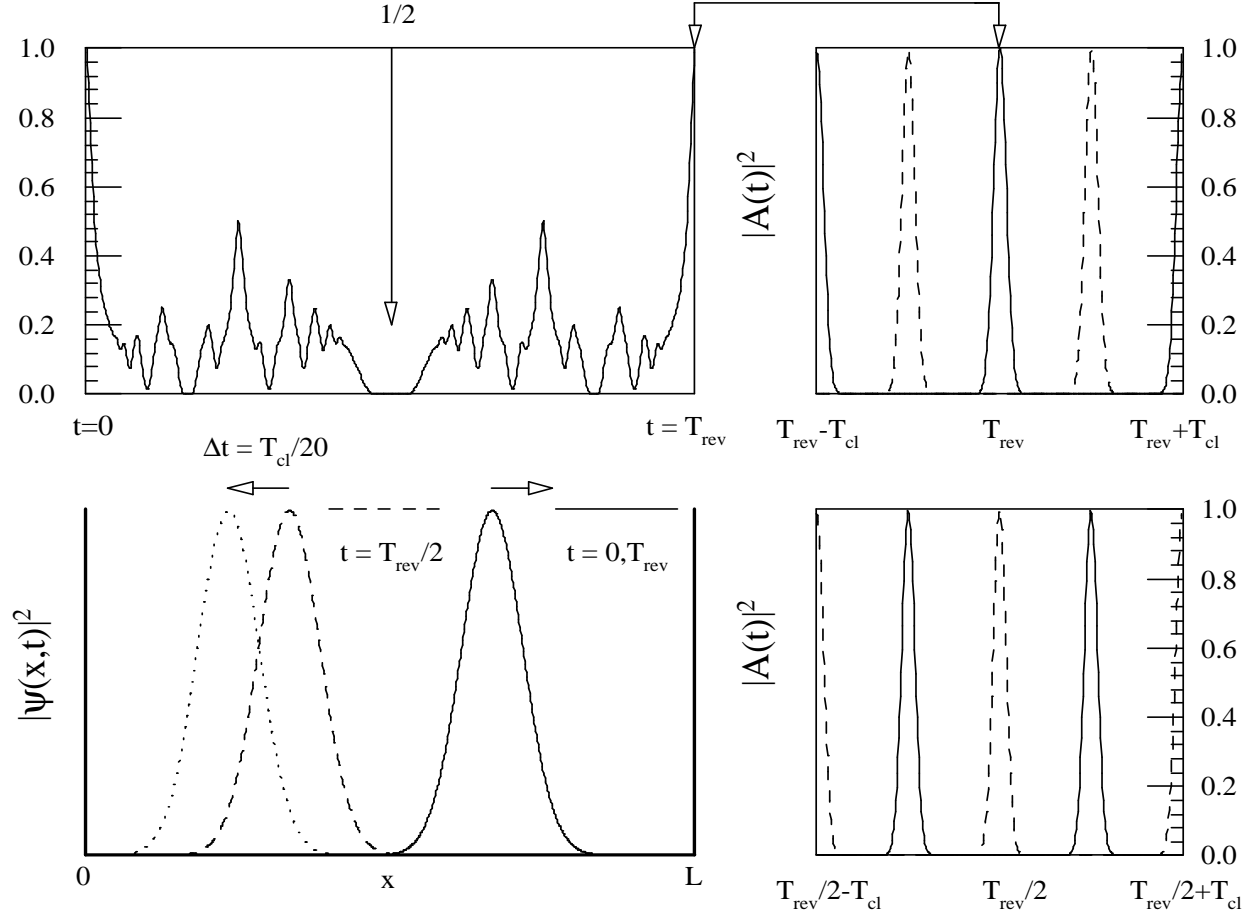


FIG. 13 Plots of $|A(nT_{CL})|^2$ over one revival time (upper left) and $|A(t)|^2$, $|\bar{A}(t)|^2$ over two classical periods, centered about T_{rev} (upper right). The autocorrelation and anti-correlation functions near $t = T_{rev}/2$ (lower right) and the position-space probabilities at $t = T_{rev}/2$ (dashed) and $T_{rev}/2 + T_{cl}/20$ (dotted) are shown, illustrating the mirror revival, the wave packet being reformed on the opposite side of the well from the $t = 0$ packet (solid) centered at $x_0/L = 2/3$.

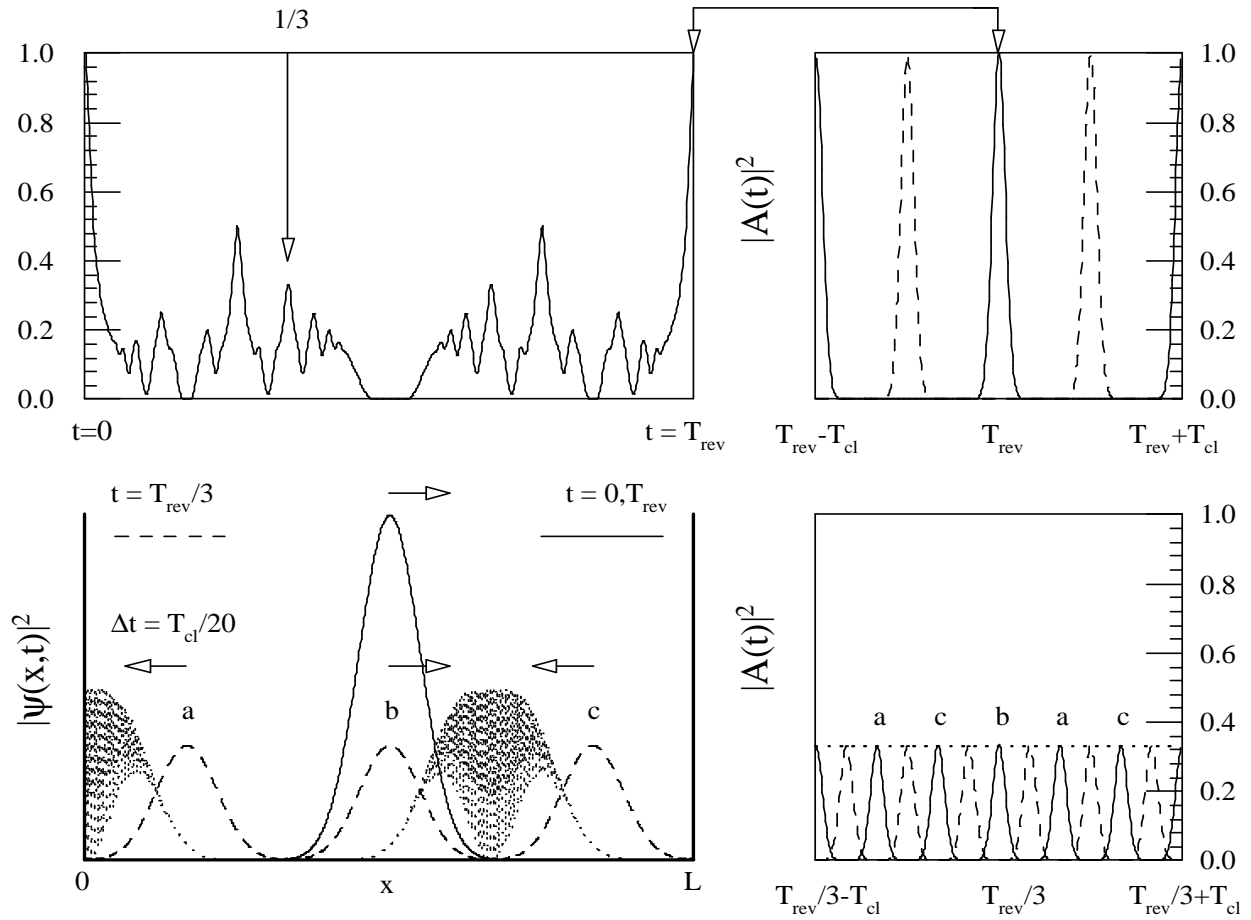


FIG. 14 Same as Fig. 13, except illustrating the fractional revival at $T_{rev}/3$. The horizontal dotted line corresponds to $|A(t)|^2 = 1/3$, and $x_0/L = 1/2$ was used. The same fractional revival is also visualized using the Wigner distribution in Fig. 29.

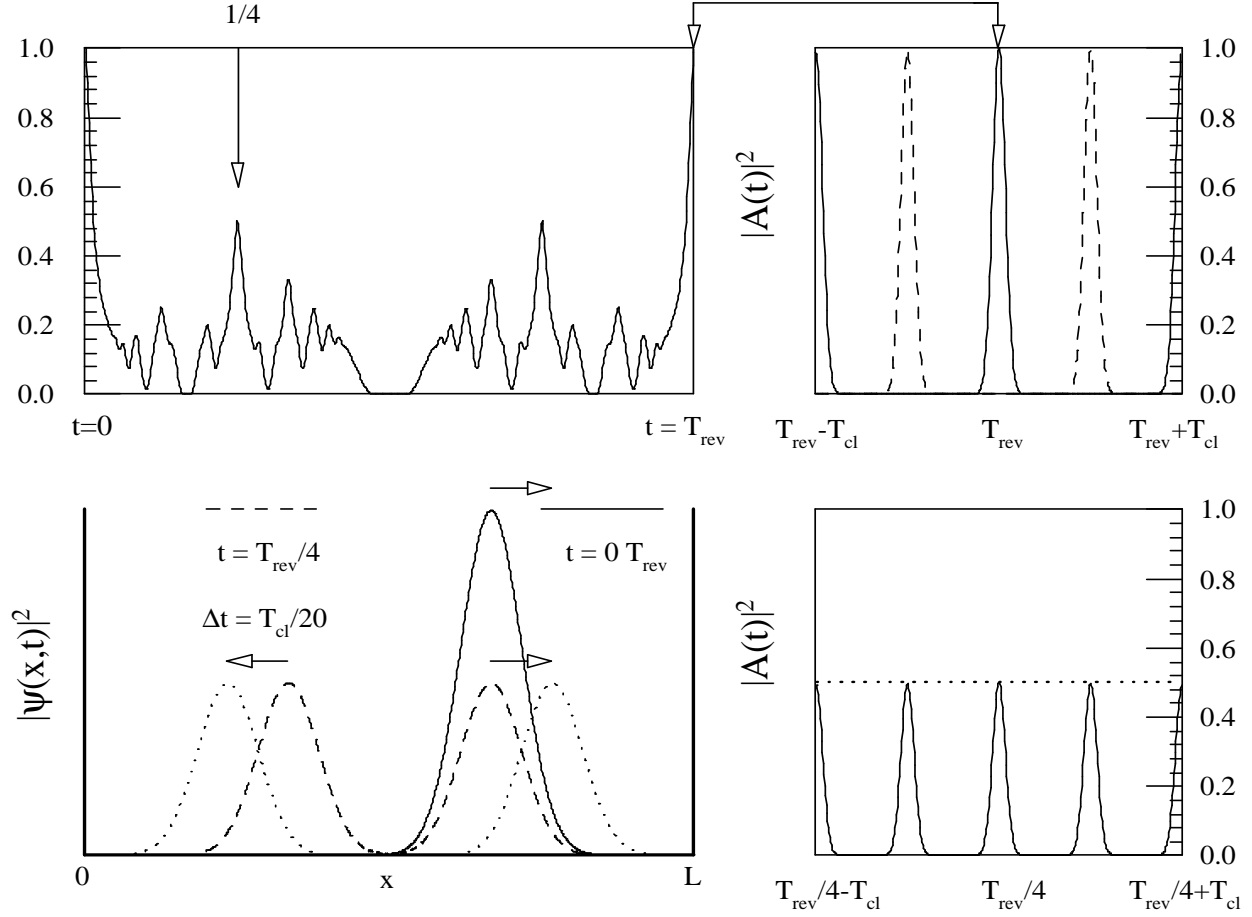


FIG. 15 Same as Fig. 13, except illustrating the fractional revival at $T_{rev}/4$. The horizontal dotted line corresponds to $|A(t)|^2 = 1/2$, and $x_0/L = 2/3$ was used. The same fractional revival is also visualized using the Wigner distribution in Fig. 30.

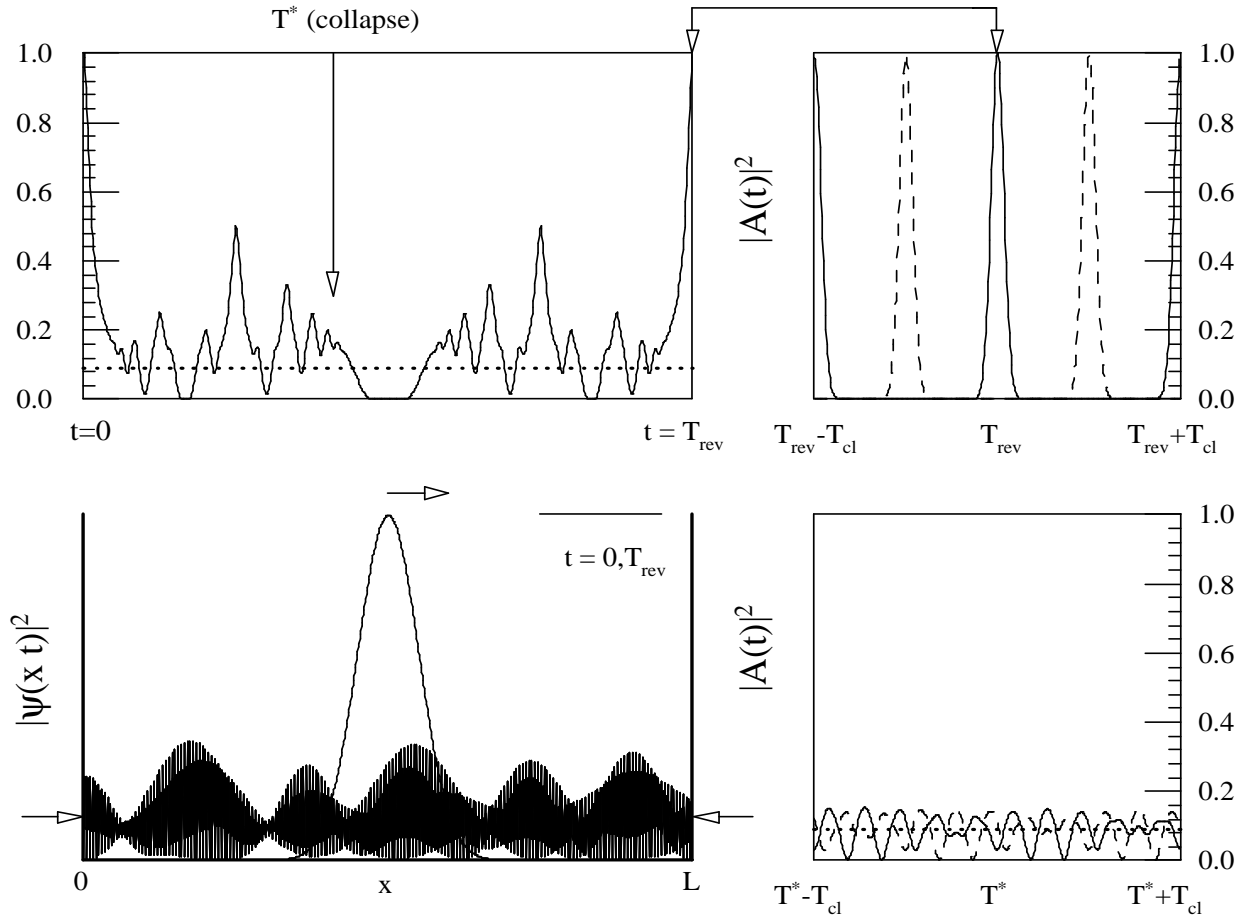


FIG. 16 Same as Fig. 13, except illustrating the behavior of both the probability density (bottom left) and $A(t), \bar{A}(t)$ (bottom right) during the collapsed phase, where $P(x,t) = |\psi(x,t)|^2$ is more consistent with the uniform or ‘flat’ value of $P(x) = 1/L$ (which is indicated by the two horizontal arrows.) The values of $|A(t)|^2, |\bar{A}(t)|^2$ can be compared to the incoherent value in Eqn. (166) shown as the horizontal dotted line.

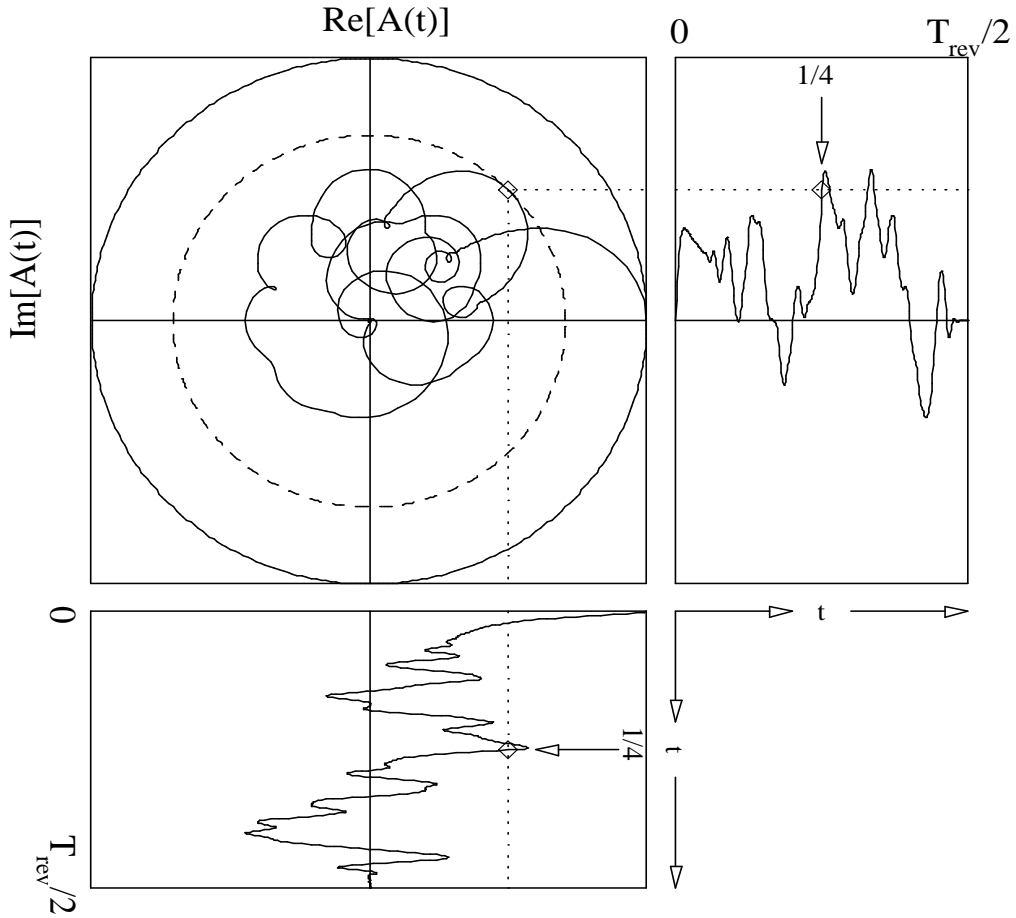


FIG. 17 Plots of the real (bottom) and imaginary (right) parts of $A(t)$ versus time (over half a revival time) as well as a parametric plot (Argand diagram) of the same data. In this case, $A(t)$ is evaluated at integral multiples of T_{cl} , as in Figs. 13 - 16. The solid circle corresponds to $|A(t)|^2 = 1$, while the dashed circle corresponds to $|A(t)|^2 = 1/2$; the location of a quarter-revival ($T_{rev}/4$) is denoted by the diamond, illustrating how at fractional revivals the autocorrelation function (sampled at these intervals) is tangent to the circle.

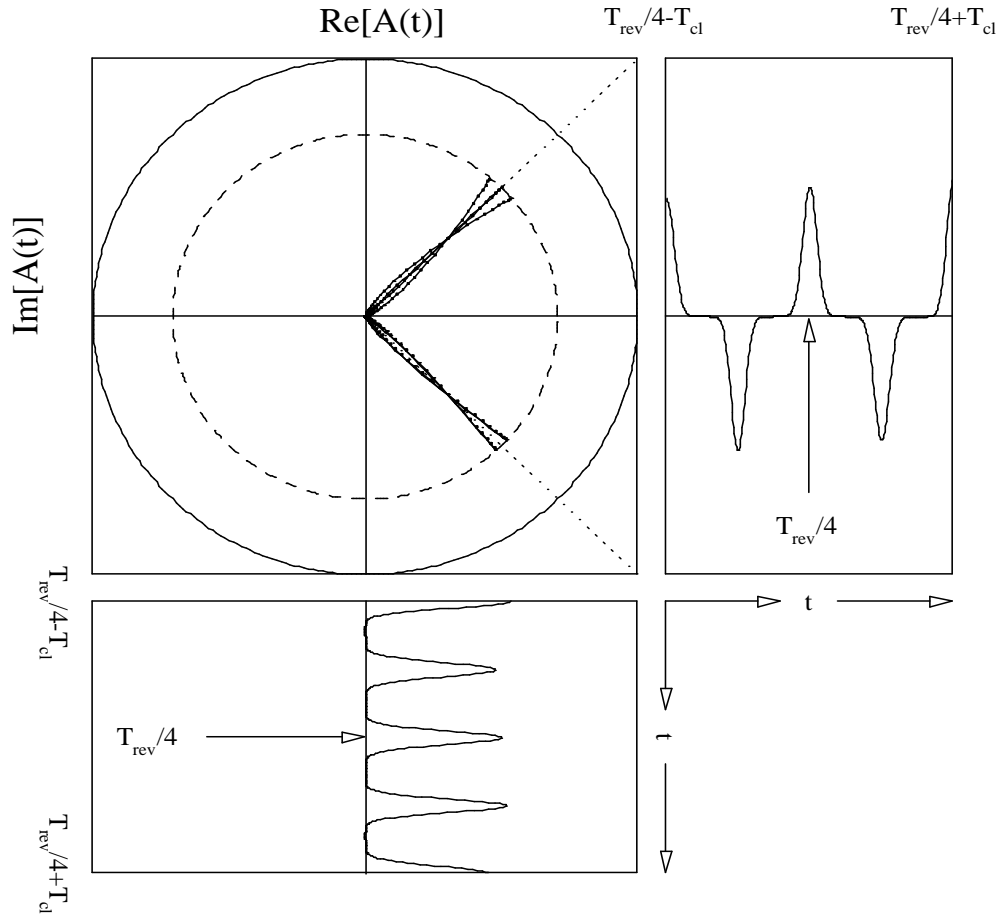


FIG. 18 Same as Fig. 17, but for the time period T_{cl} on either side of the $T_{rev}/4$ fractional revival to be compared to the general wavefunction in Eqn. (43) and the correlations predicted by Eqn. (167). The dashed circle corresponds to $|A(t)| = 1/\sqrt{2}$. The dotted lines correspond to the directions $e^{+i\pi/4}$ and $e^{-i\pi/4}$.

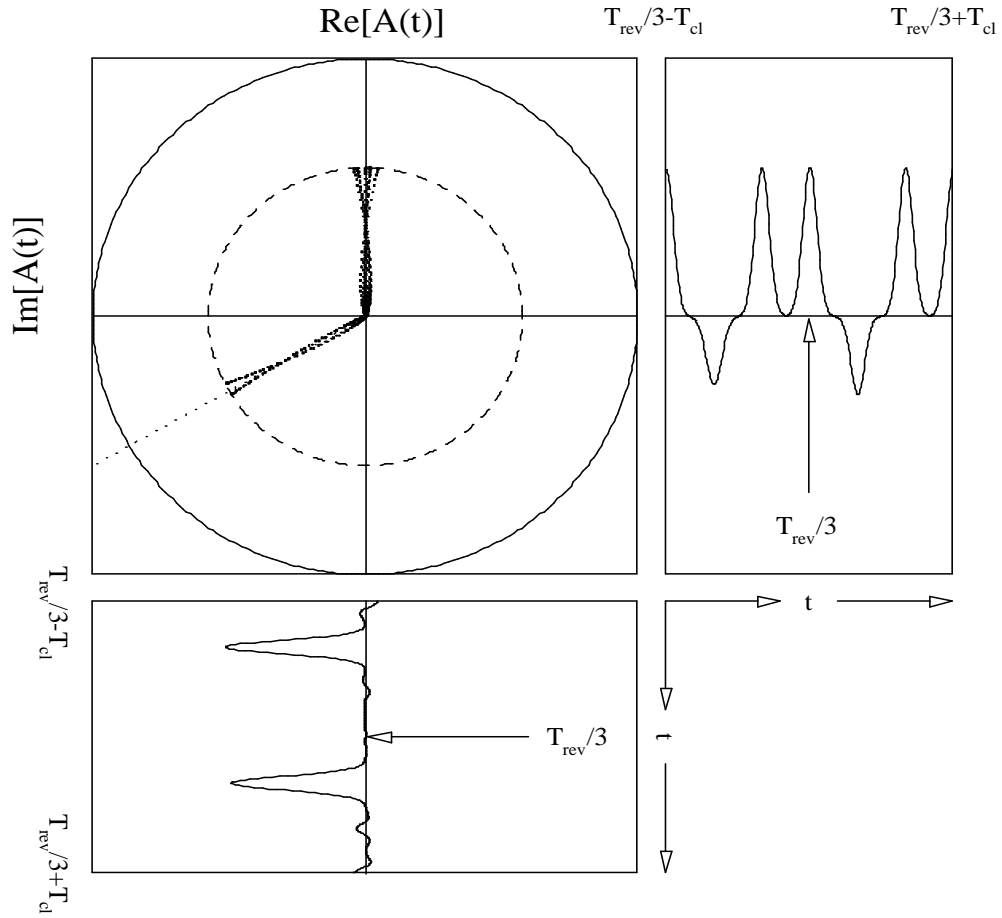


FIG. 19 Same as Fig. 17, but for the time period T_{cl} on either side of the $T_{rev}/3$ fractional revival and for all times, not just multiples of T_{cl} . Note the highly correlated phase relationship consistent with the general results of Eqn. (58) and in Eqn. (169). In this case, the dashed circle corresponds to $|A(t)| = 1/\sqrt{3}$.

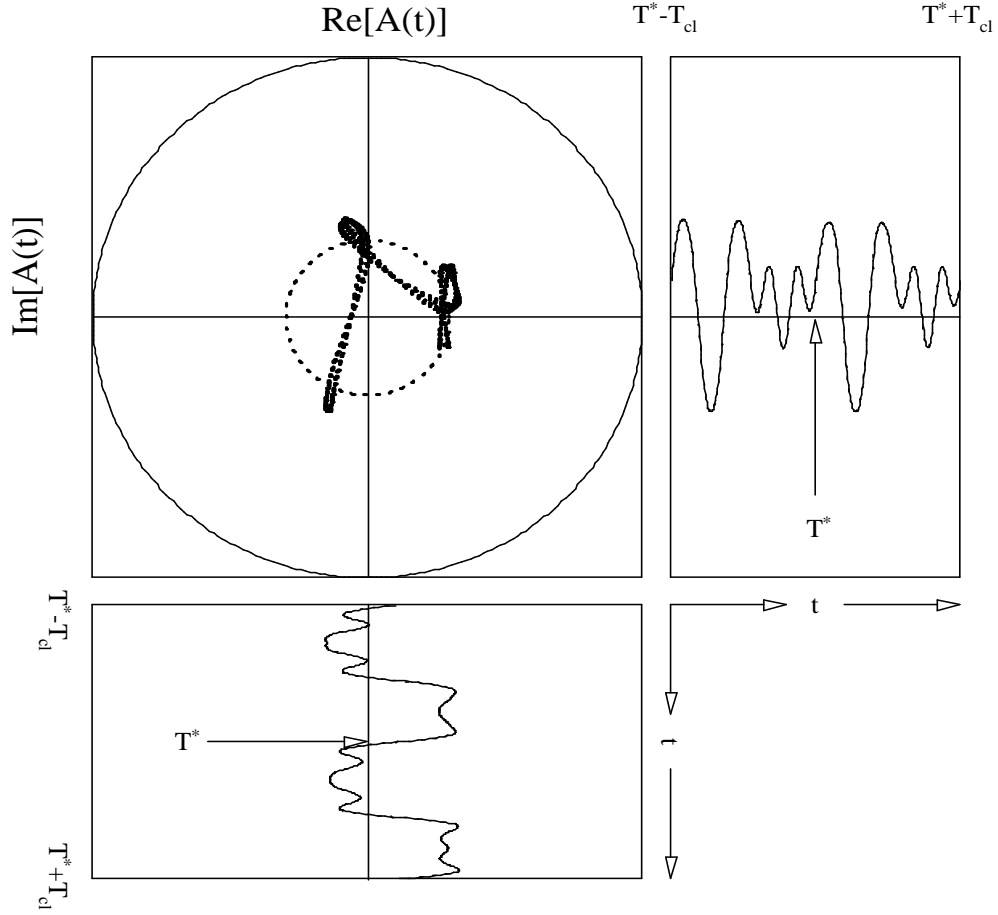


FIG. 20 Same as Fig. 17, but for the time period T_{cl} on either side of a typical time (T^*) during the collapsed phase, not near any resolvable fractional revival. In this case, the dotted circle corresponds to $|A_{inc}|^2 = \sum |a_n|^4 = 1/\Delta n 2\sqrt{\pi}$, typical of the incoherent sum of many eigenstates, with little or no phase relationship obvious.

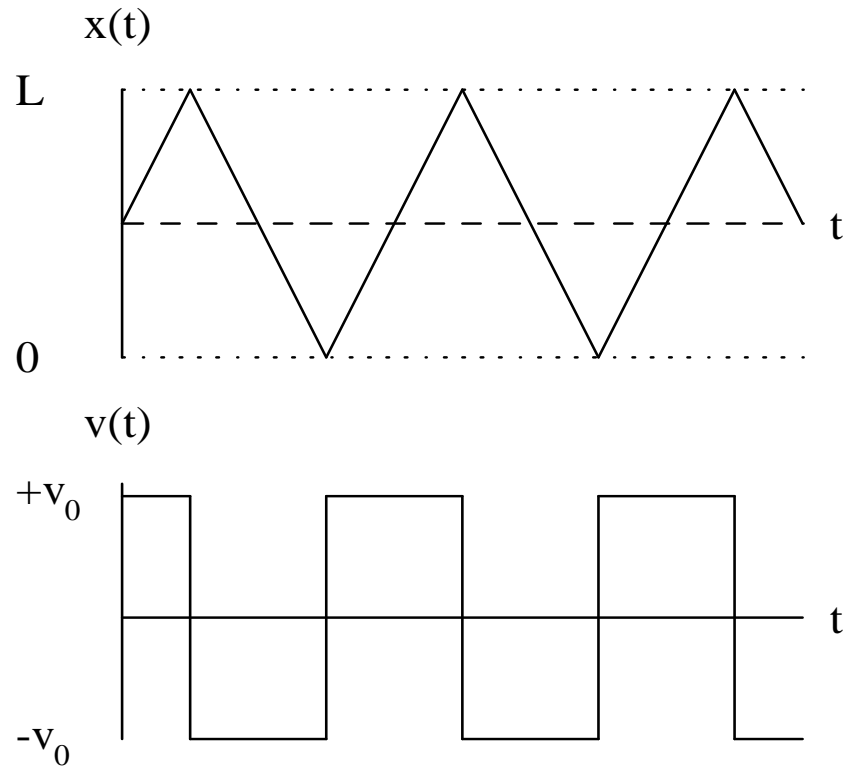


FIG. 21 The classical motion of a particle in an infinite well potential.

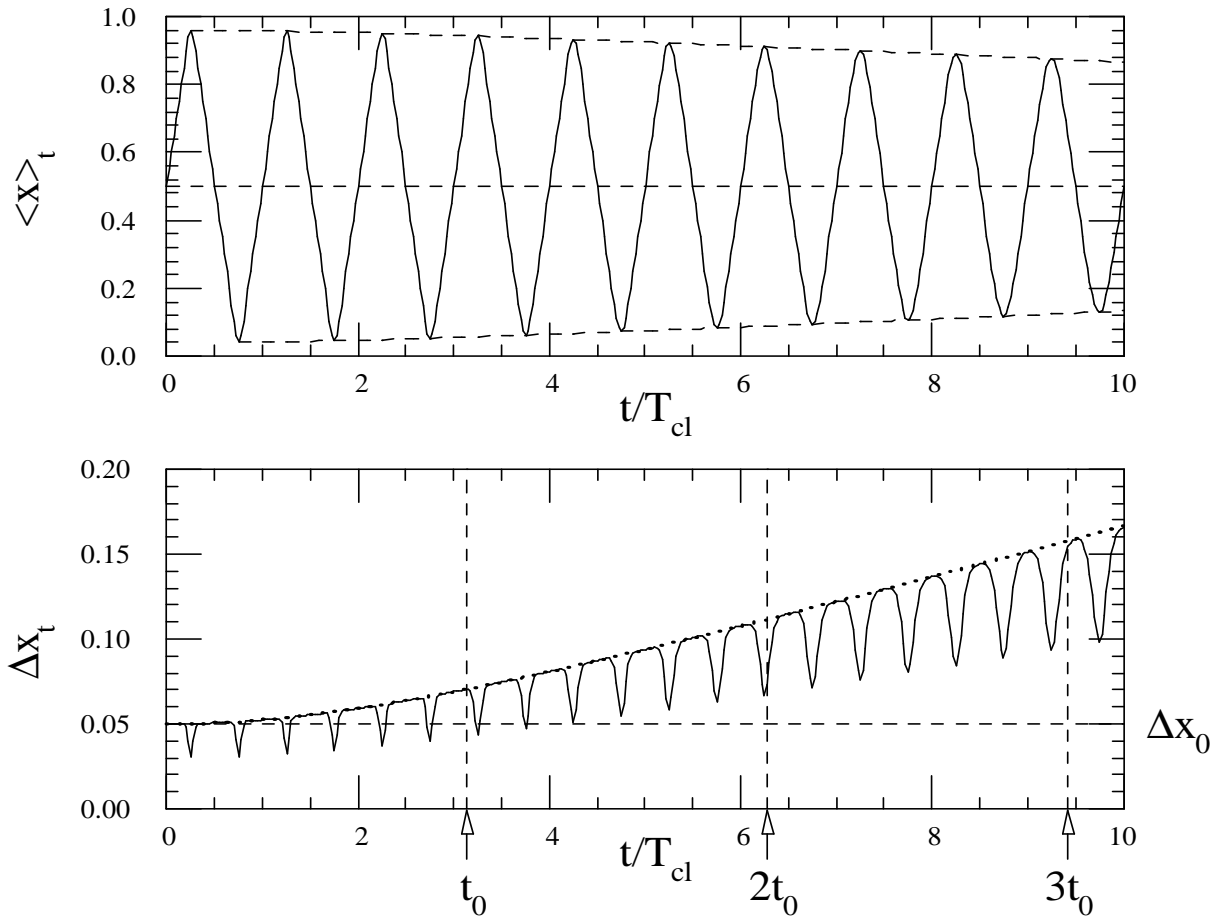


FIG. 22 The expectation value, $\langle x \rangle_t$ (top), and uncertainty, Δx_t (bottom), for the infinite Gaussian wave packet over the first ten classical periods, measured in units of L . The dotted line which forms the envelope for the Δx_t curve is the free-particle spread given by Eqn. (170a). (Reprinted from Ref. (94).)

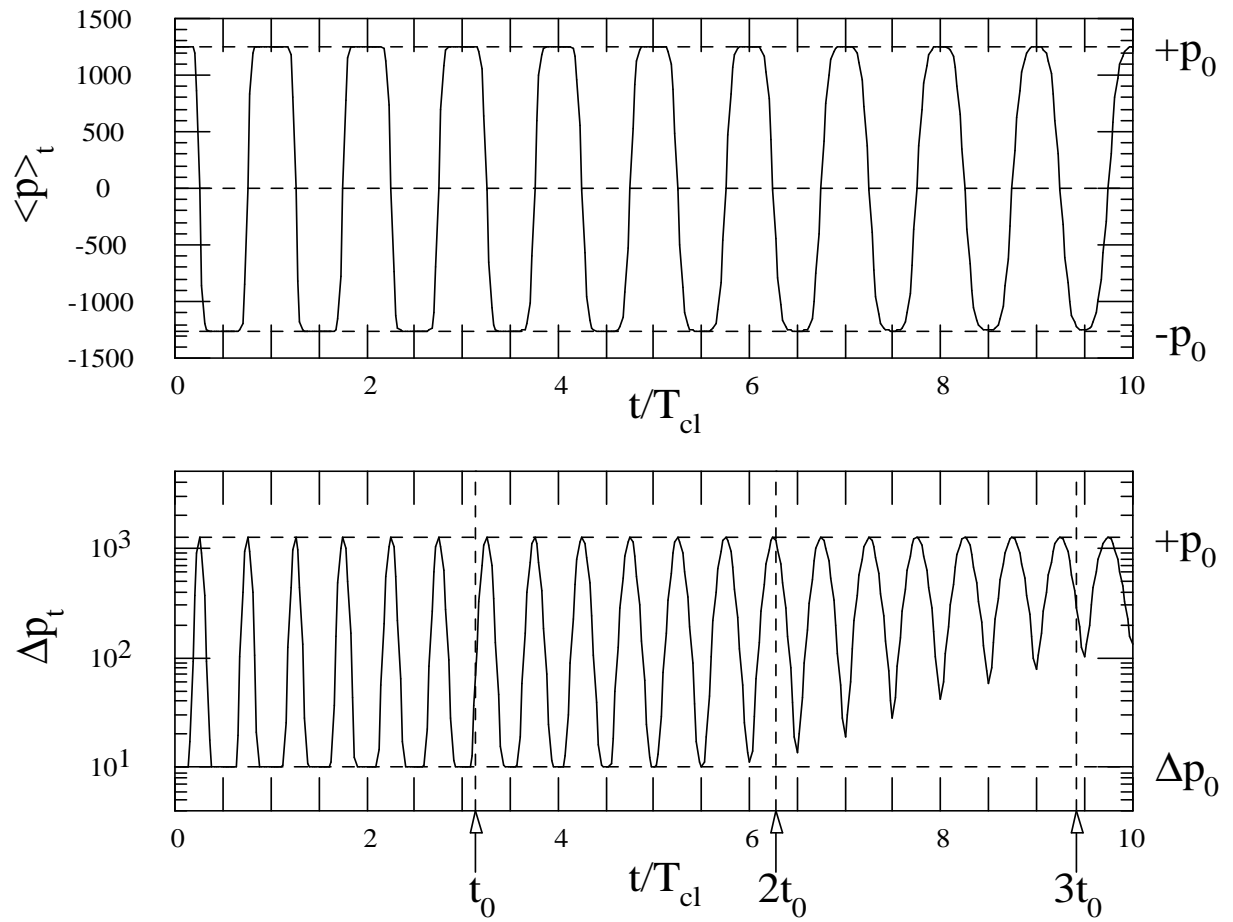


FIG. 23 Same as for Fig. 22, but for $\langle p \rangle_t$ (top), and Δp_t (bottom). (Reprinted from Ref. (94).)

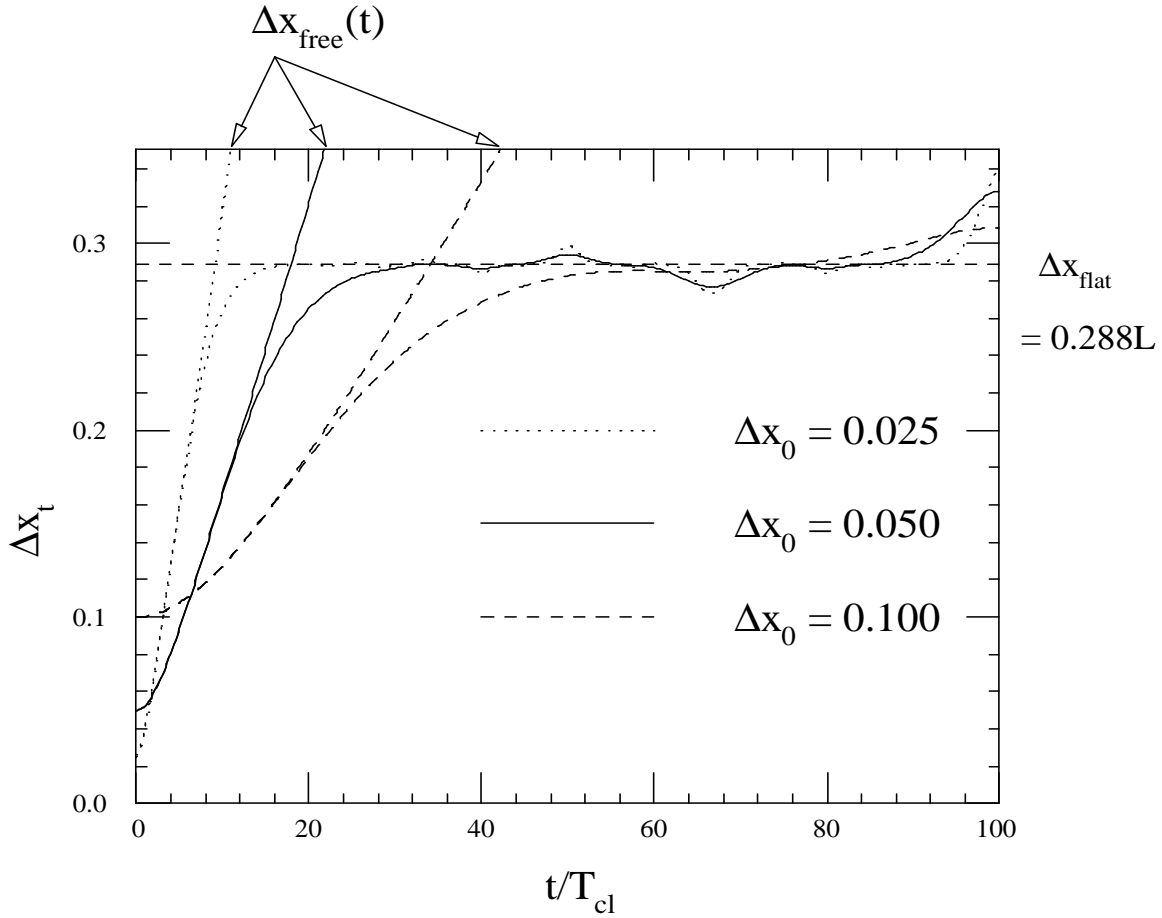


FIG. 24 The position-spread, Δx_t versus t , for various initial width Gaussian states, and the approach to the collapsed state, characterized by $\Delta x_{cl} = L/\sqrt{12}$, evaluated at integral values of the classical period. (Reprinted from Ref. (94).)

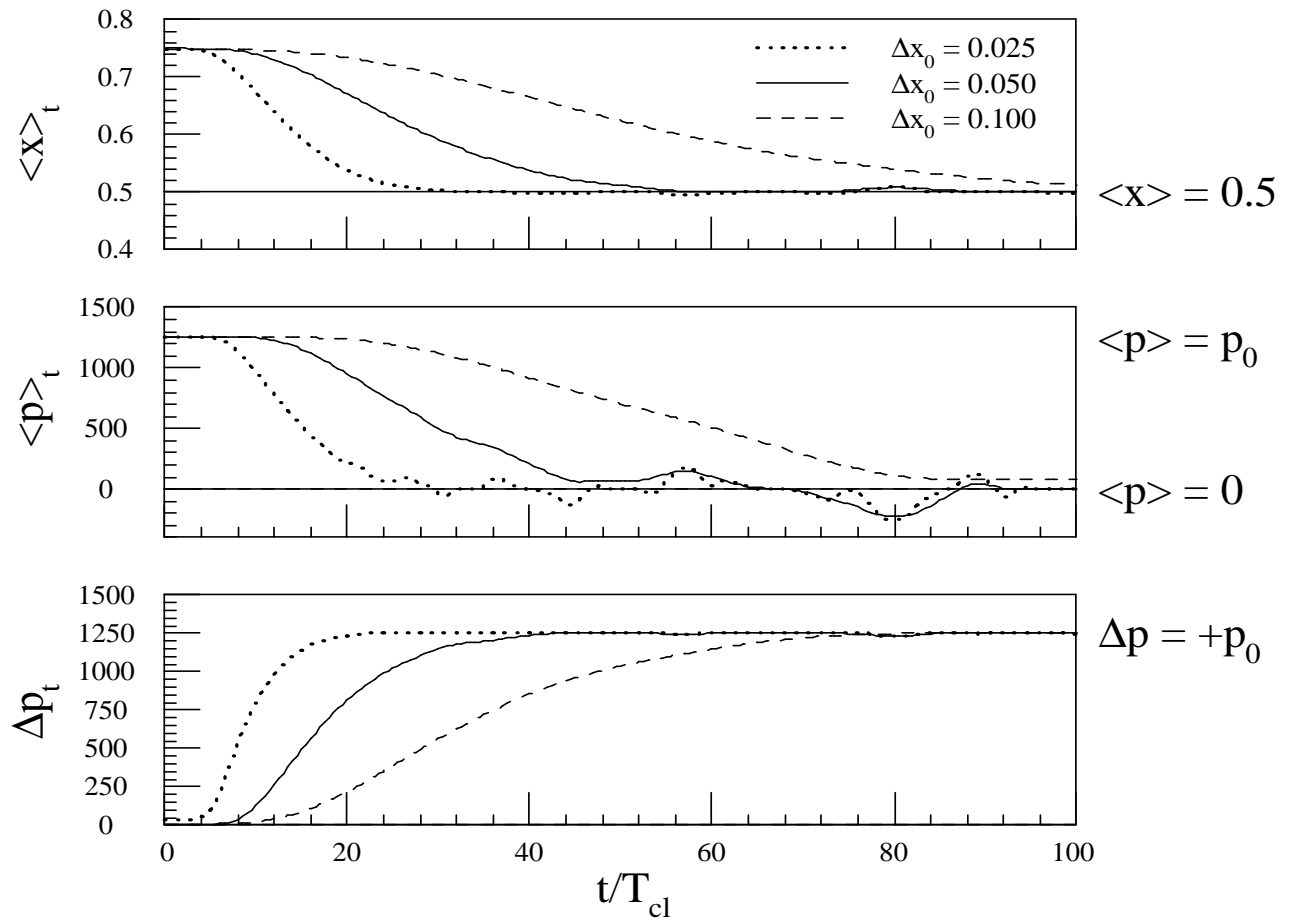


FIG. 25 The same as Fig. 24, but for $\langle x \rangle_t$ (top), $\langle p \rangle_t$ (middle), and Δp_t (bottom). (Reprinted from Ref. (94).)

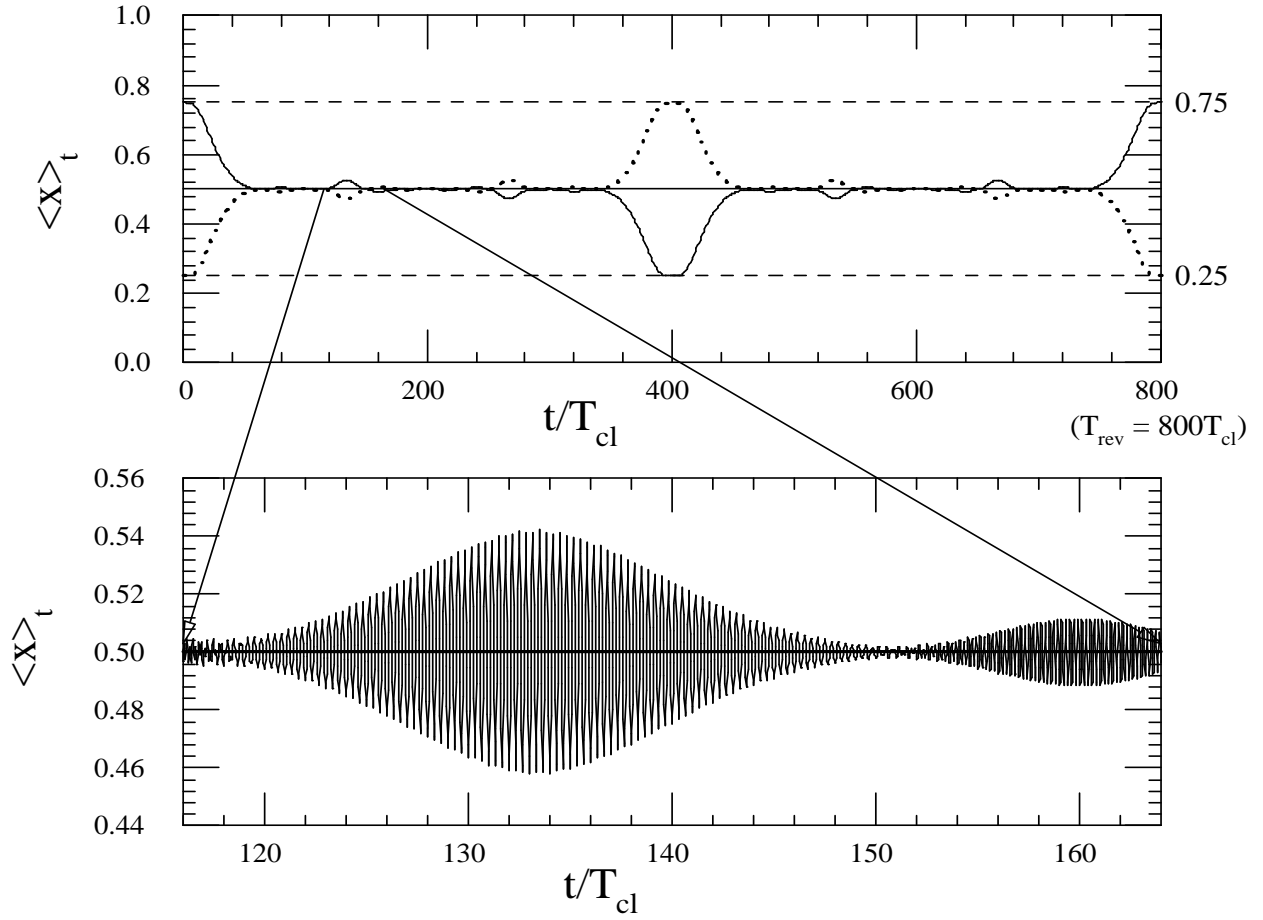


FIG. 26 The expectation value of position $\langle x \rangle_t$ evaluated at $t = (n + 1/8)T_{cl}$ (solid) and $t = (n + 5/8)T_{cl}$ (dashed) over an entire revival time. The mirror revival, where the wave packet is reversed, at $t = T_{rev}/2$ is apparent. (Reprinted from Ref. (94).)

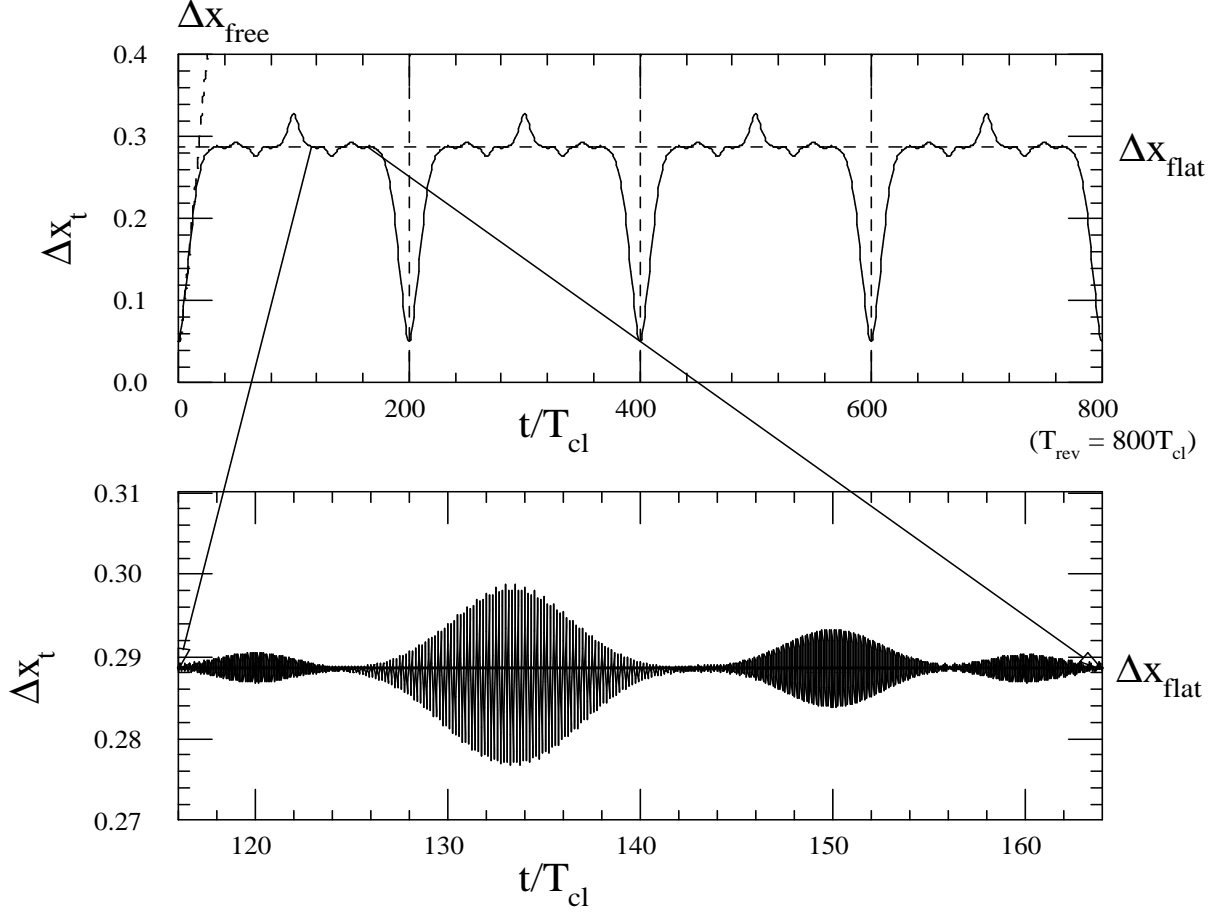


FIG. 27 Same as for Fig. 26, but for Δx_t over one revival time. The return of Δx_t to its original (small) value at T_{rev} (revival time) and $T_{rev}/2$ (mirror revival) are familiar, while the small values at the $T_{rev}/4$ and $3T_{rev}/4$ fractional revivals are special features of an initial state centered at $x_0 = L/2$. At those points, the wave packet consists of two 'mini' packets, superimposed and hence of small width, but with opposite momenta. (Reprinted from Ref. (94).)

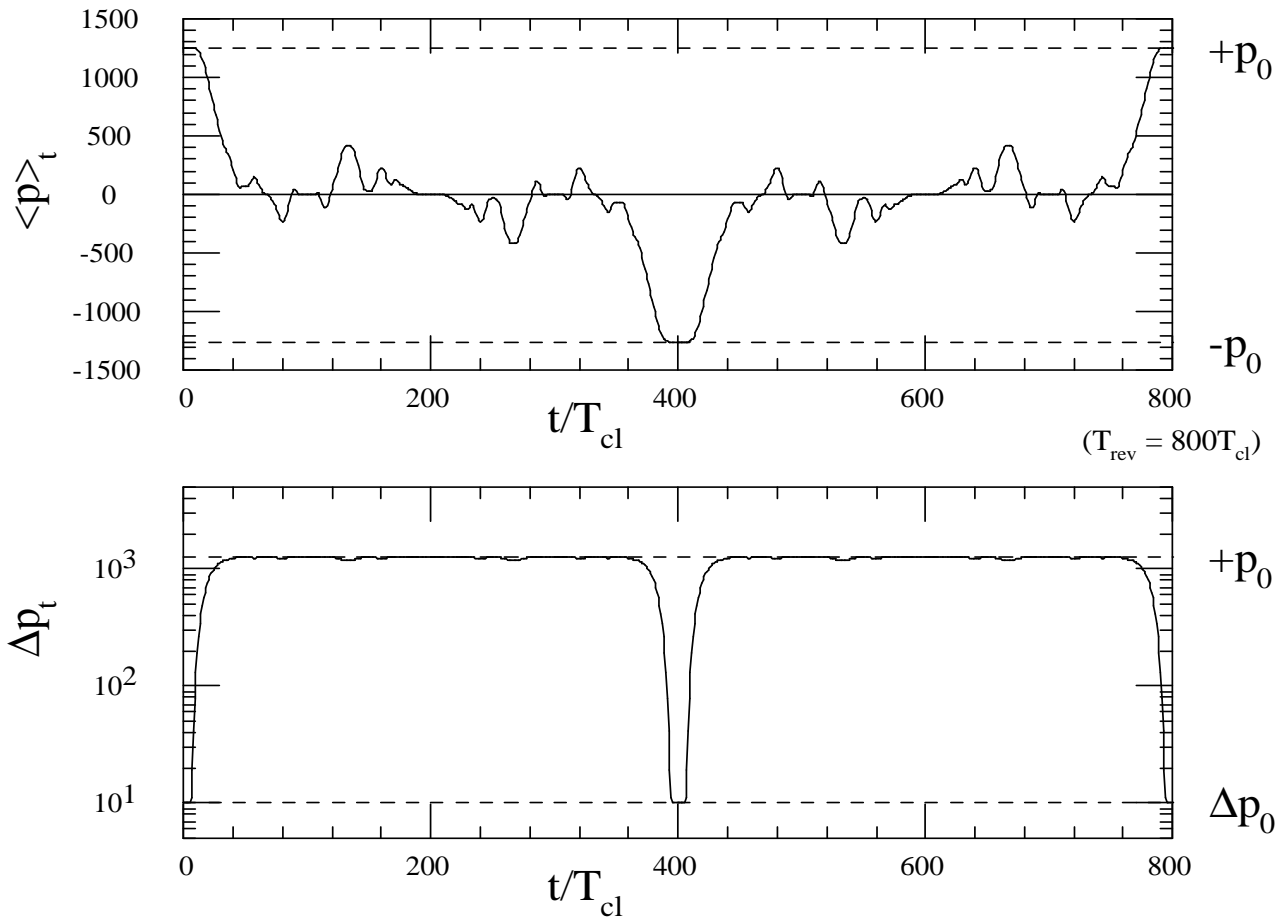


FIG. 28 Same as for Fig. 26, but for $\langle p \rangle_t$ and Δp_t . Note that there are no obvious deviations from the collapsed value of $\Delta p_{cl} = +p_0$ at $T_{rev}/4$ ($200T_{cl}$) or $3T_{rev}/4$ ($600T_{cl}$), even though Δx_t returns to its original (small) size. (Reprinted from Ref. (94).)

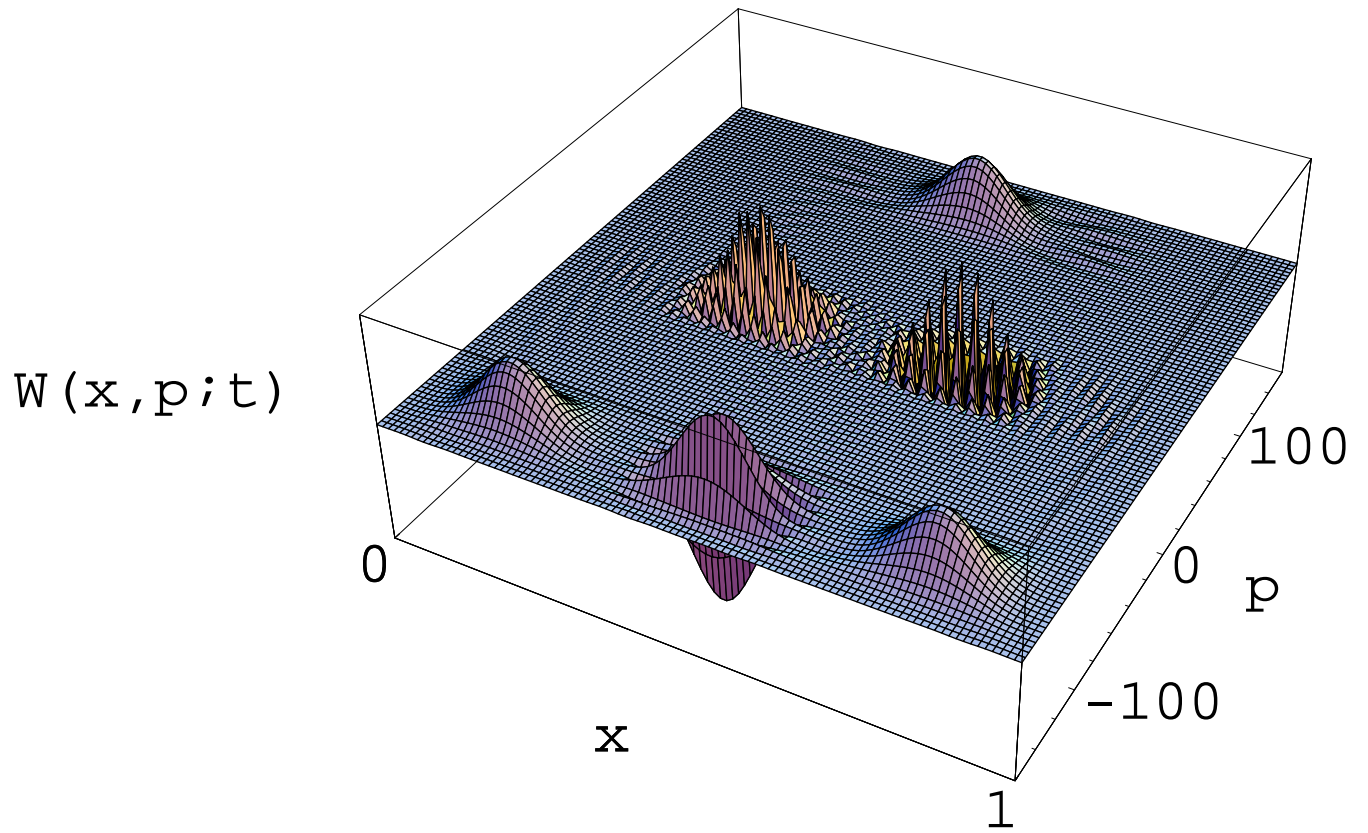


FIG. 29 Phase-space structure of the $T_{rev}/3$ fractional revival using the Wigner distribution. The parameters of Eqns. (24) and (26) are used, with $x_0/L = 1/2$, but with $n_0 = 40$ used to make the oscillatory ‘cross-terms’ more obvious.

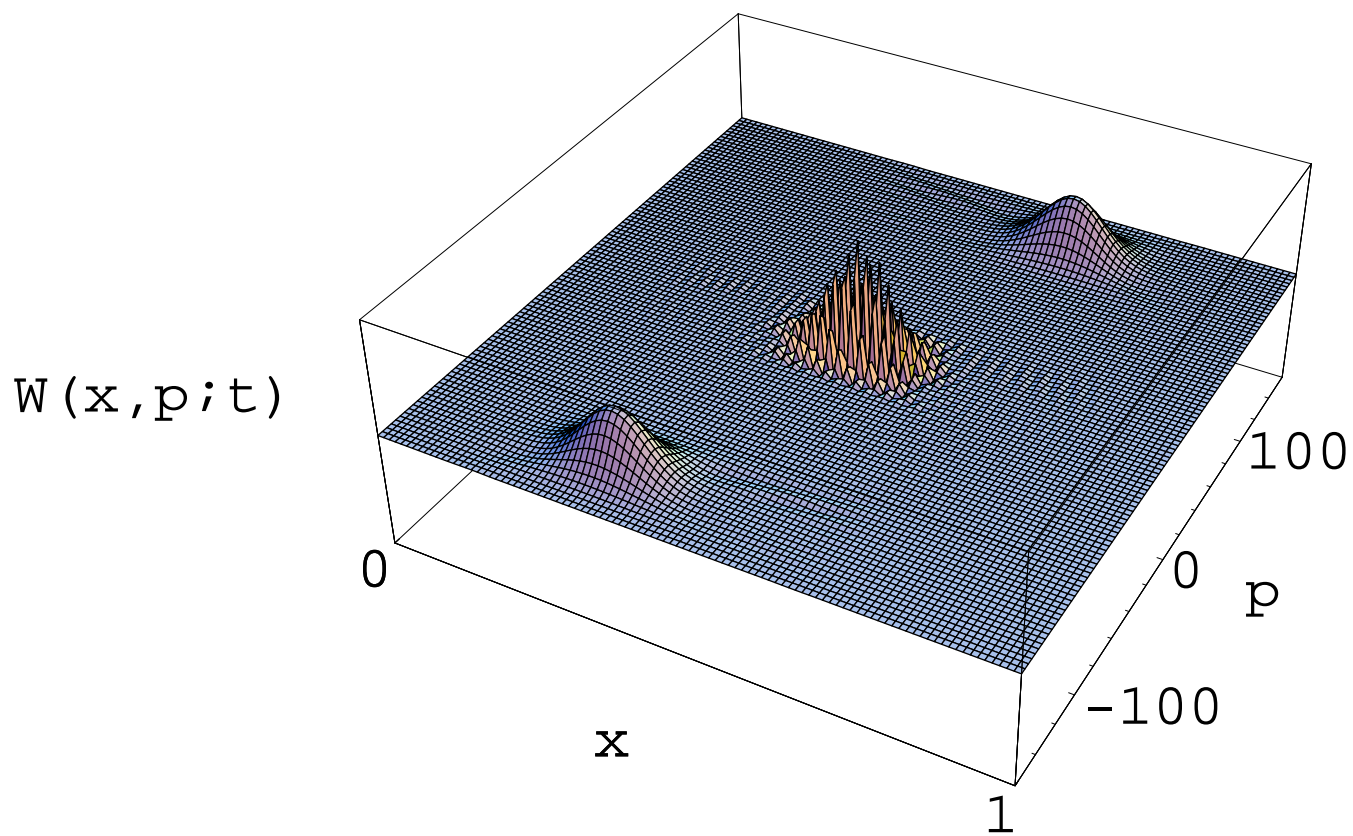


FIG. 30 Same as Fig. 29, but for the fractional revival at $t = T_{rev}/4$, where $x_0/L = 2/3$ is used.

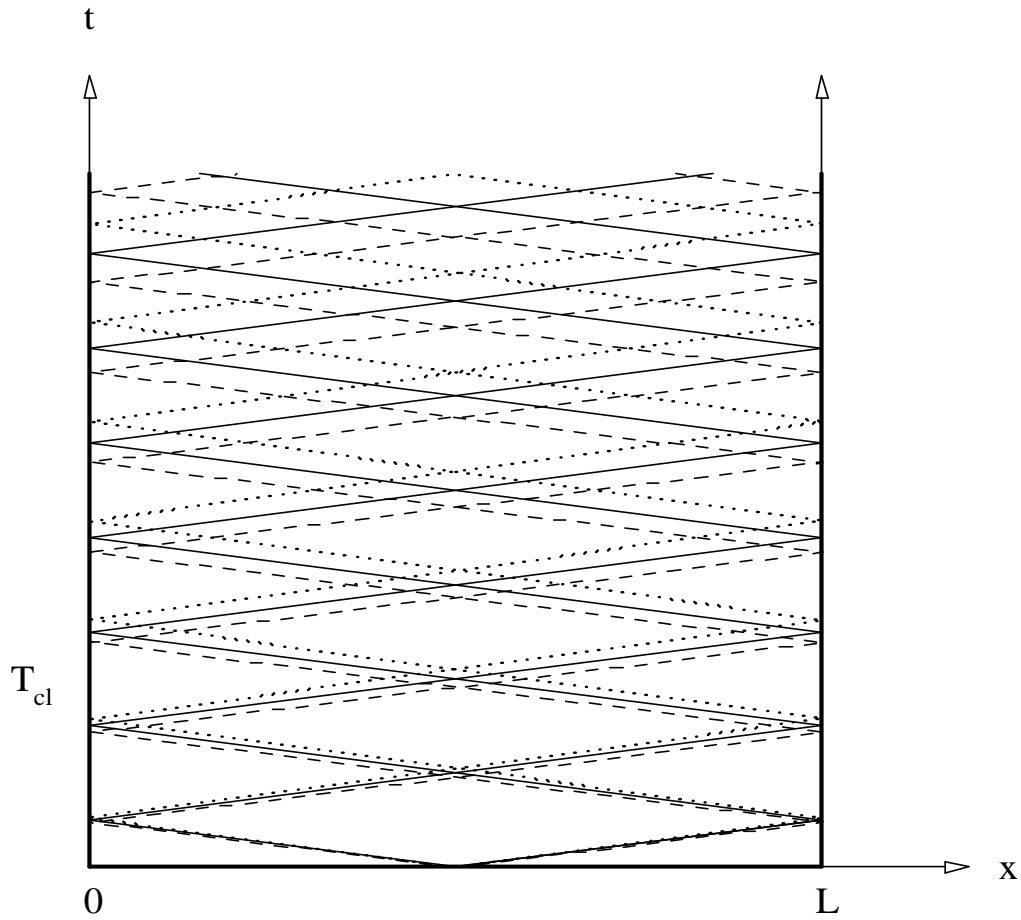


FIG. 31 Plot of the classical trajectories (or world-lines), shown in the (x, t) plane, of three point particles with slightly different speeds, illustrating wave packet spreading in the infinite well with walls at $x = 0, L$, as first discussed by Born (101), (102).

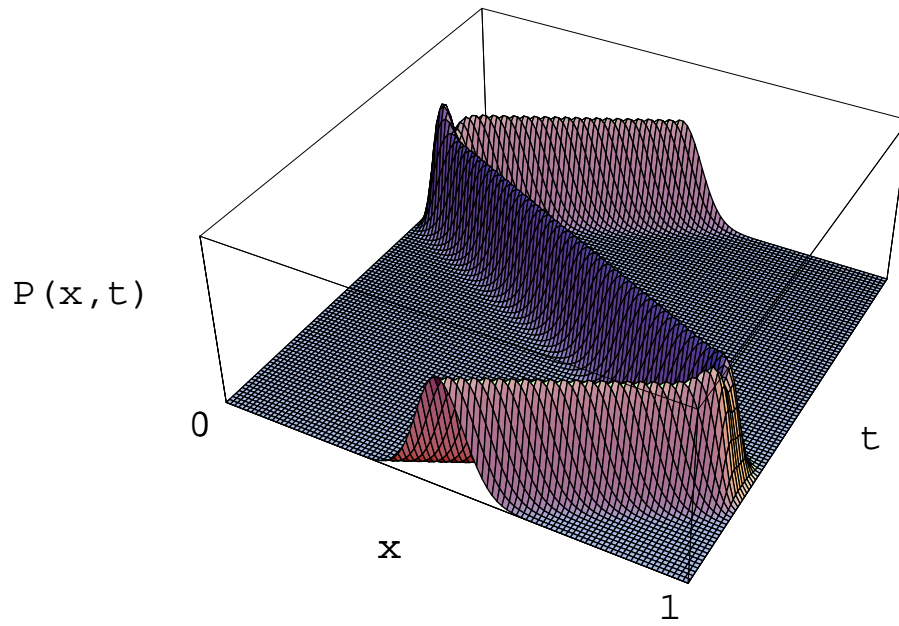


FIG. 32 Plot of the position-space probability density, $P(x, t) = |\psi(x, t)|^2$, versus x, t in the infinite well, for a Gaussian wave packet, over the first classical period. The parameters in Eqn. (159), with $n_0 = 400$, are used, so the infinite well is over the interval $x \in (0, 1)$.

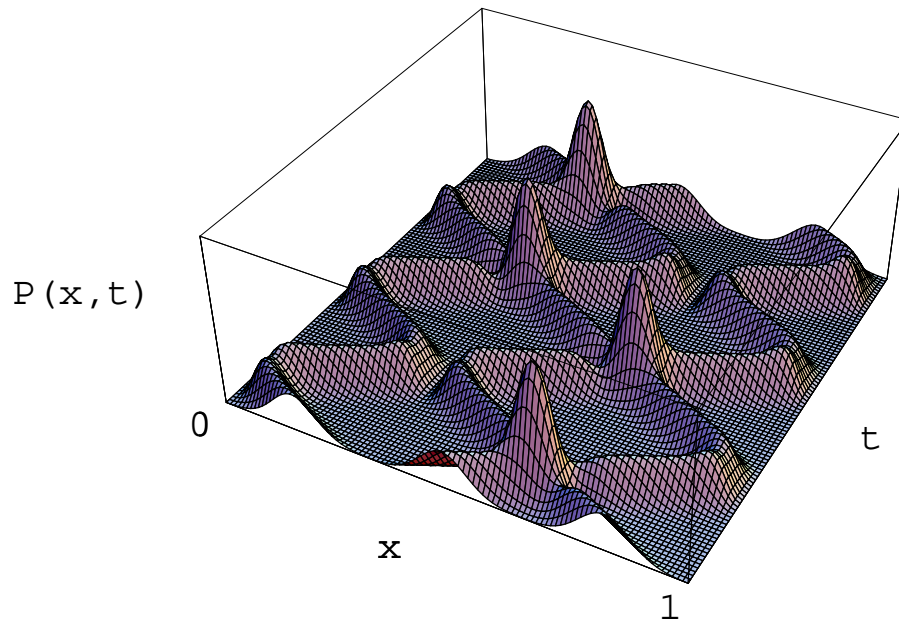


FIG. 33 Same as Fig. 32, but over one classical period, starting at $T_{rev}/3$.

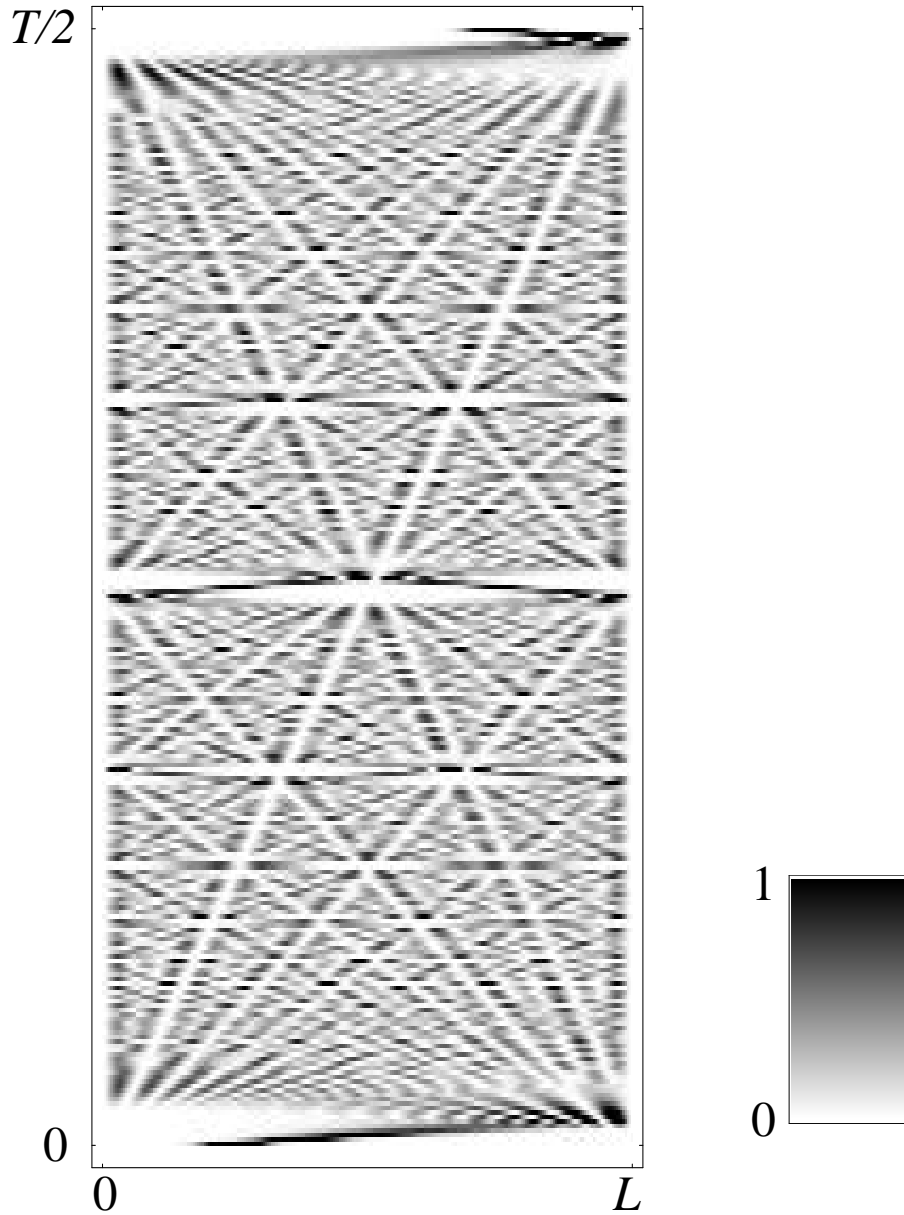


FIG. 34 Contour plot of the probability density, $|\psi(x,t)|^2$ versus x,t for the infinite well with $x \in (0,L)$ over the interval $(0,T_{rev}/2)$, with darker areas corresponding to higher probability, illustrating the pattern of ridges and canals described as a quantum carpet. A Gaussian wavepacket with $n_0 = 15$, $x_0 = L/4$, and $\Delta x_0 = L/20$ is used. (Adapted from Fig. 1 of Ref. (128), courtesy of I. Marzoli.)

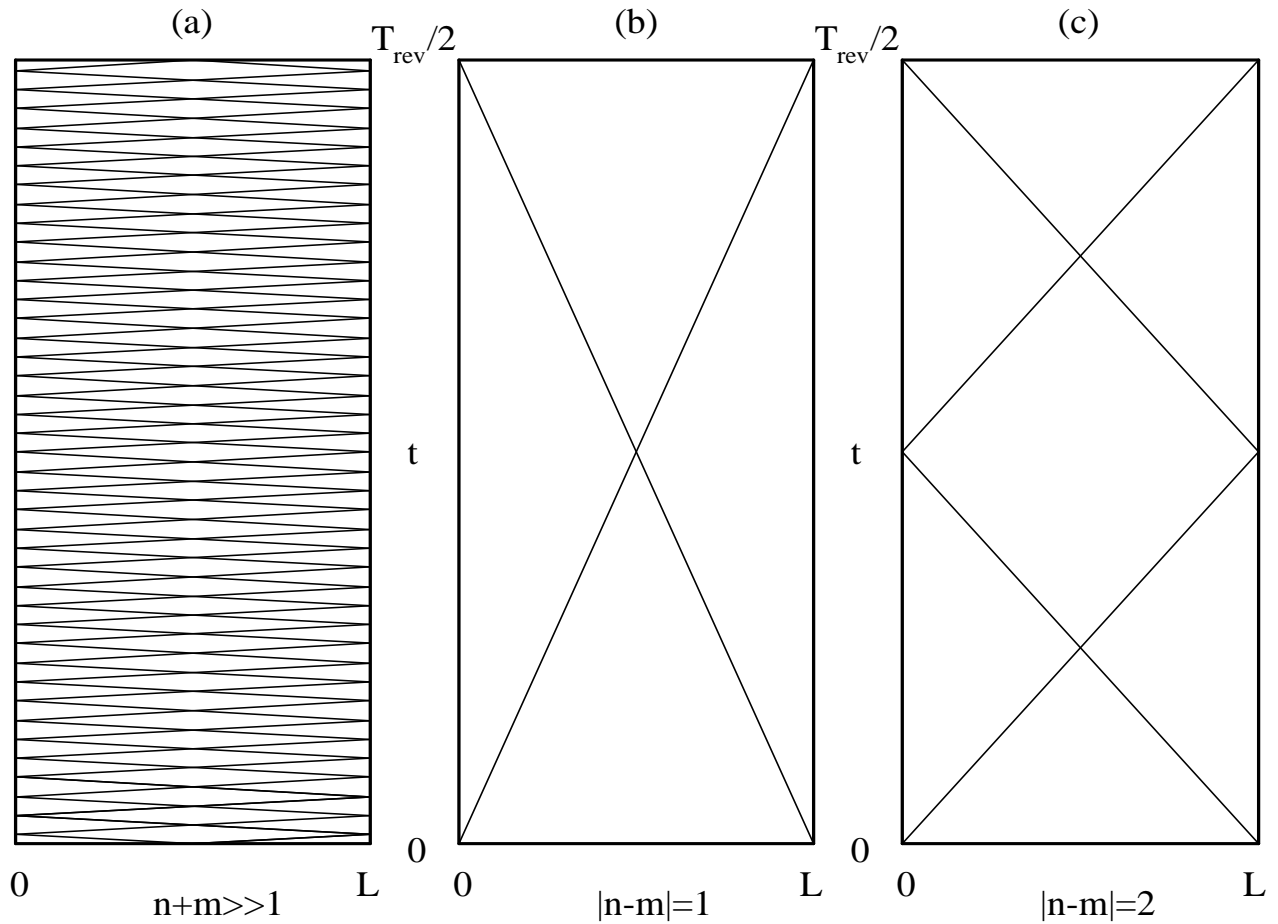


FIG. 35 Plots of typical worldlines in the (x, t) plane corresponding to the classical contribution to the probability density in Eqn. (195) where $n + m \gg 1$ (a), and two cases from the *quantum carpet* terms in Eqn. (196) corresponding to $|n - m| = 1$ (b) and $|n - m| = 2$ (c).

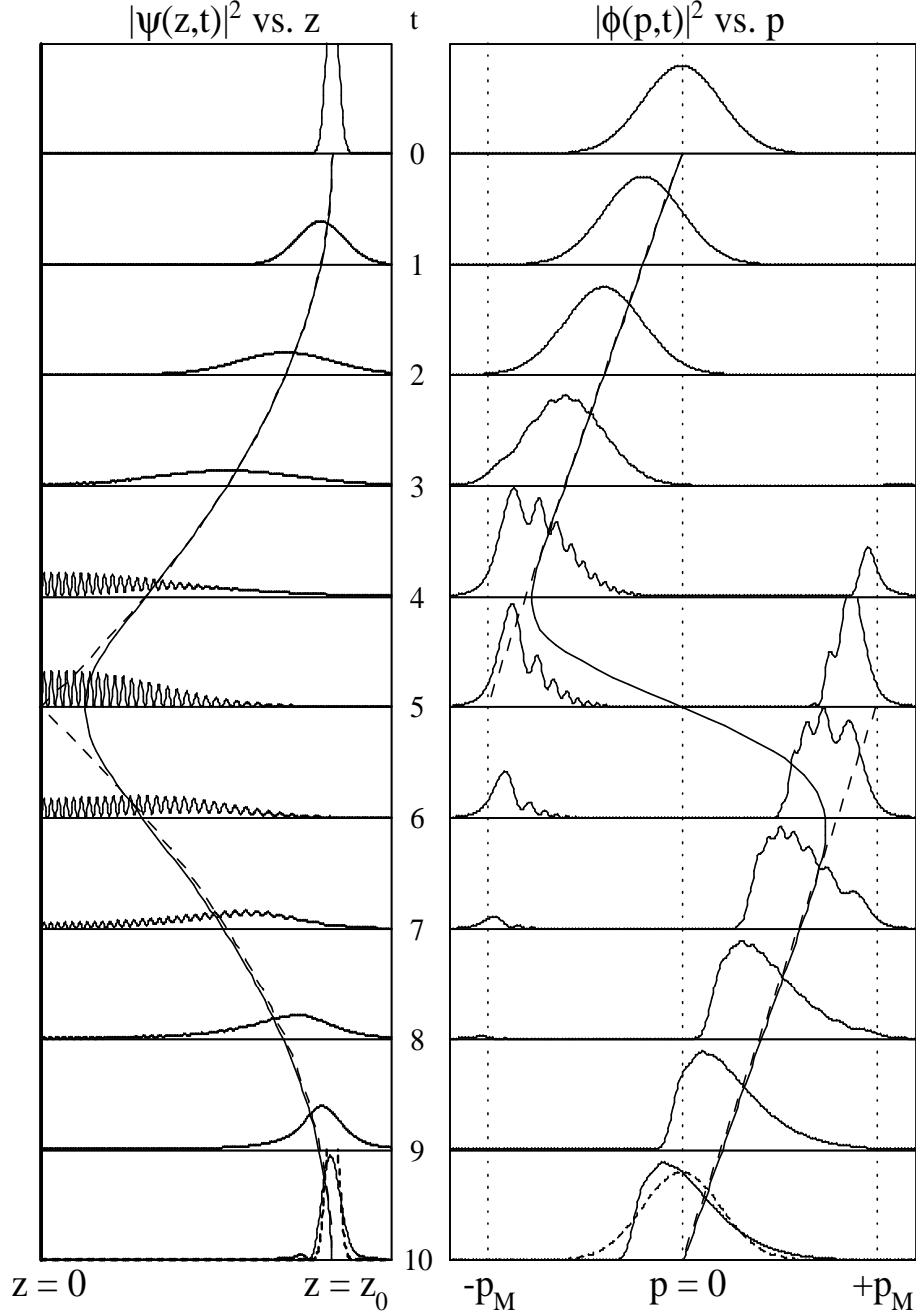


FIG. 36 Gaussian wave packet solutions for the quantum bouncer in position-space ($|\psi(z,t)|^2$ versus z , left) and momentum-space ($|\phi(p,t)|^2$ versus p , right) for various times during the first classical period. The solid curves represent the time-dependent expectation values of position ($\langle z \rangle_t$, left) and momentum ($\langle p \rangle_t$, right) for these solutions. The similar dashed curves are the classical trajectories, $z(t)$ (left) and $p(t)$ (right), superimposed. The wave packet parameters in Eqns. (217) and (218) are used. For the momentum-space figure, the vertical dotted lines represent the values $p = 0$ and the classical extremal values of momentum, $\pm p_M = \pm\sqrt{2mFz_0}$. (Reprinted from Ref. (151).)

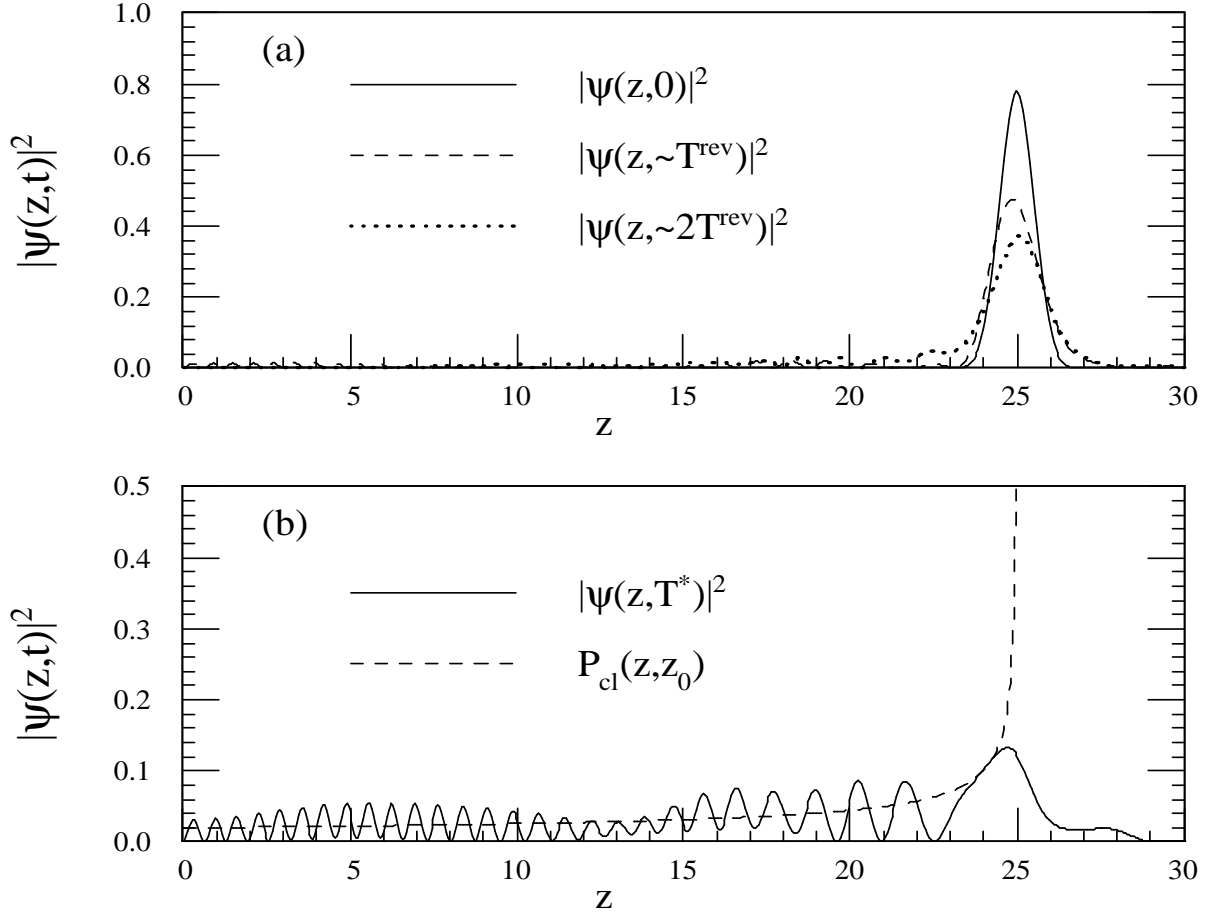


FIG. 37 The top plot (a) shows the position-space probability density, $|\psi(z,t)|^2$ for the initial Gaussian wave packet (solid), at at times near the first (dashed) and second (dotted) revival times. The bottom plot (b) shows $|\psi(z,T^*)|^2$ at a typical time, T^* , not close to any fractional revival, during the collapsed phase (solid), while the dashed curve is the classical probability density given by Eqn. (221) (but note the change in scale.)

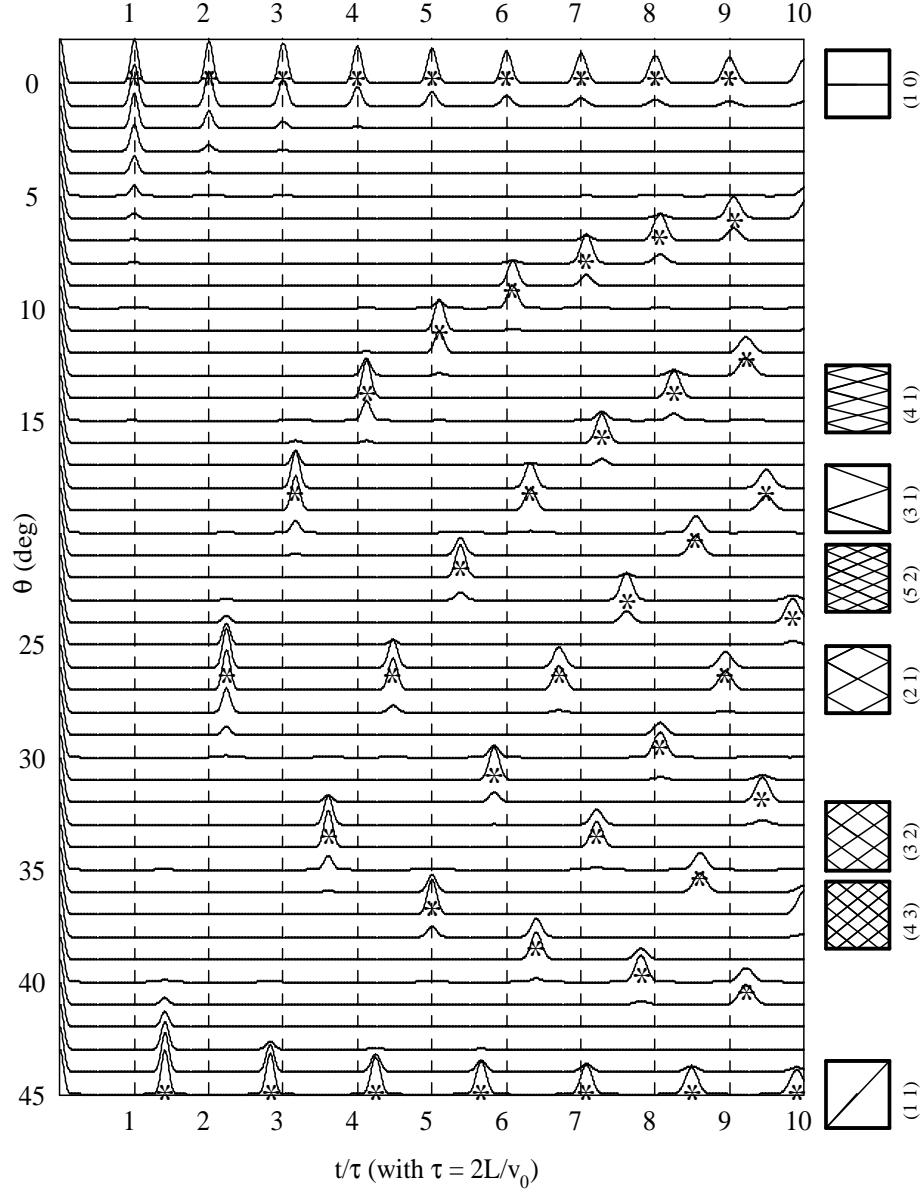


FIG. 38 Plots of the auto-correlation function, $|A(t)|^2$ versus t , for the 2-D square billiard. The plots are over a time period equal to ten classical ‘back-and-forth’ periods, 10τ , where $\tau \equiv 2L/v_0$. Plots for different values of the initial angle, $\tan(\theta) = p_{0y}/p_{0x}$ are shown. The stars indicate the positions of classical closed orbits (and recurrences) as given by Eqn. (238). (Reprinted from Ref. (97).)

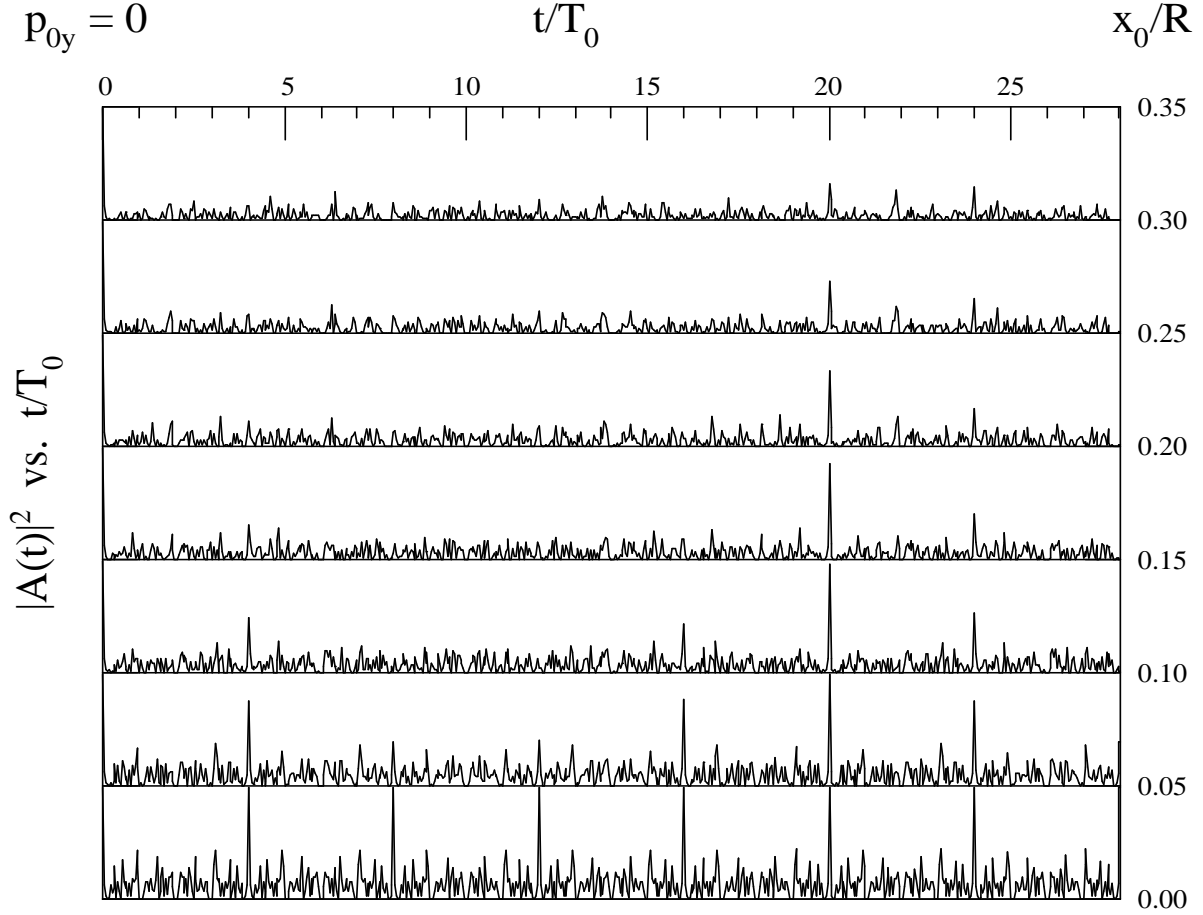


FIG. 39 Plot of the autocorrelation function, $|A(t)|^2$ versus t , in units of $T_0 \equiv 2\mu R^2/\hbar\pi$. The numerical values of Eqn. (293) are used, along with $y_0 = 0$ and $p_{0x} = p_{0y} = 0$. The results for $|A(t)|^2$ versus t , as one varies the x_0 of the initial wave packet away from the center of the circular billiard, are shown on horizontal axes. (Reprinted from Ref. (177).)

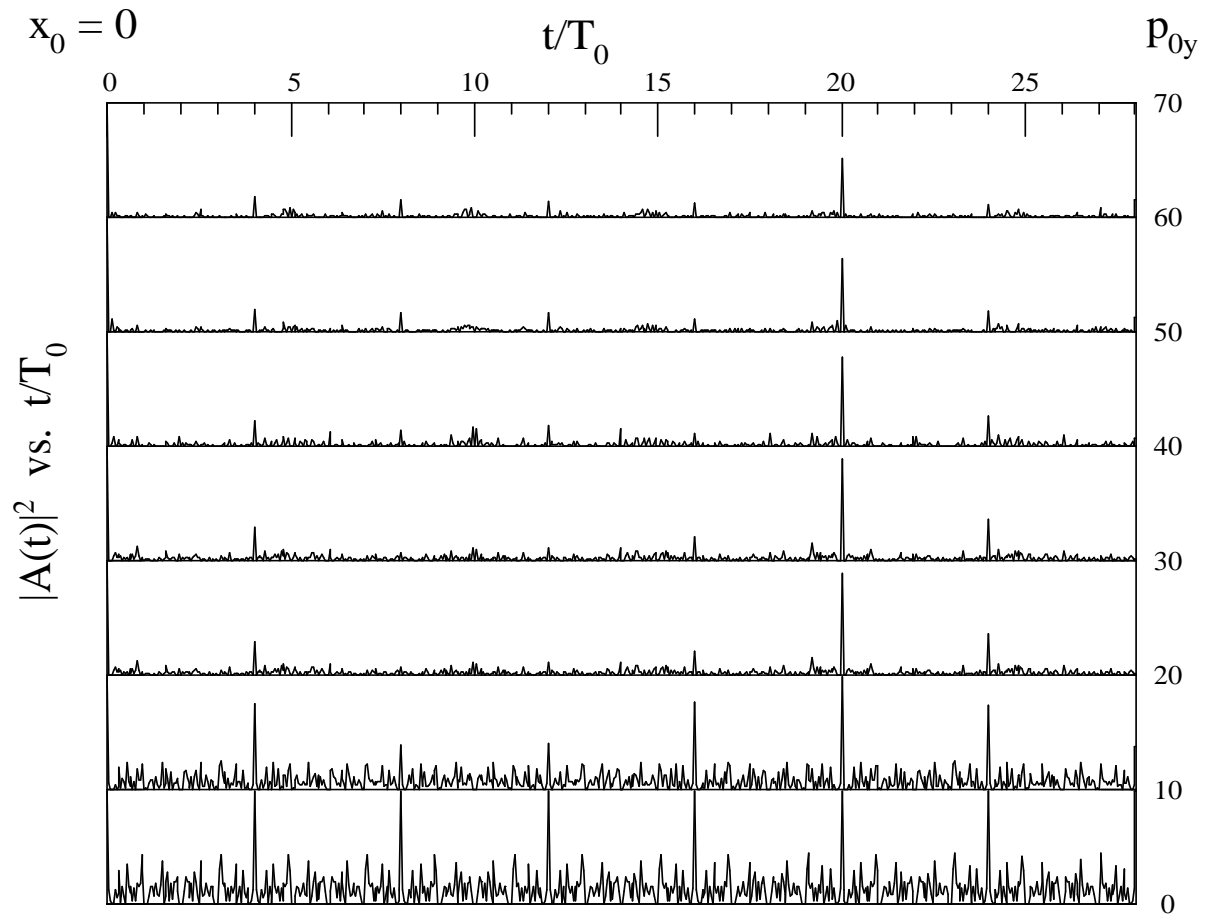


FIG. 40 Same as Fig. 39, but with $x_0 = y_0 = 0$ and $p_{0x} = 0$, as one increases p_{0y} . (Reprinted from Ref. (177).)

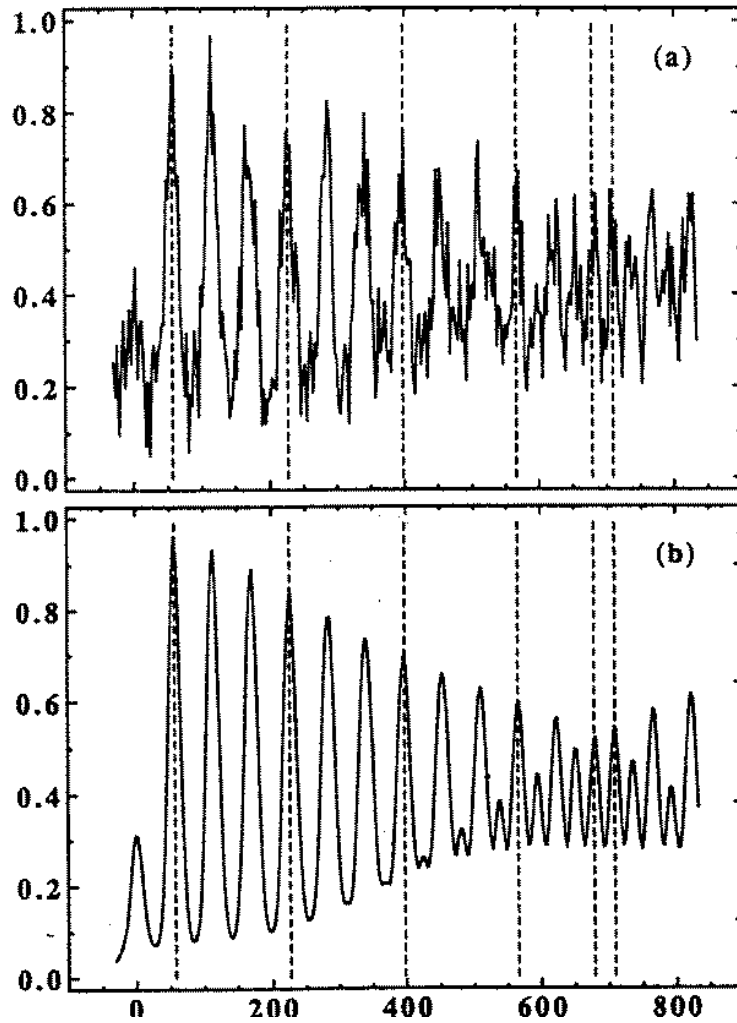


FIG. 41 Experimental (top) and theoretical (bottom) photoionization signal from Rydberg atoms as a function of the time delay after the initial probe pulse (a) compared with theoretical predictions (b). A fractional revival of order $p/q = 1/4$, with half the classical periodicity, is apparent near 680 ps . (Reprinted from Ref. (31).)

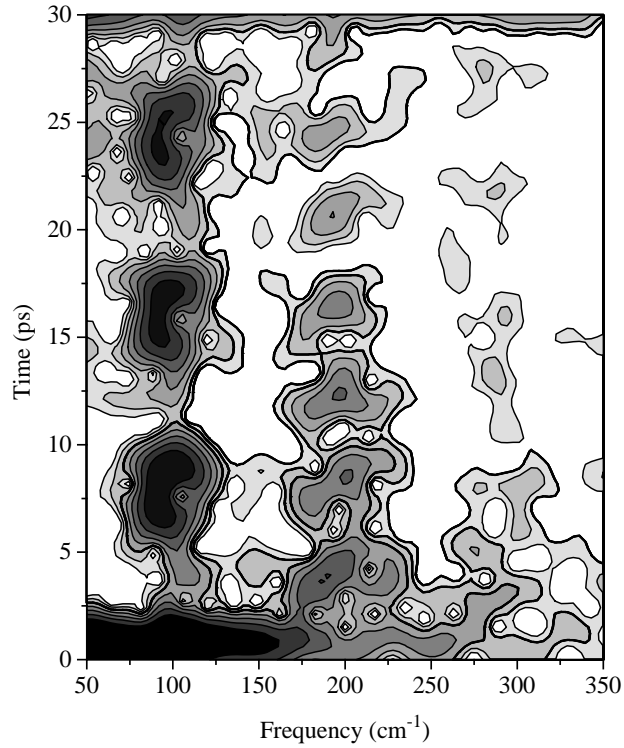


FIG. 42 Log spectrogram contour plot of data from Br_2 showing the spectral content of the observed signal as a function of time delay, defined by Eqn. (311). Evidence for full and fractional revivals at multiples of $f = 95 \text{ cm}^{-1}$ are clear. (Reprinted from Ref. (35), courtesy of D. Villeneuve.)

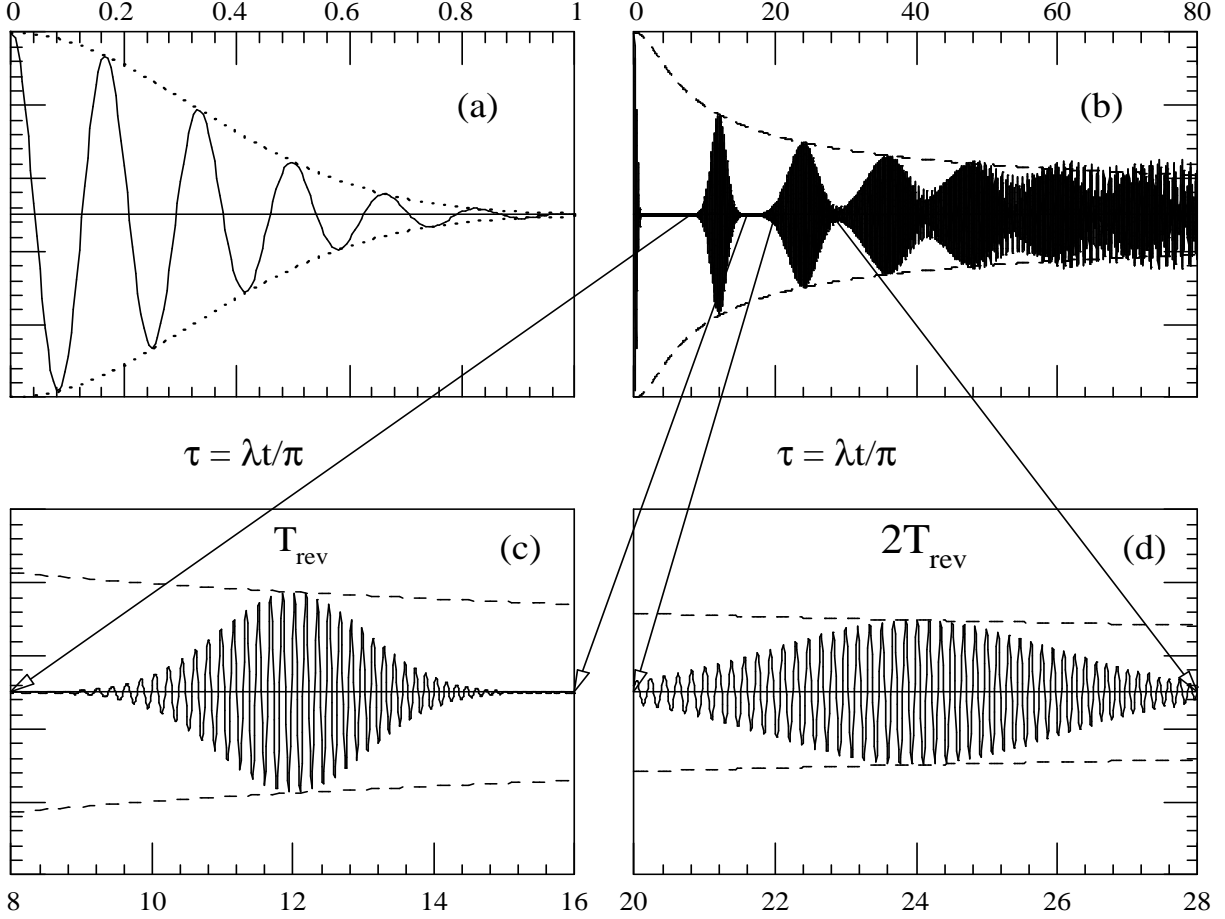


FIG. 43 Plots of $P_e(t)$ versus scaled time ($\tau = \lambda t / \pi$) from the solution in Eqn. (318) over (a) the first few Rabi cycles and (b) over a number of revivals times, showing the first (c) and second (d) revivals in detail. Values of $\bar{n} = 36$ and $\lambda = 0.01$ are used. The dotted curve corresponds to the initial Gaussian de-phasing envelope ($\exp(-(\lambda t)^2/2)$), while the dashed curves correspond to the long-term suppression given by Eqn. (321).

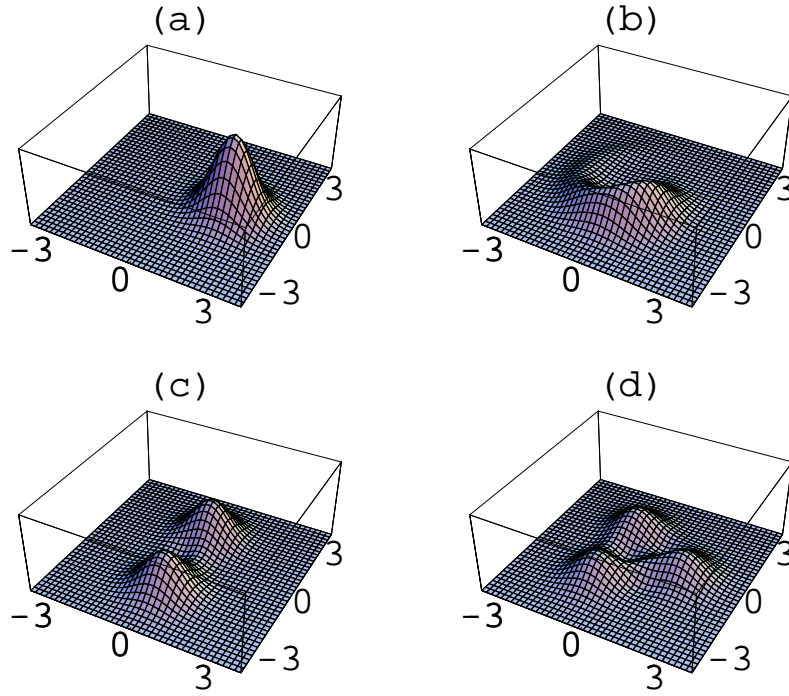


FIG. 44 Plots of $P(\beta; t) = P(\text{Re}(\beta), \text{Im}(\beta); t)$ versus $(\text{Re}(\beta), \text{Im}(\beta))$ from Eqn. (328). Values for (a) $t = 0$, (b) $0.1T_{rev}$, (c) $T_{rev}/2$, and (d) $T_{rev}/3$ are shown. An initial coherent state with $\alpha = (3, 0)$ is used for illustration.

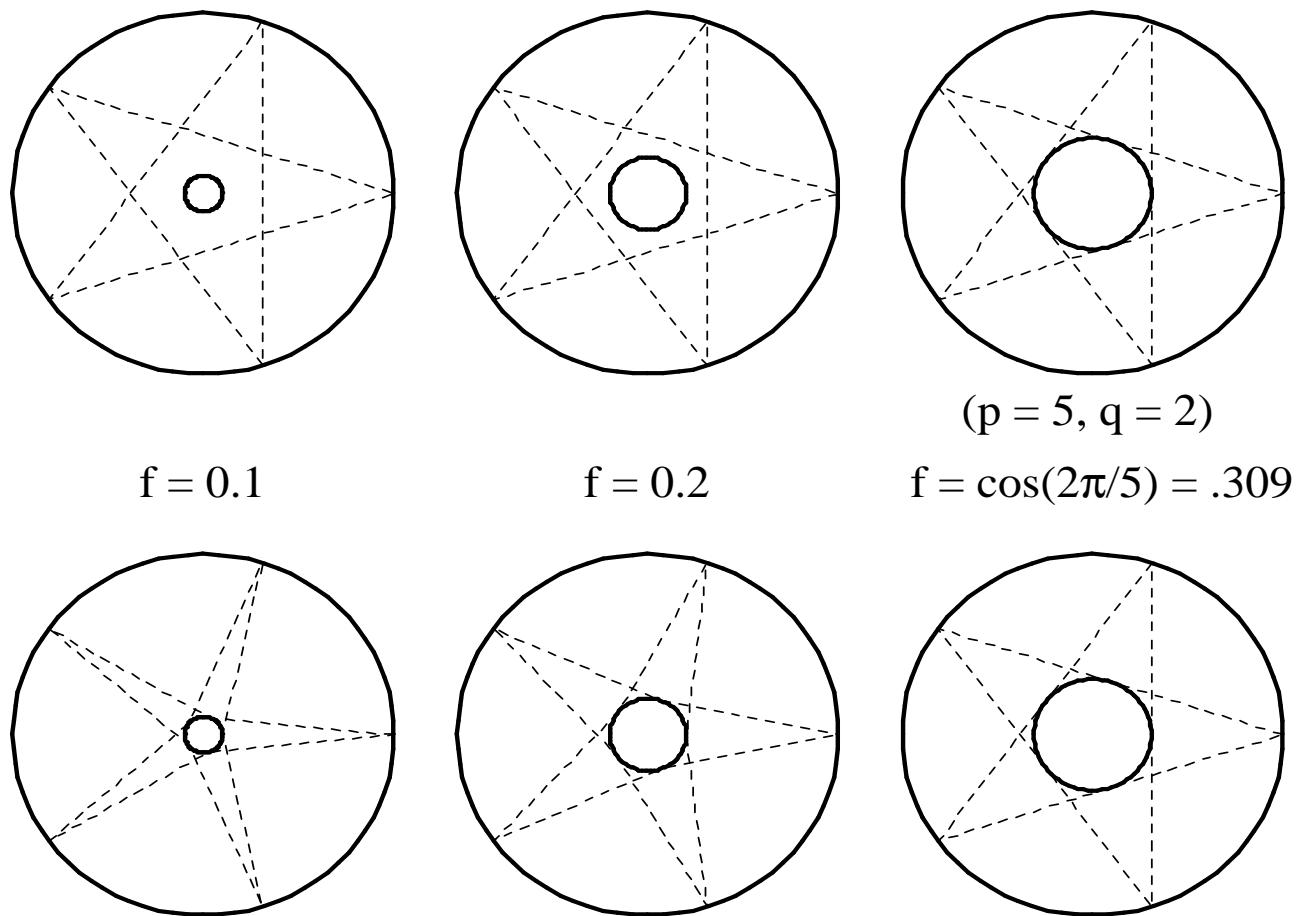


FIG. 45 An example of two possible closed orbits in the annular billiard, with $(p, q) = (5, 2)$, corresponding to the path lengths in Eqns. (E1) (top) and Eqn. (E17) (bottom), illustrating as well the critical value of $f_{max} = \cos(\pi q/p)$, beyond which neither orbit can be supported in this geometry.

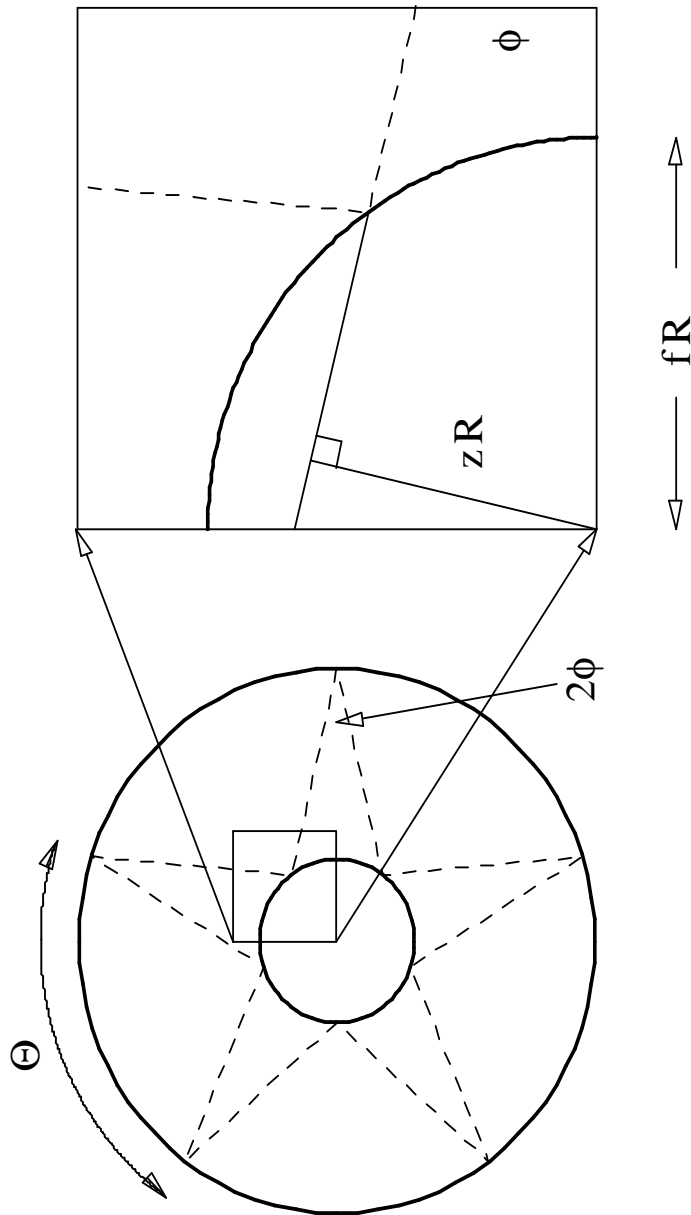


FIG. 46 The geometry defining the effective distance of closest approach for the ‘inner touching’ closed orbits for the annular billiard, leading to Eqn. (E18).